DEVELOPMENT OF ELECTROCHEMICAL DNA SENSORS BASED ON THE INCORPORATION OF FERROCENE LABELLED DATP

Ivan Magriñá Lobato

UNIVERSITAT ROVIRA i VIRGILI

Development of electrochemical DNA sensors based on the incorporation of ferrocene labelled dATP

IVAN MAGRIÑÁ LOBATO

Doctoral Thesis 2019

UNIVERSITAT ROVIRA I VIRGILI
DEVELOPMENT OF ELECTROCHEMICAL DNA SENSORS BASED ON THE INCORPORATION OF FERROCENE LABELLED DATP
Ivan Magriñá Lobato

Doctoral Thesis

Development of electrochemical DNA sensors based on the incorporation of ferrocene labelled dATP

IVAN MAGRIÑÁ LOBATO

Supervised by:
Prof. Ciara K. O'Sullivan
Dr. Mayreli Ortiz

Interfibio – Departament d'enginyeria Química

UNIVERSITAT
ROVIRA i VIRGILI

Tarragona
2019

UNIVERSITAT ROVIRA I VIRGILI
DEVELOPMENT OF ELECTROCHEMICAL DNA SENSORS BASED ON THE INCORPORATION OF FERROCENE LABELLED DATP
Ivan Magriñá Lobato

UNIVERSITAT ROVIRA i VIRGILI

Tribunal members:

Prof. Anne Varenne
(Unité de Technologies Chimiques et Biologiques pour la Santé, École nationale supérieure de chimie de Paris)

Prof. Taane Clark
(London School of Hygiene and Tropical Medicine)

Dr. Mònica Campàs Homs
(Institute of agrifood research and technology – IRTA)

Prof. Ioanis Katakis
(INTERFIBIO consolidated research group, University Rovira i Virgili)

Dr. Luis A. Tortajada-Genaro
(Institute of Molecular Recognition and Technological Development, Polytechnic University of Valencia)

Dr. Herbert Tomaso
(Friedrich-Loeffler-Institut)

External examiners:

Prof. Emmanuel Iwuoha
(Nanoelectrochemistry and Sensor Technology, University of Western Cape)

Prof. Terry Smith
(School of Natural Sciences, University of Galway)

UNIVERSITAT ROVIRA I VIRGILI
DEVELOPMENT OF ELECTROCHEMICAL DNA SENSORS BASED ON THE INCORPORATION OF FERROCENE LABELLED DATP
Ivan Magriñá Lobato

UNIVERSITAT ROVIRA i VIRGILI

DEPARTAMENT D'ENGINYERIA QUÍMICA
Universitat Rovira i Virgili
Av. Països Catalans 26
43007 Tarragona, Spain
Tel: 977 55 96 58
Fax: 977 55 96 67

Dr. MAYRELI ORTIZ and Dr. CIARA K. O'SULLIVAN

CERTIFY:
That the doctoral thesis entitled: "Development of electrochemical DNA sensors based on the incorporation of ferrocene labelled dATP" submitted by Ivan Magriñá Lobato in order to achieve the Degree of Doctor, has been carried out under our supervision, at Department of Chemical Engineering at Universitat Rovira i Virgili and that it fulfils all the requirements to be eligible for the International Doctorate Award.

Tarragona, September 3rd, 2019

Dr. Mayreli Ortiz

Dr. Ciara K. O'Sullivan

UNIVERSITAT ROVIRA I VIRGILI
DEVELOPMENT OF ELECTROCHEMICAL DNA SENSORS BASED ON THE INCORPORATION OF FERROCENE LABELLED DATP
Ivan Magriñá Lobato

AGRAÏMENTS

Escriure aquestes paraules m'està resultant més difícil que escriure qualsevol capítol de la tesis. Mai podré expressar en paraules la gratitud que sento per totes les persones que m'han acompanyat en aquest viatge.

La primera persona que vull mencionar és la meva mare, **Carmen** o **"momichi"** com m'agradava dir-li carinyosament. Ets i has sigut la persona més important de la meva vida, la que m'ho ha donat tot esperant res a canvi, la que sempre m'ha apoyat en tota i cadascuna de les decisions que he pres. Recordo perfectament lo contenta que et vas posar en saber que m'havien acceptat al doctorat, i a tu et dedico tots els fruits del meu esforç. No estàs avui entre nosaltres però se que allà on estigues et brillen els ulls, orgullosa del teu fill i del que ha aconseguit. Sempre estaràs en el meu cor, t'estimo i t'estimaré sempre.

Vull continuar agraint infinitament a la meva supervisora, **Ciara K. O'Sullivan**, la oportunitat de realitzar el doctorat a Interfibio Research Group. Ha estat una experiència molt enriquidora en molts aspectes, més enllà de l'àmbit científic i acadèmic. Treballant sota la teva supervisió m'he sentit escoltat, valorat, còmode, m'he sentit com un més de la família. T'agraeixo el temps i els esforços que m'has dedicat, els consells, les suggerències, la supervisió i la confiança que sempre has depositat en mi. Mai et podré agrair suficientment les vegades que m'has ajudat quan ho he passat malament i les oportunitats acadèmiques que m'has donat: poder assistir a cursos, congressos, estades a altres grups de recerca... i per acabar, et voldria agrair també per les magistrals classes que ens vas donar durant el màster de Nanociència, inspiradores, apassionants, brillants...! Un cop més, gràcies per tot!

A qui també vull agrair el seu esforç, temps i dedicació és a **Mayreli Ortiz**, la meva co-supervisora! Companya de batalla colze a colze al laboratori, sempre amb un somriure a la cara i una de les persones més positives i "risueñas" que conec! Gràcies per estar sempre quan t'he necessitat i per tota la teva ajuda.

No puc deixar d'agrair tampoc a **Bàrbara** i **Núria** per tota l'ajuda rebuda en temes burocràtics i per ser per a mi un referent de la diligència i organització!

Vull agrair també tota l'ajuda tècnica i científica que he rebut per part de **Anna, Miriam**, **Marketa** i **Vasso** en temes relacionats amb la biologia molecular, a **Jonathan, Mayreli, Jos, Julio, Ianis** i **Robert** per l'ajuda relacionada en l'electroquímica; a **Jonathan**, **Lukas**, **Eric** i **Mariana** amb temes relacionats amb el cleanroom i finalment a **Anna**, **Alessandro** i **Pedro** per l'ajuda en la síntesis de nucleòtids modificats.

Durant el doctorat m'han acompanyat moltes més persones, amb algunes d'elles vaig començar el viatge junts, d'altres ja han marxat i d'altres seguiran molt després de que jo marxi, però totes elles sempre ocuparan un lloc especial a la meva memòria.

Gràcies **Jonathan** per ser el meu amic i guia. Per introduir-me al grup, per ensenyar-me els primers passos, per les discussions científiques i per ser com ets.

A vosaltres **Nihad** i **Nassif** per acompanyar-me des de que vam començar, per les penes i glòries i els deliris col·lectius que hem passat junts gràcies a la nostra estimada electroquímica, i gracies per la vostra amistat. A tu **Jos** per compartir molts moments de divagació científica, política i personal, ets per a mi un referent de la humilitat i del respecte. Gràcies **Carmen** i **Mary Luz** per consentir-me, per l'ajuda, pels riures i per les converses que hem mantingut. A **Tete** pel seu sentit de l'humor i per donar-me a conèixer a San Turcio. A **Santi** per les hores

extra, el bon sentit de l'humor i les sessions de música que vam passar junts el primer nadal sofrint plegats uns experiments que no volien funcionar mai. A tu **Sallam**, per ser la personificació de l'esperit ZEN i aportar pau, tranquil·litat al laboratori i a tu **Olena** per tots els moments delirants que hem compartit.

Gràcies **Mònica** per obrir-me les portes de l'IRTA i per tota l'ajuda que em vau oferir juntament amb **Anna**.

Moltes gràcies **Prof. Michal Hocek** per totes les suggerències i aportacions que has fet a n'aquesta tesis, i també per oferir-me l'estada a l'IOCB de Praga. No només va ser una experiència científica i cultural i personal molt enriquidora sinó que em va permetre conèixer persones tant genials com **Anna**, **Pedro**, **Alessandro**, **Fabrizzia**, **Gloria**, **Marek** o **Nemanja**.

Moltes gràcies a tu també **Prof. Robert Forster** per acollir-me al teu grup de recerca a Dublin durant l'estiu del 2018 i per les teves excel·lents aportacions a n'aquesta tesis. A **Fionn** i **Adalberto** per ser els companys de laboratori més esbojarrats que he tingut mai i a **Ausra** per la seva amistat, el seu suport i per treure'm el sobrenom de Megamind!

També vull agrair i recordar a persones que han passat pels grup uns poquets mesos o amb els que he coincidit poc temps, però que no per això han deixat una petjada menys intensa. Gràcies a **Eugeni, Vibol, Àngel, Eolann, Aimee, Tin, Resmond, Valerie, Cristoph, James, Shaira, Sharmaine, Emelina, Nerissa, Keylin, James, Iván, Havva**... per tots els moments compartits.

Durant la meva etapa de doctorat he tingut l'honor de supervisar juntament amb Mayreli i Ciara a **Cansu** una brillant i prometedora estudiant! Gràcies per la paciència, les converses hilarants i per les hores de compartides dins i fora del laboratori. Sempre et recordaré! Teşekkür ederim!

Vull agrair també a **Xhensila, Laura i Zaida** per ser "los Ángeles de Ivan". Pel suport, per l'amistat, per tot el que hem fet junts i per formar part de la meva vida. Teniu reservat un racó especial del meu cor per a vosaltres.

Finalment vull agrair el suport rebut per les persones més properes. Al meu pare **Agustí**, a **Teresa** i al meu germà **Eloi** pel suport incondicional i per sempre confiar en mi i també als meus amics més propers: **Franc, Albert, Michelle, Jonathan, Laura and Laia, Miriam, Marta, Eloi, Fèlix, Kilian, Alfonso, Anna, Eric, Andrés, Xhensila i Laura** per fer de crossa en els moments més difícils.

Gràcies a tots de tot cor.

ACKNOWLEDGMENTS

This words are harder to write than any chapter in this thesis. I will never be able to express in words the gratitude I feel for all the people who joined me on this trip.

The first person I want to mention is my mother, **Carmen** or "**momichi**" as I liked to call her with love. You are and you have been the most important person in my life, who has given me everything, waiting for nothing in return, which has always supported me in every one of the decisions that I have taken. I remember perfectly how happy you were the moment you knew I was accepted in the PhD program, and I dedicate all the fruits of my effort to you. You are not among us today but I know that wherever you are, your eyes shine, proud of your son and what I have achieved. You will always be in my heart, I love you and I will always love you.

I want to continue to thank infinitely **Ciara K. O'Sullivan**, my supervisor, for the opportunity to make a doctorate at the Interfibio Research Group. It has been a very enriching experience in many aspects, beyond the scientific and academic field. Working under your supervision I felt listened, valued, comfortable, I have felt like one more in the family. I am grateful for the time and the efforts that you have dedicated to me, the advice, the suggestions, the supervision and the trust you have always placed in me. I will never be able to thank you for the times you helped me when I had problems and the academic opportunities that you gave me: to be able to attend courses, conferences, stays to other research groups ... and to finish, I would like to thank you as well for the classes that you gave us during the Master's degree in Nanoscience, inspiring, exciting, brilliant...! Once again, thanks for everything!

To whom I also want to thank for her effort, time and dedication is to **Mayreli Ortiz**, my co-supervisor! Battle partner, side by side in the lab, always with a smile in the face and one of the most positive and smiley person that I know! Thank you for always being there when I needed you and for all your help.

I would also like to thank **Bàrbara** and **Núria** for all the help received in bureaucratic issues and for being a reference of diligence and organization!

I would also like to thank all the technical and scientific help I have received from **Miriam, Marketa and Vasso** on topics related to molecular biology; to **Jonathan, Mayreli, Jos, Julio, Ianis and Robert** on electrochemistry; to **Jonathan, Lukas, Eric and Mariana** with issues related to the cleanroom and microfabrication and finally to **Anna, Alessandro and Pedro** for the help in the synthesis of modified nucleotides.

During my Ph.D. I've met many wonderful people. I started the trip with some of them, others have already left and others will continue long after I leave, but all of them will always have a special place on my memories.

Thanks **Jonathan** for being my friend and guide, for introducing me to the group, for teaching me the first steps, for the scientific discussions and for being as you are.

To you **Nihad** and **Nassif**, for starting the journey together, for the pains and the glories, and the collective delusions that we experienced together due to our beloved electrochemistry, thanks for your friendship. To you **Jos**, for all the scientific, political and personal discussions we had. Thank you **Carmen** and **Mary Luz** for spoiling me, for the laughs and for the conversations. To you **Tete**, for your endless sense of humor and for getting me to know San Turcio. To you Santi, for the fun, the music sessions and the extra hours that we spent together the first Christmas of my PhD, suffering from some experiments that never wanted to work. To

you **Sallam**, for being the incarnation of the ZEN spirit and bringing peace to the lab, and to you **Olena**, for all the delirious moments we have shared together.

Thank you **Mònica** for opening me the doors of IRTA and for all the help you offered me along with **Anna.**

Thank you very much **Prof. Michal Hocek** for all the suggestions and contributions you have made to this thesis, and also for offering me to stay in your research group at the IOCB in Prague. Not only was a very enriching scientifically, culturally and personally, but also it allowed me to meet great people including **Anna, Pedro, Alessandro, Fabrizzia, Gloria, Marek and Nemanja**.

Many thank also to **Prof. Robert Forster** to welcome me at your research group in DCU, Dublin, during last summer, and also thank you for your excellent contributions to this thesis. To you **Fionn**(cé) and **Adalberto** for being the most hilarious labmates I have ever had and to you **Ausra** for your friendship, your support and for the funny nickname you got me: Megamind!

I would also like to thank and remind people that stayed in the group for few months or with those that I met for a short period of time. Thanks **Eugeni, Vibol, Àngel, Eolann, Aimee, Tin, Resmond, Valerie, Cristoph, James, Tomi, Serena, Melike, Buket, Shaira, Sharmaine, Emelina, Nerissa, Keylin, James, Ivan, Havva** ... for all the shared moments.

During my PhD I was honored to supervise **Cansu** along with Mayreli and Ciara. A brilliant and promising student! Thank you for the patience, the hilarious conversations and for the hours that we shared inside and outside the laboratory. I will always remember you! Teşekkür ederim!

I would also like to thank **Xhensila, Laura** and **Zaida** for being "the Angels of Ivan." For the support, for the friendship, for everything we have done together. Thank you for being part of my life. A piece of my heart will always belong to you.

Finally, I would like to thank all the support received from my closest people. My father **Agustí**, **Teresa** and my brother **Eloi** for unconditional support and for always trusting me. Many thanks also to my closest friends: **Franc, Albert, Michelle, Jonathan, Miriam, Laura and Laia, Marta, Eloi, Félix, Kilian, Alfonso, Anna, Èric, Andrés, Xhensila** and **Laura** for being a foothold in the hardest moments.

Thank you all from the bottom of my heart.

TABLE OF CONTENTS

Summary

The detection of specific DNA sequences has a plethora of diverse applications in many fields including clinical diagnostics, disease monitoring, food analysis, forensics, bioterrorism and environmental control. However, traditional DNA analysis methods are multi-step, time-consuming, expensive, require bulky equipment and trained personnel, thus restricting their use. As a consequence, there is a considerable time-lag between sample acquisition and response, limiting the decision-making capacity, which in some cases might be life-threatening. To overcome this problem, miniaturized, accurate, simpler and affordable analytical devices (biosensors) have been developed during the last decades. DNA electrochemical sensors are excellent candidates for point-of-need DNA analysis that combine the high sensitivity and robustness of electrochemistry based sensors with the selectivity provided by the specific DNA hybridization that occurs between complementary DNA sequences. Nevertheless, the use of electrochemical DNA sensors as point-of–need devices is still limited because they require several steps including the amplification of the target sequence, the generation of single stranded DNA following amplification, target hybridization with a complementary capture probe and finally other reporting steps to detect the hybridized target DNA sequence. In order to reduce the number of steps and bring electrochemical DNA sensors closer to the point-of-need we proposed the combination of two strategies. The first consists in the use of ferrocene labelled dATP ($dA^{EFc}TP$) to obtain labelled target amplicons, thus avoiding the need for further labelling steps. The second consists in the use tailed primers during the liquid phase primer extension or DNA amplification to obtain amplicons with a single stranded DNA (ssDNA) tail for direct hybridization, thus avoiding the need for the post-amplification generation of single stranded DNA. In this thesis we explore the combination of the aforementioned strategies to develop electrochemical DNA sensors and their use to detect target DNA sequences in genomic DNA. Fundamental aspects related to the biosensor performance are studied, such as the optimum surface chemistry to enhance hybridization and detection, as well as the study of parameters affecting the electron transfer process between the ferrocene centers tethered to the DNA and the electrode surface. Finally, the use of other ferrocene modified dNTPs with different formal redox potentials are used in combination with $dA^{EFc}TP$ to demonstrate that is possible to directly measure the relative abundance of nucleotides in an unknown target sequence.

The thesis has been divided in the following chapters:

Chapter 1 reviews the state of the art on electrochemical DNA sensors. Sensor components including recognition elements and transducer materials are described as well as available methodologies used to immobilize nucleic acids on transducer materials. DNA biosensor technologies and detection strategies are broadly covered with special emphasis on those based on DNA hybridization. Finally, the chapter focuses on two relevant topics for this thesis: the use of redox labelled dNTPs to obtain labelled DNA amplicons and the different strategies available to generate ssDNA.

Chapter 2 describes the synthesis of $dA^{EFc}TP$ and studies its incorporation in a primer extension (PEX) experiment using tailed primers and a target sequence related to human papilloma virus 16 (HPV16) as a model. To maximize the hybridization of the PEX product on a gold electrode array and the subsequent electrochemical signal obtained, the surface chemistry of the capture probe vs backfiller is optimized. Additionally, the effect of $dA^{EFc}TP$:dATP ratio on the extension yield and the electrochemical signal obtained are explored.

Chapter 3 reports the development of a singleplex electrochemical DNA sensor for the detection of a toxic microalgae, *Karlodinium armiger*, in genomic DNA extracted from seawater samples, a method that was validated by qPCR. Additionally, the effect of $dA^{EFc}TP$:dATP ratio on the PCR amplification yield and the electrochemical sensitivity obtained are explored, as well as the stability of the electrode array.

Chapter 4 reports a duplex electrochemical DNA sensor for the detection of the causative agent of anthrax, *Bacillus anthracis*, in genomic DNA, a method that was also validated by qPCR. The duplex amplification in a single-pot reaction and duplex hybridization and detection in a single-electrode array are described. Additionally, the effect of the electrolyte composition and concentration on the electrochemical signal obtained are studied.

Chapter 5 explores the effect of electrolyte concentration and the initial electrode potential on the rate of heterogeneous electron transfer from ferrocene centers tethered to the DNA to the electrode surface. Additionally, electrode interfacial capacitance is also measured to determine the potential of zero charge (PZC) on the electrode. Both, rate of heterogeneous electron transfer and PZC obtained are employed to understand how electrolyte concentration and initial electrode potential influence the DNA monolayer structure.

Chapter 6 describes the synthesis of ferrocene, octamethylferrocene and ferrocenecarboxamide labelled dATP and dCTP in order to obtain redox labelled dNTPs with distinguishable electrochemical signals. The incorporation of both dATP and dCTP bearing ferrocene and ferrocenecarboxamide, respectively, in the same target sequence in a PEX experiment is performed to demonstrate the potential use of these labels for the direct electrochemical measurement of the relative ratios of nucleobases in an unknown sequence of DNA.

Chapter 7 summarizes the general conclusions of the thesis and the future perspectives and applications of the presented research.

CHAPTER 1

Introduction

INTRODUCTION

This chapter introduces the reader to basic concepts about biosensors and specifically about electrochemical nucleic-acid based sensors. Aspects such as: recognition element, transducer, DNA immobilization and amplification methods and different strategies to build a DNA sensor are reviewed and discussed. The chapter puts special emphasis on the use of redox labelled dNTPs as a method of labelling DNA as is one of the main goals of this thesis. Finally, the objectives of the thesis are outlined.

1.1 ELECTROCHEMICAL NUCLEIC-ACID BASED SENSORS

The detection of specific DNA sequences in a sample has applications in many fields including clinical diagnostics and disease monitoring[1–4], food analysis[5], forensics[6], bioterrorism[7] and environmental control[8]. Traditional analytical methods rely on time consuming protocols that require several steps, multiple reagents, expensive intrumentation and trained personnel, and are inherently restricted to laboratories. Biosensors[9] appeared during the last 4 decades as an alternative to laboratory based methods. They are portable devices ready to be used at the point-of-need, normally to detect only one or a small number of analytes, with analytical performances similar to laboratory based methods but in a quicker, simpler, more affordable, easier to manipulate format. Biosensors consist of 3 main blocks as depicted in Figure 1, a bioreceptor, a transducer, and a signal and data processing module[10]. The bioreceptor provides specificity to the target of interest. Bioreceptors include antibodies, enzymes, nucleic acids, a whole cell or a part of a living organism such as a tissue. The role of the transducer is to transform the biorecognition event into a measurable signal. Depending on the nature of the signal generated, transducer can be optical, piezoelectric, electrochemical or thermometric. Finally, the signal produced is processed and quantified by the processing module. Electrochemical nucleic acid based biosensors[11] are a specific type of biosensors that contain nucleic acids as a recognition element immobilized on the surface of a solid electrode that acts as an electrochemical transducer (see Figure 1.1). The complementary DNA base pairing described by Watson and Crick is the basis for the biorecognition process in this type of biosensors.

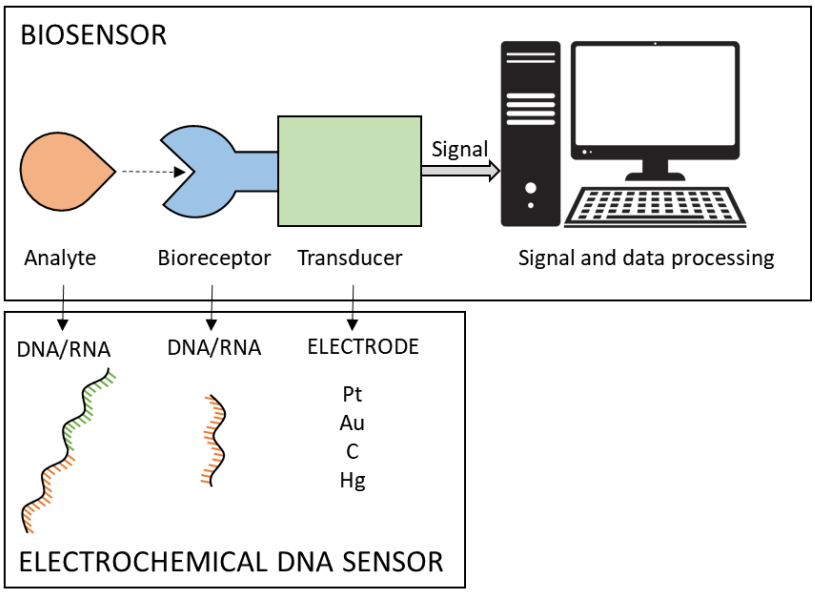

Figure 1.1. Biosensor scheme and components of an electrochemical nucleic acid-based sensor

1.2 BIORECOGNITION ELEMENTS

The nucleic acids used for DNA sensors can be classified mainly in two, regarding the kind of target they recognize:

a) Nucleic acids, when the binding is performed by hybridization to another nucleic acid target. This family includes DNA/RNA (that can be synthetic, chromosomal DNA, viral DNA or plasmids) and synthetic DNA mimics suchs as locked nucleic acids (LNA) or peptide nucleic acids (PNA) (Figure 1.2).

In LNA the the ribose sugar is modified, and it includes an extra methylene bridge that connect the 2' oxygen to the 4' carbon. The bridge locks the ribose in the 3'-endo (north) conformation which results in a significant increase of hybridization stability, resulting in an increase of the melting temperature of the DNA/LNA duplex. In PNA the ribose/desoxyribo sugar found in RNA/DNA respectively is substituted by a 2-aminoethylglycine linker. DNA-PNA duplexes are very influenced by a single-mismatch, which makes PNA probes particularly suited to detect single-base mismaches.

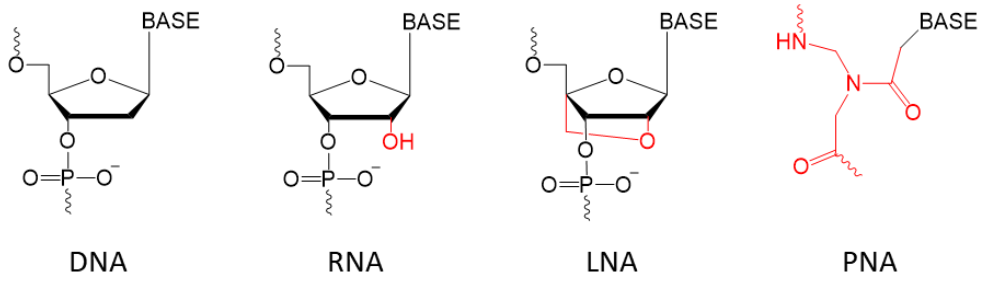

Figure 1.2. Chemical structure differences between DNA, RNA, LNA and PNA.

b) Nucleic acid aptamers. When the binding to the target (any class of proteins, peptides, drugs, toxins, small molecules, ions…) is performed by stacking, shape complementarity, electrostatics and hydrogen bonding interactions, rather than hybridization. Upon target recognition, aptamers often undergo a conformational change, forming a 3D complex in which the target contributes to the aptamer structure. Aptamers are single-stranded oligonucleotides (mainly DNA or RNA) selected from a random sequence library after many cycles of SELEX where the population of secuences with high affinity for the target is enriched in every cycle. Aptamers are also known as nucleic acid antibodies due to their similarities. Main advantages over antibodies include chemical synthesis, cost-effective production, high affinity and selectivity, high thermal stability, easy to tailor with functional groups. Figure 1.3 depicts the differences between nucleic acids and aptamers used as recognition elements.

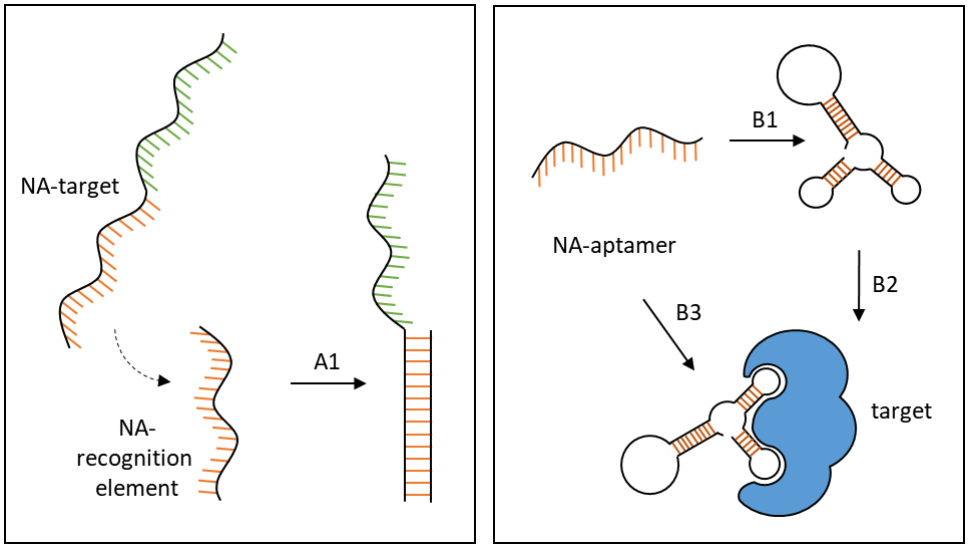

Figure 1.3. Distinction between nucleic acid (NA)-recognition elements used to hybridize (A1) complementary ssDNA/RNA strands vs NA-aptamers used to bind to other types of targets after the proper aptamer self-folding (B1-B2) or target induced folding (B3).

1.3 TRANSDUCERS

Traditionally, the transducers used in electrochemical nucleic acid biosensor preparation were bulky and made of carbon (glassy carbon, carbon paste, graphite, graphite-epoxy composite), gold, indium tin oxide (ITO) and solid mercury amalgams.

Recent developments allowed the fabrication of thin and thick film electrodes on insulator materials suitable for mass production, thus increasing the reproducibility while decreasing the cost. The most popular materials for thin electrodes are gold and carbon. Thin film electrodes can be prepared by thermal evaporation or sputtering of gold. Thick film electrodes are made basically by screen-printing technology, in with

the transducer material is suspended on a polymeric matrix, that is used as an ink to print the electrode design on the insulator material. The most common thick film electrode are screen-printed carbon electrodes (SPCE) but screen-printed gold electrodes (SPGE) are also available.
The chose of the transducer material depends on the electrochemical process that has to be interrogated. For redox processes that require very negative potentials, mercury is the material of choice due to the high hydrogen overpotential shown by this material. The working potential window for the rest of transducer materials is shifted aproximately 1V to a more positive potential as compared to mercury based electrodes. This characteristic makes mercury suitable to develop sensors based on the reduction of nucleobase residues, while the other materials, specially carbon, are more suited to study the oxidation of the nucleobase residues. More recently, nanomaterials such as gold and carbon nanoparticles (nano-onions, nanodiamonds, carbon nanotubes, graphene) have been used in transducers due to their unique electronic, mechanical and chemical properties to enhance the current signal.

1.4 NUCLEIC ACID IMMOBILIZATION STRATEGIES

The material of choice as transducer material influence the immobilization method option for capture probe attachment on the electrode surface. Different strategies available to immobilize capture probes on electrodes are depicted in Figure 1.4 and revised elsewhere[12].

NAs can be adsorbed on electrode materials by hydrophobic and/or electrostatic interactions between the NA and the surface of the electrode in a process called physisorption. Thin films of physisorbed material can be obtained by electrode immersion in a solution containing the NAs, or by evaporation of small volumes of the NA solution to dryness. Due to the interactions between the capture probe and the electrode surface, the availability and spatial orientation of the capture probes is not optimum, which leads to poor hybridization efficiencies.

A way to enhance the capture probe stability on the electrode surface is to use conducting polymer films. The films can be created via different processes including dropcasting and electropolymerization, a very interesting approach for the individual modification of electrodes in electrode arrays. Nevertheless, the entrapment of the NA within the polymeric film can decrease the conformational mobility of the capture probe, decreasing the hybridization ability, and can also hinder the diffusion of the target to the capture probe.

Another way to immobilize the capture probes is by affinity binding in which the electrode material is covalently modified with avidin or streptavidin and the capture probe is modified with biotin. The extremely strong (strept)avidin/biotin interaction provides an excellent stability of the capture probe on the surface, while providing conformational mobility.

Capture probe layers can also be obtained by the formation of self-assembled monolayers of thiolated capture probes on metals (silver, platinium, palladium, iron, mercury and gold). Capture probe can be immobilized with other thiolated molecules to form self organized monolayer films, minimizing the non-specific adsorption of other species on the electrode surface whilst retaining the conformation mobility of the capture probe.

Lastly, the capture probe can also be attached to the electrode surface by covalenty binding between a functional group on the capture probe and a suitable functional group on the surface of the substrate. Thiolated capture probe can be immobilized with maleimide moieties, whilst aminated capture probes can be linked to aldehyded, carboxylic acid or epoxy groups, to mention a few examples.

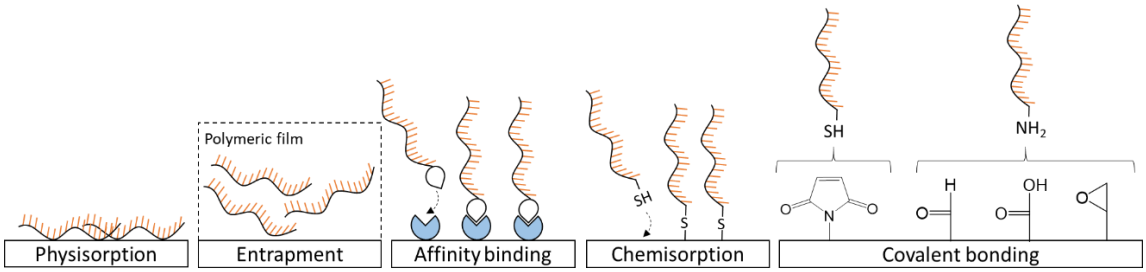

Figure 1.4 Capture probe immobilization strategies.

1.5 TYPES OF DNA-BIOSENSORS

DNA HYBRIDIZATION AND SEQUENCE SPECIFIC DNA SENSING

DNA hybridization sensors take advantage of the spontaneous hybridization that occurs between 2 complementary DNA strands. Normally, a sequence complementary to the target sequence, termed a capture probe, is immobilized on the electrode surface and used as a recognition sequence. In the presence of the complementary target, hybridization between the capture probe and the target takes places, forming the double stranded DNA (dsDNA) hybrid. The formation and stability of the dsDNA depends on the pH, temperature and ionic strength, which can be tuned to allow 0, 1 or multiple mismatches.

The hybridization event can be monitored using different strategies, as depicted in Figure 1.5:

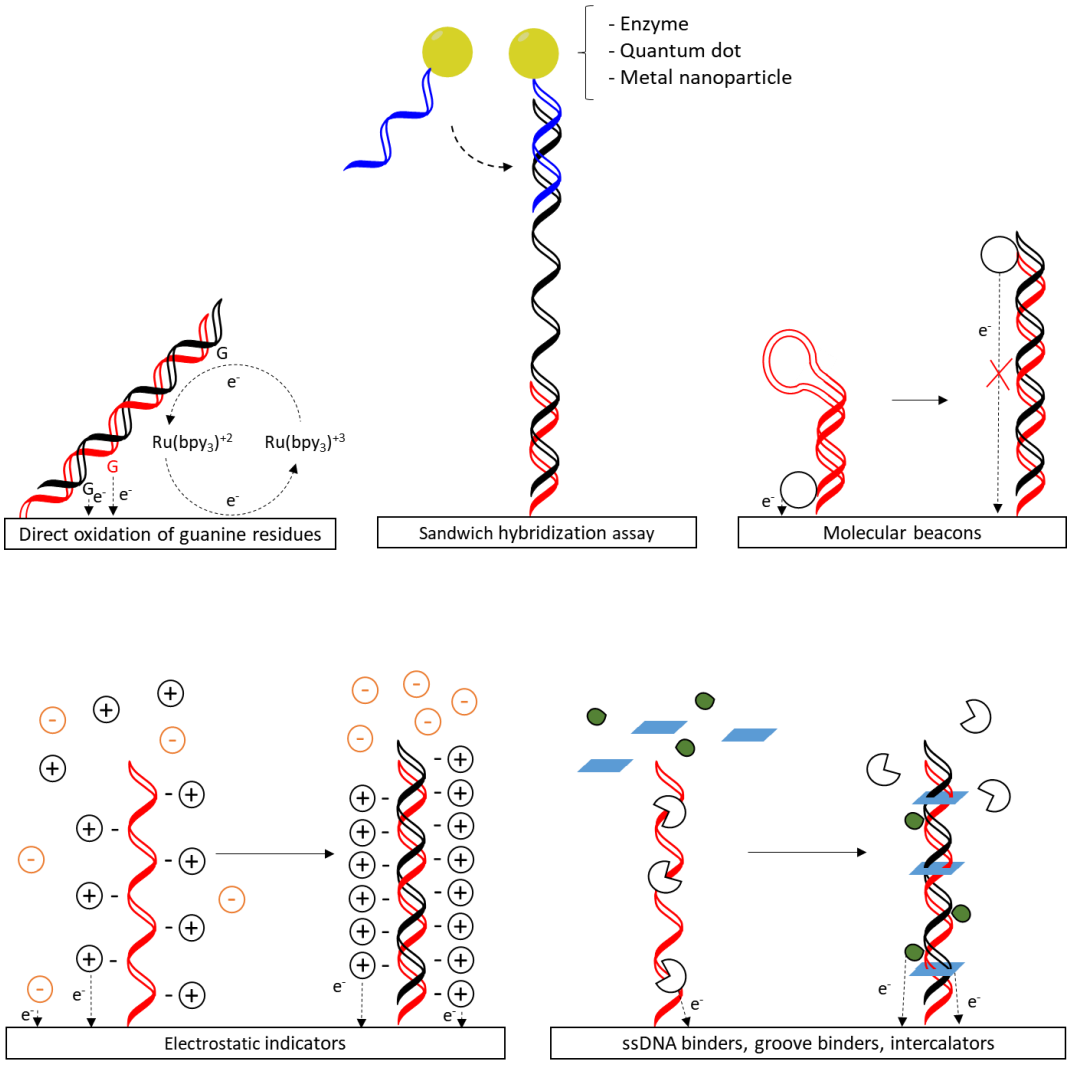

Figure 1.5. DNA sensors based on detection via hybridization.

a) Direct oxidation of guanine residues present in the DNA.

Guanine oxidation does not allow discrimination between the probe and target strands, and only the closest guanine residues to the electrode surface undergo oxidation, which is translated into low current intensities. To solve the problem of the distance from guanine to the electrode surface, redox mediator such as rhodium or ruthenium complexes can be used to shuttle the electrons from the distant guanine. Another problem with this method is the irreversible oxidation of the probes, which prevents the re-use of the recognition layer for further experiments.

b) Sandwich hybridization assay

In order to enhance the selectivity of the hybridization assay and to amplify the electrochemical signal a reporter probe can be used. This reporter probe typically consists of a NA sequence complementary to the target, but using a part of the target sequence different than that recognized by the capture probe. Labels covalently attached to reporter probes include redox active moieties, enzymes, metallic nanoparticles, or quantum dots. One single or multiple redox active moieties can be attached to the reporter probe to enhance the electrochemical signal. Enzymes are very advantageous because they catalyse the reaction of a electroactive substrate that accumulates with time, massively increasing the signal. Common enzymes used in NA based electrochemical sensors include alkaline phosphatase (ALP) and horseradish peroxidase (HRP). On the other hand, metallic and semiconductor nanoparticles can be detected by stripping voltammetry after dissolution of the particles in the appropriate solvent.

c) Molecular beacons

Capture probe can be designed to adopt a hairpin structure with the end of the oligonucleotide close to the electrode surface and bearing a reversible redox molecule, including ferrocene and methylene blue. In the absence of target, there is an oxidation peak due to the presence of the redox label close to the surface. Following target hybridization, the hairpin structure is destabilized, and the rigid dsDNA formed by the capture probe and the target moves the electroactive moiety away from the surface, resulting in a reduction in the electrochemical signal.

d) Electrostatic indicators

Positively and negatively charged redox molecules can accumulate or be repelled by an accumulation of negative charges provided by the phosphate backbone of the DNA immobilized on the electrode surface. The number of negative charges on the electrode surface increases following hybridization due to the acumulation of more negatively charged DNA. This creates an electrostatic barrier for negatively charged redox molecules such as hexacianofferrate (II/III) $[Fe(CN)_6]^{3-/4-}$ hindering its access to the electrode surface, thus decreasing the redox signal. The effect is the opposite for positively charged redox molecules such as ruthenium hexaamine (II/III) $[Ru(NH_3)_6]^{2+/2-}$ that accumulates on the surface following target hybridization, thus increasing the redox signal.

e) Indicators with binding preference for ssDNA, groove binders and intercalators.
Indicators such as phenothiazine or methylene blue preferentially bind to unpaired guanine residues, thus being specific for ssDNA molecules. After hybridization these indicators are displaced from the capture probe and moved away from the electrode surface, resulting in a decrease in electrochemical signal. Groove binders such as daunomycin and intercalators such as tris(2,2'-bipyridine)ruthenium(III) $[Ru(bpy)_3]^{3+}$ on the other hand, are able to recognize specific structural features of dsDNA which results in an accumulation of the indicator following hybridization, thus increasing the signal.

1.6 DIRECT LABELLING OF TARGET USING REDOX LABELLED DNTPs

The use of modified dNTPs to functionalize DNA is a concept that has been explored during the last decades. The possibilities are almost endless and include the addition of fluorescent[13], Raman[14], spin[15] or redox probes[16], the addition of moieties susceptible to attack by DNAzymes[17] or the addition of moieties that avoid restriction endonuclease mediated cleavage[18], the addition of reactive groups for cross coupling reactions[19], as well as the addition of groups that modulate transcription[20]. Among all the possibilities, the use of redox labels represents a very attractive idea for the development of electrochemical DNA sensors. The advantages include a) Following extension or amplification the amplicon obtained is ready to be electrochemically detected with no extra labelling steps, b) the incorporation of multiple redox labels per amplicon produces signal amplification and c) the redox labels can be selected to work in mild redox potentials compatible with most common transducer materials such as carbon and gold.

Wlassoff *et al*.[21] was the first visualizing in agarose gel electrophoresis the incorporation of dUTP modified with ferrocenecarboxamidopropenyl ($dU^{capFc}TP$) and ferroceneacetamidopropenyl ($dU^{aapFc}TP$) moieties in a primer extension (PEX) experiment using 100% of the ferrocene modified dUTP and Klenow(exo-). Surprisingly they discovered that a subtle difference of just one methylene group in the linker between the nucleotide and ferrocene, provoked an early PEX termination for $dU^{aapFc}TP$ but not for $dU^{capFc}TP$ when the template sequence had 2 consecutive A. Later, in 2008, Yeung *et al*.[22] used the same $dU^{capFc}TP$ to develop a real time solid phase electrochemical microchip demonstrating that the $dU^{capFc}TP$ is not only being incoporated into the DNA but still electrochemically active and measurable after the amplification.

It is known that the incorporation of modified nucleotides into DNA depends on many factors including the polymerase employed, the dNTPs used, the position of the modification, the sequence to extend or amplify, the linker and the bulkiness of the modification. Nevertheless, there are mechanistic and structural studies[23–29] demonstrating that the major groove direction on the complex of polymerase, primer and template has significant available free room, which enables efficient incorporation

of dNTPs, even those bearing bulky substituents if they are linked to position 5 of pyrimidines or position 7 of 7-deazapurines. However, it is still necessary to determine experimentally if a modified dNTP is a good substrate for incorporation in PEX/PCR experiment to a certain polymerase.

After Wlassof's and Yeung's experiments, a new generation of redox labeled dNTPs were reported, including aminophenyl and nitrophenyl[16], tetrathiafulvalene[30], $Ru(bpy)_3$ and $Co(bpy)_3$[31], anthraquinone[32], benzofurazane[33], azidophenyl[34], phenothiazine[35] and polyoxometalates (POMs)[36] among others (Figure 1.6). The addition of diverse redox molecules to different nucleotides facilitates their electrochemical discrimination, which is of particular interest in electrochemical sequencing and the electrochemical detection of single nucleotide polymorphisms (SNPs).

A visual comparison of the redox potentials of the reported redox labels and the intrinsic redox peaks of nucleobases residues in DNA can be seen in Figure 1.7.

The new generation of redox labels were coupled directly to base of the dNTPs or through an ethynyl linker. Direct linking was achieved using the Suzuki-Miyaura cross-coupling reaction between the halogenated dNTPs and the boronic acid modified redox label. Redox labeling via an ethynyl linker was achieved using the Palladium-catalyzed Sonogashira cross-coupling reactions between the halogenated dNTPs and the ethynyl modified redox labels. Both reactions are single-step, aqueous-phase, straightforward and result in satisfactory reaction yields.

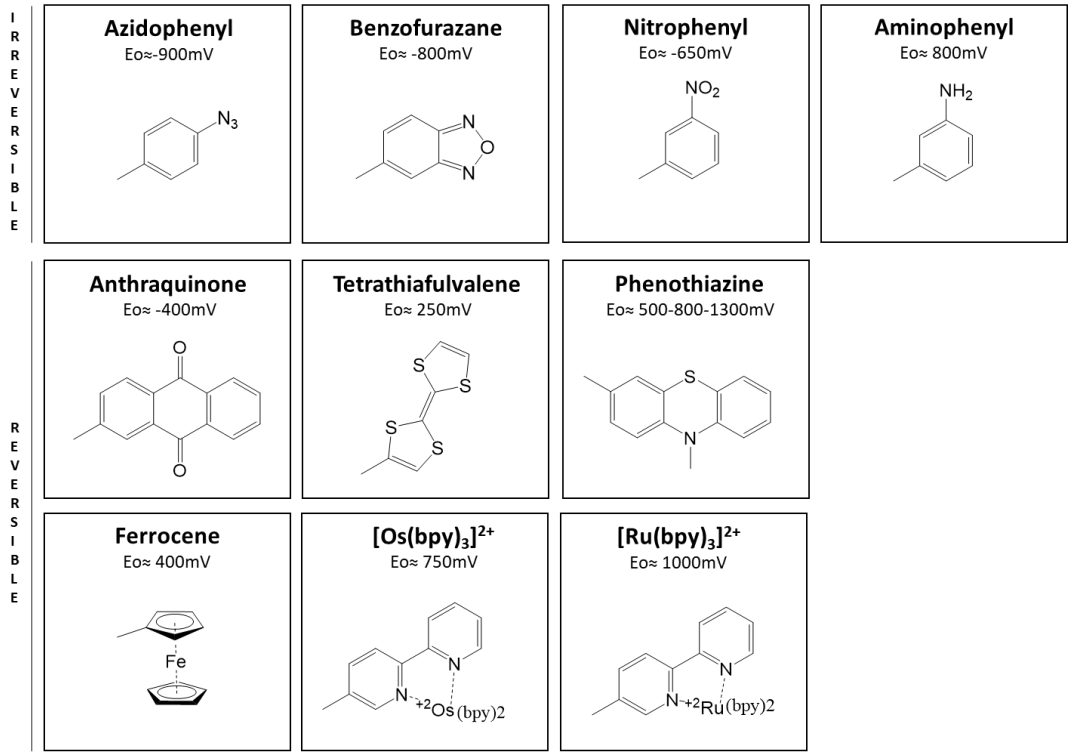

Figure 1.6. Reported redox labels linked to dNTPs with their respective standard potentials.

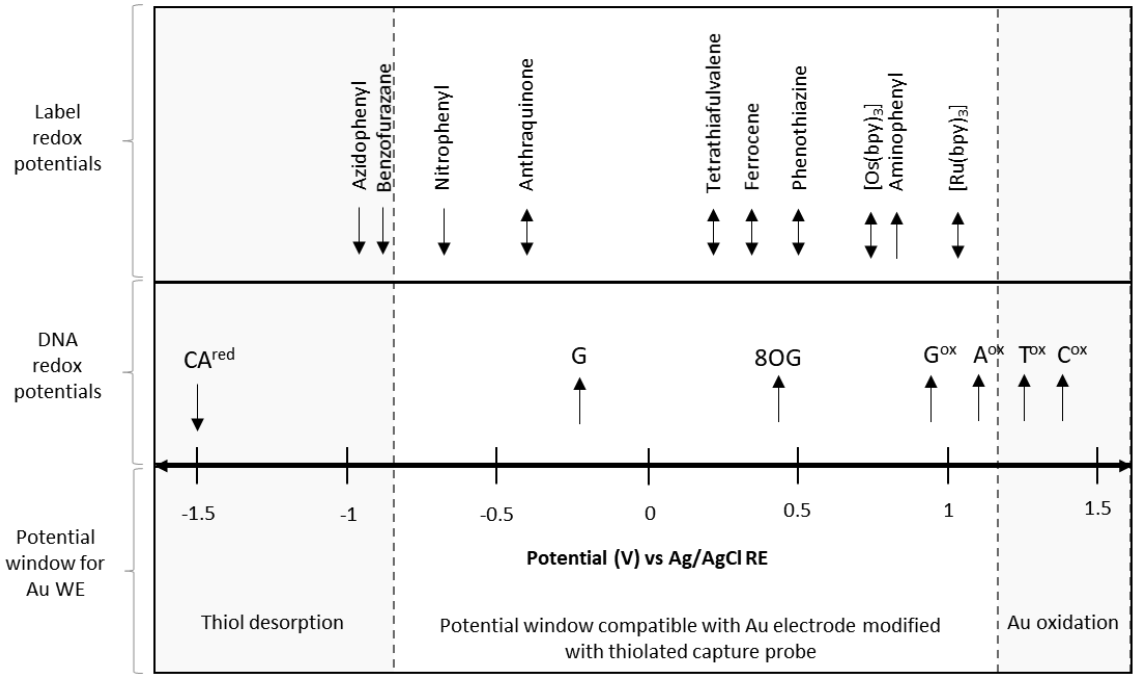

Figure 1.7. Scheme of redox potentials observed for DNA and some electroactive species used to label dNTPs. ↑ represents a non-reversible oxidation peak, ↓ represents a non-reversible reduction peak and ↕ represents reversible redox peaks. DNA redox peaks are obtained at mercury/amalgam electrode for negative potentials and at carbon electrodes for positive potentials. CA: reduction of cytosine and adenine, G: re-oxidation of an electrochemically generated reduction product of guanine, G^{ox}, A^{ox}, T^{ox}, C^{ox}: oxidation of guanine, adenine, thymine and cytosine, 8-OG: oxidation of a common DNA damage marker, 8-oxoguanine. All synthetized nucleotides were incorporated in a PEX where the natural dNTP was 100% replaced by the modified dNTP, demonstrating the ability of the polymerases tested to incorporate them. The linkers used in each of the redox labelled dNTPs, the electron transfer of the redox label, its reversibility, interactions with DNA and polymerases tested among other experimental details is summarized in Table 1.1

Table 1.1. Reported redox labels linked to dNTPs and main characteristics.

Redox label	Linker to the nucleotide	Electrons transfered	Reversible?	DNA Intercalator	Polymerases tested	PEX and/or PCR	Modified bases	Ratio modified dNTP:dNTP	Comments	Ref
Aminophenyl	Direct	-	no	no	Klenow(exo-) DyNAzyme	PEX	A,T,C	100%		[16]
Nitrophenyl	Direct	4	no	no	Klenow(exo-) DyNAzyme	PEX	A,T,C	100%	Intense cathodic peak	[16]
Benzofurazane	Direct	6	no	no	Pwo KODXL	PEX	A,T,C	100%	Very intense cathodic peak	[33]
Phenothiazine	Direct Ethynyl	1 + 1	1, yes 1, no	yes	KOD XL Vent(exo-) PWO	PEX PCR	C,A	100% PEX 50% PCR	Not good PCR substrate	[35]
Anthraquinone	Ethynyl	2	yes	yes	KOD XL	PEX	C,A	100%	Reversible	[32]
Tetrathiafulvalene	Ethynyl	1 1	yes	No	Klenow, Vent(exo-), Pwo, Dynazyme Klenow(exo-)	PEX	C,T,G,A	100%	Problems to incorporate 2 consecutive labels. Weak redox signal	[30]
Azidophenyl	Direct	2	no	No	KOD XL, Pwo, Vent(exo-)	PEX	C,A	100%	Can be clicked with other moieties after incorporation in DNA but this increases number of steps.	[34]
$[Ru(bpy)_3]^{+2}$	Ethynyl	1	yes	yes	Klenow(exo-), Vent(exo-), DyNAzyme, Pwo		C,T,G,A	100%	Very bulky, PEX termination when 2 consecutive incorporations	[31]
$[Os(bpy)_3]^{+2}$	Ethynyl	1	yes	yes	Klenow(exo-), DyNAzyme		C,T,G,A	100%	Very bulky, PEX termination when 2 consecutive incorporations	[31]
Ferrocene	Ethynyl Carboxamido-propenyl Acetamido-propenyl	1	yes	no	Klenow(exo-), T4 Tth KODXL Dynazyme	PEX PCR	A,T	20-100%	Incorporation dependant on linker	[21,37–39]

Pavel *et al*.,[40] demonstrated with a novel methodology that 7-Aryl-7-deazaadenine 2'-deoxyribonucleoside triphosphates are, in general, better substrates than natural dATP in competitive incorporations for most of the polymerases they tested, including KODXL, Taq, Vent (exo-), Klenow (exo-), and *Bst*. They also demonstrated that *Bst* polymerase is able to incorporate modified dATP with bulky functional groups including ethynyl and phenyl derivatives, redox labels such as nitrophenyl and aminophenyl, fluorescent labels and reactive groups, but the polymerase failed to incorporate very bulky groups such as (4-Triphenylmethylsulfanyl)phenyl dNTPs. Interestingly, they observed that the same polymerases were able to incorporate the same dCTPs modified with the same moieties, but they were similar or worse substrates than natural dCTP. To explain the higher affinity of the 7-aryl $dA^{X}TPs$ to the active site of polymerases, they performed molecular modelling studies comparing dATP and $dA^{Ph}TP$ docked with the complex *Bst* polymerase, primer and template. They found a larger affinity for $dA^{Ph}TP$ over dATP probably due to π-π stacking occuring between the phenyl group in the $dA^{Ph}TP$ that was filling the space between the aliphatic chain of Arg629 and the phenyl group of Phe710 in the polymerase, a phenomena extrapolatable to other 7-aryl-7-deaza-dATP analogues.

Hana *et al*.,[41] further discovered that 7-deazapurine dNTPs with π-electron substituents (vinyl, ethynyl and phenyl) are generally better than the natural counterparts (dATP and dGTP) for *Bst* and KOD XL polymerases, but on the other hand, the 5-substituted dCTP was comparable to the natural dCTP and the 5-substituted dTTP was worse than the natural counterpart. They also found that Pwo and Vent(exo-) could incoporate the modified dNTPs, but they preferred the natural dNTPs over the modified one.

Amongst the electrochemical redox labels reported for modified dNTPs, ferrocene stands out due to some specific properties: a) It is one of the most stable organometallic compounds that has been very well studied, it is a cheap and available substrate as well as being easy to functionalize and crosslink[39]. b) It has reversible redox peaks which facilitates multiple measurements, if required. This feature makes ferrocene compatible with cyclic voltammetry measurements and therefore useful to obtain kinetic data such as the electron transfer coefficients[42]. c) Additionally, ferrocene can be measured in very mild potentials (typically $E_{1/2}$ between 300-400mV vs Ag/AgCl) which makes it compatible with the most common electrode materials used in electrochemical sensors. d) If required, the ferrocene redox potential can be tuned towards more positive or more negative potentials by: i) modifying the link between the ferrocene and the nucleotide[21] (e.g..from 398mV using a carboxamidopropenyl-1 linker vs 260mV using a acetamidopropenyl-1 linker), ii) conjugate the ferrocene to the base in the nucleotide through an ethynyl linker[37] (e.g.. from 450mV for ethynylferrocene dATP vs 415mV for ethynylferrocene dUTP), or iii) by modifying the cyclopendiene rings in the ferrocene with electron donor[43] or electron withdrawing[44] functional groups.

1.7 PRIMER EXTENSION BASED METHOD

An alternative strategy to detect target hybridization is via primer extension of the 3'-end of short oligos (primers) hybridized to a longer oligo sequence (target) using the long oligo as a template. Introducing labelled dNTPs in the process, is possible to labeled the extended oligo with redox active tags, or with other tags than can be used for detection (Figure 1.8).

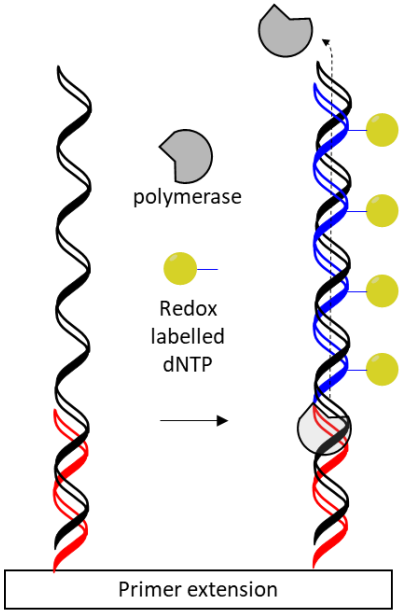

Figure 1.8. Primer extension (PEX) scheme in the presence of labelled dNTPs after hybridization with a single stranded complementary DNA target.

1.8 DETECTION OF MUTATION AND SINGLE NUCLEOTIDE POLYMORPHISMS

The detection of mutations (alterations in the nucleotide sequence that provoke pathogenesis and disease) and single nucleotide polymorphisms (harmless single point mutations that can be used for fingerprinting) can also be detected via hybridization by different strategies as depicted in Figure 1.9.

Hybridization stringency conditions (elevated temperature, low ionic strenght, or using PNA instead of DNA probes) can be applied to avoid hybridization unless the capture probe and target sequence match perfectly.

Less stringent conditions can be used to allow hybridization of the target even in the presence of a single base mismatch. The presence of the mismatch can be monitored by the ability of the duplex formed to mediate the electron transfer between a redox DNA intercalator covalently attached to the end of the capture probe. The disruption of the π stacking provoked by the mismatch, interrupt the electron transfer mediated by the dsDNA, reducing the redox signal.

Another strategy consists of the primer extension of the capture probe hybridized with the target that contains the SNP in the next upstream nucleobase. Four parallel PEX reaction can be performed including only 1 modified dNTP per reaction. Under the proper conditions, only when the base is complementary to the first free position of the target will be incorporated, and further detected, identifying the exact SNP at that position.

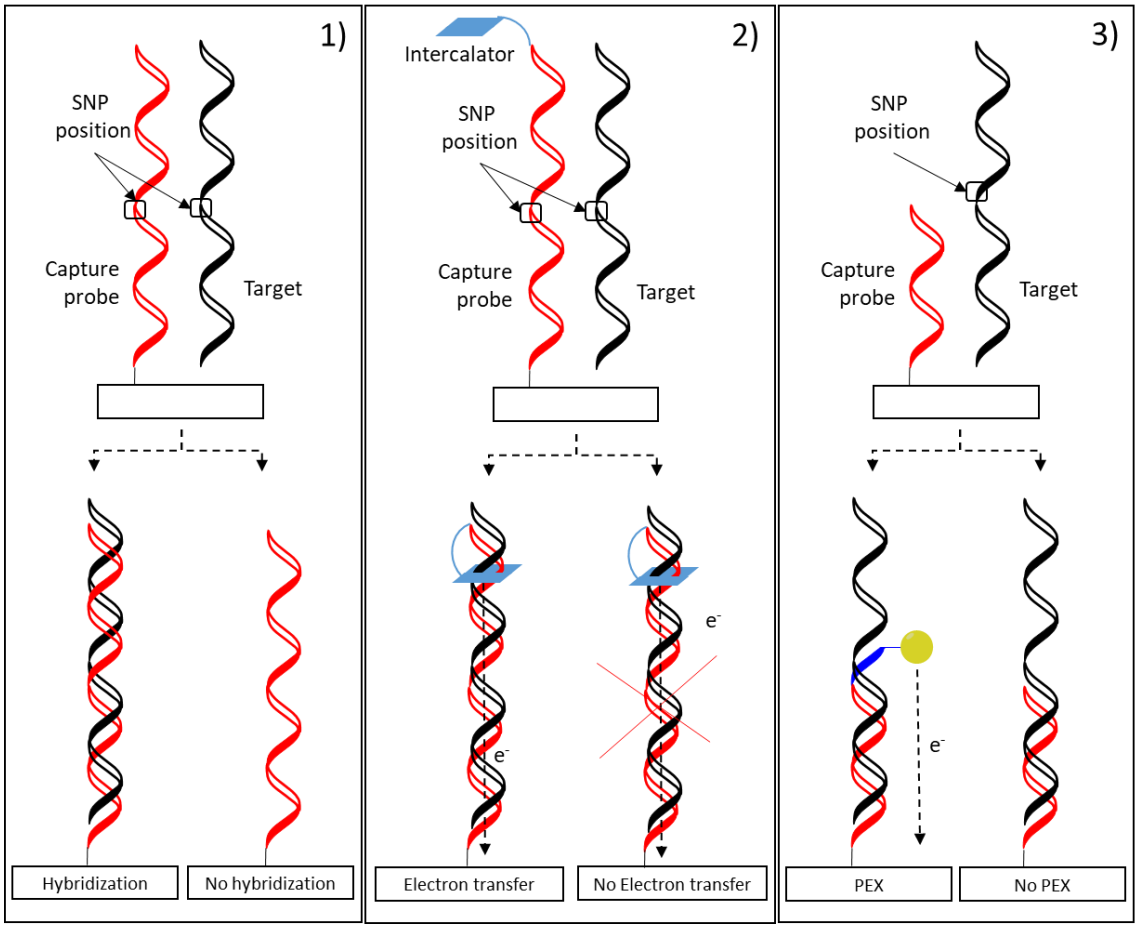

Figure 1.9. Strategies to detect mutations and SNPs in hybridization based DNA sensors. 1) Hybridization performed in high stringency, 2) using a capture probe modified covalently with a redox probe and c) PEX with a single redox tagged dNTP.

1.9 DNA AMPLIFICATION METHODS

The human genome has 3 billion base pairs. Trying to detect a target DNA sequence that is at maximum hundreds of base-pairs within the length of the genome, that is present in few copy numbers and additionally is surrounded by a complex biological matrix, is a very challenging task. Normally, it is required to purify the genomic material to get rid of the matrix, and then enrichthe target via target amplification prior to detection. Kary Mullis, back in 1983, isolated Taq polymerase, a thermophilic enzyme able to withstand high temperatures, whilst still having adequate activity at low temperatures, facilitating exponential *in vitro* amplification of a specific DNA target sequence in a easy, rapid and cost-effective way.

Polymerase chain reaction (PCR)

The polymerase chain reaction is a protocol consisting of the cyclic repetition of 3 steps (1. thermal denaturation, 2. annealing and 3. elongation, Figure 1.10) in order to achieve an exponential amplification of a target DNA sequence. The method requires the use of deoxynucleotides (dNTPs) as DNA building blocks, primers (short oligonucleotides) to define the DNA region to be amplified, and a thermostable polymerase enzyme that elongates the primers using the target as a template.

In the thermal denaturation step the sample is heated to 90-95ºC to denature and separate the two original strands of the target DNA. In the annealing step, the temperature is decreased to approximately 5ºC below the melting temperature of the primers (typically 55-60ºC) in order to allow primer-template hybridization while having enough stringency to avoid non-specific hybridization events. Finally, in the elongation step, the temperature is increased to the optimum working temperature of the polymerase which extends the 3' end of the primer and synthesizes the complementary strand to the template target. After one cycle, the number of DNA copies is multiplied by 2. Therefore, after n cycles, the number of copies is multiplied by 2^n. Taking into account that the time required per cycle oscillates between 1-3 minutes, it is possible to obtain millions of copies from 1 single DNA copy in less than 1h.

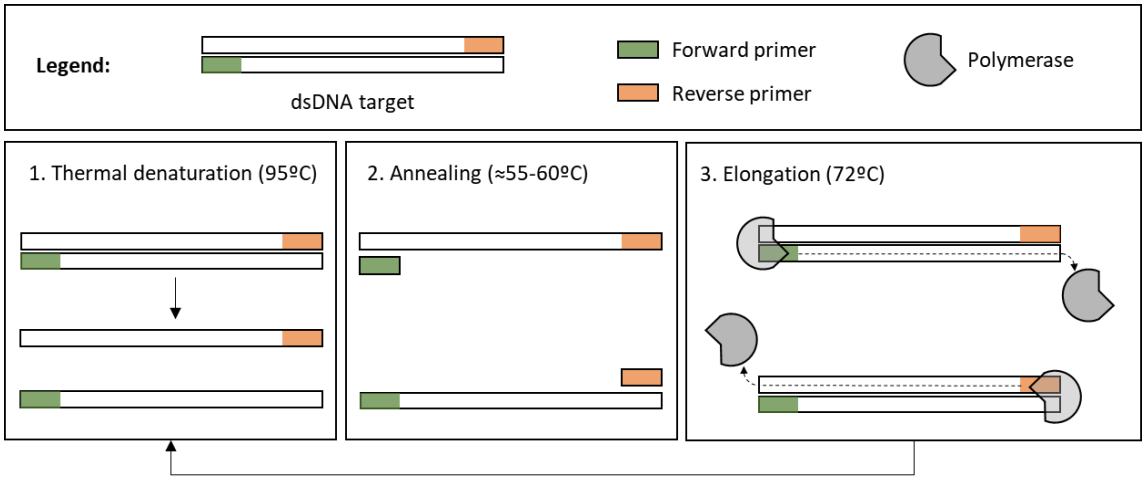

Figure 1.10. PCR amplification mechanism.

1.10 METHODS FOR GENERATION OF SINGLE STRANDED DNA (ssDNA)

Following amplification, the majority of electrochemical genosensors require the generation of single stranded DNA (ssDNA) from the PCR product for further detection via hybridization to a specifically designed and immobilized capture oligonucleotide probe. This can be achieved by different methodologies, as depicted in Figure 1.11, including:

a) Thermal denaturation and rapid cooling. Heating above 95ºC induces DNA denaturation and ssDNA generation, and a rapid cooling on ice can prevent the complete re-hybridization of all the denatured DNA leaving a few free strands for further hybridization. Whilst the method is simple, the reproducibility is poor and the amount of ssDNA generated is limited[58].

> **Thermal/basic denaturation coupled with magnetoseparation.** An alternative method is based on the use of biotinylated forward or reverse primer (not both) in the PCR mixture in order to obtain biotinylated amplicons. Following PCR, biotinylated amplicons can be captured by streptavidin coated magnetic beads and ssDNA released by thermal/pH denaturation. To prevent re-hybrisation of the released ssDNA, the complementary strand bounded to the magnetic bead is removed from the solution by magnetoseparation. This strategy however consists of several steps and it is not convenient for the development of a POC biosensor.

b) Enzymatic digestion. An attractive alternative is the selective enzymatic digestion of one of the DNA strands using, for example, T7 or lambda exonuclease and a phosphorothioate labelled forward primer. The modification on the primer prevents the digestion of the strand and following incubation it is possible to generate large amounts of ssDNA. This methodology produces large amounts of ssDNA and is often used in SELEX methodologies, but it has too many steps to be considered useful for biosensor applications [59].

c) Asymmetric nucleic acid amplification. A very simple and straightforward way to generate ssDNA is to use different amounts of primers in the amplification mixture. Following the completion of *x* number of amplification cycles, one of the primers is completely consumed and in the following cycles only the other primer will be extended, thus generating ssDNA.

d) Use of tailed primers. An alternative strategy reported recently takes advantage of the use of tailed primers, which consist of primers modified at the 5'- end with a single

stranded DNA sequence ("tail") that is used for hybridization. The tail is separated from the primer using a 3-C alkyl chain spacer to prevent the elongation of the tail during amplification[60–64]. This strategy does not generate ssDNA, but produces amplicons that bear a ssDNA tail that can be used for hybridization. Therefore the capture probe is designed to hybridize to the tail, and the primer sequence to be specific for the desired target. Using this methodology, 100% of the amplicons can be detected via hybridization.

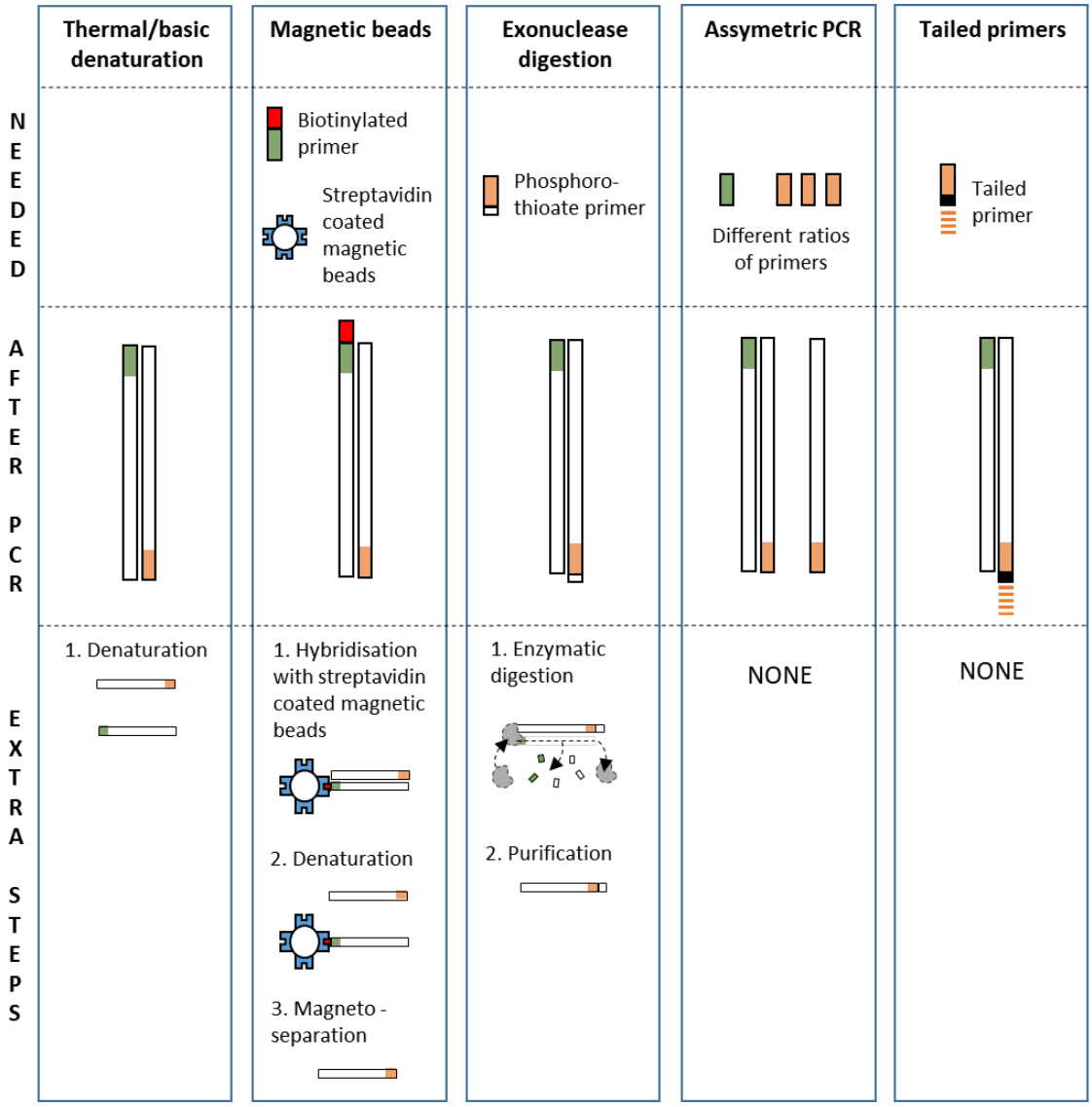

Figure 1.11. Strategies to generate ssDNA from dsDNA. Extra reagents required for the strategy, amplicons obtained after PCR amplification and extra steps needed afterwards to generate ssDNA.

1.11 OBJECTIVES

The general objective of this doctoral thesis is the development of generic, simple and sensitive electrochemical genosensors based on the incorporation of ethynyl ferrocene labelled dATP (dA^{EFc}TP) and tailed primers for the detection of genomic DNA.

To achieve this goal, the following specific objectives have been defined:

- To demonstrate that dA^{EFc}TP can be incorporated in primer extension experiments using a long 100bp DNA target.
- To apply dA^{EFc}TP in combination with tailed primers in a genosensor for the singleplex detection of the toxic microalgae, *Karlodinium armiger* in seawater samples.
- To further explore the capabilities of the previous method to develop a duplex electrochemical genosensor for the detection of *Bacillus anthracis* genomic DNA.
- To study and understand the electron transfer process between the incorporated dA^{EFc}TP and the electrode surface.
- To explore the use of dA^{EFc}TP in combination with other redox labelled dNTPs to determine the relative abundance of nucleotides in an unknown target DNA sequence.

1.12 REFERENCES

(1) Malhotra, B. D.; Chaubey, A. Biosensors for Clinical Diagnostics Industry. *Sensors Actuators, B Chem.* **2003**, *91* (1–3), 117–127. https://doi.org/10.1016/S0925-4005(03)00075-3.

(2) Bora, U. Nucleic Acid Based Biosensors for Clinical Applications. *Biosens. J.* **2013**, *2* (1), 1–8. https://doi.org/10.4172/2090-4967.1000104.

(3) D'Orazio, P. Biosensors in Clinical Chemistry. *Clin. Chim. Acta* **2003**, *334* (1–2), 41–69. https://doi.org/10.1016/S0009-8981(03)00241-9.

(4) Janegitz, B. C.; Cancino, J.; Zucolotto, V. Disposable Biosensors for Clinical Diagnosis. *J. Nanosci. Nanotechnol.* **2014**, *14* (1), 378–389. https://doi.org/10.1166/jnn.2014.9234.

(5) Martín-Fernández, B.; Manzanares-Palenzuela, C. L.; Sánchez-Paniagua López, M.; de-los-Santos-Álvarez, N.; López-Ruiz, B. Electrochemical Genosensors in Food Safety Assessment. *Crit. Rev. Food Sci. Nutr.* **2017**, *57* (13), 2758–2774. https://doi.org/10.1080/10408398.2015.1067597.

(6) Yáñez-Sedeño, P.; Agüí, L.; Villalonga, R.; Pingarrón, J. M. Biosensors in Forensic Analysis. A Review. *Anal. Chim. Acta* **2014**, *823*, 1–19. https://doi.org/10.1016/j.aca.2014.03.011.

(7) Nikoleli, G.; Karapetis, S. Biosensors for Security and Bioterrorism Applications. *Biosens. Secur. Bioterrorism Appl.* **2016**, No. March, 431–442. https://doi.org/10.1007/978-3-319-28926-7.

(8) Palchetti, I.; Mascini, M. Nucleic Acid Biosensors for Environmental Pollution Monitoring. *Analyst* **2008**, *133* (7), 846–854. https://doi.org/10.1039/b802920m.

(9) Thévenot, D. R.; Toth, K.; Durst, R. A.; Wilson, G. S. Electrochemical Biosensors: Recommended Definitions and Classification. *Pure Appl. Chem.* **1999**, *71* (12), 2333–2348.

(10) Bhalla, N.; Jolly, P.; Formisano, N.; Estrela, P. Introduction to Biosensors. **2016**, No. June, 1–8. https://doi.org/10.1042/EBC20150001.

(11) Labuda, J.; Oliveira Brett, A. M.; Evtugyn, G.; Fojta, M.; Mascini, M.; Ozsoz, M.; Palchetti, I.; Paleček, E.; Wang, J. Electrochemical Nucleic Acid-Based Biosensors: Concepts, Terms, and Methodology (IUPAC Technical Report). *Pure Appl. Chem.* **2010**, *82* (5), 1161–1187. https://doi.org/10.1351/PAC-REP-09-08-16.

(12) Rashid, J. I. A.; Yusof, N. A. The Strategies of DNA Immobilization and Hybridization Detection Mechanism in the Construction of Electrochemical DNA Sensor: A Review. *Sens. Bio-Sensing Res.* **2017**, *16* (October), 19–31. https://doi.org/10.1016/j.sbsr.2017.09.001.

(13) Dziuba, D.; Jurkiewicz, P.; Cebecauer, M.; Hof, M.; Hocek, M. A Rotational BODIPY Nucleotide: An Environment-Sensitive Fluorescence-Lifetime Probe for DNA Interactions and Applications in Live-Cell Microscopy. *Angew. Chemie - Int. Ed.* **2016**, *55* (1), 174–178. https://doi.org/10.1002/anie.201507922.

(14) Manley, G. DNA Sequencing by Synthesis Using 3'-O-Azidomethyl Nucleotide Reversible Terminators and Surface-Enhanced Raman Spectroscopic Detection. *RSC Adv.* **2014**, *1* (2), 49342–49346. https://doi.org/10.1039/C4RA08398A.

(15) Obeid, S.; Yulikov, M.; Jeschke, G.; Marx, A. Enzymatic Synthesis of Multiple Spin-Labeled DNA. *Angew. Chemie - Int. Ed.* **2008**, *47* (36), 6782–6785.

https://doi.org/10.1002/anie.200802314.

(16) Cahová, H.; Havran, L.; Brázdilová, P.; Pivoňková, H.; Pohl, R.; Fojta, M.; Hocek, M. Aminophenyl- and Nitrophenyl-Labeled Nucleoside Triphosphates: Synthesis, Enzymatic Incorporation, and Electrochemical Detection. *Angew. Chemie - Int. Ed.* **2008**, *47* (11), 2059–2062. https://doi.org/10.1002/anie.200705088.

(17) Hollenstein, M.; Hipolito, C. J.; Lam, C. H.; Perrin, D. M. A Self-Cleaving DNA Enzyme Modified with Amines, Guanidines and Imidazoles Operates Independently of Divalent Metal Cations (M2+). *Nucleic Acids Res.* **2009**, *37* (5), 1638–1649. https://doi.org/10.1093/nar/gkn1070.

(18) Macíčková-Cahovthoma, H.; Hocek, M. Cleavage of Adenine-Modified Functionalized DNA by Type II Restriction Endonucleases. *Nucleic Acids Res.* **2009**, *37* (22), 7612–7622. https://doi.org/10.1093/nar/gkp845.

(19) Dadová, J.; Orság, P.; Pohl, R.; Brázdová, M.; Fojta, M.; Hocek, M. Vinylsulfonamide and Acrylamide Modification of DNA for Cross-Linking with Proteins. *Angew. Chemie - Int. Ed.* **2013**, *52* (40), 10515–10518. https://doi.org/10.1002/anie.201303577.

(20) Kielkowski, P.; MacÍčková-Cahová, H.; Pohl, R.; Hocek, M. Transient and Switchable (Triethylsilyl)ethynyl Protection of DNA against Cleavage by Restriction Endonucleases. *Angew. Chemie - Int. Ed.* **2011**, *50* (37), 8727–8730. https://doi.org/10.1002/anie.201102898.

(21) Wlassoff, W. A.; King, G. C. Ferrocene Conjugates of dUTP for Enzymatic Redox Labelling of DNA. *Nucleic Acids Res.* **2002**, *30* (12), e58. https://doi.org/e58\r10.1093/nar/gnf058.

(22) Yeung, S. S. W.; Lee, T. M. H.; Hsing, I. Electrochemistry-Based Real-Time PCR on a Microchip. **2008**, *80* (2), 363–368.

(23) Faloona, B. K. B. . M. and F. A. . Specific synthesis of DNA in vitro cia a polymerase-catalyzed chain reaction. *Methods* **1987**, *155*, 335–350.

(24) Bergen, K.; Steck, A. L.; Strütt, S.; Baccaro, A.; Welte, W.; Diederichs, K.; Marx, A. Structures of KlenTaq DNA Polymerase Caught While Incorporating C5-Modified Pyrimidine and C7-Modified 7-Deazapurine Nucleoside Triphosphates. *J. Am. Chem. Soc.* **2012**, *134* (29), 11840–11843. https://doi.org/10.1021/ja3017889.

(25) Obeid, S.; Bußkamp, H.; Welte, W.; Diederichs, K.; Marx, A. Snapshot of a DNA Polymerase While Incorporating Two Consecutive C5-Modified Nucleotides. *J. Am. Chem. Soc.* **2013**, *135* (42), 15667–15669. https://doi.org/10.1021/ja405346s.

(26) Obeid, S.; Bußkamp, H.; Welte, W.; Diederichs, K.; Marx, A. Interactions of Non-Polar And “click-Able” nucleotides in the Confines of a DNA Polymerase Active Site. *Chem. Commun.* **2012**, *48* (67), 8320–8322. https://doi.org/10.1039/c2cc34181f.

(27) Betz, K.; Streckenbach, F.; Schnur, A.; Exner, T.; Welte, W.; Diederichs, K.; Marx, A. Structures of DNA Polymerases Caught Processing Size-Augmented Nucleotide Probes. *Angew. Chemie - Int. Ed.* **2010**, *49* (30), 5181–5184. https://doi.org/10.1002/anie.200905724.

(28) Bergen, K.; Betz, K.; Welte, W.; Diederichs, K.; Marx, A. Structures of KOD and 9°N DNA Polymerases Complexed with Primer Template Duplex. *ChemBioChem* **2013**, *14* (9), 1058–1062. https://doi.org/10.1002/cbic.201300175.

(29) Obeid, S.; Baccaro, A.; Welte, W.; Diederichs, K.; Marx, A. Structural Basis for the

Synthesis of Nucleobase Modified DNA by Thermus Aquaticus DNA Polymerase. *Proc. Natl. Acad. Sci. U. S. A.* **2010**, *107* (50), 21327–21331. https://doi.org/10.1073/pnas.1013804107.

(30) Riedl, J.; Horáková, P.; Šebest, P.; Pohl, R.; Havran, L.; Fojta, M.; Hocek, M. Tetrathiafulvalene-Labelled Nucleosides and Nucleoside Triphosphates: Synthesis, Electrochemistry and the Scope of Their Polymerase Incorporation into DNA. *European J. Org. Chem.* **2009**, No. 21, 3519–3525. https://doi.org/10.1002/ejoc200900392.

(31) Vrábel, M.; Horáková, P.; Pivoňkovás, H.; Kalachova, L.; Černocká, H.; Cahová, H.; Pohl, R.; Šebest, P.; Havran, L.; Hocek, M.; et al. Base-Modified DNA Labeled by [Ru(bpy)3]2+ and [Os(bpy)3]2+ Complexes: Construction by Polymerase Incorporation of Modified Nucleoside Triphosphates, Electrochemical and Luminescent Properties, and Applications. *Chem. - A Eur. J.* **2009**, *15* (5), 1144–1154. https://doi.org/10.1002/chem.200801538.

(32) Balintová, J.; Pohl, R.; Horáková, P.; Vidláková, P.; Havran, L.; Fojta, M.; Hocek, M. Anthraquinone as a Redox Label for DNA: Synthesis, Enzymatic Incorporation, and Electrochemistry of Anthraquinone-Modified Nucleosides, Nucleotides, and DNA. *Chem. - A Eur. J.* **2011**, *17* (50), 14063–14073. https://doi.org/10.1002/chem.201101883.

(33) Balintová, J.; Plucnara, M.; Vidláková, P.; Pohl, R.; Havran, L.; Fojta, M.; Hocek, M. Benzofurazane as a New Redox Label for Electrochemical Detection of DNA: Towards Multipotential Redox Coding of DNA Bases. *Chem. - A Eur. J.* **2013**, *19* (38), 12720–12731. https://doi.org/10.1002/chem.201301868.

(34) Balintová, J.; Špaček, J.; Pohl, R.; Brázdová, M.; Havran, L.; Fojta, M.; Hocek, M. Azidophenyl as a Click-Transformable Redox Label of DNA Suitable for Electrochemical Detection of DNA-Protein Interactions. *Chem. Sci.* **2015**, *6* (1), 575–587. https://doi.org/10.1039/c4sc01906g.

(35) Simonova, A.; Havran, L.; Pohl, R.; Fojta, M.; Hocek, M. Phenothiazine-Linked Nucleosides and Nucleotides for Redox Labelling of DNA. *Org. Biomol. Chem.* **2017**, *15* (33), 6984–6996. https://doi.org/10.1039/c7ob01439b.

(36) Ortiz, M.; Debela, A. M.; Svobodova, M.; Thorimbert, S.; Lesage, D.; Cole, R. B.; Hasenknopf, B.; O'Sullivan, C. K. PCR Incorporation of Polyoxometalate Modified Deoxynucleotide Triphosphates and Their Application in Molecular Electrochemical Sensing of Yersinia Pestis. *Chem. - A Eur. J.* **2017**, *23*, 10597–10603. https://doi.org/10.1002/chem.201701295.

(37) Brázdilová, P.; Vrábel, M.; Pohl, R.; Pivoňková, H.; Havran, L.; Hocek, M.; Fojta, M. Ferrocenylethynyl Derivatives of Nucleoside Triphosphates: Synthesis, Incorporation, Electrochemistry, and Bioanalytical Applications. *Chem. - A Eur. J.* **2007**, *13*, 9527–9533. https://doi.org/10.1002/chem.200701249.

(38) Magriñá, I.; Toldrà, A.; Campàs, M.; Ortiz, M.; Simonova, A.; Katakis, I.; Hocek, M.; O'Sullivan, C. K. Electrochemical Genosensor for the Direct Detection of Tailed PCR Amplicons Incorporating Ferrocene Labelled dATP. *Biosens. Bioelectron.* **2019**, *134* (January), 76–82. https://doi.org/10.1016/j.bios.2019.03.060.

(39) Astruc, D. Why Is Ferrocene so Exceptional? *Eur. J. Inorg. Chem.* **2017**, *2017* (1), 6–29. https://doi.org/10.1002/ejic.201600983.

(40) Kielkowski, P.; Fanfrlík, J.; Hocek, M. 7-Aryl-7-Deazaadenine 2'-

Deoxyribonucleoside Triphosphates (dNTPs): Better Substrates for DNA Polymerases than dATP in Competitive Incorporations. *Angew. Chemie - Int. Ed.* **2014**, *53*, 7552–7555. https://doi.org/10.1002/anie.201404742.

(41) Cahová, H.; Panattoni, A.; Kielkowski, P.; Fanfrlîk, J.; Hocek, M. 5-Substituted Pyrimidine and 7-Substituted 7-Deazapurine dNTPs as Substrates for DNA Polymerases in Competitive Primer Extension in the Presence of Natural dNTPs. *ACS Chem. Biol.* **2016**, *11* (11), 3165–3171. https://doi.org/10.1021/acschembio.6b00714.

(42) Steentjes, T.; Jonkheijm, P.; Huskens, J. Electron Transfer Processes in Ferrocene-Modified Poly(ethylene Glycol) Monolayers on Electrodes. *Langmuir* **2017**, *33* (43), 11878–11883. https://doi.org/10.1021/acs.langmuir.7b02160.

(43) Noviandri, I.; Brown, K. N.; Fleming, D. S.; Gulyas, P. T.; Lay, P. A.; Masters, A. F.; Phillips, L. The Decamethylferrocenium/Decamethylferrocene Redox Couple: A Superior Redox Standard to the Ferrocenium/Ferrocene Redox Couple for Studying Solvent Effects on the Thermodynamics of Electron Transfer. *J. Phys. Chem. B* **2002**, *103* (32), 6713–6722. https://doi.org/10.1021/jp991381+.

(44) Waniek, S. D.; Klett, J.; Förster, C.; Heinze, K. Polysubstituted Ferrocenes as Tunable Redox Mediators. *Beilstein J. Org. Chem.* **2018**, *14*, 1004–1015. https://doi.org/10.3762/bjoc.14.86.

(45) Li, J.; Macdonald, J. Advances in Isothermal Amplification: Novel Strategies Inspired by Biological Processes. *Biosens. Bioelectron.* **2015**, *64* (2015), 196–211. https://doi.org/10.1016/j.bios.2014.08.069.

(46) Deng, H.; Gao, Z. Bioanalytical Applications of Isothermal Nucleic Acid Amplification Techniques. *Anal. Chim. Acta* **2015**, *853*, 30–45.

(47) Ma, Z.; Lee, R. W.; Li, B.; Kenney, P.; Wang, Y.; Erikson, J.; Goyal, S.; Lao, K. Isothermal Amplification Method for next-Generation Sequencing. *Proc. Natl. Acad. Sci.* **2013**, *110* (35), 14320–14323. https://doi.org/10.1073/pnas.1311334110.

(48) Craw, P.; Balachandran, W. Isothermal Nucleic Acid Amplification Technologies for Point-of-Care Diagnostics: A Critical Review. *Lab Chip* **2012**, *12*, 2469–2486.

(49) Isothermal Amplification of Nucleic Acids on a Solid Support, 2011.

(50) Kim, J.; Easley, C. J. Isothermal DNA Amplification in Bioanalysis: Strategies and Applications. *Bioanalysis* **2011**, *3* (2), 227–239. https://doi.org/10.4155/bio.10.172.

(51) Fakruddin, M.; Mazumdar, R.; Chowdhury, A.; Mannan, K. Nucleic Acid Sequence Based Amplification (NASBA)-Prospects and Applications. *Int J Life Sci Pharma Res* **2012**, *2* (1), 106.

(52) Mueller, J. D.; Pütz, B.; Höfler, H. Self-Sustained Sequence Replication (3SR): An Alternative to PCR. *Histochem. Cell Biol.* **1997**, *108* (4–5), 431–437. https://doi.org/10.1007/s004180050183.

(53) Walker, G. T.; Fraiser, M. S.; Schram, J. L.; Little, M. C.; Nadeau, J. G.; Malinowski, D. P. Strand Displacement Amplification - an Isothermal, in Vitro DNA Amplification Technique. *Nucleic Acids Res.* **1992**, *20* (7), 1691–1696. https://doi.org/10.1093/nar/20.7.1691.

(54) Goo, N. I.; Kim, D. E. Rolling Circle Amplification as Isothermal Gene Amplification in Molecular Diagnostics. *Biochip J.* **2016**, *10* (4), 262–271. https://doi.org/10.1007/s13206-016-0402-6.

(55) Wong, Y. P.; Othman, S.; Lau, Y. L.; Radu, S.; Chee, H. Y. Loop-Mediated Isothermal Amplification (LAMP): A Versatile Technique for Detection of Micro-Organisms. *J. Appl. Microbiol.* **2018**, *124* (3), 626–643. https://doi.org/10.1111/jam.13647.

(56) Barreda-García, S.; Miranda-Castro, R.; de-los-Santos-Álvarez, N.; Miranda-Ordieres, A. J.; Lobo-Castañón, M. J. Helicase-Dependent Isothermal Amplification: A Novel Tool in the Development of Molecular-Based Analytical Systems for Rapid Pathogen Detection. *Anal. Bioanal. Chem.* **2018**, *410* (3), 679–693. https://doi.org/10.1007/s00216-017-0620-3.

(57) Lobato, I. M.; O'Sullivan, C. K. Recombinase Polymerase Amplification: Basics, Applications and Recent Advances. *TrAC - Trends Anal. Chem.* **2018**, *98*, 19–35. https://doi.org/10.1016/j.trac.2017.10.015.

(58) Tosar, J. P.; Brañas, G.; Laíz, J. Electrochemical DNA Hybridization Sensors Applied to Real and Complex Biological Samples. *Biosens. Bioelectron.* **2010**, *26*, 1205–1217. https://doi.org/10.1016/j.bios.2010.08.053.

(59) Svobodová, M.; Pinto, A.; Nadal, P.; O'Sullivan, C. K. Comparison of Different Methods for Generation of Single-Stranded DNA for SELEX Processes. *Anal. Bioanal. Chem.* **2012**, *404*, 835–842. https://doi.org/10.1007/s00216-012-6183-4.

(60) Jauset-Rubio, M.; Svobodová, M.; Mairal, T.; McNeil, C.; Keegan, N.; El-Shahawi, M. S.; Bashammakh, A. S.; Alyoubi, A. O.; O'Sullivan, C. K. Aptamer Lateral Flow Assays for Ultrasensitive Detection of β-Conglutin Combining Recombinase Polymerase Amplification and Tailed Primers. *Anal. Chem.* **2016**, *88*, 10701–10709. https://doi.org/10.1021/acs.analchem.6b03256.

(61) Jauset-Rubio, M.; Svobodová, M.; Mairal, T.; McNeil, C.; Keegan, N.; Saeed, A.; Abbas, M. N.; El-Shahawi, M. S.; Bashammakh, A. S.; Alyoubi, A. O.; et al. Ultrasensitive, Rapid and Inexpensive Detection of DNA Using Paper Based Lateral Flow Assay. *Sci. Rep.* **2016**, *6*, 37732. https://doi.org/10.1038/srep37732.

(62) Jauset-Rubio, M.; Tomaso, H.; El-Shahawi, M. S.; Bashammakh, A. S.; Al-youbi, A. O.; O'Sullivan, C. K. Duplex Lateral Flow Assay for the Simultaneous Detection of Yersinia Pestis and Francisella Tularensis. *Anal. Chem.* **2018**, *90*, 12745–12751. https://doi.org/10.1021/acs.analchem.8b03105.

(63) Al-madhagi, S.; Joda, H.; Jauset-rubio, M.; Ortiz, M.; Katakis, I.; O'Sullivan, C. K. Isothermal Amplification Using Modi Fi Ed Primers for Rapid Electrochemical Analysis of Coeliac Disease Associated DQB1*02 HLA Allele. *Anal. Biochem.* **2018**, *556*, 16–22. https://doi.org/10.1016/j.ab.2018.06.013.

(64) Joda, H.; Beni, V.; Willems, A.; Frank, R.; Höth, J.; Lind, K.; Strömbom, L.; Katakis, I.; O'Sullivan, C. K. Modified Primers for Rapid and Direct Electrochemical Analysis of Coeliac Disease Associated HLA Alleles. *Biosens. Bioelectron.* **2015**, *73*, 64–70. https://doi.org/10.1016/j.bios.2015.05.048.

CHAPTER 2

Ferrocenylethynyl-dATP: synthesis, incorporation and electrochemical detection

Ferrocenylethynyl dATP: Synthesis, incorporation and electrochemical detection

Ivan Magriñá[1], Anna Simonova[2], Michal Hocek[2,3], Ciara K. O'Sullivan[1,4]
[1] INTERFIBIO Consolidated Research Group, Departament d'Enginyeria Química, Universitat Rovira i Virgili, Avinguda Països Catalans 26, 43007 Tarragona, Spain
[2] Institute of Organic Chemistry and Biochemistry, Czech Academy of Sciences, Flemingovo nám. 2, CZ-16610, Prague, Czech Republic
[3] Department of Organic Chemistry, Faculty of Science, Charles University in Prague, Hlavova 8, CZ-12843, Prague 2, Czech Republic
[4] Institució Catalana de Recerca i Estudis Avançats, Passeig Lluís Companys, 23, 08010 Barcelona, Spain

2.1 ABSTRACT

We report the synthesis of the ferrocenylethynyl-dATP ($dA^{EFc}TP$) from a 7-iodo-7-deaza-dATP (dA^{I}) precursor in 3 simple and straighforward reactions. The incorporation of varying ratios of $dA^{EFc}TP$:natural dATP using primer extension (PEX) of a tailed primer is described. The resulting PEX product is thus tethered with a single stranded tail which can be directly hybridised to a surface immobilised complementary probe avoiding the need to generate single stranded DNA for subsequent detection via hybridization. The ratio of a short alkanethiol to the thilated DNA probe was optimised to yield the best surface chemistry for maximum hybridisation of the PEX product, which was measured using square wave voltammetry and cyclic voltammetry.

2.2 INTRODUCTION

The modification of the nucleobases of DNA for a plethora of diverse applications has been reported, including labelling with fluorescent[1], raman[2], spin[3] or redox probes[4]. The addition of moieties susceptible to attack by DNAzymes[5] or moieties that avoid restriction endonuclease mediated cleavage[6] has also been described, as has the addition of reactive groups for cross coupling reactions[7] and the addition of groups that can modulate the transcription[8].
Specifically for the development of electrochemical DNA sensors, the labelling of DNA with redox active moieties is of particular interest. The direct incorporation of electrochemical modifed dNTPs combine the advantages of a positive detection signal, a signal amplification proportional to the number of incorporated dNTPs[9], a low background and the option to introduce different electrochemically distinguishable tags[10]. Several electrochemical labels have been described, including aminophenyl and nitrophenyl[4], tetrathiafulvalene[11], $Ru(bpy)_3$ and $Co(bpy)_3$[12], anthraquinone[13], benzofurazane[14], azidophenyl[15], phenothiazine[16] and polyoxometalates (POMs)[17].
Ferrocene has been widely used in electrochemical biosensors as it is one of the most stable organometallic compounds, that is well characterised, is inexpensive and easily available, facile to functionalise and crosslink[18], and has reversible redox behaviour[19]. Furthermore, ferrocene can be measured at very mild potentials (typically $E_{1/2}$ between 300-400mV vs Ag/AgCl), compatible with the most common electrode

materials used in electrochemical sensors. Additionally, the ferrocene redox potential can be tuned towards more positive or more negative potentials by: i) modifying the link between the ferrocene and the nucleotide[20] (i.e.: from 398mV using a carboxamidopropenyl-1 linker vs 260mV using a acetamidopropenyl-1 linker), ii) conjugating the ferrocene to the base in the nucleotide through an ethynyl linker[10] (i.e: from 450mV for ethynylferrocene dATP vs 415mV for ethynylferrocene dUTP), or iii) by modifying the cyclopendiene rings in the ferrocene with electron donor[21] or electron withdrawing[22] funtional groups. However, ferrocene is a quite bulky label that can negatively impact DNA amplification mediated by polymerases, and can effect both the enzymatic incorporation of the ferrocene labelled dNTPs and the ability of the polymerase to read through a modified template with ferrocene when compared with a template build with natural dNTPs.

Nevertheless, there are reports detailing primer extension (PEX) and polymerase chain reaction (PCR) with ferrocene labelled dNTPs, including ferrocenecarboxamidopropenyl-dUTP ($dU^{capFc}TP$)[20,23], ferroceneacetamidopropenyl-dUTP ($dU^{aapFc}TP$)[20] and ferrocenethynyl-dATP/dUTP ($dA^{EFc}TP$ and $dU^{EFc}TP$).

Wlassoff et al.[20] reported the incorporation of $dU^{capFc}TP$ and $dU^{aapFc}TP$ in a PEX experiment using 100% ferrocene modified dUTP and Klenow(exo-) polymerase fragment. Interestingly, they used a sequence that had 2 consecutive U as a template demonstrating that it was possible to efficiently incorporate two consecutive $dU^{capFc}TP$. However, the same results were not applicable to the incorporation of $dU^{aapFc}TP$, which resulted in an early PEX termination. These results highlight the effect of subtle changes in the linker (only one methylene group difference) on the incorporation of the modified nucleobase. They also studied the ability of the thermal stable Tth DNA polymerase to amplify a 998 bp amplicon using the same $dU^{capFc}TP$ at different $dU^{capFc}TP$:dTTP ratios, and whilst they observed a poor amplification yield for 100% $dU^{capFc}TP$, ratios of 25, 50 and 75% produced the expected amplicon size. Amplicon mobility in gel electrophoresis was decreased with increasing $dU^{capFc}TP$:dTTP ratios indicative of an extensive incorporation of the $dU^{capFc}TP$. Furthermore, they studied that the melting temperature (T_m) of the amplicon with and without ferrocene labels and they found a relatively small decrease of 4ºC for the ferrocene modified amplicon.

In 2008, Yeung et al.[23] used the same $dU^{capFc}TP$ to develop a real time solid phase electrochemical amplification within a microchip, demonstrating that the $dU^{capFc}TP$ is still electrochemically active after incorporation into DNA.

Brádzilová P. et al.[10] described the synthesis of $dA^{EFc}TP$ and $dU^{EFc}TP$ and their 100% incorporation in PEX, mediated by Klenow(exo-) and thermostable DyNAzyme polymerases. They observed that both $dA^{EFc}TP$ and $dU^{EFc}TP$ could be incorporated at non-adjacent positions using both enzymes. However, the incorporation at adjacent positions was less feasible, resulting in early PEX termination when using the DyNAzyme, thus limiting the use of this enzyme with homopolymers, which are commonly found in natural sequences.

In general it is established that the incorporation of modified nucleotides into DNA depends on several factors including, the polymerase employed, the dNTP used, the position of the modification, the sequence to extend or amplify[24], the linker as well as the bulkiness of the modification. Surprisingly, recent studies found that for Bst and KOD XL polymerase, some 7-aryl-7-deaza dATP analogues are better substrates than natural dATP even in the presence of bulky functional groups[24,25]. KOD XL is a

particularly attractive polymerase for use with modified nucleotides as it is thermostable and thus compatible with PCR. To date, there are no reports of the evaluation of the ability of KODXL polymerase to incorporate $dA^{EFc}TP$ in PEX reactions with full length target sequences. A demonstration of the ability of KODXL to incorporate the $dA^{EFc}TP$ in PEX reactions would form the basis for its use in PCR based electrochemical genosensors.

To electrochemically measure the PEX or PCR products via hybridisation to an immobilised probe, it is normally necessary to purify the amplicons from the the PEX or PCR mixtures, generate single stranded DNA (ssDNA), hybridise the ssDNA to a probe functionalised electrode, hybridise a second labelled reporter probe, and finally measure. Purification and ssDNA generation can be achieved using a biotinylated template and mangetoseparation using streptavidin-coated magnetic beads with thermal or alkaline denaturation[10]. This process is time consuming, requires several steps and can result in loss of DNA. An interesting alternative to avoid the purification and the ssDNA generation after PEX or PCR is the use of tailed primers. The so-called tailed primers are primers modified with a tail linked through a C3/C9/C18 spacer that prevents elongation of the tail sequence during PEX or PCR. Amplicons produced with tailed primer(s), are duplexes flanked by one/two single stranded tail(s), ready to be hybridised by a complementary probe(s)[26].

In this paper we describe the synthesis of $dA^{EFc}TP$, the incorporation of the $dA^{EFc}TP$ in a PEX experiment, the direct hybridisation of the PEX product to probes immobilised on the surface of electrodes of a microarray, and the detection of the PEX product, with incorporated $dA^{EFc}TP$ by using square wave and cyclic voltammetry. We used a clinically relevant target for screening of Human Papilloma Virus (HPV-16 [27]) as a model template. PEX was carried out using a tailed primer and the thermostable and PCR compatible KOD XL polymerase for the incorporation of the $dA^{EFc}TP$. We studied the effect of different $dA^{EFc}TP$:dATP ratios on the amplification yield and the ferrocene peak currents and finally we optimised the surface chemistry to facilitate maximum hybridisation and ferrocene peak currents.

2.3 EXPERIMENTAL SECTION

Reagents and materials

For the PEX reaction we used KOD XL polymerase obtained from Merck Millipore (Madrid, Spain), synthetic oligonucleotides produced by Biomers (Ulm, Germany), natural dNTPs from ThermoFischer Scientific (Barcelona, Spain) and the **dA^{EFc}TP** synthesised in-house following the Sonogashira reaction[10]. For agarose gel electrophoresis, we employed certified molecular biology agarose gel powder from ThemoFischer Scientific (Barcelona, Spain), GelRed™ Nucleic Acid Gel Stain from Biotium (Barcelona, Spain), TBE buffer prepared in house (10.8 g TRIS-base, 5.5 g boric acid and 4 ml ETDA 0.5 M per liter of solution), and the DNA gene ruler Low range DNA Ladder from Thermo Scientific. All other chemicals were obtained from Sigma-Aldrich S.A. (Barcelona, Spain) and used as received. We used DNA free water provided by Fisher Bioreagents to prepare PCR solutions, and high purity deionised water (18MΩ) produced with a Milli-Q RG system (Millipore Ibérica, Spain) for all other solutions.

Synthesis of 7-Deaza-7-(ferrocene-1-yl-ethynyl)-2'-deoxyadenosine-5'-triphosphate, dA^{EFc}TP

We synthesised the dA^{EFc}TP following 3 consecutives reactions as shown in **Figure 2.1.**

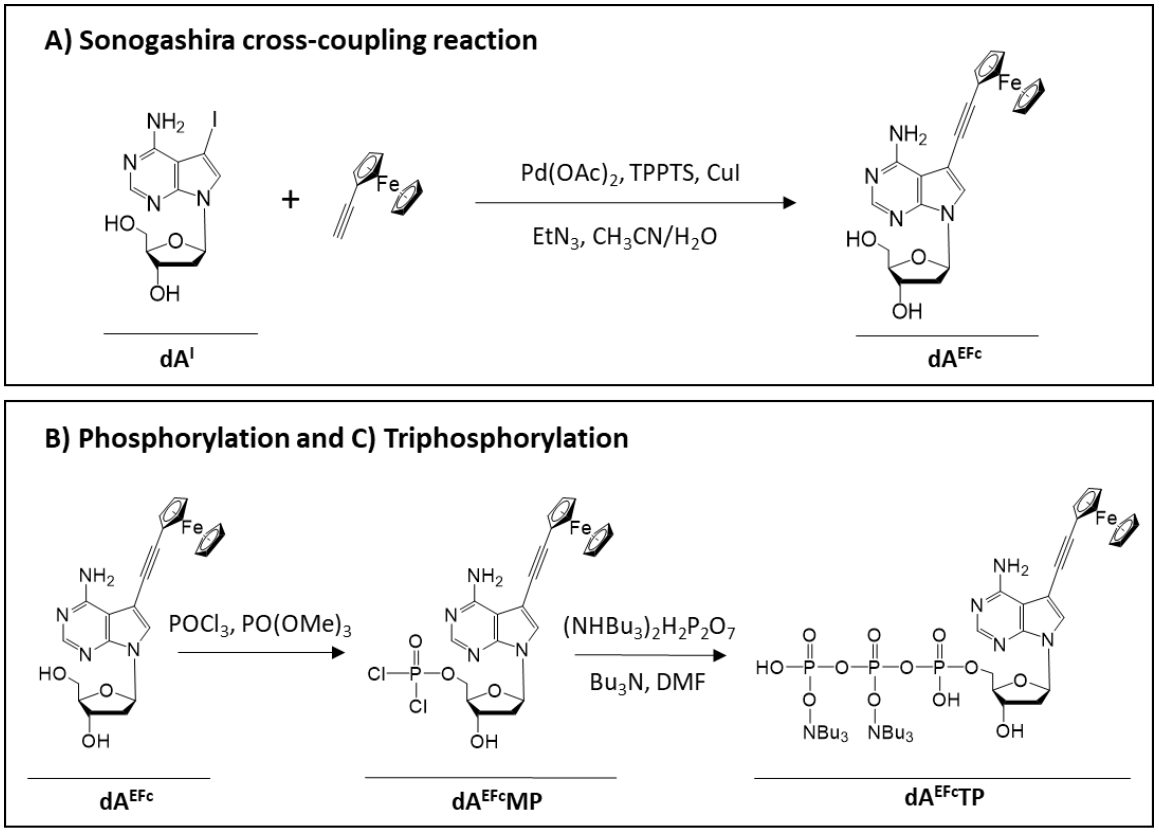

Figure 2.1 Synthesis of ethynyl ferrocene dATP

Cross-coupling reaction

In a vial A we introduced 7-iodo-7-deaza-dATP (dA^{I}) (50 mg, 0.133 mmol, 1 eq.), the ethynyl ferrocene (41.9 mg, 0.199 mmol, 1.5 eq.) and a small magnet. Then we sealed the vial with a septum, purged with N_2, introduced deareated Et_3N (148 µL, 8 eq.) and CH_3CN/H_2O 1:1 (0.75 µL) and we stirred until the solid reagents were completely dissolved.
In a second vial B, we introduced the catalyst $Pd(OAc)_2$ (1.6 mg, 0.07 mol, 0.05 eq.), the 3',3''-Phosphanetriyltris(benzenesulfonic acid) trisodium salt (TPPTS) (20 mg, 5 eq. to Pd) and then we sealed the vial with a septum, purged with N_2, introduced deareated $CH_3CN/H2O$ 1:1 (0,75 µL) and mixed with the needle until the solid reagents were dissolved. We then transferred the content of vial B to vial A with a syringe and allowed the reaction to take place under continuous stirring conditions for 1 hour at 60ºC, in an oil bath. Subsequently, we dried the solvent in a rotary evaporator and purified the 7-Deaza-7-(ferrocene-1-yl-ethynyl)-2'-deoxyadenosine (dA^{EFc}) product using flash chromatography, starting with 100% chloroform to remove the excess of unreacted ethynyl ferrocene, and then using an increasing gradient from chloroform to methanol to collect the product. Finally, we dried the solvents in a rotary evaporator.

Phosphorylation and triphosphorylation

In vial A we introduced the dA^{EFc} purified product (46mg, 0.1 mmol, 1eq), a small magnet and we then sealed the vial with a septum lid. We warmed the vial contents to 50-60ºC under vacuum and continuous stirring conditions to remove the air/solvents for 1 h and finally we added Ar. We then cooled down the vial with a ice-water bath and added $PO(OMe)_3$ (650 uL) and $POCl_3$ (12.1 uL, 1.3 eq.) and allowed the phosporylation reaction to take place for 1h.
In a vial B we weighed $(NHBu_3)H_2P_2O_7$ (275mg, 0.5mmol, 5 eq), then sealed with a septum lid and purged with vaccum/Ar 3 times. Subsequently, we injected DMF (3mL) and Bu_3N (0.1 ml, 4 eq). Following dissolution of the $(NHBu_3)H_2P_2O_7$, we transferred the contents of vial B to vial A and allowed the triphosphorylation reaction to take place for 2 h.
To stop the reaction, we added tryethylammonium bicarbonate (TEAB) 2 M until bubbles stopped appearing. We then transferred the reaction product to a round bottomed flask and we performed co-evaporation with Milli-Q 4 times. We filtered the product with a syringe filter and added water to a final volume of 4mL prior to injection for RP-HPLC purification, after which we co-evaporated the collected RP HLPC product 4 times with Milli-Q and exchanged the NBu^{3+} ion by Na^+ using a Dowex-Na^+ column. Finally, we lyophilised the product.

Electrode fabrication and functionalisation

We fabricated gold sputtered electrode arrays consisting in 3 groups of 3 circular 1mm^2 working electrodes (9 working electrodes in total), fabricated on a glass substrate as described previously[28]. Prior to functionalisation, we washed and cleaned the electrodes as follows: 5 minutes sonication in acetone, 5 minutes sonication in isopropanol, rinse with milli-Q water, dry with N_2, electrochemical cleaning with KOH 0,1M 10 cycles at 100mV/s from 0 to -1,2 V vs Ag/AgCl reference electrode, rinse with milli-Q water, dry with N_2, electrochemical cleaning with H_2SO_4 0,1 M 10 cycles at 100mV/s from 0 to 1,6V vs Ag/AgCl rinse with milli-Q water, dry with N_2.

A capture probe cocktail solution was prepared to contained 1 µM capture probe, 100 µM of mercaptohexanol and 1 M KH_2PO_4. For surface probe optimisation, mercaptohexanol concentrations tested were 0-1-10-100-1000-10,000 µM. One microlitre of the capture probe cocktail was dropcasted on to each working electrode and the array was then incubated for 3 h at 22 ºC in a humidity saturated chamber. After functionalisation, we rinsed the electrodes with copious amounts of Milli-Q and dried them with N_2. Once dried we created a 7 µL volume chamber to host the PEX purified products for hybridisation and electrochemical detection, by placing a PMMA cover over a patterned double adhesive gasket. Once assembled, we washed the microfluidic chambers with 200 µL of PBS Tween-20, then 200 µL of milli-Q and finally dried them with N_2 prior to use.

Primer extension (PEX)

We performed PEX in a T100 thermal cycler (Biorad) by heating the sample to 60ºC for 30 minutes, and cooling down to 4ºC prior to amplicon hybridisation. Each 10 µL reaction mixture contained 0.6 units of KOD XL, KOD XL buffer 1X, Primer 150 nM, template 225 nM, dGTP, dCTP, dTTP at 200 µM and the sum of dATP + **dA^{EFc}TP** at 200 µM. Following PEX we hybridised the PEX product directly to a probe complementary to the ssDNA tail, which was immobilised on individual electrodes of an array or we purified the product using the commercial kit DNA Clean and Concentrator – 5 from Zymo Research following the general protocol described in the kit. The DNA was recoverd in 18µL of Milli-Q and then mixed with 2 µL of PBS x10.

Table 2.1. List of oligonucleotide sequences and their respective modifications

Oligo	Sequence
Capture probe	5'- **TTC ATT GAG TTC GTC GTA ATT** TTT TTT TTT TTT TT-3'-C6-SH
Non-specific capture probe	5'- **CTA GGA ATT CGG CTA CTT AG**T TTT TTT TTT TTT TT-3'-C6-SH
Primer	5'- **ATT ACG ACG AAC TCA ATG AA** – C3 – *TGA GCA ATT AAA TGA CAG CTC AGA GGA GGA GG* – 3'
Template	5'- ACC GAA GCG TAG AGT CAC ACT TGC AAC AAA AGG TTA CAA TAT TGT AAT GGG CTC TGT CCG GTT CTG CTT GTC CAG CTG GAC CAT CTA TTT CAT *CCT CCT CCT CTG AGC TGT CAT TTA ATT GCT CA* – 3'
Thiolated primer	*SH-C6-5'-TGA GCA ATT AAA TGA CAG CTC AGA GGA GGA GG* – 3'

(T: 14 TT: 5 TTT: 1)

Agarose gel electrophoresis

We visualised the PEX products using agarose gel electrophoresis (Figure 2.2). We prepared the gel with ultra low pure agarose (4% w/v) in 1× Tris-Borate-EDTA buffer (TBE) and stained with GelRed™nucleic acid stain. We loaded 3 µL of PEX product with 3 µL of loading buffer 2x per well, performed electrophoresis at 100 V for 40min and imaged the gels in a UV transilluminator at λ = 254 nm

Hybridisation for liquid phase PEX products

We incubated 7 µL of PEX product in each electrode array chamber (3 working electrodes/chamber, for triplicate measurements) for 30 minutes, at 22ºC in a humidity saturated chamber. Following hybridisation we flushed the electrode array chambers with 3x200 µL of PBS Tween and finally with 200 µL of 0,1M $Ca(NO_3)_2$.

Electrochemical detection. Square wave voltammetry

We performed square wave voltammetry using a potentiostat/galvanostat PBSTAT 12 Autolab controlled with Nova 2.1.3 software. We took the measurements following hybridisation in a $Ca(NO_3)_2$ 0.1M electrolyte solution using an external Ag/AgCl reference electrode and the internal counter and working gold electrodes on the electrode array. For square wave voltammetry experiments, we stepped the potential from 0.2 V to 0.6 V with a 5 mV step, 25 mV modulation amplitude and 50 Hz frequency. For cyclic voltammetry experiments we cycled the potential for 0 to 0.6V vs Ag/AgCl at 100mV/s.

2.4 RESULTS AND DISCUSSION

Synthesis of dA^{EFc}TP

The synthetic approach presented here is straightforward and similar to the one previously described by Petra et at. [10], who synthesised the dA^{EFc}TP from the dA^{I}TP precursor, instead of the dA^{I} precursor used in this work.
The dA^{EFc}TP produced was purified as previously described and characterised using ^{31}P NMR, and mass spectroscopy (see supplemetary information Figure S2.1 and Figure S2.2, respectively). The spectras obtained confirmed the proper synthesis of the ferrocene labelled nucleotide. We used the purified dA^{EFc}TP for futher PEX experiments.

Primer extension

We performed primer extension with different ratios of dAE^{Fc}TP:dATP including 0% (all natural dNTPs), 20-40-60-80-100%. In agarose gel, see **Figure 2.2**, we could observe that the PEX reaction worked for all the ratios tested. The PEX product band (125-mer) appears in the gel higher than the template (*75-mer) and the duplex primer-template (*88,5-mer) bands. The exces of template non-hybridised to the primer produces a template-template dimer that appears lower than the desired PEX product band (see supplementary information Figure S2.3 for band assignment). This by-product do not interefere with further electrochemical detection because it lacks the tail present only in the primer and therefore it can not hybridise on the electrode.

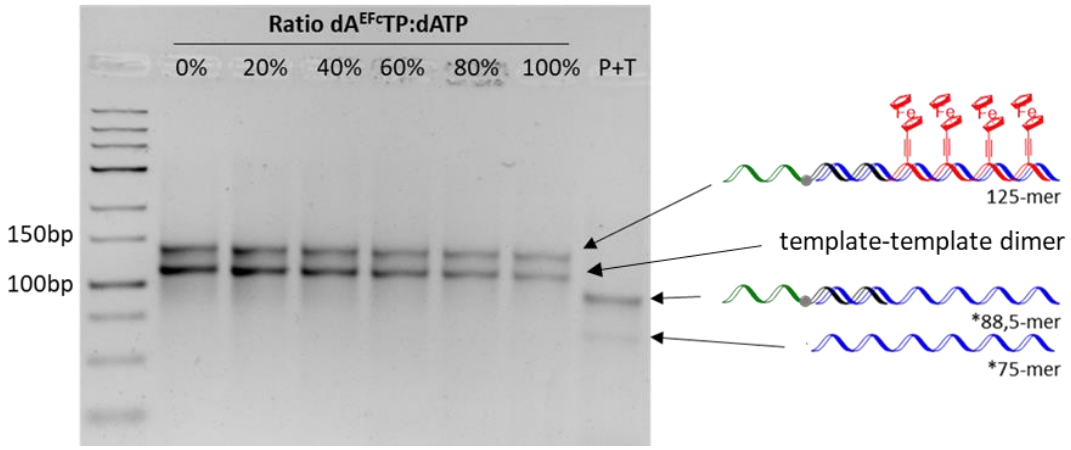

Figure 2.2 Agarose gel electrophoresis of all dAE^{Fc}TP:dATP ratios tested (0-20-40-60-80-100%) for the PEX experiment. *length stimated by dividing by 2 the number of oligo bases because it is ssDNA or and hybrid ssDNA/dsDNA

It is important to notice that the template sequence correponds to a real DNA fragment of the HPV16 and it contains a non-periodic distribution of A across the sequences. It contains A monomers separated by different numbers of the other nucleobases and it also contains 5 A homodimers and 1 A homotrimer. It is relevant to observe that even in this heterogeous distribution of A across the sequence did not provoke a premature termination of the product as observed previously when

DyNAzyme was used as polymerase and the template contained a dimer AA in the sequence[10].

Electrochemical detection

We developed a generic method to perform PEX experiments, followed by direct hybridisation and electrochemical detection as depicted in Figure 2.3.

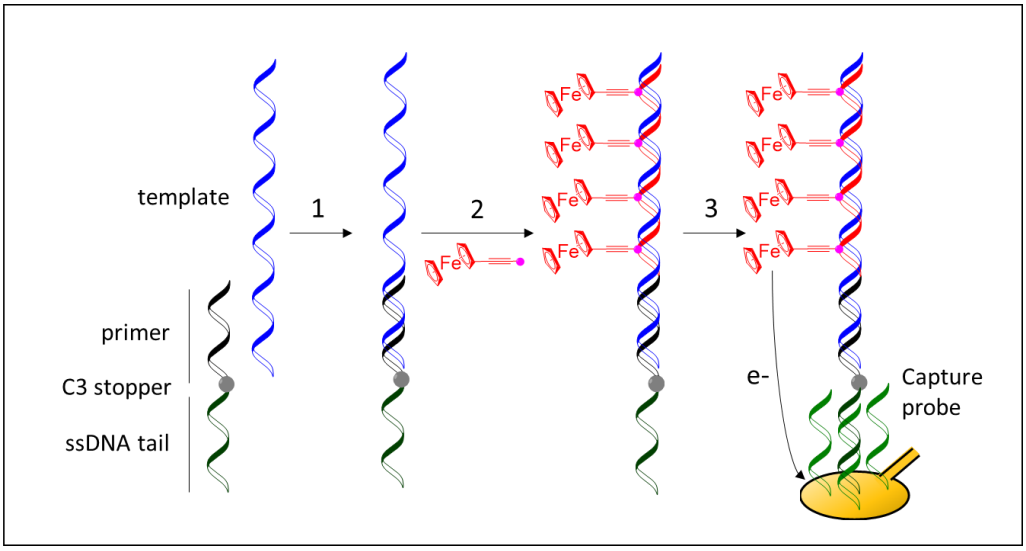

Figure 2.3 Scheme for primer extension, hybridisation and electrochemical detection. The tailed primer hybridises with the complementary target (1), then the primer is extended in the presence of $dA^{EFc}TP$ (2), and finally, the PEX product is hybridised on a gold electrode functionalised with a complementary capture probe, and the incorporated ferrocenes are electrochemically detected using square wave voltammetry or cyclic voltammetry (3).

Surface chemistry optimization

The hybridisation of the target ssDNA on a electrode surface with a complementary capture probe has three main advantages: a) pre-concentration of the target, b) an easy way to remove non-specific products after a washing step, and c) a close proximity of the target to the electrode surface to facilitate electrochemical detection. Nevertheless, DNA hybridisation on surfaces also suffers from three main constraints: a) electrostatic repulsions, b) steric hinderance between neighbour capture probes immobilised on the surface, and c) non-specific adsorption of target DNA and other components in solution to the electrode surface.
Several strategies has been reported to minimise these constraints, including the addition of a vertical spacer between the capture probe and the electrode surface, optimisation of the surface probe density and the use of thiolated backfillers[29].
To propulse the capture probe from the electrode surface and increase the availability of the recognition sequence at the electrode/solution interface we added a 15

polythymine vertical spacer between the thiol moiety and the capture probe sequence (Table 2.1). Polythymine is routinely used as a vertical spacer because it tends to stand upright and away from the surface due to the low affinity for gold whilst maintaining the flexibility and mobility of a ssDNA oligonucleotide[30].

In order to optimise the surface probe density and to avoid non-specific adsorption of PEX solution components on the gold electrode surface we performed co-immobilisation of the thiolated capture probe with the the shortchain alkanethiol mercaptohexanol as a co-immobiliser at different ratios (1:0, 1:1, 1:10, 1:100, 1:1.000, 1:10.000). We then added the PEX product obtained with 100% $dA^{EFc}TP$ and allowed it to hybridise for 30 minutes and after washing square wave voltammetry was performed. As can be seen in Figure 2.4, we observed that when no backfiller is used (ratio 1:0), the ferrocene oxidation peak current is minimum, which is also seen for the 1:1 and 1:10 ratios, which can be attributed to the high capture probe density on the electrode surface with the capture probes in a "brush-like state[31]" as well as a high electrostatic barrier that prevents the target oligo penetrating into the capture probe layer to hybridise. For the ratio 1:100, a maximum ferrocene oxidation peak current is observed, and we attribute this to a larger spacing between neighbourg capture probes, which allows a "cross-over state[31]" with minimised electrostatic repulsions and an appropiate conformation of the capture probe for hybridisation. When the spacing between captures the probes is further increased (ratio 1:1.000) the target hybridisation and ferrocene peak currents are still better as compared to the more densely packed capture probe ratios (1:0, 1:1, 1:10) but worse than for the ratio 1:100. This can be explained by the decrease of available capture probes on the surface and more space between them that results in a "mushroom-like state[31]"a less favorable conformation of the capture probe. Finally, for the ratio 1:10.000, the capture probe density is too low to capture enough target that can be electrochemically detected. The results obtained indicate that the optimum ratio capture probe:mercaptohexanol is 1:100, which is in agreement with

with previous reports[32], and all further experiments were carried out using a 1:100 probe:mercaptohexanol ratio.

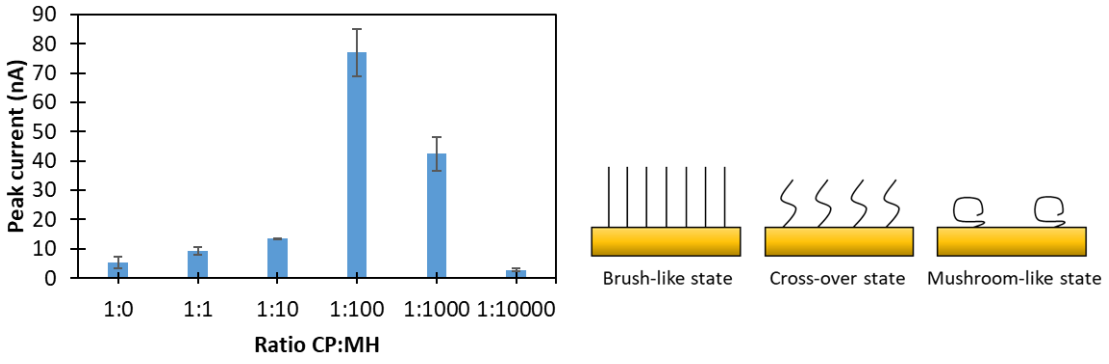

Figure 2.4 Ferrocene peak intensities obtained for different ratios capture probe : mercaptohexanol for the PEX product obtained with 100% $dA^{EFc}TP$ (left) and schematic representation of the capture probe conformation on gold electrode surfaces depending on the capture probe density.

Effect of dA^{EFc}TP:dATP ratio on ferrocene peak intensity

PEX products obtained for the different ratios dA^{EFc}TP:dATP (0-20-40-60-80-100%) and visualised using agarose gel electrophoresis (Figure 2.2) were hybridised to probes immobilised on the surface of individual electrodes of an array, the electrodes were then washed and square wave voltammetry used to measured the ferrocene incorporated into the PEX product (Figure 2.5 i) and ii)).
As expected, there is no ferrocene peak current in the absence of dA^{EFc}TP (ratio 0%). For the ratios from 20 to 100% there is an increase in the ferrocene peak current with an increasing dA^{EFc}TP:dATP ratio, suggesting a proportional incorporation of the dA^{EFc}TP with the ratio, as previously observed.[20] using dU^{capFc}TP. We did not observe any ferrocene oxidation peak following hybridisation of the PEX product in the presence of 100% dA^{EFc}TP on a electrode modified with a non-specific capture probe, demonstrating that the ferrocene oxidation peaks observed were due to incorporated dA^{EFc}TP and not due to non-specific adsorption of the dA^{EFc}TP or the PEX product (Figure 2.5 ii).
The results obtained reinforce the results obtained by Cahová H. et al.[25] who demonstrated that modified dNTPs bearing π-electron-containing substituents vinyl, ethynyl and phenyl are comparable or better substrates than natural dNTP for DNA polymerases.

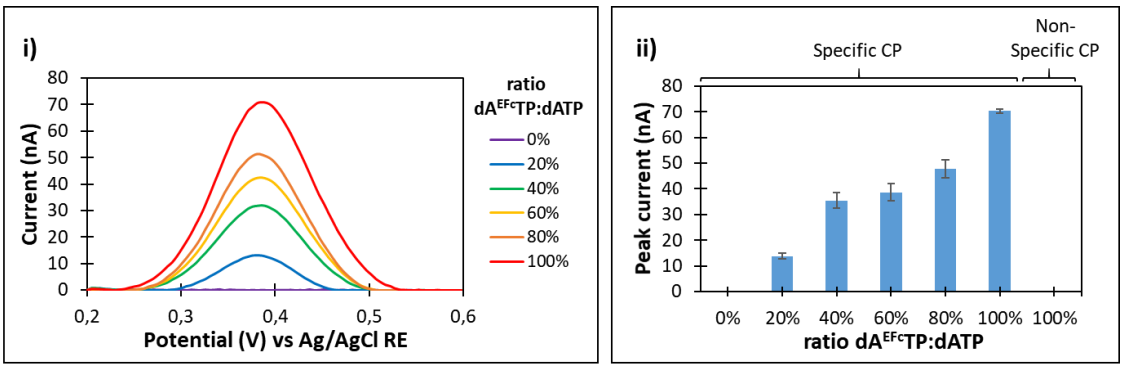

Figure 2.5 Electrochemical detection. i) Square wave voltammogram and ii) Current intensities obtained for the different ratios dA^{EFc}TP:dATP after baseline correction. CP= Capture probe; RE=Reference electrode

Surface confinement of ferrocene on electrode surface

To further demonstrate that dA^{EFc}TP was enzymatically incorporated by KOD XL polymerase during PEX, we carried out a cyclic voltammetry experiment after PEX product hybridisation on the electrode array in the presence of 100mM $Ca(NO_3)_2$. We observed the characteristic voltammogram shape for a fast and reversible surface confined redox species (ferrocene attached to the captured DNA), with negligible peak to peak separation (Eo-Er=10mV, ideally 0mV) and no tailing of the baseline, Figure 2.6. In contrast, a solution containing dA^{EFc}TP 100µM in $Ca(NO_3)_2$ 100mM shows the typical voltammogram for a difussion controlled system, with a characteristic peak to peak separation (Eo-Er=70mV, ideally 60mV) and the diffusional tails[33].

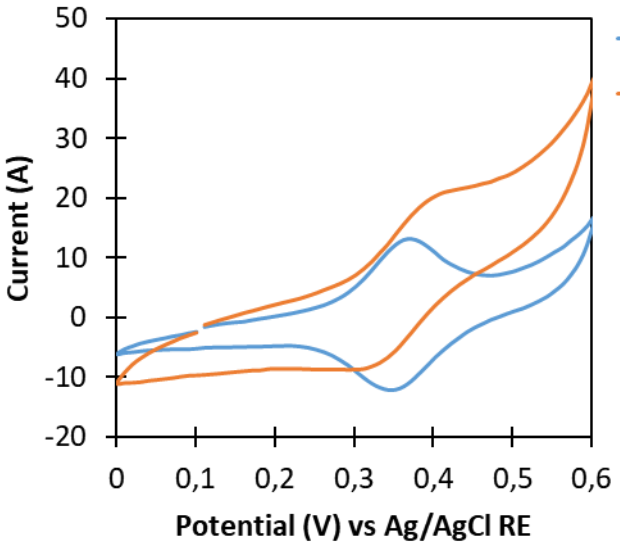

	Fc-DNA	dA^{EFc}TP
Eo (mV)	363	393
Er (mV)	352	322
Eo-Er (mV)	10	70

Figure 2.6 Cyclic voltammograms obtained at 100mV/s in presence of 100mM $Ca(NO_3)_2$ as electrolyte solution for ferrocene modified DNA (Fc-DNA) hybridised on the electrode and dA^{EFc}TP 100µM free in solution.

2.5 CONCLUSIONS

We presented a novel, simple and generic approach for the direct electrochemical detection of a primer extension product of the HPV16 genotype. The method consisted of the PEX reaction in the presence of tailed primers to produce tailed amplicons ready to be hybridised with no need for post-primer extension purification or generation of single stranded DNA. We demonstrated that KOD XL polymerase is able to incorporate dA^{EFc}TP in a 100 bases and complex template that contains 2 and 3 repetitions of A within the sequence, without an early termination of the PEX even when 100% dA^{EFc}TP is used in the PEX mixture. We confirmed the incorporation of the dA^{EFc}TP using agarose gel electrophoresis, square wave voltammetry and by cyclic voltammetry. Finally, we confirmed that capture probe:mercaptohexanol 1:100 ratio is the best in terms of hybridisation of the PEX product.

2.6 REFERENCES

(1) Dziuba, D.; Jurkiewicz, P.; Cebecauer, M.; Hof, M.; Hocek, M. A Rotational BODIPY Nucleotide: An Environment-Sensitive Fluorescence-Lifetime Probe for DNA Interactions and Applications in Live-Cell Microscopy. *Angew. Chemie - Int. Ed.* **2016**, *55* (1), 174–178.

(2) Manley, G. DNA Sequencing by Synthesis Using 3'-O-Azidomethyl Nucleotide Reversible Terminators and Surface-Enhanced Raman Spectroscopic Detection. *RSC Adv.* **2014**, *1* (2), 49342–49346.

(3) Obeid, S.; Yulikov, M.; Jeschke, G.; Marx, A. Enzymatic Synthesis of Multiple Spin-Labeled DNA. *Angew. Chemie - Int. Ed.* **2008**, *47* (36), 6782–6785.

(4) Cahová, H.; Havran, L.; Brázdilová, P.; Pivoňková, H.; Pohl, R.; Fojta, M.; Hocek, M. Aminophenyl- and Nitrophenyl-Labeled Nucleoside Triphosphates: Synthesis, Enzymatic Incorporation, and Electrochemical Detection. *Angew. Chemie - Int. Ed.* **2008**, *47* (11), 2059–2062.

(5) Hollenstein, M.; Hipolito, C. J.; Lam, C. H.; Perrin, D. M. A Self-Cleaving DNA Enzyme Modified with Amines, Guanidines and Imidazoles Operates Independently of Divalent Metal Cations (M2+). *Nucleic Acids Res.* **2009**, *37* (5), 1638–1649.

(6) Macíčková-Cahovthoma, H.; Hocek, M. Cleavage of Adenine-Modified Functionalized DNA by Type II Restriction Endonucleases. *Nucleic Acids Res.* **2009**, *37* (22), 7612–7622.

(7) Dadová, J.; Orság, P.; Pohl, R.; Brázdová, M.; Fojta, M.; Hocek, M. Vinylsulfonamide and Acrylamide Modification of DNA for Cross-Linking with Proteins. *Angew. Chemie - Int. Ed.* **2013**, *52* (40), 10515–10518.

(8) Kielkowski, P.; MacÍčková-Cahová, H.; Pohl, R.; Hocek, M. Transient and Switchable (Triethylsilyl)Ethynyl Protection of DNA against Cleavage by Restriction Endonucleases. *Angew. Chemie - Int. Ed.* **2011**, *50* (37), 8727–8730.

(9) Di Giusto, D. A.; Wlassoff, W. A.; Giesebrecht, S.; Gooding, J. J.; King, G. C. Enzymatic Synthesis of Redox-Labeled RNA and Dual-Potential Detection at DNA-Modified Electrodes. *Angew. Chemie - Int. Ed.* **2004**, *43* (21), 2809–2812.

(10) Brázdilová, P.; Vrábel, M.; Pohl, R.; Pivoňková, H.; Havran, L.; Hocek, M.; Fojta, M. Ferrocenylethynyl Derivatives of Nucleoside Triphosphates: Synthesis, Incorporation, Electrochemistry, and Bioanalytical Applications. *Chem. - A Eur. J.* **2007**, *13*, 9527–9533.

(11) Riedl, J.; Horáková, P.; Šebest, P.; Pohl, R.; Havran, L.; Fojta, M.; Hocek, M. Tetrathiafulvalene-Labelled Nucleosides and Nucleoside Triphosphates: Synthesis, Electrochemistry and the Scope of Their Polymerase Incorporation into DNA. *European J. Org. Chem.* **2009**, No. 21, 3519–3525.

(12) Vrábel, M.; Horáková, P.; Pivoňkovás, H.; Kalachova, L.; Černocká, H.; Cahová, H.; Pohl, R.; Šebest, P.; Havran, L.; Hocek, M.; et al. Base-Modified DNA Labeled by [Ru(Bpy)3]2+ and [Os(Bpy)3]2+ Complexes: Construction by Polymerase Incorporation of Modified Nucleoside Triphosphates, Electrochemical and Luminescent Properties, and Applications. *Chem. - A Eur. J.* **2009**, *15* (5), 1144–1154.

(13) Balintová, J.; Pohl, R.; Horáková, P.; Vidláková, P.; Havran, L.; Fojta, M.; Hocek, M. Anthraquinone as a Redox Label for DNA: Synthesis, Enzymatic

Incorporation, and Electrochemistry of Anthraquinone-Modified Nucleosides, Nucleotides, and DNA. *Chem. - A Eur. J.* **2011**, *17* (50), 14063–14073.

(14) Balintová, J.; Plucnara, M.; Vidláková, P.; Pohl, R.; Havran, L.; Fojta, M.; Hocek, M. Benzofurazane as a New Redox Label for Electrochemical Detection of DNA: Towards Multipotential Redox Coding of DNA Bases. *Chem. - A Eur. J.* **2013**, *19* (38), 12720–12731.

(15) Balintová, J.; Špaček, J.; Pohl, R.; Brázdová, M.; Havran, L.; Fojta, M.; Hocek, M. Azidophenyl as a Click-Transformable Redox Label of DNA Suitable for Electrochemical Detection of DNA-Protein Interactions. *Chem. Sci.* **2015**, *6* (1), 575–587.

(16) Simonova, A.; Havran, L.; Pohl, R.; Fojta, M.; Hocek, M. Phenothiazine-Linked Nucleosides and Nucleotides for Redox Labelling of DNA. *Org. Biomol. Chem.* **2017**, *15* (33), 6984–6996.

(17) Ortiz, M.; Debela, A. M.; Svobodova, M.; Thorimbert, S.; Lesage, D.; Cole, R. B.; Hasenknopf, B.; O'Sullivan, C. K. PCR Incorporation of Polyoxometalate Modified Deoxynucleotide Triphosphates and Their Application in Molecular Electrochemical Sensing of Yersinia Pestis. *Chem. - A Eur. J.* **2017**, *23*, 10597–10603.

(18) Astruc, D. Why Is Ferrocene so Exceptional? *Eur. J. Inorg. Chem.* **2017**, *2017* (1), 6–29.

(19) Steentjes, T.; Jonkheijm, P.; Huskens, J. Electron Transfer Processes in Ferrocene-Modified Poly(Ethylene Glycol) Monolayers on Electrodes. *Langmuir* **2017**, *33* (43), 11878–11883.

(20) Wlassoff, W. A.; King, G. C. Ferrocene Conjugates of DUTP for Enzymatic Redox Labelling of DNA. *Nucleic Acids Res.* **2002**, *30* (12), e58.

(21) Noviandri, I.; Brown, K. N.; Fleming, D. S.; Gulyas, P. T.; Lay, P. A.; Masters, A. F.; Phillips, L. The Decamethylferrocenium/Decamethylferrocene Redox Couple: A Superior Redox Standard to the Ferrocenium/Ferrocene Redox Couple for Studying Solvent Effects on the Thermodynamics of Electron Transfer. *J. Phys. Chem. B* **2002**, *103* (32), 6713–6722.

(22) Waniek, S. D.; Klett, J.; Förster, C.; Heinze, K. Polysubstituted Ferrocenes as Tunable Redox Mediators. *Beilstein J. Org. Chem.* **2018**, *14*, 1004–1015.

(23) Yeung, S. S. W.; Lee, T. M. H.; Hsing, I. Electrochemistry-Based Real-Time PCR on a Microchip. *Anal. Chem.* **2008**, *80* (2), 363–368.

(24) Kielkowski, P.; Fanfrlík, J.; Hocek, M. 7-Aryl-7-Deazaadenine 2'-Deoxyribonucleoside Triphosphates (DNTPs): Better Substrates for DNA Polymerases than DATP in Competitive Incorporations. *Angew. Chemie - Int. Ed.* **2014**, *53*, 7552–7555.

(25) Cahová, H.; Panattoni, A.; Kielkowski, P.; Fanfrlík, J.; Hocek, M. 5-Substituted Pyrimidine and 7-Substituted 7-Deazapurine DNTPs as Substrates for DNA Polymerases in Competitive Primer Extension in the Presence of Natural DNTPs. *ACS Chem. Biol.* **2016**, *11* (11), 3165–3171.

(26) Joda, H.; Beni, V.; Willems, A.; Frank, R.; Höth, J.; Lind, K.; Strömbom, L.; Katakis, I.; O'Sullivan, C. K. Modified Primers for Rapid and Direct Electrochemical Analysis of Coeliac Disease Associated HLA Alleles. *Biosens. Bioelectron.* **2015**, *73*, 64–70.

(27) So, K. A.; Lee, I. H.; Lee, K. H.; Hong, S. R.; Kim, Y. J.; Seo, H. H.; Kim, T. J. Human

Papillomavirus Genotype-Specific Risk in Cervical Carcinogenesis. *J. Gynecol. Oncol.* **2019**, *30* (4), e52.

(28) del Río, J. S.; Yehia Adly, N.; Acero-Sánchez, J. L.; Henry, O. Y. F.; O'Sullivan, C. K. Electrochemical Detection of Francisella Tularensis Genomic DNA Using Solid-Phase Recombinase Polymerase Amplification. *Biosens. Bioelectron.* **2014**, *54*, 674–678.

(29) Ravan, H.; Kashanian, S.; Sanadgol, N.; Badoei-Dalfard, A.; Karami, Z. Strategies for Optimizing DNA Hybridization on Surfaces. *Anal. Biochem.* **2014**, *444* (1), 41–46.

(30) Park, S. J.; Lazarides, A. A.; Storhoff, J. J.; Pesce, L.; Mirkin, C. A. The Structural Characterization of Oligonucleotide-Modified Gold Nanoparticle Networks Formed by DNA Hybridization. *J. Phys. Chem. B* **2004**, *108* (33), 12375–12380.

(31) Brittain, W. J.; Minko, S. A Structural Definition of Polymer Brushes. *J. Polym. Sci. Part A Polym. Chem.* **2007**, *45* (16), 3505–3512.

(32) Henry, O. Y. F.; Perez, J. G.; Sanchez, J. L. A.; O'Sullivan, C. K. Electrochemcial Characterisation and Hybridisation Efficiency of Co-Assembled Monolayers of PEGylated SsDNA and Mercaptohexanol on Planar Gold Electrodes. *Biosens. Bioelectron.* **2010**, *25* (5), 978–983.

(33) Gomez, M. E.; Kaifer, A. E. Voltammetric Behavior of a Ferrocene Derivative: A Comparison Using Surface-Confined and Diffusion-Controlled Species. *J. Chem. Educ.* **2009**, *69* (6), 502.

2.7 SUPPLEMENTARY INFORMATION

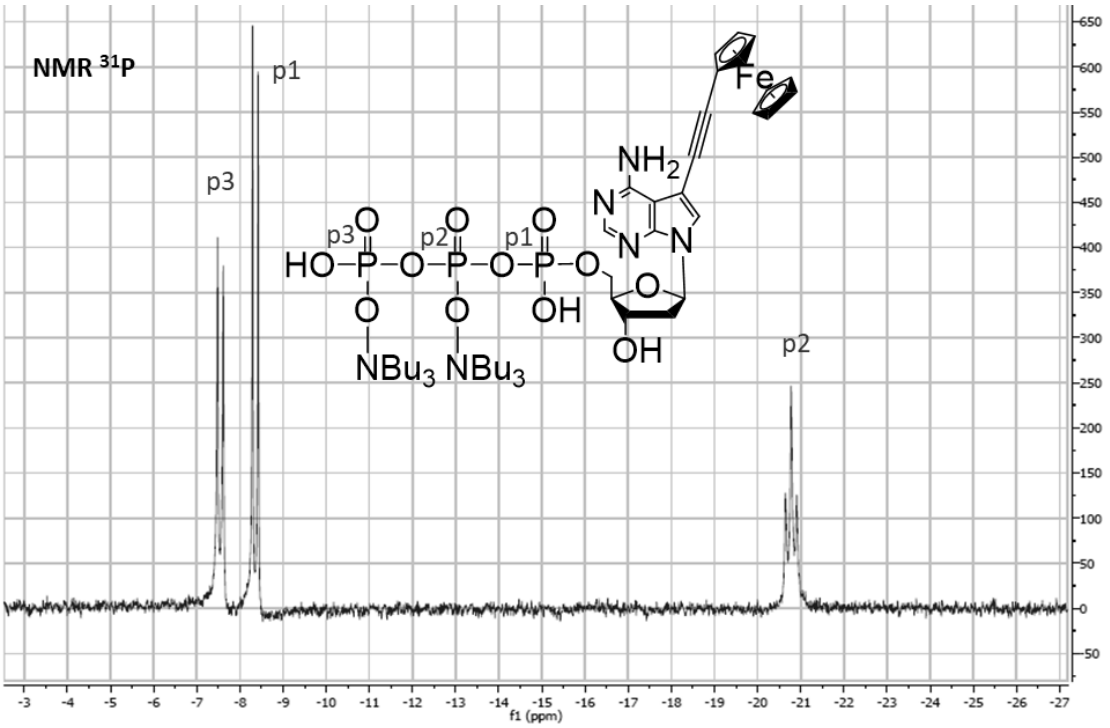

Figure S2.1 dA^{EFc}TP NMR ^{31}P. (202.3 MHz, D2O). Performed in a Bruker AVANCE 500 instrument.

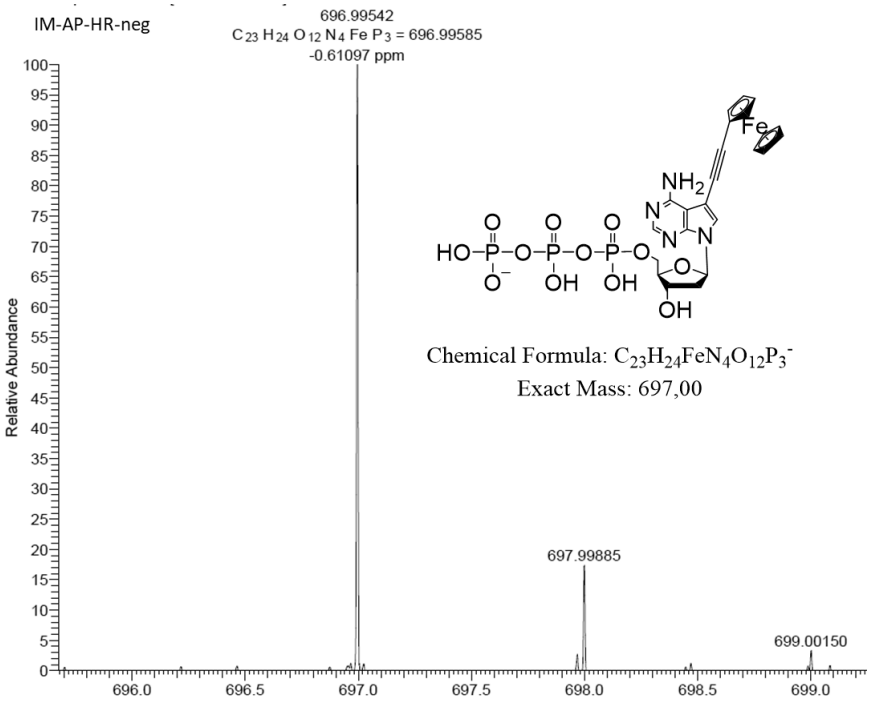

Figure S2.2 Mass spectra. ESI with negative ionization. Performed in LTQ Orbitrap XL spectrometer (Thermo Fisher Scientific).

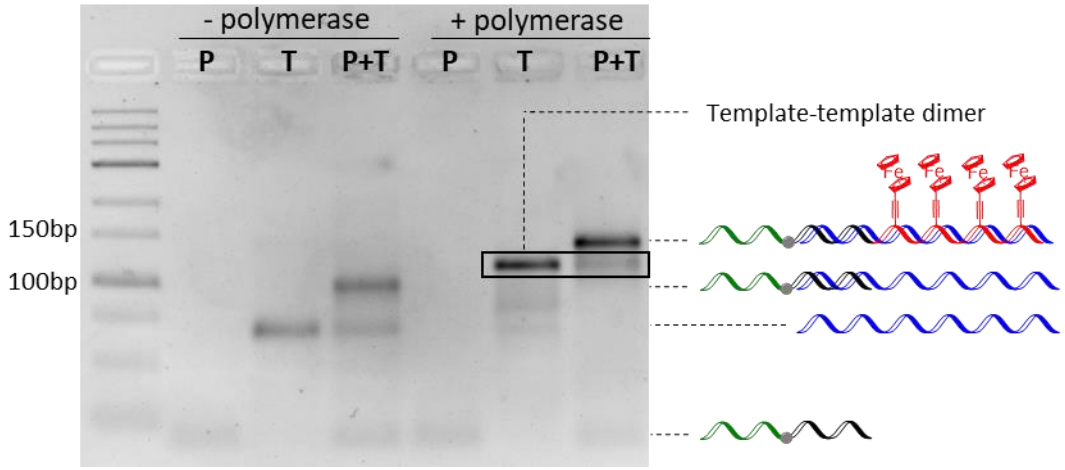

Figure S3.2 Agarose gel obtained for primer (P), template (T) and the combination of primer + template (P+T) in presence (+) or absence (-) of klenow(exo-) polymerase using 100% $dA^{EFc}TP$. Two different PEX products are obtained: a template-template dimer and the desired primer-template PEX product.

CHAPTER 3

Electrochemical genosensor for the direct detection of tailed PCR amplicons incorporating ethynyl ferrocene labelled dATP

Electrochemical genosensor for the direct detection of tailed PCR amplicons incorporating ethynyl ferrocene labelled dATP

Ivan Magriñá[1], Anna Toldrà[2], Mònica Campàs[2], Mayreli Ortiz[1], Anna Simonova[3,4], Ioanis Katakis[1], Michal Hocek[3,4]*, Ciara K. O'Sullivan[1,5]*

[1] INTERFIBIO Consolidated Research Group, Departament d'Enginyeria Química, Universitat Rovira i Virgili, Avinguda Països Catalans 26, 43007 Tarragona, Spain
[2] IRTA, Sant Carles de la Ràpita, Spain
[3] Institute of Organic Chemistry and Biochemistry, Czech Academy of Sciences, Flemingovo nám. 2, CZ-16610, Prague, Czech Republic
[4] Department of Organic Chemistry, Faculty of Science, Charles University in Prague, Hlavova 8, CZ-12843, Prague 2, Czech Republic
[5] Institució Catalana de Recerca i Estudis Avançats, Passeig Lluís Companys, 23, 08010 Barcelona, Spain

3.1 ABSTRACT

An electrochemical genosensor for the detection and quantification of *Karlodinium armiger* is presented. The genosensor exploits tailed primers and ferrocene labelled dATP analogue to produce PCR products that can be directly hybridised on a gold electrode array and quantitatively measured using square wave voltammetry. Tailed primers consist of a sequence specific for the target, followed by a carbon spacer and a sequence specifically designed not to bind to genomic DNA, resulting in a duplex flanked by single stranded binding primers. The incorporation of the 7-(ferrocenylethynyl)-7-deaza-2'-deoxyadenosine triphosphate was optimised in terms of a compromise between maximum PCR efficiency and the limit of detection and sensitivity attainable using electrochemical detection via hybridisation of the tailed, ferrocene labelled PCR product. A limit of detection of 277 aM with a linear range from 315 aM to 10 fM starting DNA concentration and a sensitivity of 122 nA·decade^{-1} was achieved. The system was successfully applied to the detection of genomic DNA in real seawater samples.

3.2 INTRODUCTION

Karlodinium is a dinoflagelate genus involved in harmful algal blooms (HAB) that produces huge fish killing-events around the world including areas in South Africa, Europe, North America, and Australia with impact in aquaculture ponds and local wild fauna [1]. Identification and quantification of karlodinium species can be used as an early warning tool for the initiation of mitigation strategies to prevent HABs, including moving fish cages from the path of the algae bloom, or targeting the bloom with chemicals or other biological control agents [2]. Current monitoring programs rely on light microscopy to perform algae identification and counting. However, microscopy is inherently slow, laboratory based and prone to misidentification with other dinoflagelates such as *Alexandrium* genus [3] due to the poor morphology features of *Karlodinium* genus. Furthermore, it is impossible to distinguish between *Karlodinium*

species, which is very important as their rate of proliferation and toxicity varies from one to another. Since 1994, recurrent fish killing events have been reported in Spain's Alfacs Bay, which were attributed to the proliferation of two co-existing *Karlodinium* species: *K. veneficum* and *K.armiger.* Both have been reported to be mixotrophic and combine photosynthesis with prey feeding but with notable differences [4]. Whereas *K. veneficum* relies more on photosynthesis, *K.armiger* growth rate is strongly dependant on prey feeding. In fact, *K. armiger* shows a pronounced swarming behaviour, with the ability to form a feeding aggregate allowing ingestion of prey several times larger than itself, including larvae of commercially important bivalves and finfish, and as a consequence *K.armiger* represents a threat for different trophic levels and is also more toxic than *K. veneficum* [4]**.**

To distinguish between *K. armiger* and *K. veneficum* a chloroplast counting per cell can be implemented but this method is extremely time consuming limiting its use in monitoring programs [1]. Flow cytometry, a high throughput analytical tool that allows the discrimination and quantification of cells, whilst also providing information regarding the life cycle stages of dinoflagellates, is another alternative. However, it is more suited to mono-specific blooms of one or two species and the instrumentation required is expensive and complex [3]**.** Molecular tools such as qPCR has also been employed for the identification and quantification of different algae species, such as that developed to detect and quantify *K.armiger* and *K.veneficum* in seawater samples [5], and whilst it is specific, robust and relatively rapid, it is quite expensive and requires trained personnel and infrastructure.

Here, we present a new generic approach for use in electrochemical genosensing exploiting a combination of tailed primers and redox labelled dNTPs (Hocek and Fojta, 2011), using the detection of *K. armiger* in seawater samples as a model system. The use of tailed primers in both the PCR and isothermal amplification has previously been reported [6,7], and also the electrochemical detection of PCR products using the ferrocene labelled dATP analogue (7-(ferrocenylethynyl)-7-deaza-2'-deoxyadenosine 5'-triphosphate, **dA^{EFc}TP**) [8], but this is the first demonstration of their combination and direct detection of the PCR product on microfabricated gold electrode arrays (Figure 3.1).

The vast majority of reports detailing DNA biosensors require the generation of post-amplification generation of single-stranded DNA for its subsequent hybridisation to a surface-immobilised probe [9], and this is often followed by another hybridisation with a labelled reporter probe, to generate a signal proportional to the quantity of DNA.

Among the different transduction options, electrochemical transduction have some advantages over other techniques, including high sensitivity, compatibility with microfabrication and miniaturization, simple and inexpensive instrumentation required, with an inherent low cost and power consumption as well as its tolerance to sample turbidity [10]. The electrochemical detection of DNA hybridisation is mainly based on the electrochemical detection of labels (organic dyes, metal complexes, enzymes or metal particles) that intercalate within the double stranded DNA, are

electrostatically adsorbed on the dsDNA phosphate backbone or hybridise to the target through a secondary labelled reporting probe [11].

In our approach we overcome the need to generate single stranded DNA exploiting a specifically designed tailed forward primer, which consist of a single stranded DNA sequence ("tail") that is added to the 5'-end of the primer using a 3-C alkyl chain spacer, preventing elongation of the tail during amplification. This results in a PCR product that is a duplex of the targeted sequence tethered with a single stranded tail that hybridises with a surface immobilised probe (Figure 3.1b).

To avoid the use of labels that require to be added in a further step following hybridisation, an alternative is to totally or partially replace the natural dNTPs employed in PCR with modified dNTPs tethered with electrochemically active moieties such as, for example, ferrocene [8], anthraquinone [12], or benzofurazane [13]. We chose to use the ferrocene labelled dATP analogue, as ferrocene is a reversible and stable label, its oxidation peak when incorporated into DNA is within the gold electrode potential window (450mV vs Ag/AgCl 3M KCl reference electrode) and the **dA^{EFc}TP** has been demonstrated to be a good substrate for several DNA polymerases such as Klenow (exo) or DyNAzyme [8].

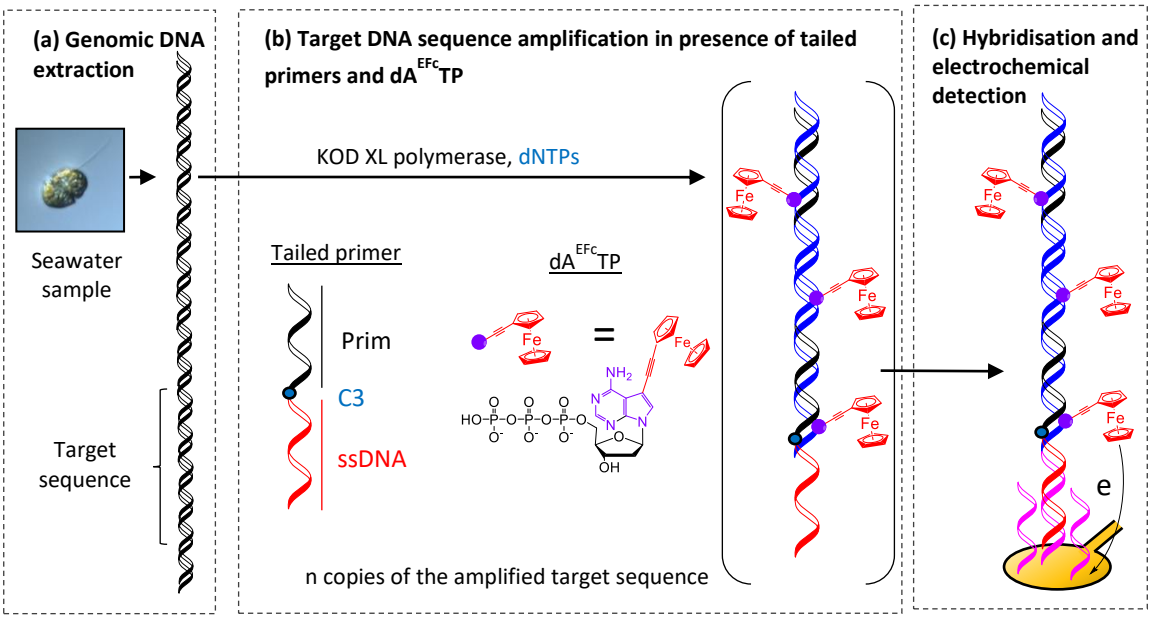

Figure 3.1. Schematic of the assay (a) Extraction of *K. Armiger* genomic DNA from seawater; (b) DNA is amplified by PCR using KOD XL polymerase in the presence of tailed primers and ferrocene labelled dATP (**dA^{EFc}TP**); (c) Redox labelled PCR product hybridises to a short capture probe complementary to the tail sequence, which is immobilised on the surface of individual gold electrodes of a microfabricated array.

3.3 MATERIALS AND METHODS

Reagents

Synthetic oligonucleotides were purchased from Biomers (Ulm, Germany), KOD XL polymerase was purchased from Merck illipore (Madrid, Spain), the SYBR Green dye was purchased from Applied Biosystems (Spain), HRP substrate formulation tetramethylbenzidine (TMB) enhanced one component HRP membrane was purchased from Diarect AG (Germany), GelRed™ Nucleic Acid Gel Stain from Biotium (Barcelona, Spain) and the certified molecular biology agarose gel powder from Bio-Rad Laboratories S.A. (Barcelona, Spain). Three-millimetre thick polymethylmethacrylate (PMMA) was purchased from La Indústria de la Goma (Tarragona, Spain) and double-sided medical grade adhesive foil ARSeal 90880 from Adhesive Research (Ireland). All other chemicals were obtained from Sigma-Aldrich S.A. (Barcelona, Spain) and used as received. Natural dNTPs were purchased from ThermoFischer Scientific (Barcelona, Spain) and $dA^{EFc}TP$ was synthesised following the Sonogashira reaction [8]

DNA free water from Fisher Bioreagents was used to prepare all reagents involved in PCR and the rest of the solutions were prepared using high purity deionised water (18MΩ) produced with a Milli-Q RG system (Millipore Ibérica, Spain).

Oligonucleotide sequences

Primers used were designed to be specific for *K. armiger* target [5] and avoid cross-reactivity with other related toxic microalgae such as *K. veneficum* and the tails in the tailed primers were designed to avoid cross-reactivity between them and also with the primers.

Table 3.1. List of oligonucleotide sequences and their respective modifications

Oligo	Sequence
Karlo FwP T	5'-ATT ACG ACG AAC TCA ATG AA – C3 – ATA GCT TCA CAG CAG AGG TTA CAA C-3'
Karlo RvP	5'-ACA CAC ATC CAA CCA TYT CAC TG-3'
Karlo RvP T	5'-TGT AAA ACG ACG GCC AGT – C3 – ACA CAC ATC CAA CCA TYT CAC TG-3'
KA target	5'-ATA GCT TCA CAG CAG AGG TTA CAA CAC CAA TGC TGC TCC GCT ACC CGC GAT CTC ATG CAC CAG GGA GCG GCA AGA AGC CAG AGC TTC AAG ACA CCC CTA CCC CCG TGC AGG AGC TCA CAA AGA AAG TTC ACA GTG AGA TGG TTG GAT GTG TGT-3'
KA SP	5'- TTC ATT GAG TTC GTC GTA ATT TTT TTT TTT TTT TT-3'-C6-SH
NS SP	5'- GTC GTG ACT GGG AAA ACT TTT TTT TTT TTT - 3'-C6-SH
Reporter probe-HRP	HRP-5'-ACA CAC ATC CAA CCA TYT CAC TG-3'

Y represent the wobble C+T.

[Note: Whilst in the final format of the assay using the ferrocene labelled dNTPs only tailed forward primer would be used, for developmental work both the reverse and forward primers were tailed. This renders a double tailed amplicon, with one tail for hybridising to the surface immobilised probe, and the other tail to hybridise to a horse radish peroxidase labelled probe. This was simply used to confirm that amplification with the tailed primers and hybridisation of the PCR amplicon was successful.]

DNA extraction from samples

Seawater samples were spiked with cultured *K. armiger* and *K. veneficum* cells at two different concentration levels (**Alert level≈** 200.000 cells/L and **Mortality level≈** 1.000.000 cells/L). (Figure 3.5b). Genomic DNA was extracted using the Biomeme (BIM) isolation kit (Biomeme, Philadelphia, USA) following a protocol previously developed [5]. Briefly, 50mL of sample is centrifuged at 3700g for 25min to harvest all cells in suspension. Then, the pellet is re-suspended in 300µL of lysis buffer (1M NaCl, 70mM Tris, 30mM EDTA, pH 8.6), transferred to a 2ml cryotube that contains ~50µg of 0.5mm diameter zirconium glass beads (Biospec, USA) and lysed using a BeadBeater-8 (BioSpec, USA) pulsed for 45s at full speed. Subsequently, 250µL of the lysed sample is pumped through an ion-exchange cartridge coupled to a syringe up and down 10 times (10 pumps) to capture all the DNA. Then, the ion cartridge is washed with 500µL of Biomeme Protein Wash solution (1 pump), then with 750µL of Biomeme Wash Buffer (1 pump) and finally the genomic DNA is eluted with 500µL of Biomeme Elution buffer (5 pumps).

qPCR

The qPCR assay was performed using an ABI 7300 thermocycler (Applied Biosystems, Thermo Fisher Scientific, Spain) with previously optimised parameters [5]. Briefly, a two-step cycling protocol was carried out, with an initial denaturation step at 95ºC for 10 min, followed by 45 cycles at 95 °C for 20 s and 58 °C for 30 s. Reaction mixture contained 10µL SYBR Green dye 2x, 2uL of primers (Karlo FwP T and Karlo RvP) at 5µM concentration stock each, 2µL of DNA extracts or calibration curve patrons made by serial solution of DNA target and 2µL of DNA free water.

PCR

The PCR was performed with a T100 thermal cycler (Biorad) using the following cycling protocol: 95ºC for 2 minutes, followed by 45 cycles at 95ºC for 30 seconds, 60ºC for 30 seconds, and 72ºC for 30 seconds, followed by a final elongation step at 72ºC for 5 minutes. Each 10µL reaction mixture contained 0,1units of KODXL and KODXL buffer 1X, both forward and reverse primers (Karlo FwP T and Karlo RvP) at 100µM, dGTP, dCTP, dTTP at 200µM and different ratios **dA^{EFc}TP**:dATP whilst maintaining [**dA^{EFc}TP**+dATP]=200µM as final concentration. To check DNA hybridisation on the electrodes, Karlo RvP was replaced by Karlo RvP T in the PCR mixture.

Agarose gel electrophoresis

Amplification products were checked by agarose gel electrophoresis. The gel was made with ultralow pure agarose (3% w/v) in 1× Tris-Borate- EDTA buffer (TBE) and stained with GelRed™nucleic acid stain. A mixture of 2µL of PCR product with 4µL of loading buffer 2x was loaded per gel well, electrophoresis was performed at 100 V for 22 min and gels were visualized in a UV transilluminator at λ = 254 nm.

Electrode fabrication

The electrode array was designed with a set of nine circular working electrodes (1mm^2) and a rectangular counter electrode (4mm^2). It was fabricated by sputtering on a 75x25mm soda-lime glass slides substrate (Sigma-Aldrich, Spain) as described previously with minor modifications [14]. Briefly, a positive photoresist AZ1505 (MicroChemicals GmbH, Germany) was deposited by spin coating at 4000rpm for 30sec on a pre-cleaned and dried glass slide. Then, the photoresist was exposed to UV light for 4 sec using a chromium mask in contact mode (LED Paffrath GmbH, Rose FotoMasken, Germany) and the transferred pattern was developed using the commercial developer AZ726. Following development, the glass slide was introduced into the sputtering chamber (ATC Orion 8-HV, AJA International Inc., USA) and was subjected to an oxygen plasma etching using AC O_2/Ar (5 $cm^3 \cdot s^{-1}$ of Ar, 5 $cm^3 \cdot s^{-1}$ of O_2, 50 W) for 5 minutes. Then, a layer of 30nm of Ti/TiO_2 was sputtered (oxygen flow rate: 5 $cm^3 \cdot s^{-1}$ of O_2 for the first 10 nm, then increase up to 20 $cm^3 \cdot s^{-1}$ for the last 5 nm. Ar flow rate: constant 5 $cm^3 \cdot s^{-1}$). Last step consisted in the deposition of 100 nm of Au by AC sputtering (5 $cm^3 \cdot s^{-1}$ of Ar, 5 $cm^3 \cdot s^{-1}$ of O_2, 50W). Lift-off was done by sonication during 5 minutes in acetone, then 5 minutes in isopropanol and finally rinsed with Milli-Q water.

Electrode functionalisation with capture probe

Electrodes were cleaned with soap prior to modification, then rinsed with milli-Q water and dried with N_2. One microlitre of a solution containing 1µM surface probe (KA SP or NS SP), 100µM mercaptohexanol in 1M KH_2PO_4 was dropcasted per each electrode and the array was incubated at room temperature (22ºC), for at least 16h in a humidity saturated chamber. After incubation, electrodes were rinsed with Milli-Q and dried with N_2.

Microfluidic fabrication and mounting

Microfluidics were fabricated using double adhesive gasket (Adhesive Research, Ireland) and 2 mm thickness PMMA cover plates patterned using a CO_2 laser marker (Fenix, Synrad, USA). Following electrode array functionalisation, double adhesive gasket and PMMA were aligned and bonded by pressure to produce a 7 µL microfluidic chamber where DNA hybridisation and electrochemical measurements were carried out (Figure 3.2). Microfluidic chambers were washed with 200 µL of PBS Tween-20, 200 µL of Milli-Q and dried with N_2. The arrays are stable modified with capture probe and incorporating the microfluidics are stable for at least one week if kept dried at 4ºC.

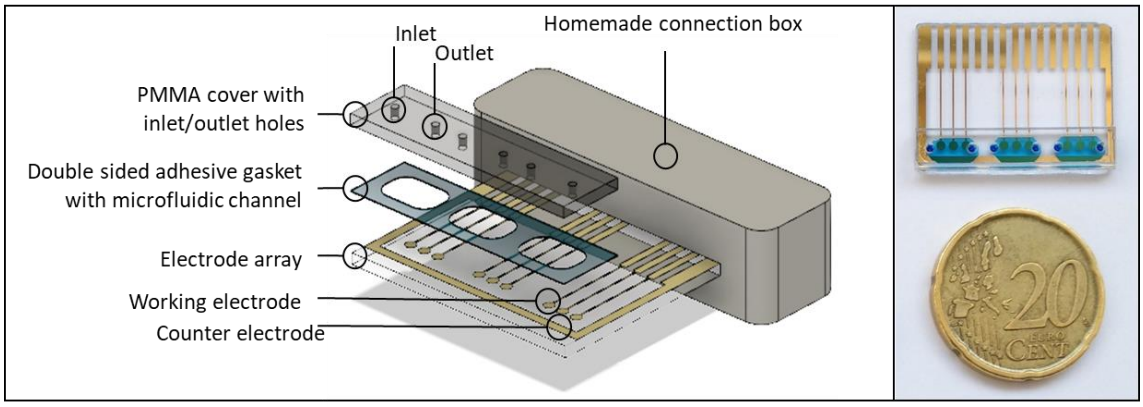

Figure 3.2. Schematic representation and real picture of the electrode array and the microfluidic cell. Electrode array, double adhesive gasket and PMMA cover are bound together to create 7 µL cells where hybridisation and electrochemical measurements are carried out. Electrode is connected to the potentiostat trough a homemade connection box.

Amplicon hybridisation on electrode arrays

Following amplification, 7 µL of PCR product was directly incubated in the microfluidic chamber for 30 minutes at room temperature (22ºC) in a humidity saturated chamber. The microfluidic chamber was then washed 3 times with 200µL of PBS Tween-20 and 200 µL of PBS containing $Ru[NH_3]_6Cl_3$ (Ruthenium(III) hexamine) 0.1 mM. Square wave voltammetry was subsequently performed by placing a Ag/AgCl (1 M KCl) reference electrode on the droplet of PBS containing ruthenium(III) hexamine formed on top of the PMMA block between the inlet and the oulet of the microfluidic cell to be measured.

Secondary hybridisation with reporting probe (only used as control to check DNA hybridisation)

After amplicon hybridisation and square wave voltammetry measurements, microfluidic chambers were then flushed with 200 µL of PBS and incubated with 7 µL of 10 nM reporter probe-HRP in PBS for 30 minutes at room temperature (22ºC) in a humidity saturated chamber. Microfluidic chambers were then flushed 3 times with 200 µL of PBS Tween-20 and 200 µL of PBS and subsequently the microfluidic chambers were filled with 100 µL of TMB enhanced one component HRP membrane and allowed to react for 5 minutes. Finally, fast chronoamperometric measurements were carried out placing the Ag/AgCl (1M KCl) reference electrode, as explained above.

Electrochemical measurements

All electrochemical measurements were performed with a potentiostat/galvanostat PBSTAT 12 Autolab controlled with Nova 2.0 Software. Electrode array was connected to the potentiostat through a homemade connector and electrochemical measurement were done using an external Ag/AgCl reference electrode, and the internal gold working and counter electrodes (Figure 3.2).

Square wave voltammetry measurements were carried out following amplicon hybridisation on electrode arrays in PBS containing Ruthenium(III) hexamine (0.1 mM) by applying a potential from 0.2 V to 0.5 V with a 5 mV step, 25 mV modulation amplitude and 50 Hz frequency.

Fast chronoamperometric measurements were carried out after a secondary hybridisation with the reporting probe by applying a potential of −0.2 V vs Ag/AgCl RE for 0.5 s and then reading the current output.

Results are represented as the mean value ± standard deviation for triplicate measurements.

3.4 RESULTS AND DISCUSSION

Direct DNA hybridisation after PCR amplification and electrochemical measurements.

Figure 3.3 illustrates the experiments carried out to demonstrate the concept of the method presented here. To prove that tailed primers can be used to capture PCR products specifically on a gold electrode, and that the incorporated ferrocene could be measured, PCR was carried out using tailed forward and reverse primers [**Note:** Reverse primer with tail is only used as a control in this experiment but will not be used in the final method].

One electrode was modified with a thiolated non-specific surface probe (NS SP) (electrode A) and two electrodes with a thiolated specific surface probe (KA SP) (electrodes B and C). Subsequently, electrodes A and B were incubated with PCR product that was amplified in the presence of tailed primers, 100% **dA^{EFc}TP** and 10nM initial DNA target concentration (Figure 3.3a). After the excess of PCR product was removed by washing, square wave voltammogram was recorded in the presence of PBS and ruthenium (III) hexamine[15]. An oxidation peak at 450mV with a peak intensity of 100±5 nA was only observed at the electrode modified with the specific surface probe shown (Figure 3.3b). To determine that the oxidation peak was coming from ferrocene and not from the DNA itself, electrode C was incubated with an amplicon produced by PCR in the presence of tailed primers and natural primers but not containing **dA^{EFc}TP** and no oxidation peak was observed, further confirming that the signal was specifically coming from the ferrocene incorporated into the DNA (Figure 3.3a).

To confirm that amplicons were captured on the gold electrodes A, B and C, all electrodes were exposed to a reporter probe-HRP and chronoamperometry was performed in the presence of precipitating TMB (Figure 3.3c). As expected, amperometric signals were observed at Electrode B and C (-380±12 nA and -736±22 nA, respectively), with only negligible currents observed at Electrode A (-17±6 nA) (Figure 3.3d).

The higher current observed at Electrode C as compared to B can be explained by the higher amount of amplicon generated using natural dNTPs, as described below (Figure 3.4a).

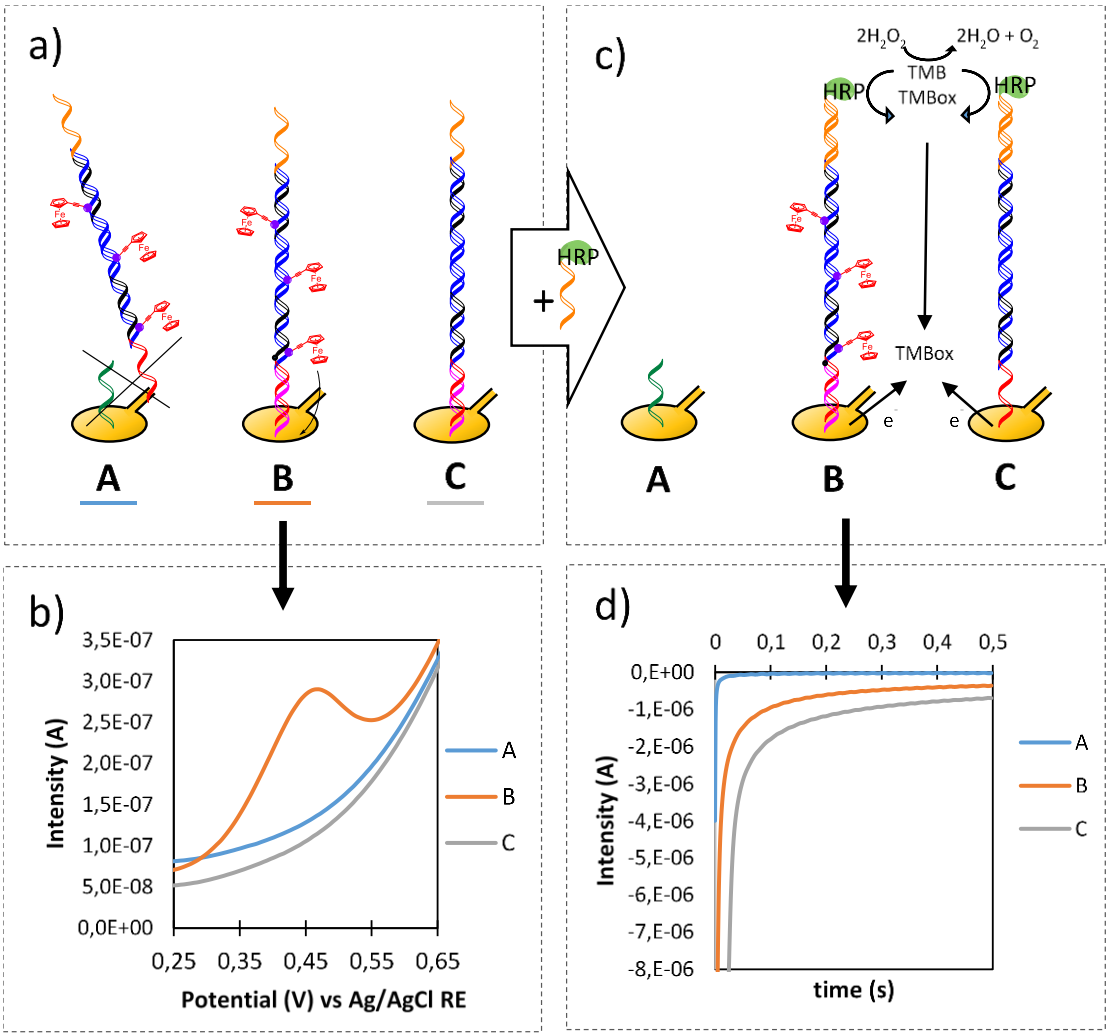

Figure 3.3. Schematic of demonstration of proof-of-concept of detection of double tailed PCR amplicons incorporating ferrocene labelled dNTPs as detailed in the text.

Effect of dA^{EFc}TP:dATP ratio on PCR amplification yield and electrochemical sensitivity.

Although **dA^{EFc}TP** is a good substrate for DNA polymerases [8], similar to other related 7-alkynyl or 7-aryl-7-deazapurine dNTPs [16], in PCR amplification the bulkier modified dNTPs often give lower yields due to the difficult reading of the polymerase through hypermodified templates. Therefore, once the incorporation and electrochemical detection of the modified dNTPs had been demonstrated using 100% **dA^{EFc}TP** in the PCR mixture, mixtures of **dA^{EFc}TP** with natural dATP in different ratios (100%, 80%, 60%, 40% and 20%) were evaluated in terms of PCR yield and electrochemical signal detected.

Calibration curves were performed at different starting concentrations of DNA target, ranging from 10nM to 1fM for each **dA^{EFc}TP**:dATP ratio. It is known that modified dNTPs decrease polymerase activity, leading to a decreased amplification efficiency [17], and as can be seen in Figure 3.4a, decreasing the **dA^{EFc}TP**:dATP ratio does indeed

improve the limit of detection. This effect can be exploited to tune the linear range and the limit of detection of the method according to the specific needs of the assay.

To ensure that the **dA^{EFc}TP** is still incorporated using the different **dA^{EFc}TP**:dATP ratios, PCR product from a 10nM starting concentration of target, were hybridised to the gold electrode immobilised probes and detected using SWV. As can be observed in Figure 3.4b, **dA^{EFc}TP** is incorporated in all the ratios tested but the peak intensity depends on two factors - the amplification yield and the ratio **dA^{EFc}TP**:dATP used. For saturated PCR reactions (20-60%, which show the same band intensity on the gel), the lower ratio results in a decreased ferrocene peak intensity, attributable to a reduced incorporation of the modified dATP into the amplicon with the lower **dA^{EFc}TP**:dATP ratios. The peak intensity dependence on the number of **dA^{EFc}TP** incorporated on the DNA was previously reported [8]. At the higher ratios of 80-100%, the PCR amplification yield is lower and thus less molecules of DNA are captured on the electrode, consequently less molecules of ferrocene would available to be measured and lower ferrocene peak intensities would be obtained.

In order to be able to detect the *K. armiger* in a relevant concentration range (10-1fM, when *K. armiger* population starts to be dangerous) the **dA^{EFc}TP/dATP** ratio has to be between 20-40%. We chose 30% as the best ratio in terms of LOD and sensitivity because it is enough to reach 1fM and provides more sensitivity than 20% (data not shown).

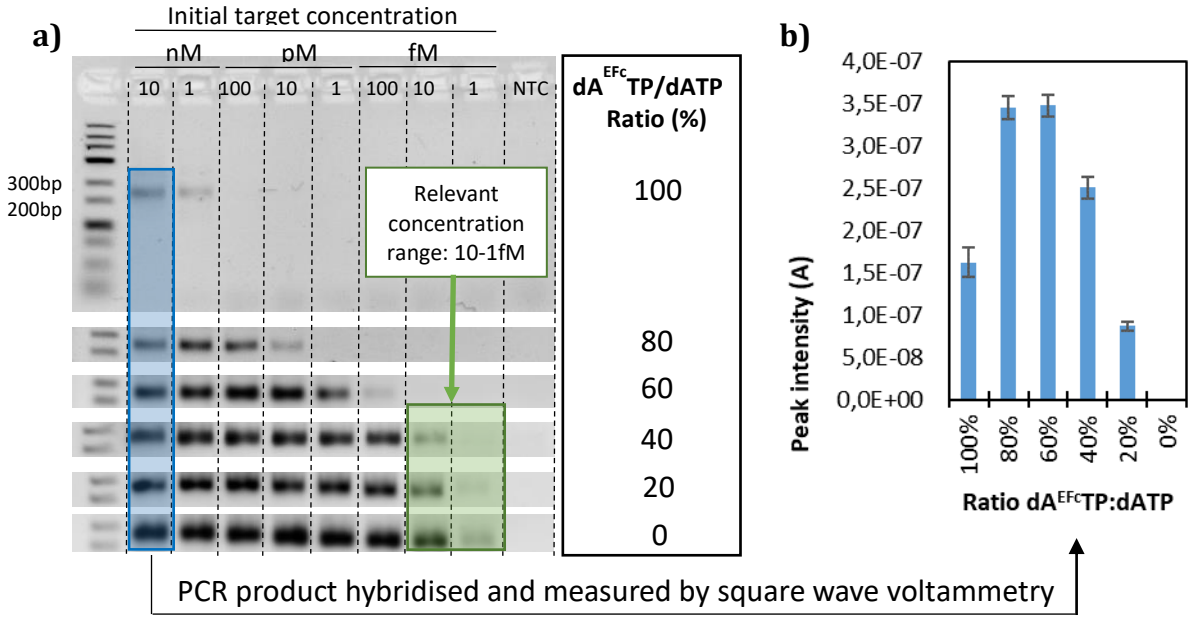

Figure 3.4 Effect of dA^{EFc}TP:dATP on calibration curve and ferrocene peak intensity. (a) Agarose gel obtained for calibration curves using different **dA^{EFc}TP**:dATP ratios**;** (b) PCR products obtained from a 10nM starting DNA concentration using different **dA^{EFc}TP**:dATP ratios were hybridised and measured by square wave voltammetry.

Calibration curve

A calibration curve was constructed over a wide range of concentrations (315 aM to 3.15 pM (from -15.5 to 11.5 log M) using a 30% **dA^{EFc}TP**:dATP ratio (see voltammograms in supplementary information, Figure S3.1). Gel electrophoresis was carried out with the PCR products (Figure 3.5a), and the resulting electrochemical calibration curve can be seen in Figure 3.5. The assay was completed within 2,5h (PCR amplification (100 min), hybridisation (30 min) and detection (2 min). The limit of detection (LOD) achieved, defined as the concentration of the analyte at three times the standard deviation of the mean blank signal, was 277aM. The sensitivity was 122nA·decade^{-1} with a linear range of 1.5 orders of magnitude, from 10fM to 315aM starting DNA concentration.

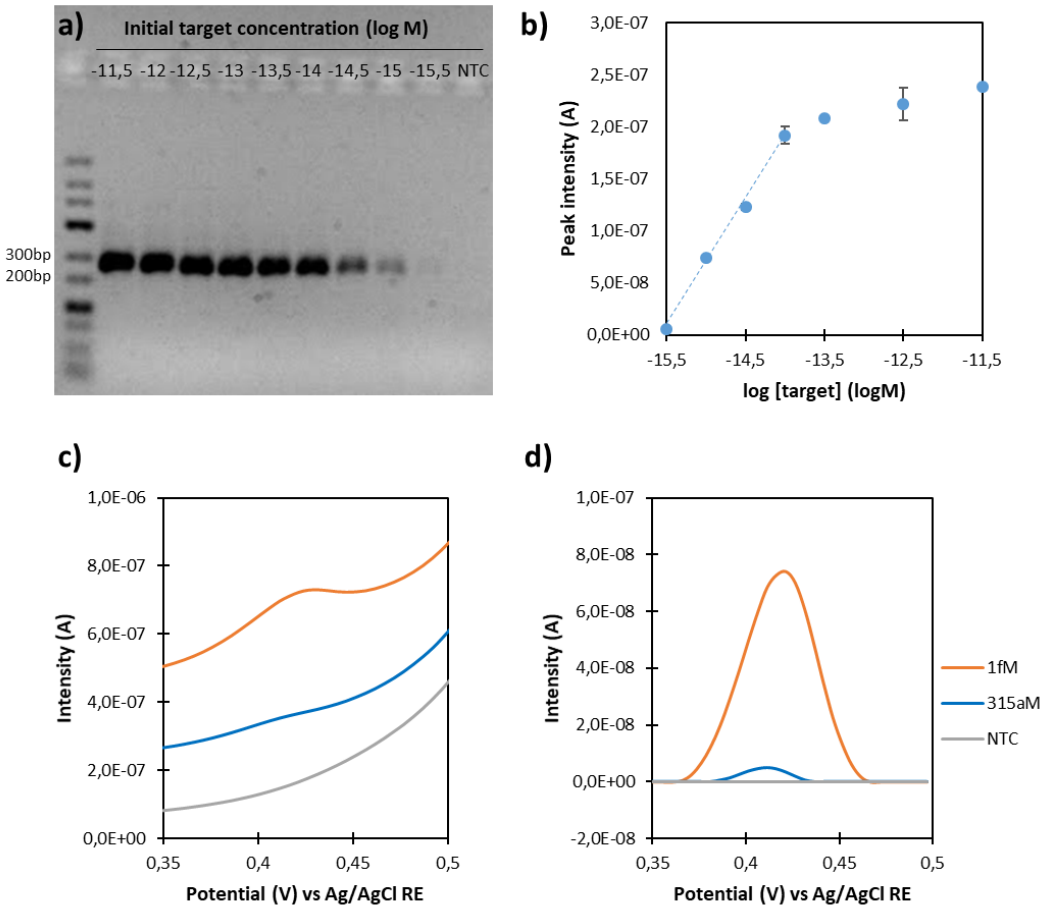

Figure 3.5. Calibration curve (a) Agarose gel obtained for calibration curve using 30% **dA^{EFc}TP**:dATP ratio; and (b) electrochemical signal obtained for each concentration of the calibration curve. c) and d) are an example of the voltammograms obtained for the non-template control (NTC), 315aM and 1fM target concentration before and after baseline correction, respectively.

Detection of *K. armiger* genomic DNA in seawater samples.

Seawater samples were spiked with cultured *K.armiger* and *K.veneficum* at two different levels of concentration, alert level (200.000 cells/L) and mortality level (1.000.000 cells/L). Genomic DNA was extracted and the concentrations estimated by the method developed in this work correlated very well with the concentrations estimated by the qPCR method developed previously [5]. No cross-reactivity with *K. veneficum* was observed, or with any other organisms present in the seawater used in this work (Figure 3.6). Voltammograms are shown in supplementary information, Figure S3.2.

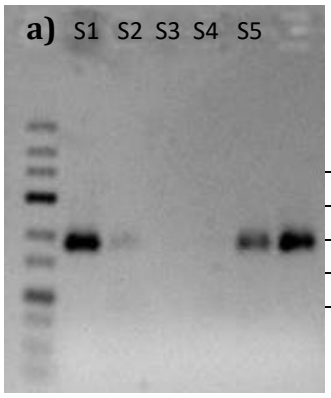

*Alert level: 200.000 cells/L
**Mortality level: 1.000.000

b) Sample	Spiked cells	[target DNA] (fM) qPCR	[target DNA] (fM) present method	Recovery (%)
S1**	*K. armiger*	7.6	6.7	90
S2*	*K. armiger*	0.5	0.7	120
S3*	*K. veneficum*			
S4**	*K. veneficum*			
S5*	*K. armiger + K. veneficum*	1.3	1.3	100
S6**	*K. armiger + K. veneficum*	11	6.7	60

Figure 3.6. Real samples. (a) Agarose gel electrophoresis obtained after PCR amplification of 6 seawater samples spiked with *K.armiger* and *K.veneficum*; (b) Sample composition and target DNA concentration estimated by qPCR and the method presented in this paper.

Electrode array stability

The stability of functionalised electrodes was tested over 1 week. First, electrode arrays were modified, functionalised, washed and dried with N_2 as described previously. Then, inlet and oulet holes for each microfluidic chamber were sealed with adhesive gasket to isolate the electrodes, and the arrays were stored at 4ºC. Adhesive was removed and microfluidic chamber washed as usual with 3x200µL PBS tween and with 200µL of milli-Q and dried with N_2 prior amplicon hybridization. The same electrode array but different microfluidic chambers were used to detect a PCR product amplified with 30% $dA^{EFc}TP$:dATP ratio and initial target concentration of 10pM. In between measurements, the electrode was kept in the fridge at 4ºC. Figure 3.7 shows there is no significant difference between ferrocene signal obtained for the PCR product in day 1 and day 7 proving the electrode stability of the arrays over 1 week when they are stored sealed in the fridge at 4ºC.

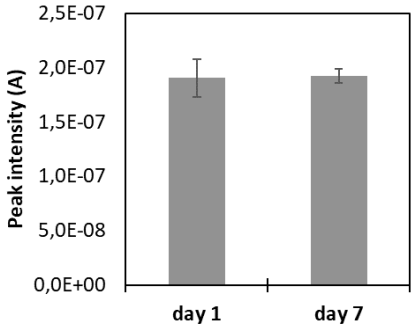

Figure 3.7 Electrode array stability when stored at 4ºC ready to be used for PCR product hybridization and detection.

3.5 CONCLUSIONS

A novel and simple DNA electrochemical platform for the detection of genomic DNA after amplification by combining tailed primers and ferrocene labelled dATP analogue was demonstrated. As a proof of concept the method was applied to the detection of *K. armiger* genomic DNA in seawater samples. The assay was completed within 2,5h and yielded a limit of detection of 277aM with a linear range from 315aM to 10fM starting DNA concentration and a sensitivity of 122nA·decade^{-1}. The developed assay eliminates the need for a single stranded DNA generation step prior to DNA hybridisation due to the use of tailed primers, and also avoids the need for any post hybridisation labelling for detection purposes due to the use of **dA^{EFc}TP**. The methodology is generic and ongoing work is focusing to extending to other genomic DNA targets in singleplex, duplex and multiplex formats, as well as replacing PCR with isothermal amplification, bringing the platform closer to deployment at the point-of-need.

ACKNOWLEDGMENTS

This work has been carried out with partial financial support from Spanish Ministerio de Economía y Competitividad for CIGUASENSING BIO2017-87946-C2-1-R and SEASENSING BIO2014-56024-C2-1. The work was also supported by the Czech Academy of Sciences (Praemium Academiae to M.H.), and by the European Regional Development Fund; OP RDE (No. CZ.02.1.01/0.0/0.0/16_019/0000729 to M.H.). The authors also acknowledge support from CERCA Programme/Generalitat de Catalunya.

3.6 REFERENCES

(1) Garcés, E.; Fernandez, M.; Penna, A.; Lenning, K. Van; Gutierrez, A.; Camp, J.; Zapata, M. Characterization of Nw Mediterranean Karlodinium Spp. (Dynophyceae) Strains Using Morphological, Molecular, Chemical and Physiological Methodologies. *Phycol. Soc. Am.* **2006**, *42*, 1096–1112.

(2) Fernández-Tejedor, M.; Soubrier-Pedreño, M. Á.; Furones, M. D. Mitigation of Lethal Effects of Karlodinium Veneficum and K. Armiger on Sparus Aurata: Changes in Haematocrit and Plasma Osmolality. *Dis. Aquat. Organ.* **2007**, *77* (1), 53–59.

(3) Figueroa, R. I.; Garcés, E.; Bravo, I. The Use of Flow Cytometry for Species Identification and Life-Cycle Studies in Dinoflagellates. *Deep. Res. Part II Top. Stud. Oceanogr.* **2010**, *57* (3–4), 301–307.

(4) Berge, T.; Poulsen, L. K.; Moldrup, M.; Daugbjerg, N.; Juel Hansen, P. Marine Microalgae Attack and Feed on Metazoans. *ISME J.* **2012**, *6* (10), 1926–1936.

(5) Toldrà, A.; Andree, K. B.; Fernández-tejedor, M.; Diogène, J.; Campàs, M. Dual Quantitative PCR Assay for Identification and Enumeration of Karlodinium Veneficum and Karlodinium Armiger Combined with a Simple and Rapid DNA Extraction Method. **2018**.

(6) Jauset-Rubio, M.; Svobodová, M.; Mairal, T.; McNeil, C.; Keegan, N.; El-Shahawi, M. S.; Bashammakh, A. S.; Alyoubi, A. O.; O'Sullivan, C. K. Aptamer Lateral Flow Assays for Ultrasensitive Detection of β-Conglutin Combining Recombinase Polymerase Amplification and Tailed Primers. *Anal. Chem.* **2016**, *88*, 10701–10709.

(7) Jauset-Rubio, M.; Svobodová, M.; Mairal, T.; McNeil, C.; Keegan, N.; Saeed, A.; Abbas, M. N.; El-Shahawi, M. S.; Bashammakh, A. S.; Alyoubi, A. O.; et al. Ultrasensitive, Rapid and Inexpensive Detection of DNA Using Paper Based Lateral Flow Assay. *Sci. Rep.* **2016**, *6*, 37732.

(8) Brázdilová, P.; Vrábel, M.; Pohl, R.; Pivoňková, H.; Havran, L.; Hocek, M.; Fojta, M. Ferrocenylethynyl Derivatives of Nucleoside Triphosphates: Synthesis, Incorporation, Electrochemistry, and Bioanalytical Applications. *Chem. - A Eur. J.* **2007**, *13*, 9527–9533.

(9) Junhui, Z.; Hong, C.; Ruifu, Y. DNA Based Biosensors. *Biotechnol. Adv.* **1997**, *15* (1), 43–58.

(10) Wang, J. Towards Genoelectronics: Electrochemical Biosensing of DNA Hybridization. *Chem. - A Eur. J.* **1999**, *5* (6), 1681–1685.

(11) Kerman, K.; Kobayashi, M.; Tamiya, E. Recent Trends in Electrochemical DNA Biosensor Technology. *Meas. Sci. Technol.* **2004**, *15*, R1-11.

(12) Balintová, J.; Pohl, R.; Horáková, P.; Vidláková, P.; Havran, L.; Fojta, M.; Hocek, M. Anthraquinone as a Redox Label for DNA: Synthesis, Enzymatic Incorporation, and Electrochemistry of Anthraquinone-Modified Nucleosides, Nucleotides, and DNA. *Chem. - A Eur. J.* **2011**, *17*, 14063–14073.

(13) Balintová, J.; Plucnara, M.; Vidláková, P.; Pohl, R.; Havran, L.; Fojta, M.; Hocek, M. Benzofurazane as a New Redox Label for Electrochemical Detection of DNA: Towards Multipotential Redox Coding of DNA Bases. *Chem. - A Eur. J.* **2013**, *19*, 12720–12731.

(14) del Río, J. S.; Svobodova, M.; Bustos, P.; Conejeros, P.; O'Sullivan, C. K. Electrochemical Detection of Piscirickettsia Salmonis Genomic DNA from Salmon Samples Using Solid-Phase Recombinase Polymerase Amplification. *Anal. Bioanal. Chem.* **2016**, *408*, 8611–8620.

(15) Das, J.; Ivanov, I.; Safaei, T. S.; Sargent, E. H.; Kelley, S. O. Analytical Methods Combinatorial Probes for High-Throughput Electrochemical Analysis of Circulating Nucleic Acids in Clinical Samples Angewandte. **2018**, 3711–3716.

(16) Kielkowski, P.; Fanfrlík, J.; Hocek, M. 7-Aryl-7-Deazaadenine 2'-Deoxyribonucleoside Triphosphates (DNTPs): Better Substrates for DNA Polymerases than DATP in Competitive Incorporations. *Angew. Chemie - Int. Ed.* **2014**, *53*, 7552–7555.

(17) Wlassoff, W. A.; King, G. C. Ferrocene Conjugates of DUTP for Enzymatic Redox Labelling of DNA. *Nucleic Acids Res.* **2002**, *30* (12), e58.

3.7 SUPPLEMENTARY INFORMATION

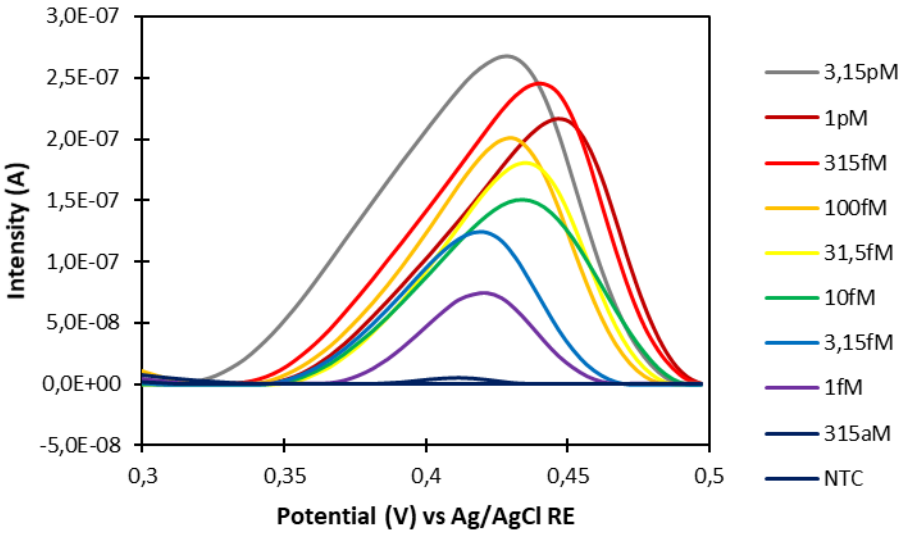

Figure S3.1. Voltammograms obtained for the calibration curve after baseline correction (moving average with a windows size equal to 1).

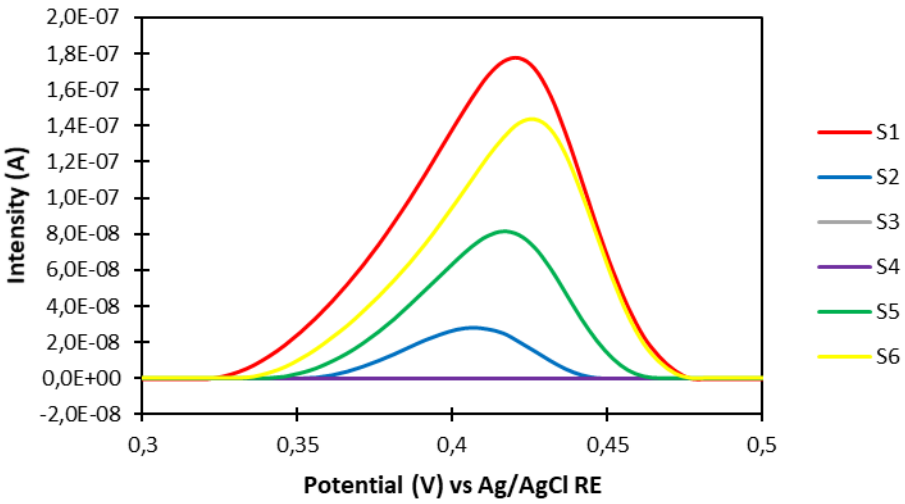

Figure S3.2. Voltammograms obtained for the real samples after baseline correction (moving average with a windows size equal to 1).

UNIVERSITAT ROVIRA I VIRGILI
DEVELOPMENT OF ELECTROCHEMICAL DNA SENSORS BASED ON THE INCORPORATION OF FERROCENE LABELLED DATP
Ivan Magriñá Lobato

CHAPTER 4

Duplex electrochemical DNA sensor to detect B. anthracis CAP and PAG targets based on the incorporation of tailed primers and ferrocene labelled dATP

Duplex electrochemical DNA sensor to detect *B.anthracis CAP and PAG* DNA targets based on the incorporation of tailed primers and ferrocene labelled dATP

Ivan Magriñá[1], Miriam Jauset-Rubio[1], Mayreli Ortiz[1], Herbert Tomaso[2], Anna Simonova[3,4], Michal Hocek[3,4*], Ciara K. O'Sullivan[1,5*]

4.1 ABSTRACT

We report the duplex amplification of 2 plasmid DNA markers involved in the virulence of *Bacillus anthracis*: CAP and PAG, and the direct electrochemical detection of these amplicons. The method consists of the simultaneous amplification of the 2 targets in a single-pot reaction via PCR using tailed primers and ferrocene labelled dATP. Following amplification, the PCR products hybridize to probes immobilized on electrodes in a microfabricated electrode array chip. The incorporated ferrocene labelled dATP is then detected using square wave voltammetry- We evaluated the effect of electrolyte cations, anions and concentration to condense, bend and shrink double stranded DNA, and their effect on the intensity of the ferrocene signal. We obtained detection limits of 0,8fM and 3,4fM for CAP and PAG targets respectively. We successfully developed a method to detect the presence of both targets in genomic DNA extracted from real samples.

4.2 INTRODUCTION

Bacillus anthracis is a non motile, gram-positive, rod shaped and spore-forming bacteria, known for being the causative agent of Anthrax[1]. It is an enzootic disease in most countries in Africa and Asia, but it also occurs sporadically in Europe, America and Australia. Anthrax affects mainly herbivores but all mammals, including humans, are susceptible to infection. The infection starts when spores of *B. anthracis* enter the host body through skin injuries, an insect bite, by consuming contaminated food and/or by inhalation of airbone spores. Generally, gastrointestinal and pulmonary infections are more severe, but even cutaneous infection, the most common form of infection in humans, can lead to fatal systemic anthrax[2]. The World Health Organization has published an extensive review on anthrax covering different aspects of the disease, including the disease and its importance, the etiology and ecology, the incidence, the transmission, the clinical manifestations, the treatment and prophylaxis in humans and animals, as well as directions for Anthrax control and surveillance[1].
There are several reports describing methods for the detection of *B. anthracis*[3], and those based on the detection of nucleic acids are very interesting due to the higher sensitivity and specificity that can be achieved as compared to antigen-antibody/aptamer based detection systems. Most of the reports focus on the detection of two virulence plasmids, pXO1 and pXO2, which have been used to distinguish from other bacteria in the *B. cereus* group, such as *B. anthracis, B. cereus, B. thuringiensis, B. mycoides, B. psuedomycoides and B. wihenstephanensis*[3]. The pXO1 plasmid contains the genes for the toxin proteins: protective antigen [pagA], edema factor [cya] and lethal factor [lef], which work in tandem to produce edema and cell

death. On the other hand, the pXO2 bears the genes capA, capB and capC required for the capsule synthesis that facilitates evasion of the immune system. The number of pXO1 and pXO2 plasmid copies differes from strain to strain and are between 2-41 copies of pXO1 plasmid and 1-2 copies of pXO2 plasmid [4].
The lose of any of the plasmids, which is common for pXO2 plasmid in nature, but rare for the toxin plasmid pXO1 results in a strong strain attenuation[2]. In fact, vaccines for *B. anthracis* are made of strains that do not contain pXO1 plasmid (Pasteur vaccine) or strains that do not contain pXO2 plasmid (Sterne vaccine), because the absence of one of them highly decreases its virulence. Consequently, when developing a method to identify *B. anthracis* and assess its risks and potential effect on health it is important not only to identify the species, but also to determine if it contains both virulent plasmids.

Determination of pXO1 and pXO2 plasmids is reported for qPCR setups due to its high sensitivity and the self-contained nature of the assay. Nevertheless qPCR requires expensive and bulky instrumentation that hinders its applicability as a point-of-need method. As an alternative, electrochemical genosensors are emerging as an alternative approach to qPCR with advantages that include portability, low cost and good analytical performance[5].

Electrochemical genosensors combine the high sensitivity and robustness of electrochemistry based sensors[6] with the selectivity provided by the specific DNA hybridization that occurs between complementary DNA strands. In most cases, genosensors require an initial enrichment of the target sequence to increase the target concentration to detectable levels, a step that is usually performed using PCR[7]. Following amplification, the majority of electrochemical genosensors require the generation of single stranded DNA (ssDNA) from the PCR product for detection via hybridization to a specifically designed and immobilized capture oligonucleotide probe. Generation of ssDNA can be achieved using assymetric PCR, where different ratios of primers are exploited[7], or alternatively, via thermal denaturation and rapid cooling[7]. An attractive alternative is the selective enzymatic digestion of one of the DNA strands using, for example, T7 or lambda exonuclease and a phosphorothioate labelled forward primer, whilst another approach uses biotinylated primer and following capture of the amplicon on streptavidin magnetic beads, thermal/pH denaturation to release ssDNA[8]. A different strategy reported recently takes advantage of the use of tailed primers, which consist of primers modified at the 5'- end with a single stranded DNA sequence ("tail") that is used for hybridization. The tail is separated from the primer using a 3-C alkyl chain spacer to prevent the elongation of the tail during amplification[9–13].

The detection of DNA following hybridization to the immobilized oligonucleotide probe can be achieved directly by direct oxidation of guanines[14], but the majority of the reports to date describe the use of labels (organic dyes, metal complexes, enzymes or metal particles) that bind to the target through a secondary labelled reporting probe or, alternatively, intercalate within the dsDNA, or, are electrostatically adsorbed on the dsDNA backbone[15].

The use of dNTPs modified with redox active labels presents a very interesting approach to directly produce a labelled amplicon and avoid the necessity of introducing a secondary labelled probe. Several redox labelled dNTPs has been reported including ferrocene[16], anthraquinone[17], benzofurazane[18] and polyoxometalates (POMs)[19]. Ferrocene is particularly of interest because it is a reversible and stable label with redox peaks within the potential window of a gold electrode, and furthermore, Fc-labelled dNTPs are efficiently incorporated by several DNA polymerases such as Klenow (exo-), DyNAzyme[16] and Vent (exo-)[20]. We have chosen 7-ferrocenyl-ethynyl-7-deaza-dATP (**dA^{EFc}TP**) because it was previously shown that 7-alkynyl-7-deazaadeninen are particularly good substrates for polymerases, even better than natural dATP[21].
We recently reported a singleplex genosensor to determine the presence of *K. armiger* in seawater samples as a proof-of-concept of a novel approach where we combined the use of tailed primers and **dA^{EFc}TP**[22]. This feasibility study highlighted the possibility of using this approach for detection of a single DNA sequence. In the work reported here, we wished to further show the immense possibilities of the approach by moving forward to a more challenging target that requires duplex parallel detection of two sequences. Duplex detection with two sets of tailed primers requires optimisation to facilitate a single-pot amplification with duplex-target detection as opposed to two individual PCR reactions being detected on a single microarray. Probes designed to hybridise to the tails of each of the targets were immobilised on individual electrodes of a microarray were evaluated for their specificity. Furthermore, we studied the effect of the electrolyte solution on the ferrocene oxidation peak due to shrinking, bending and shielding effects, evaluating the effect of monovalent (K^+, Na^+) and divalent (Mg^{2+}, Sr^{2+}, Ca^{2+}) cations, as well as the effect of a range of anions and the effect of the electrolyte concentration and pH. Using conditions optimised to provide maximum specificity and sensitivity, the genosensor array was exploited for the detection of of the *B. anthracis* virulence factors CAP and PAG genes in real samples, and the assay flow-through is schematically depicted in Figure 4.1.

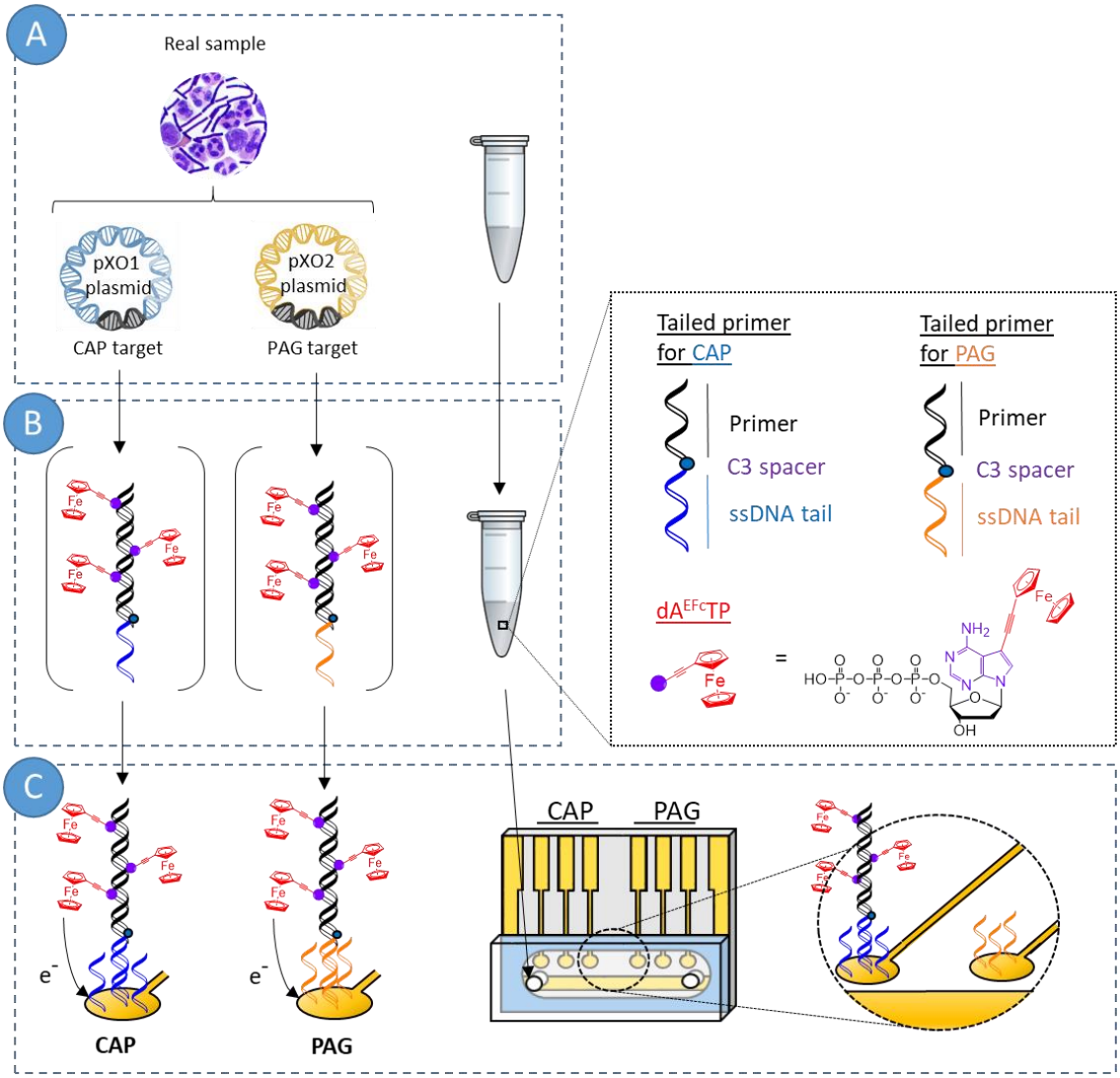

Figure 4.1. Schematic of the assay (A) Genomic DNA extraction from real samples including pXO1 and pXO2 plasmids, in case they are present. (B) Duplex DNA amplification in presence of **dA^{EFc}TP** and tailed primers for CAP and PAG targets. (C) PCR product hybridization on a microarray electrode modified with a capture probe specific for each one of the targets, wash and electrochemical detection.

4.3 MATERIALS AND METHODS

Reagents and materials

For PCR experiments, we used KOD XL polymerase purchased from Merck Millipore (Madrid, Spain), synthetic oligonucleotides obtained from Biomers (Ulm, Germany), natural dNTPs from ThermoFischer Scientific (Barcelona, Spain) and **dA^{EFc}TP** synthesised following the Sonogashira reaction[16]. For qPCR experiments we used the PowerUp SYBRGreen master mix from Applied Biosystems.
For agarose gel electrophoresis, we employed certified molecular biology agarose gel powder from ThemoFischer Scientific (Barcelona, Spain), GelRed™ Nucleic Acid Gel Stain from Biotium (Barcelona, Spain), TBE buffer prepared in house (10.8 g TRIS-base, 5.5 g boric acid and 4 ml ETDA 0.5 M per liter of solution), and the DNA gene ruler Low range DNA Ladder from Thermo Scientific.
To fabricate the electrode array and microfluidics, we used soda-lime glass slides from Sigma-Aldrich (Spain), three-millimetre thick polymethylmethacrylate (PMMA) from La Indústria de la Goma (Tarragona, Spain) and double-sided adhesive gasket ARSeal 90880 from Adhesive Research (Ireland).
All other chemicals were obtained from Sigma-Aldrich S.A. (Barcelona, Spain) and used as received.
We used DNA free water provided by Fisher Bioreagents to prepare PCR solutions, and high purity deionised water (18MΩ) produced with a Milli-Q RG system (Millipore Ibérica, Spain) for all other solutions.

Oligonucleotide sequences

We modified previously published primers for the detection of CAP and PAG genes[37,38] by the addition of two different tails on the forward primers: CAP FwP and PAG FwP. The specificity of these primers was checked using the Primer Blast software. In addition, the multiple primer analyser from ThermoFischer Scientific was used to test the cross-reactivity between the different primers designed, so that the designed primers avoid the formation of self-dimers and primer-dimers. Table 4.1 details the oligonucleotides and modifications used in this work.

Table 4.1. List of oligonucleotides

Oligo name	Sequence
CAP FwP	*5'- ATT ACG ACG AAC TCA ATG AA*-**C3-**TTG GGA ACG TGT GGA TGA TTT-3'
CAP RvP	5'- TCA GGG CGG CAA TTC ATA AT-3'
CAP CP	5'- *TTC ATT GAG TTC GTC GTA AT*T TTT TTT TTT TTT TT-3'-**C6-THIOL**
CAP target	5'- TTG GGA ACG TGT GGA TGA TTT TGG ATA TAG TAA TCT AGC TCC AAT TGT AAT TAT GAA TTG CCG CCC TGA-3'
PAG FwP	5'- *CTA AGT AGC CGA ATT CCT AG*-**C3-**CGG ATA GCG GCG GTT AAT C-3'
PAG RvP	5'- CAA ATG CTA TTT TAA GGG CTT CTT TT-3'
PAG CP	5'- *CTA GGA ATT CGG CTA CTT AG*T TTT TTT TTT TTT TT-3'-**C6-THIOL**
PAG target	5'- CGG ATA GCG GCG GTT AAT CCT AGT GAT CCA TTA GAA ACG ACT AAA CCG GAT ATG ACA TTA AAA GAA GCC CTT AAA ATA GCA TTT G-3'

In bold: oligo modifications
In italics and underlined: sequences used for DNA hybridization: tails and surface probe.

Real samples

The Friedrich-Loeffler-Institut (FLI) kindly provided us with purified genomic DNA samples, positive for *Bacillus anthracis,* following the protocol described in the QIAamp DNA Mini Kit from Qiagen. Table 4.3 shows the presence of the plasmid pXO1, and/or the plasmid pXO2 for each of the samples according to the FLI Institute, to the qPCR experiments and to the method presented here.

Polymerase Chain Reaction (PCR)

We performed PCR in a T100 thermal cycler (Biorad) following the next step cycling protocol: 95ºC for 2 minutes, followed by 34 cycles at 95ºC for 30 seconds, 60ºC for 30 seconds, and 72ºC for 45 seconds, with a final elongation step at 72ºC for 5 minutes. Each 10µL reaction mixture had 0.1 units of KOD XL, KOD XL buffer 1X, CAP primers (CAP FwP and CAP RvP) at 100 nM each one, PAG primers (PAG FwP and PAG RvP) at 100 nM each one, dGTP, dCTP, dTTP at 200 µM, dATP at 160 µM and **dA^{EFc}TP** at 40 µM and finally 1µL of the sample.

Table 4.2. Reagents used in the PCR mixture

	Sample name				
Reagents	**CAP-Fc**	**CAP**	**PAG-Fc**	**PAG**	**CAP-Fc + PAG-Fc**
dA^{EFc}TP/dATP ratio 20%	+	-	+	-	+
CAP target 100fM	+	+	-	-	+
PAG target 100fM	-	-	+	+	+

Agarose gel electrophoresis

We visualized the PCR products using agarose gel electrophoresis. The gel was prepared with ultra low pure agarose (4% w/v) in 1× Tris-Borate-EDTA buffer (TBE) and stained with GelRed™nucleic acid stain. We loaded 3 µL of PCR product with 3 µL of loading buffer 2x per well, performed electrophoresis at 100 V for 1h and imaged the gels in a UV transilluminator at λ = 254 nm.

qPCR

We performed qPCR assay using a real time thermocycler 7900HT from Applied Biosystems and a two-step cycling protocol with an initial denaturation step at 95ºC for 10 min, followed by 40 cycles at 95°C for 20 s and 60ºC for 30 seconds. The reaction mixture contained SYBR Green dye 1x, CAP primers (CAP FwP and CAP RvP) at 100nM each one, 100 nM of each of the PAG primers (PAG FwP and PAG RvP), and different concentrations of the target DNA or the sample diluted in the qPCR mixture 10 times. The amplification plots for CAP and PAG targets and genomic DNA samples are included in the supplementary information (Figures S4.1 and S4.2).

Electrode fabrication

We designed an electrode array with a set of six circular gold working electrodes (1 mm^2) and a rectangular gold counter electrode (8 mm^2), Figure 4.2. To fabricate the array we used soda-lime glass slides as substrate and we deposited the 30 nm Ti layer and a 100 nm Au layer by sputtering, as described previously[39]. Briefly, we deposited a positive photoresist AZ1505 (MicroChemicals GmbH, Germany) via spin coating at 4000 rpm for 30 s on a pre-cleaned and dried glass slide. We then placed and aligned a chromium mask in contact mode on the photoresist coated glass slide, which was subsequently exposed to UV light for 4 s (LED Paffrath GmbH, Rose FotoMasken, Germany) and the photoresist was developed using the commercial developer AZ726. We then introduced the glass slide into the sputtering chamber (ATC Orion 8-HV, AJA Interna- tional Inc., USA) for oxygen plasma etching using AC O_2/Ar (5 $cm^3 \cdot s^{-1}$ of Ar, 5 $cm^3 \cdot s^{-1}$ of O_2, 50 W) for 5 min, using a sputtering deposition of 30nm of Ti/TiO2 layer (oxygen flow rate: 5 $cm^3 \cdot s^{-1}$ of O_2 for the first 10 nm, which was then increased to 20 $cm^3 \cdot s{-}1$ for the last 5 nm. Ar flow rate: constant 5 $cm^3 \cdot s^{-1}$) and a sputtering deposition on a 100nm of Au layer by AC sputtering (5 $cm^3 \cdot s^{-1}$ of Ar, 5 $cm^3 \cdot s^{-1}$ of O_2, 50 W). Finally, we performed the lift-off step by sonication in acetone for 5 min, then sonication in isopropanol for 5 min and finally we rinsed the glass slide with Milli-Q water and dried with N_2.

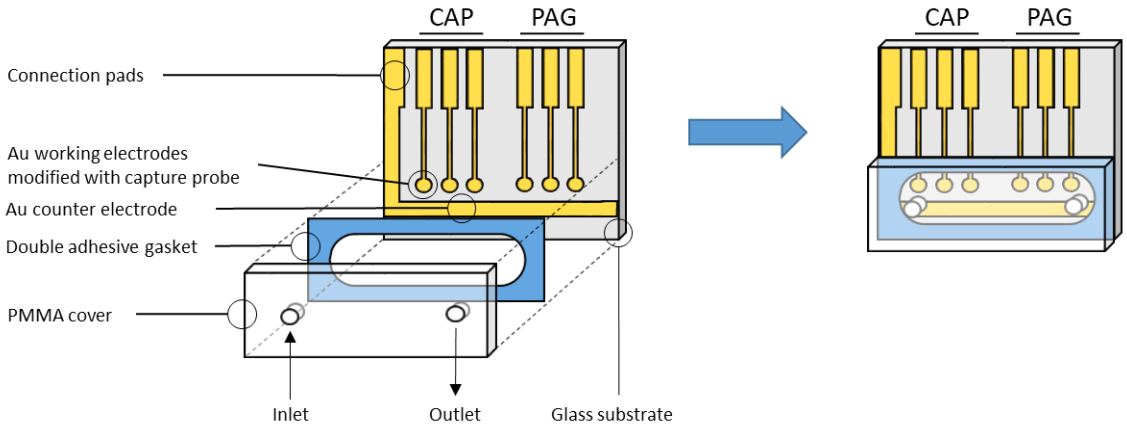

Figure 4.2. Scheme of the electrode array and the microfluidic cell.

Electrode functionalization with capture probe

Prior to funcionalization, we washed the electrode arrays with soap, then rinsed them with milli-Q water and finally dried them with N_2. We then dropcasted 1 µL of a surface probe cocktail on each working electrode and the array was then incubated overnight (at least 16 h) at room temperature (22ºC) in a humidity saturated chamber. The probe cocktail contained 1 µM capture probe (CAP capture or PAG capture), 100 µM mercaptohexanol and 1 M KH_2PO_4. After functionalization, we rinsed the electrodes with abundant milli-Q and dried them with N_2.

Microfluidic fabrication and mounting

We designed microfluidic chambers of 15 µL volume to host the PCR product for amplicon hybridization and electrochemical detection (Figure 4.2). The chamber is achieved by adhering the electrode array to a PMMA cover using double adhesive gasket. We used Winrad software to design the patterns, and a CO_2 laser marker (Fenix, Synrad, USA) to cut the materials. Once assembled, we washed the microfluidic chambers with 200 µL of PBS Tween-20, then 200 µL of milli-Q and finally dried them with N_2 prior to use.

Amplicon hybridization on electrode arrays

After PCR, we injected 15 µL of the PCR product into the microfluidic chamber housing the electrode array. Hybridization took place at room temperature (22ºC) in a humidity saturated chamber for 30 minutes. We then flushed the microfluidic chamber 3 times, with 200 µL of PBS Tween-20 and then with 200 µL of $Mg(NO_3)_2$ 0.1M.

Electrochemical measurements

We performed square wave voltammetry using a potentiostat/galvanostat PBSTAT 12 Autolab controlled with Nova 2.1.3 software. We took the measurements following hybridization in a $Mg(NO_3)_2$ 0.1M electrolyte solution using an external Ag/AgCl

reference electrode and the internal counter and working gold electrodes on the electrode array. We stepped the potential from 0 V to 0.6 V with a 5 mV step, 25 mV modulation amplitude and 50 Hz of frequency. The potentiostat and electrode array were connected using an "in-house" connector.

4.4 RESULTS AND DISCUSSION

PCR product hybridization and cross reactivity

To demonstrate the method presented in this paper, we carried out 5 different PCR reactions, to produce: #1. CAP-Fc, #2. CAP, #3. PAG-Fc, #4. PAG and #5. CAP-Fc + PAG-Fc where CAP or PAG referes to amplicon containing the CAP or PAG target sequence, repectively, and Fc indicates the presence of **dA^{EFc}TP** in the PCR mixture (see table 4.2). As we previously reported, the ratio **dA^{EFc}TP**:dATP affects the PCR amplification yield and the electrochemical signal obtained[22]. For most of applications where the target concentration is in the range of fM, the ratio should be below 40% to amplify the target to detectable levels. We performed all the experiments with 20% **dA^{EFc}TP**:dATP ratio as it allowed us to amplify both targets at the same time and obtain good electrochemical signals.
As can be seen in Figure 4.3a, gel electrophoresis analysis revealed that the duplex PCR product with the **dA^{EFc}TP** incorporated produce two distinguishable bands, with band intensities similar to the singleplex amplification of each of CAP and PAG with **dA^{EFc}TP**. The difference in band intensities between both the CAP and PAG, with and without the **dA^{EFc}TP** is probably caused by the presence of bulky ferrocene moiety in the template which can lower the PCR yield due to the difficult reading of the polymerase through the hypermodified DNA strand[23].
Subsequently, we added each of the PCR products (#1-5) to a different electrode array and then allowed them to incubate for 30 minutes at room temperature (22ºC), washed the arrays with PBS Tween and detected the presence of ferrocene using square wave voltammetry in the presence of 100mM $Ca(NO_3)_2$. Figure 4.3b shows as an example of the voltammograms obtained for array number 3. The voltammograms obtained for the other electrode arrays can be seen in supplementary information (Figure S4.1). Only the electrodes modified with the capture probe for PAG target showed a ferrocene oxidation peak at 360 mV when incubated with the PCR product #3. There was no ferrocene oxidation peak observed for the electrodes modified with the capture probe for the CAP target, indicating that there is no non-specific adsorption on the electrodes or cross-reactivity between the tails. Figure 4.3c shows the ferrocene peak currents obtained for the rest of the PCR products when incubated, washed and measured with the electrode array. As expected, only the PCR products containing ferrocene give an oxidation peak, and the peak is only observed for the electrodes modified with the specific capture probe. We observed that the ferrocene peak obtained for PAG is higher than the ferrocene peak obtained for CAP, even if the starting DNA concentration for both targets in the PCR mixture is the same. We attribute this difference to the different content of adenosine in the target sequences (PAG has 45 and CAP 36). Brázdilova *et al.*[16] previously reported the peak intensity dependence on the number of **dA^{EFc}TP** incorporated in the DNA. Additionally, we also

observed no significant differences between the singleplex product and the duplex product for each of the targets, which suggests that neither of the targets supress or inhibit the amplification of the other target.

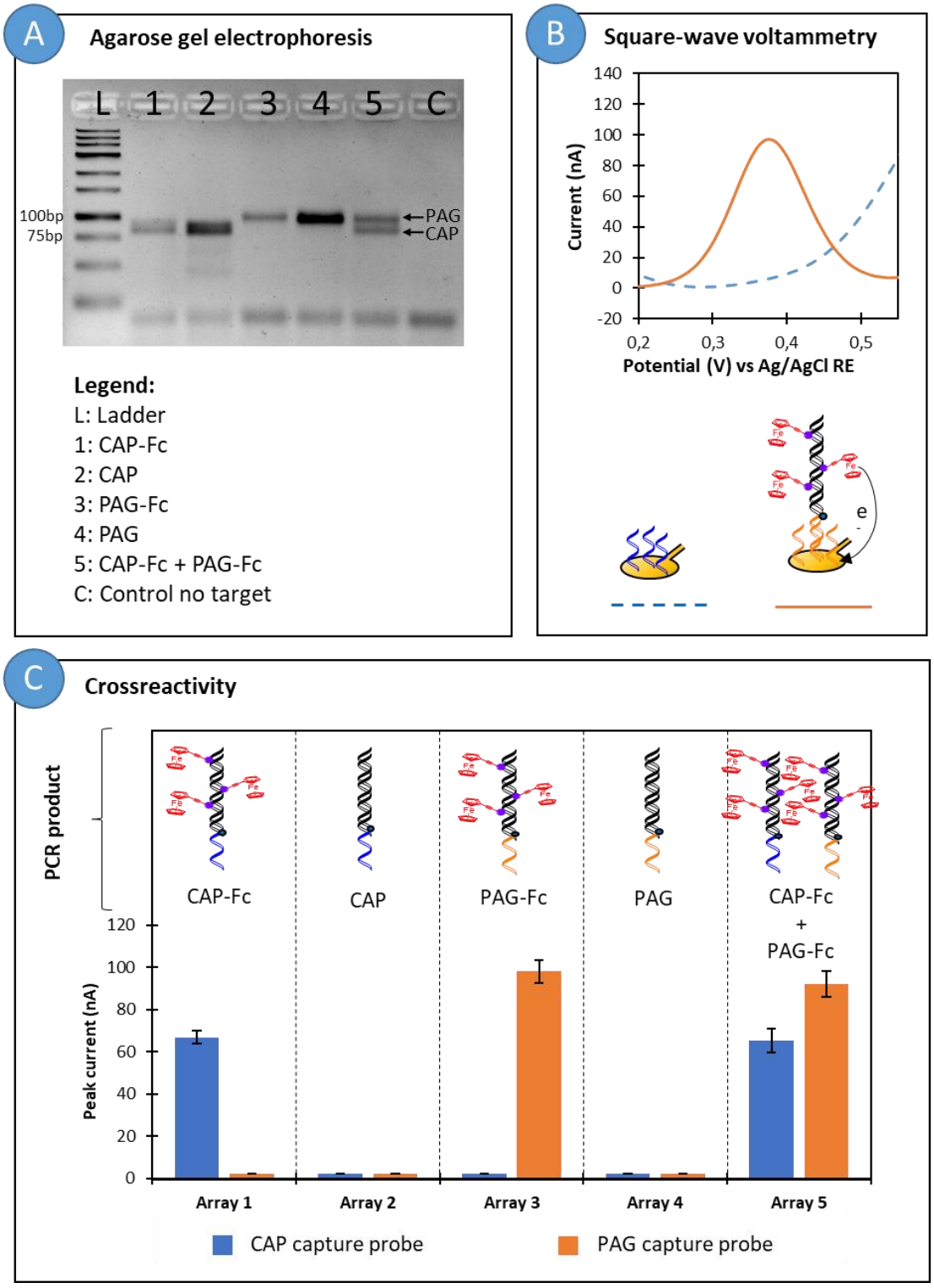

Figure 4.3. Hybridization and detection of amplified PCR products on the electrode array. A) Agarose gel electrophoresis obtained after PCR amplification. B) Voltamogram obtained for hybridization of PCR product #3 on the electrode array. C) Peak intensites obtained for the other PCR products.

Effect of electrolyte on ferrocene oxidation peak.

We studied the effect of the electrolyte solution on the ferrocene oxidation peak. We assessed the effect of the cation, the effect of the anion, and the effect of the electrolyte concentration in the pH range between 6-7.4 and at a constant temperature of 25ºC (Figure 4.4). We could not observe the ferrocene oxidation peak in the presence of PBS and other electrolytes containing monovalent cations such as K^+ and Na^+. We hypothesise that the ferrocenes could not reach the electrode surface to allow the electron transfer due to the two main factors: a) The poor mobility of the ferrocene confined in the double stranded DNA (dsDNA) structure and b) the repulsion experienced by captured PCR amplicons hybridized to the electrode-tethered probes, with neigbouring PCR amplicons and the ssDNA capture probes immobilized on the electrode surface. However, we clearly observed the ferrocene oxidation peak in the presence of the divalent cations: Ca^{2+}, Mg^{2+}, and Sr^{2+}. We postulate that this is due to the ability of divalent cations to: a) condense and shrink dsDNA[24]; b) bend dsDNA[25] and c) shield the electrostatic repulsions between neighbouring DNA strands[26], with the combination of these effects contributing to bringing the ferrocenes closer to the electrode surface, facilitating electron transfer.
We also observed a decrease in the ferrocene peak intensity when we decreased the concentration of the electrolyte $Ca(NO_3)_2$ from 0.1M to 0.001M, which we attribute due to less cation molecules being available at lower electrolyte concentrations, and less notable shrinking, bending and shielding effect thus occurs.
Finally, we observed that the ferrocene peak intensity also depends on the nature of the anion present in the solution we tested: NO_3^-, acetate$^-$, SO_4^{2-} and Cl^-. This phenomena is more difficult to explain because anions are rarely considered in the first hydration shell of the DNA due to the negatively charged nature of the DNA phosphate backbone which repeals anions and attract cations. However, there are studies that demonstrate that DNA has electropositive edges which involve amino, imino and hydroxyl groups that can act as binding points for anions[27].
We chose $Ca(NO_3)_2$ 0.1M as the preferred electrolyte solution to perform further experiments, but $Mg(NO_3)_2$ 0.1M or $Sr(NO_3)_2$ 0.1M could also be used and the same results obtained.

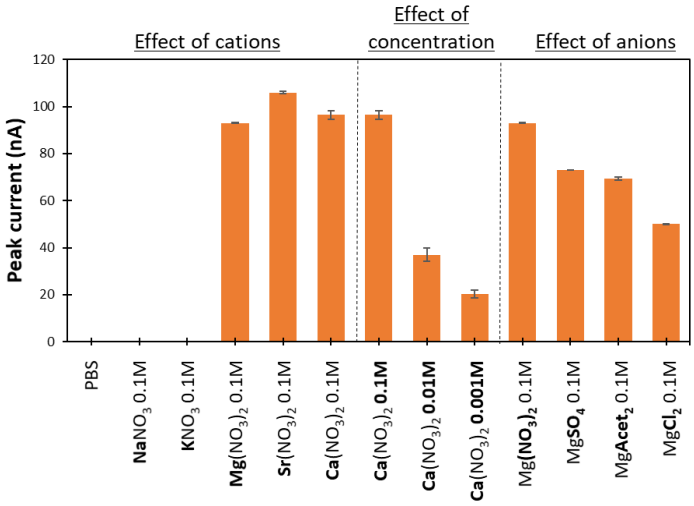

Electrolyte	pH	Peak current (nA) dsDNA	dsDNA-Fc
PBS	7.4	0	0
$NaNO_3$ 0.1M	6.5	0	0
KNO_3 0.1M	6.5	0	0
$Mg(NO_3)_2$ 0.1M	6.8	0	93.0 ± 0.2
$Sr(NO_3)_2$ 0.1M	6.4	0	105.9 ± 0.4
$Ca(NO_3)_2$ 0.1M	6.6	0	96.4 ± 1.9
$Ca(NO_3)_2$ 0.01M	6.6	0	36.9 ± 2.8
$Ca(NO_3)_2$ 0.001M	6.5	0	20.4 ± 1.7
$MgSO_4$ 0.1M	7.2	0	73.0 ± 0.1
$MgAcet_2$ 0.1M	6.5	0	69.3 ± 0.7
$MgCl_2$ 0.1M	6.6	0	50.0 ± 0.2

Figure 4.4 Effect of cations, anions and electrolyte concentration on intensity of ferrocene signal

Duplex calibration curve and real samples

We performed a PCR duplex calibration curve covering a wide range of starting DNA concentrations, from 100 aM to 10 pM using a 20% **dA^{EFc}TP**:dATP ratio. We observed that the ferrocene signal is saturated for both CAP and PAG targets at concentrations between from 100 fM and 10 pM to, and that no signal is observed for concentrations equal or below to 100 aM. We used GraphPad Prism software to plot the peak current vs initial target concentration and applied a sigmoidal curve fit. The limit of detection (LOD) was calculated as the blank value plus three times the standard desviation of the blank value. We obtained detection limits of 0,8fM and 3,4fM, for CAP and PAG target respectively (Figure 4.5). A higher number of PCR cycles could be used to decrease the LOD, but this also results in non-specific amplicons bearing the tail, that will be detected as false positives.
The same PCR conditions were used to determine the presence of CAP and PAG targets in 4 genomic DNA extracts fom real samples: S1, S2, S3 and S4. We only observed ferrocene peaks for CAP and/or PAG for the samples where we expected to find the targets, according to the data provided by FLI and the qPCR experiment carried out in house (Table 4.3).

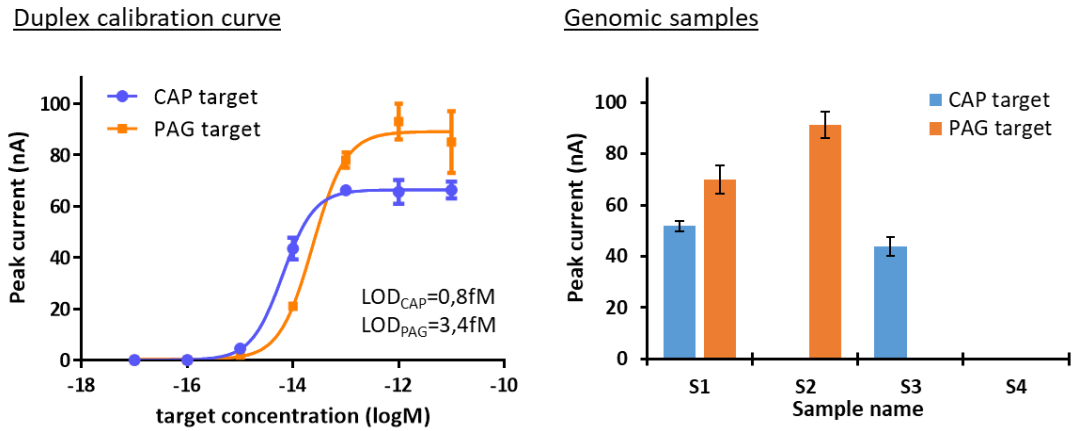

Figure 4.5 Duplex calibration curve performed with synthetic DNA and genomic samples.

Table 4.3 Samples and presence of plasmids

Genomic samples	Provided by collaborator		Estimated by qPCR		Estimated by this method	
	pOX1 plasmid	pOX2 plasmid	PAG presence	CAP presence	PAG presence	CAP presence
S1	+	+	+	+	+	+
S2	+	-	+	-	+	-
S3	-	+	-	+	-	+
S4	-	-	-	-	-	-

In order to identify the presence of *B. anthracis* and its virulence we chose to detect the pag and cap genes present in the virulence plasmids pXO1 and pXO2, respectively. The bases are similar to commercial kits that are based on the target amplification of virulence plasmid markers cya, lef of pag for pXO1, and cap for pXO2, where the main differences rely on the detection strategy of the amplification product. Whilst we used ferrocene labelled dATP to generate redox active amplicons that we detected following hybridization to specifically designed probes immobilised on individual gold electrodes of an array, the commercial kits are based on detection of the amplicon using fluorescent probes. Examples of commercially available kits include: Applied Biosystems® TaqMan® Bacillus anthracis Detection Kit, based on a dual singleplex assay for pXO1 and pXO2, AmpliSens Bacillus anthracis-FRT based on the triplex detection of pagA, capA genes and an internal control, and RealArt Bacillus anthracis PCR from Arthus Biotech, based on the detection of lef and capA targets.

Apart from the commercially available kits there are many reports describing nucleic based methods to detect *B. anthracis*[3]. The majority of these are based on the detection of the mentioned virulent plasmid markers, but there are other non-plasmid targets described in the literature, including the chromosomal markers BA-5449[28], BA-5510[29], gyrA[30], rpoB[31] plcR[32] and AC-390[33] as well as variable number tandem repeats (VNTRs) present in an open reading frame[34]. Whilst these markers are useful for the identification of *B. anthracis*, they cannot be used to predict the virulence of the strain, as this is dependant on the presence of the virulence plasmids pXO1 and pXO2.

An electrochemical genosensor to detect the specific *B. anthracis* regulatory gene atxA was recently reported[35], based on the post-asymmetric amplification hybridisation of the target, with differential pulse voltammetric detection of the redox intercalator methylene blue. The LOD is higher than the one presented in this paper (1pM vs 1fM) and the amplification time is longer (132 min vs 90min), and whilst the method was useful for the identification of *B. anthracis*, it did not determine the presence of pXO1 and pXO2, and thus could not predict its virulence.

Another recent approach consisted of the isothermal real time recombinase polymerase amplification (RPA) of 4 different markers,the BA-5345 chromosomal marker, lef factor (pXO1), capA (pxO2) and adk marker from *B. cereus* group. The method has been used and validated in field achieving a LOD of 10 copies in less than 10 minutes, but requires 4 singleplex reactions, instead of a single one-pot multiplex reaction[36].

Our approach is significantly more facile than many of these reported approaches, being able to simultaneously but individually quantitatively detect each of the pXO1 and pXO2, at low femtomolar detection limits using duplex amplification and detection. The use of the tailed primers overcomes the need for the generation of ssDNA, which is not only laborious and costly, but significant and uncontrollable amounts of DNA are often lost whilst producing the ssDNA. The use of the Fc-dATP facilitates direct electrohemical detection of the tailed amplicon product, significantly simplifying the assay, and we are currently working on the use of isothermal amplification to further move this approach towards an effective platform, which can be deployed and used at the point-of-need/care.

4.5 CONCLUSIONS

We presented a novel duplex electrochemical genosensor for the simultaneous amplification and detection of 2 DNA sequences, i.e. two plasmid DNA markers involved in the virulence of *B. Anthracis*, CAP and PAG, in genomic DNA extracted from real samples. The main advantages of the method include the amplification of both targets in a single pot reaction and the direct hybridization and detection of the PCR product on an electrode microarray. The method overcomes some of the limitations of classic genosensors, including the need to generate ssDNA for hybridization purposes, thanks to the use of tailed primers, as well as the need for post-hybridization labelling methods, due to the use of ferrocene labelled dATP, the combination of both decreasing the number of steps required. We also studied the effect of electrolyte cations, anions and concentration on the ferrocene signal, and postulated that the enhancement in signal observed in the presence of divalent cations is due to their ability to condense, bend and shrink double stranded DNA, whilst shielding the electrostatic repulsions between neighbouring DNA strands, culminating in the ferrocenes being closer to the electrode surface, thus enhancing electron transfer. The method presented here is completely generic in nature and transferable to other targets for duplex or multiplex simultaneous detection of several DNA targets. In order to implement the use of tailed primers and **dA^{EFc}TP** for use at the point of need, we are currently exploring multiplex isothermal amplification combined with electrochemical detection using a handheld potentiostat.

ACKNOWLEDGMENTS

The authors gratefully acknowledge the financial support from Spanish Ministerio de Economía y Competitividad for CIGUASENSING BIO2017-87946-C2-1-R and SEASENSING BIO2014-56024-C2-1. The work was also supported by the Czech Academy of Sciences (Praemium Academiae to M.H.), and by the European Regional Development Fund; OP RDE (No. CZ.02.1.01/0.0/0.0/16_019/0000729 to M.H.).

4.6. REFERENCES

(1) WHO. Anthrax in Humans and Animals. *World Organ. Anim. Heal.* **2008**, 219.
(2) Mock, M. and Fouet, A. Anthrax. *Annu. Rev. Microbiol.* **2001**, *55*, 647–671.
(3) Rao, S. S.; Mohan, K. V. K.; Atreya, C. D. Detection Technologies for Bacillus Anthracis: Prospects and Challenges. *J. Microbiol. Methods* **2010**, *82*, 1–10.
(4) Straub, T.; Baird, C.; Bartholomew, R. A.; Colburn, H.; Seiner, D.; Victry, K.; Zhang, L.; Bruckner-Lea, C. J. Estimated Copy Number of Bacillus Anthracis Plasmids PXO1 and PXO2 Using Digital PCR. *J. Microbiol. Methods* **2013**, *92*, 9–10.
(5) Manzanares-palenzuela, C. L.; Martín-fernández, B.; López, M. S.; López-ruiz, B. Trends in Analytical Chemistry Electrochemical Genosensors as Innovative Tools for Detection of Genetically Modified Organisms. *Trends Anal. Chem.* **2015**, *66*, 19–31.

(6) Wang, J. Towards Genoelectronics: Electrochemical Biosensing of DNA Hybridization. *Chem. - A Eur. J.* **1999**, *5* (6), 1681–1685.
(7) Tosar, J. P.; Brañas, G.; Laíz, J. Electrochemical DNA Hybridization Sensors Applied to Real and Complex Biological Samples. *Biosens. Bioelectron.* **2010**, *26*, 1205–1217.
(8) Svobodová, M.; Pinto, A.; Nadal, P.; O'Sullivan, C. K. Comparison of Different Methods for Generation of Single-Stranded DNA for SELEX Processes. *Anal. Bioanal. Chem.* **2012**, *404*, 835–842.
(9) Jauset-Rubio, M.; Svobodová, M.; Mairal, T.; McNeil, C.; Keegan, N.; El-Shahawi, M. S.; Bashammakh, A. S.; Alyoubi, A. O.; O'Sullivan, C. K. Aptamer Lateral Flow Assays for Ultrasensitive Detection of β-Conglutin Combining Recombinase Polymerase Amplification and Tailed Primers. *Anal. Chem.* **2016**, *88*, 10701–10709.
(10) Jauset-Rubio, M.; Svobodová, M.; Mairal, T.; McNeil, C.; Keegan, N.; Saeed, A.; Abbas, M. N.; El-Shahawi, M. S.; Bashammakh, A. S.; Alyoubi, A. O.; et al. Ultrasensitive, Rapid and Inexpensive Detection of DNA Using Paper Based Lateral Flow Assay. *Sci. Rep.* **2016**, *6*, 37732.
(11) Jauset-Rubio, M.; Tomaso, H.; El-Shahawi, M. S.; Bashammakh, A. S.; Al-youbi, A. O.; O'Sullivan, C. K. Duplex Lateral Flow Assay for the Simultaneous Detection of Yersinia Pestis and Francisella Tularensis. *Anal. Chem.* **2018**, *90*, 12745–12751.
(12) Al-madhagi, S.; Joda, H.; Jauset-rubio, M.; Ortiz, M.; Katakis, I.; O'Sullivan, C. K. Isothermal Amplification Using Modi Fi Ed Primers for Rapid Electrochemical Analysis of Coeliac Disease Associated DQB1*02 HLA Allele. *Anal. Biochem.* **2018**, *556*, 16–22.
(13) Joda, H.; Beni, V.; Willems, A.; Frank, R.; Höth, J.; Lind, K.; Strömbom, L.; Katakis, I.; O'Sullivan, C. K. Modified Primers for Rapid and Direct Electrochemical Analysis of Coeliac Disease Associated HLA Alleles. *Biosens. Bioelectron.* **2015**, *73*, 64–70.
(14) Ferapontova, E. E. DNA Electrochemistry and Electrochemical Sensors for Nucleic Acids. *Annu. Rev. Anal. Chem.* **2018**, *11*, 197–218.
(15) Kerman, K.; Kobayashi, M.; Tamiya, E. Recent Trends in Electrochemical DNA Biosensor Technology. *Meas. Sci. Technol.* **2004**, *15*, R1-11.
(16) Brázdilová, P.; Vrábel, M.; Pohl, R.; Pivoňková, H.; Havran, L.; Hocek, M.; Fojta, M. Ferrocenylethynyl Derivatives of Nucleoside Triphosphates: Synthesis, Incorporation, Electrochemistry, and Bioanalytical Applications. *Chem. - A Eur. J.* **2007**, *13*, 9527–9533.
(17) Balintová, J.; Pohl, R.; Horáková, P.; Vidláková, P.; Havran, L.; Fojta, M.; Hocek, M. Anthraquinone as a Redox Label for DNA: Synthesis, Enzymatic Incorporation, and Electrochemistry of Anthraquinone-Modified Nucleosides, Nucleotides, and DNA. *Chem. - A Eur. J.* **2011**, *17*, 14063–14073.
(18) Balintová, J.; Plucnara, M.; Vidláková, P.; Pohl, R.; Havran, L.; Fojta, M.; Hocek, M. Benzofurazane as a New Redox Label for Electrochemical Detection of DNA: Towards Multipotential Redox Coding of DNA Bases. *Chem. - A Eur. J.* **2013**, *19*, 12720–12731.
(19) Ortiz, M.; Debela, A. M.; Svobodova, M.; Thorimbert, S.; Lesage, D.; Cole, R. B.; Hasenknopf, B.; O'Sullivan, C. K. PCR Incorporation of Polyoxometalate Modified Deoxynucleotide Triphosphates and Their Application in Molecular

Electrochemical Sensing of Yersinia Pestis. *Chem. - A Eur. J.* **2017**, *23*, 10597–10603.

(20) Wlassoff, W. A.; King, G. C. Ferrocene Conjugates of DUTP for Enzymatic Redox Labelling of DNA. *Nucleic Acids Res.* **2002**, *30* (12), e58.

(21) Kielkowski, P.; Fanfrlík, J.; Hocek, M. 7-Aryl-7-Deazaadenine 2'-Deoxyribonucleoside Triphosphates (DNTPs): Better Substrates for DNA Polymerases than DATP in Competitive Incorporations. *Angew. Chemie - Int. Ed.* **2014**, *53*, 7552–7555.

(22) Magriñá, I.; Toldrà, A.; Campàs, M.; Ortiz, M.; Simonova, A.; Katakis, I.; Hocek, M.; O'Sullivan, C. K. Electrochemical Genosensor for the Direct Detection of Tailed PCR Amplicons Incorporating Ferrocene Labelled DATP. *Biosens. Bioelectron.* **2019**, *134*, 76–82.

(23) Zhu, Z.; Waggoner, A. S. Molecular Mechanism Controlling the Incorporation of Fluorescent Nucleotides into DNA by PCR. *Cytometry* **1997**, *28* (3), 206–211.

(24) Tongu, C.; Kenmotsu, T.; Yoshikawa, Y.; Zinchenko, A. A.; Chen, N.; Yoshikawa, K. Competitive Effects of 2 + and 3 + Cations on DNA Compaction. 1–15.

(25) Rouzina, I.; Bloomfield, V. A. DNA Bending by Small , Mobile Multivalent Cations. *Biophys. J.* **1998**, *74*, 3152–3164.

(26) Springer, T.; Sípová, H.; Vaisocherová, H.; Stepánek, J.; Homola, J. Shielding Effect of Monovalent and Divalent Cations on Solid-Phase DNA Hybridization : Surface Plasmon Resonance Biosensor Study. *Nucleic Acids Res.* **2010**, *38* (20), 7343–7351.

(27) Auffinger, P.; Bielecki, L.; Westhof, E. Anion Binding to Nucleic Acids. *Structure* **2004**, *12*, 379–388.

(28) Volokhov, D.; Pomerantsev, A.; Kivovich, V.; Rasooly, A.; Chizhikov, V. Identification of Bacillus Anthracis by Multiprobe Microarray Hybridization. *Diagn. Microbiol. Infect. Dis.* **2004**, *49*, 163–171.

(29) Olsen, J. S.; Skogan, G.; Fykse, E. M.; Rawlinson, E. L.; Tomaso, H.; Granum, P. E.; Blatny, J. M. Genetic Distribution of 295 Bacillus Cereus Group Members Based on Adk-Screening in Combination with MLST (Multilocus Sequence Typing) Used for Validating a Primer Targeting a Chromosomal Locus in B. Anthracis. *J. Microbiol. Methods* **2007**, *71*, 265–274.

(30) Hurtle, W.; Bode, E.; Kulesh, D. A.; Kaplan, R. S.; Garrison, J.; Bridge, D.; House, M.; Frye, M. S.; Loveless, B.; Norwood, D. Detection of the Bacillus Anthracis GyrA Gene by Using a Minor Groove Binder Probe. *J. Clin. Microbiol.* **2004**, *42* (1), 179–185.

(31) Almeida, J. L.; Harper, B.; Cole, K. D. Bacillus Anthracis Spore Suspensions: Determination of Stability and Comparison of Enumeration Techniques. *J. Appl. Microbiol.* **2008**, *104*, 1442–1448.

(32) Gierczyński, R.; Zasada, A. A.; Raddadi, N.; Merabishvili, M.; Daffonchio, D.; Rastawicki, W.; Jagielski, M. Specific Bacillus Anthracis Identification by a PlcR-Targeted Restriction Site Insertion-PCR (RSI-PCR) Assay. *FEMS Microbiol. Lett.* **2007**, *272*, 55–59.

(33) Cherif, A.; Borin, S.; Rizzi, A.; Ouzari, H.; Boudabous, A.; Daffonchio, D. Characterization of a Repetitive Element Polymorphism-Polymerase Chain Reaction Chromosomal Marker That Discriminates Bacillus Anthracis from Related Species. *J. Appl. Microbiol.* **2002**, *93*, 456–462.

(34) Jackson, P. J.; Walthers, E. A.; Kalif, A. S.; Richmond, K. L.; Adair, D. M.; Hill, K. K.; Kuske, C. R.; Andersen, G. L.; Wilson, K. H.; Hugh-Jones, M. E.; et al. Characterization of the Variable-Number Tandem Repeats in VrrA from Different Bacillus Anthracis Isolates. *Appl. Environ. Microbiol.* **1997**, *63* (4), 1400–1405.

(35) Das, R.; Goel, A. K.; Sharma, M. K.; Upadhyay, S. Electrochemical DNA Sensor for Anthrax Toxin Activator Gene AtxA-Detection of PCR Amplicons. *Biosens. Bioelectron.* **2015**, *74*, 939–946.

(36) Bentahir, M.; Ambroise, J.; Delcorps, C.; Pilo, P.; Gala, J.-L. Sensitive and Specific Recombinase Polymerase Amplification Assays for Fast Screening, Detection, and Identification of Bacillus Anthracis in a Field Setting. *Appl. Environ. Microbiol.* **2018**, *84* (11), e00506-18.

(37) Matero, P.; Hemmilä, H.; Tomaso, H.; Piiparinen, H.; Rantakokko-Jalava, K.; Nuotio, L.; Nikkari, S. Rapid Field Detection Assays for Bacillus Anthracis, Brucella Spp., Francisella Tularensis and Yersinia Pestis. *Clin. Microbiol. Infect.* **2011**, *17*, 34–43.

(38) Skottman, T.; Piiparinen, H.; Hyytiäinen, H.; Myllys, V.; Skurnik, M.; Nikkari, S. Simultaneous Real-Time PCR Detection of Bacillus Anthracis , Francisella Tularensis and Yersinia Pestis. *Eur. J. Clin. Microbiol. Infect. Dis.* **2006**, *26*, 207–211.

(39) del Río, J. S.; Svobodova, M.; Bustos, P.; Conejeros, P.; O'Sullivan, C. K. Electrochemical Detection of Piscirickettsia Salmonis Genomic DNA from Salmon Samples Using Solid-Phase Recombinase Polymerase Amplification. *Anal. Bioanal. Chem.* **2016**, *408*, 8611–8620.

4.7 SUPPLEMENTARY INFORMATION

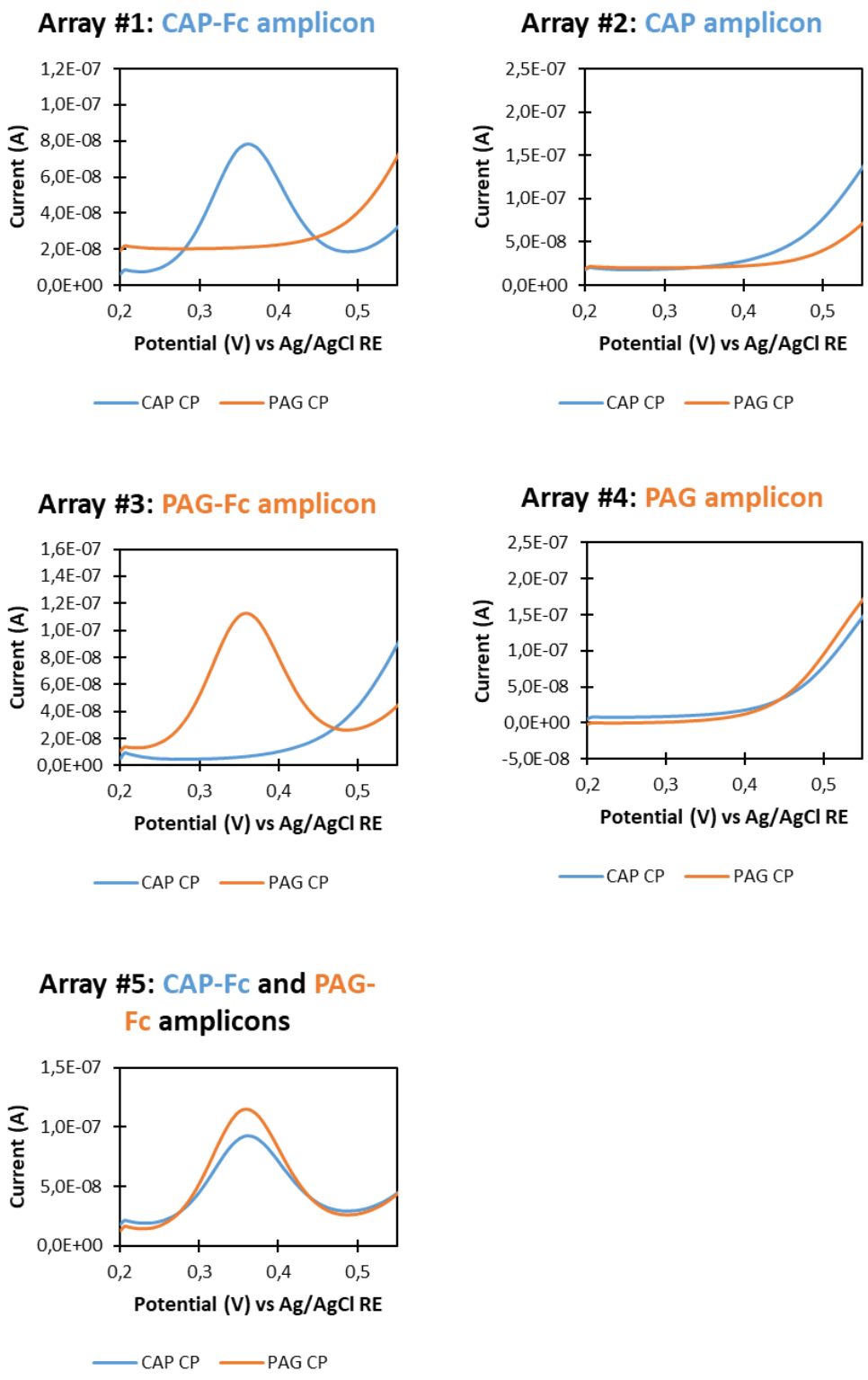

Figure S4.1. Raw voltammograms obtained from electrodes arrays incubated with different PCR products: #1. CAP-Fc, #2. CAP, #3. PAG-Fc, #4. PAG, #5. CAP-Fc + PAG-Fc.

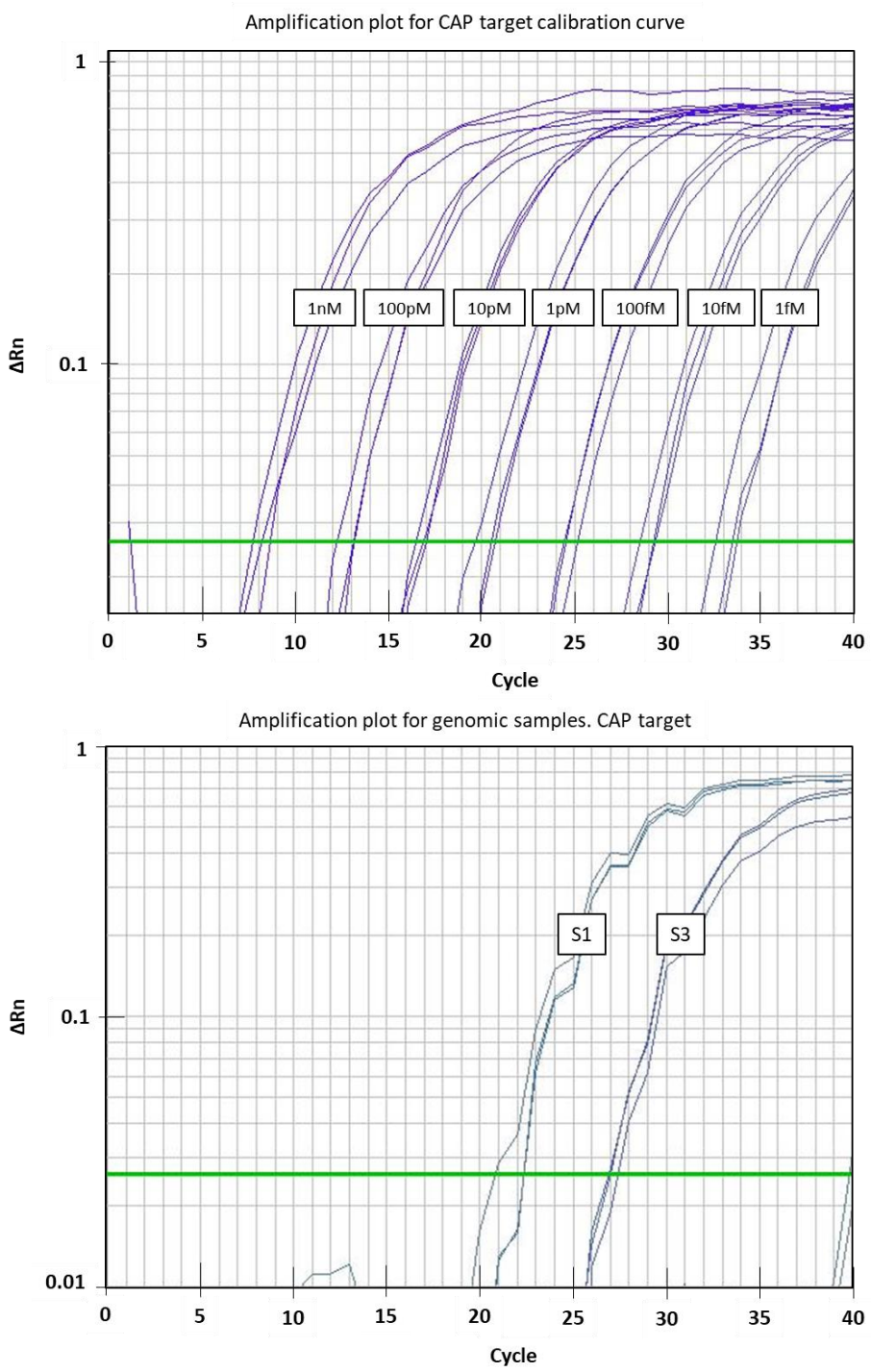

Figure S4.2. Amplification plot for CAP target calibration curve and genomic samples. Threshold: 0,026

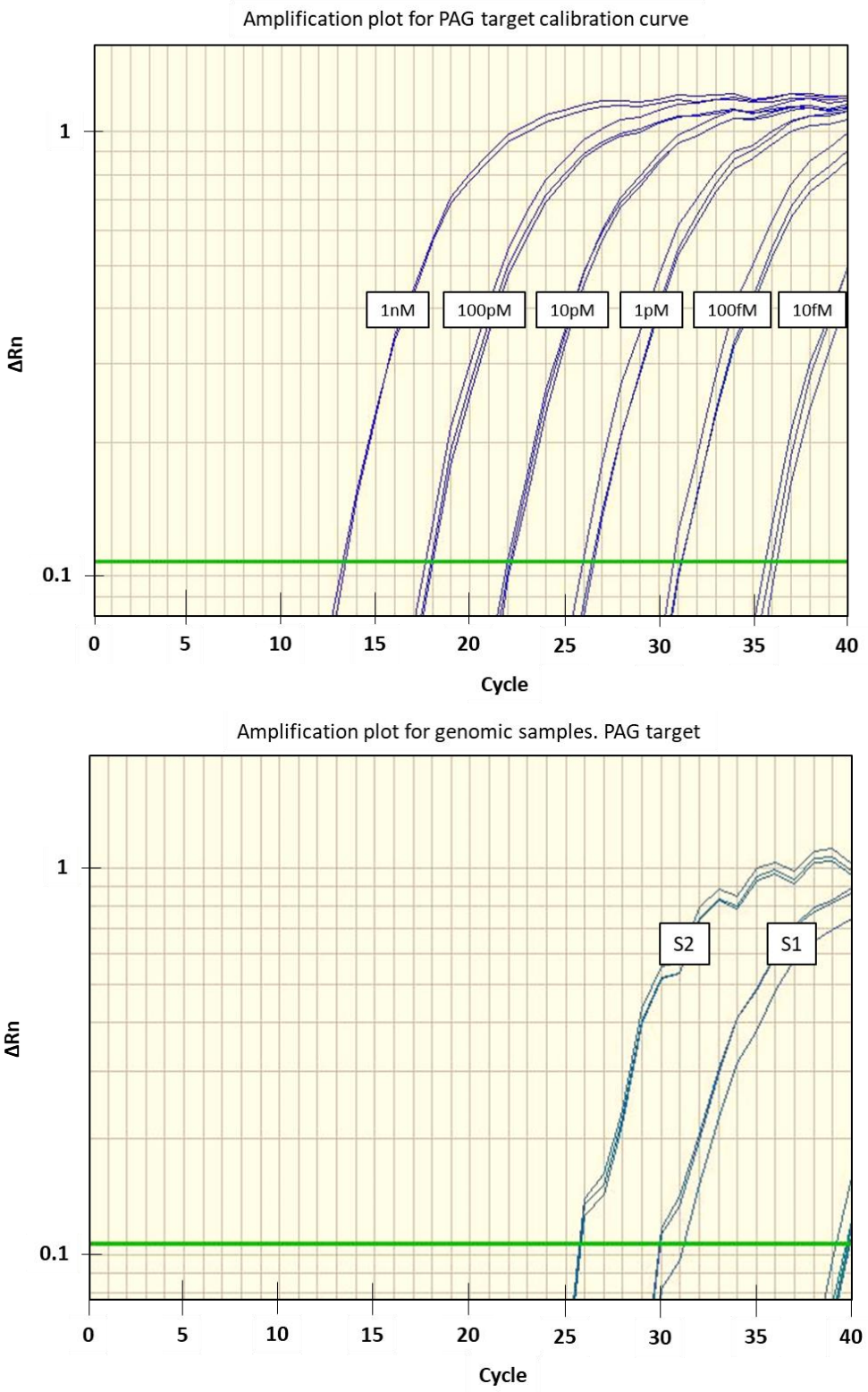

Figure S4.3. Amplification plot for CAP target calibration curve and genomic samples. Threshold: 0,1

UNIVERSITAT ROVIRA I VIRGILI
DEVELOPMENT OF ELECTROCHEMICAL DNA SENSORS BASED ON THE INCORPORATION OF FERROCENE LABELLED DATP
Ivan Magriñá Lobato

CHAPTER 5

Controlling DNA Monolayer Structure Through Electrostatics

Controlling DNA Monolayer Structure Through Electrostatics

Ivan Magriñá,[1] Mayreli Ortiz,[1] Ana Simonova,[2] Ioanis Katakis,[1] Michal Hocek,[2,3] Ciara O'Sullivan,*[1,4] and Robert Forster,*[5]

1 Departament d'Enginyeria Química, Universitat Rovira i Virgili, 26 Països Catalans, 43007 Tarragona, Spain
2 Institute of Organic Chemistry and Biochemistry of the Czech Academy of Sciences, Flemingovo nám. 2, CZ-16610, Prague, Czech Republic
3 Department of Organic Chemistry, Faculty of Science, Charles University in Prague, Hlavova 8, CZ-12843, Prague 2, Czech Republic
4 Institució Catalana de Recerca i Estudis Avançats, Passeig Lluís Companys, 23, 08010 Barcelona, Spain
5 School of Chemical Sciences, FutureNeuro SFI Research Centre, National Centre for Sensor Research, Dublin City University, Dublin 9, Ireland.

5.1 ABSTRACT

The ability to induce concertina movement in a DNA monolayer by changing the local charge distribution is demonstrated. A 153-mer target DNA was amplified using ethynyl ferrocene dATP and a tailed forward primer resulting in a duplex with a single stranded DNA tail for hybridization to a surface-tethered probe. A thiolated probe containing the sequence complementary to the tail as well as a 15 polythimine vertical spacer with a $(CH_3)_6$ spacer was immobilized on the surface of a gold electrode and hybridized to the redox modified complementary strand. Potential step chronoamperometry and cyclic voltammetry were used to probe the potential of zero charge, PZC, and the rate of heterogeneous electron transfer between the electrode and the immobilized ferrocene moieties. Chronoamperometry indicates that each strand contains ferrocene units located at different distances over a range of approximately 13 Å giving three, well resolved, exponential current-time decays. Significantly, the apparent standard heterogeneous electron transfer rate constant, k^o, observed depends on the initial potential, i.e., the rate of electron transfer at zero driving force is not the same for oxidation and reduction of the ferrocene labels. Moreover, the presence of ions, such as Sr^{3+}, that strongly ion pair with the negatively charged DNA back bone modulate the electron transfer rate significantly. Specifically, k^o is 57.7±3.5 s-1 and 3.2±0.2 s^{-1} for reduction and oxidation, respectively where the Sr^{2+} concentration is 10 mM but the corresponding values in 1M Sr^{2+} are 1.1±0.07 s^{-1} and 17.7±1.2 s^{-1}. These results are consistent with a model in which a low Sr^{2+} concentration and an initial potential that is negative of the PZC, leads to electrostatic repulsion of the negatively charged DNA backbone and the negatively charged electrode leading to the DNA adopting an extended configuration (concertina open) resulting in a slow rate of heterogeneous electron transfer. In contrast, for ferrocene reduction, the initial potential is positive of PZC and the negatively charged DNA is electrostatically attracted to the electrode (concertina closed) giving a shorter electron transfer distance and a higher rate of heterogeneous electron transfer. When the Sr^{2+} concentration is high, the charge on the DNA backbone is charge compensated

by the electrolyte and the charge on the electrode dominates the electron transfer dynamics and the opposite potential dependence is observed. These results open up the possibility of electro-mechanical switching using DNA super structures.

5.2 INTRODUCTION

The use of redox labelled DNA and dNTPs has been studied and exploited [1], and it has been demonstrated that dsDNA has an intrinsic ability to mediate long range electron transfer (ET) along its base pair stack [2] when redox indicators are intercalated into the DNA [3]. No significant drop in the currents are observed for distances up to 50Å [3] with tunneling through the much shorter σ-bonded linker to the electrode surface being the rate-limiting step [4]. This ability can be blocked by a single base pair mismatch, DNA lesions or DNA conformational perturbations, and this phenomena has in fact been exploited for the detection of DNA mismatches and the monitoring of protein/DNA interactions [5].

Long distance DNA mediated electron transfer has been reported for redox indicators covalently bound to DNA through a conjugated ethylene linker. Examples include ethylene anthraquinone or ethylene tetramethylpiperidine 1-oxyl (TEMPO) redox labels that show large electrochemical signals and are very sensitive to DNA base pair mismatches. On the other hand, when alkyl anthraquinone or ethylendiamine TEMPO probes were used, weak and non-sensitive to DNA mismatches signals were observed, attributed to direct surface charge transfer [6]. However, other reports suggest that the conjugation of the redox probe to DNA through short unsaturated linkers in some cases is not enough to provide electronic coupling between the redox probe and the dsDNA base pair π-stack required for the DNA-mediated ET. As an alternative ET could be achieved through an electronic wire formed by $Ru(NH_3)_6^{3+}$ molecules electrostatically bound to the DNA duplex phosphate backbone [7]. Interestingly, this mechanism was only observed for anthraquinone conjugated via acetylene linker but was not observed when an alkanethiol linker was used. Apart from DNA mediated or molecular wire assisted ET, direct contact of the redox indicator with the electrode surface can also facilitate ET. Nevertheless, double stranded DNA (dsDNA) is stiffer and more rigid than single stranded DNA (ssDNA) and tends to orientate perpendicularly or tilted from the electrode surface to minimize electrostatic repulsion between the negatively charged phosphate backbone between neighboring DNA strands, which propels the redox labels away from the electrode surface. Indeed, this property has been exploited in a specific genosensor design, where an immobilized ssDNA capture probe bearing a redox label is flexible enough to reach the electrode surface and undergo ET, whilst following hybridization with its complementary target, the duplex formed is rigid, moving the redox label away from the electrode surface, thus preventing direct electron transfer [8].

Despite the rigidity of the dsDNA duplex and its tendency to be oriented perpendicularly or slightly tilted from the surface, dsDNA can also approach the electrode surface to facilitate direct electron transfer via different mechanisms, including:

a) DNA motion due to free rotation of the duplex around a linker [9]
b) DNA orientation driven by an external potential [10]
c) DNA bending and compression mediated by multivalent cations [11,12] and
d) electrostatic repulsion shielding mediated by divalent cations [13–15]

Even when the negative charge of DNA is shielded using specific electrolytes, the DNA layer structure is still susceptible to the effect of external potentials. AFM measurements demonstrated that the DNA monolayer thickness can be reversibly modulated by an external potential that induces the DNA duplex to be either lying flat down on the surface or standing straight up [10]. Indeed, this phenomena has been exploited to develop a method based on potential pulses to reduce electrostatic repulsions and enhance hybridization with high density capture probes [16].
DNA is a polyelectrolyte with a high density of negative charges located along the phosphate backbone. In the absence of counterions, the electrostatic repulsive energy between two 10-bp complementary strands would be around 60kcal/mol whereas the DNA base paring and stacking energy is substantially lower, around 1-3 kcal/mol. Theoretical calculations indicate that the ion atmosphere surrounding DNA enormously shields this electrostatic repulsion between DNA strands enabling double helix formation, and this effect is more significant for divalent cations than for monovalent cations [17]. In fact, Mg^{2+} has a higher affinity for DNA than Na^{+} and in a background of 20 mM Na^{+}, only ~0.5 mM Mg^{2+} is needed to replace half of the Na^{+} ions in the ion atmosphere of a DNA duplex [18]. This is further supported by the increased efficiency of Mg^{2+} stabilization of duplex DNA on solid supports, where significantly higher hybridization is observed with 15mM Mg^{2+} as compared to 1M Na^{+} [15].
The presence of multivalent cations such as Ca^{+2}, Mg^{2+}, putrescine^{2+}, spermidine^{3+}, spermine^{4+} and cobalt(III)hexamine has been reported to decrease the persistent length of dsDNA and there are experimental evidences that dsDNA bends in presence of multivalent cations. Models suggest that multivalent cations bind to the major groove of the DNA releasing the sodium counter-ions from the neighboring phosphates which promotes a major groove collapse towards the cationic ligand. The bending angle produced by the multivalent cations depends on the charge density and the size of the cation bound to the major groove and is predicted to be large (20-40º) and smooth [11]. Another model suggests that divalent cations are also able to pull cytosine bases partially out from the helical stack in the major grooves to interact with the π-system [12]. On the other hand, divalent cations such as Mg^{2+} are routinely used to create highly packed DNA films on solid supports because Mg^{2+} not only shields the electrostatic repulsion between complementary strands but also the repulsion between neighboring strands [5]. In the presence of Mg^{2+}, surface coverages of ~40 pmol/cm^2 of close packed DNA have been reported [13], whilst in the in the absence of Mg^{2+} surface coverages of ~12 pmol/ cm^2 are reported [14].
In summary, multivalent cations appear to play an important role in the development of DNA electrochemical sensors by enhancing the hybridization efficiencies, shielding

electrostatic repulsions and bending the dsDNA to facilitate direct electron transfer from the redox labels to the electrode surface.

In the work reported herein, we study the electron transfer associated with ethynyl ferrocene incorporated into duplex DNA by amplification of labelled dNTPs. A tailed forward primer affords a PCR amplicon with a ssDNA tail, which is used to hybridize to a complementary surface-immobilized probe (Figure 5.1). Whilst the ferrocene label is tethered to DNA through an ethynyl linker, long distance DNA mediated electron transfer is not anticipated as the amplicon incorporates a C3 spacer discontinuity and the capture probe contains a 15 poly thymine ssDNA vertical spacer. The effect of the divalent cation Sr^{2+} concentration on the thermodynamic and kinetics of electron rate constant by cyclic voltammetry as well as the effect of the initial potential, and hence DNA conformation, on the apparent rate constant was studied.

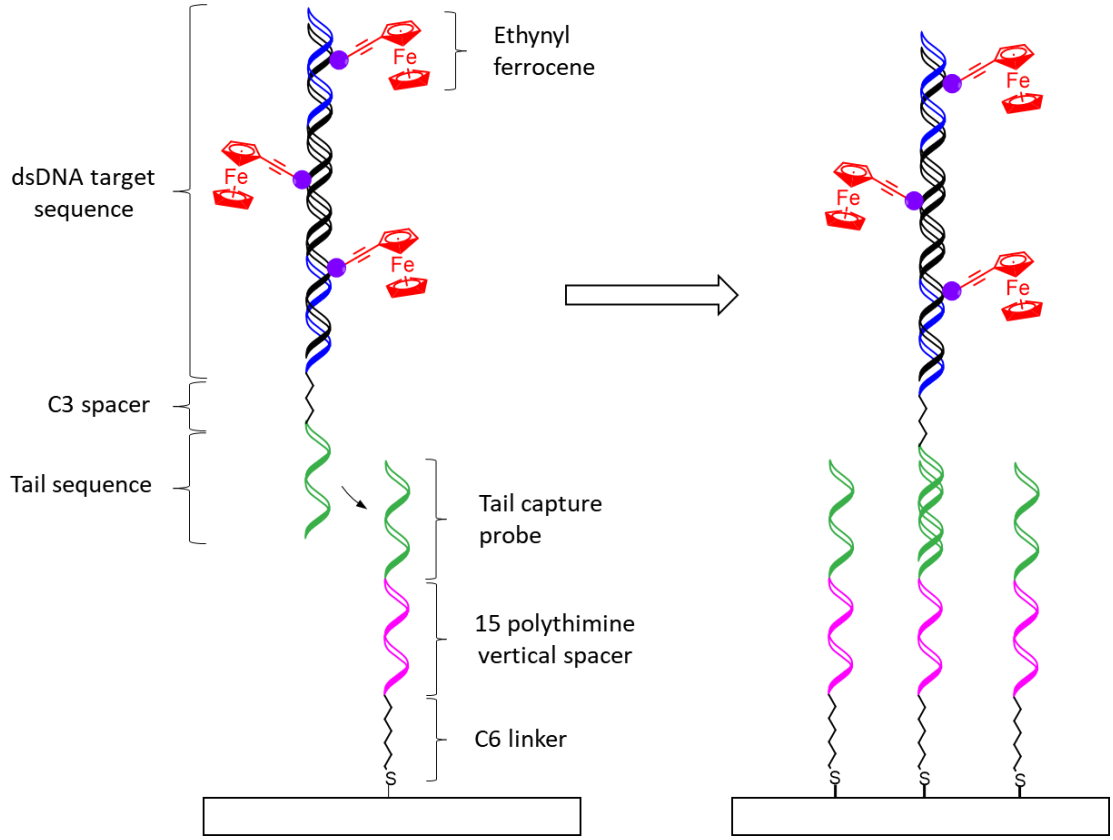

Figure 5.1. Schematic description of the oligo complex formed on the electrode surface.

5.3 MATERIALS AND METHODS

Reagents and Materials.

KOD XL polymerase was purchased from Merck Millipore (Madrid, Spain), synthetic oligonucleotides obtained from Biomers (Ulm, Germany) (Table 5.1), natural dNTPs from ThermoFisher Scientific (Barcelona, Spain) and DNA free water provided by Fisher Bioreagents. $dA^{EFc}TP$ was synthesized and characterized and synthesized following the Sonogashira reaction, as previously described [19].

Electrode arrays were fabricated using soda-lime glass slides from Sigma-Aldrich (Spain), three-millimeter thick polymethylmethacrylate (PMMA) from La Indústria de la Goma (Tarragona, Spain) and double adhesive gasket ARSeal 90880 from Adhesive Research (Ireland).
All other reagents were obtained from Sigma-Aldrich S.A. (Barcelona, Spain) and used as received. High purity deionized water (18MΩ cm^{-1}) produced with a Milli-Q RG system (Millipore Ibérica, Spain) was used throughout. As a model system, amplification and detection of the toxic dinoflagellate *Karlodinium armiger* was used.

Table 5.1. List of oligonucleotide sequences and modifications.

Oligo	Sequence
Karlodinium armiger Forward Primer with tail (FwP-T)	5'-att acg acg aac tca atg aa – C3 – ata gct tca cag cag agg tta caa c-3'
Karlodinium armiger Reverse Primer (RevP)	5'-aca cac atc caa cca tYt cac tg-3'
Karlodinium armiger target (KA)	5'-ata gct tca cag cag agg tta caa cac caa tgc tgc tcc gct acc cgc gat ctc atg cac cag gga gcg gca aga agc cag agc ttc aag aca ccc cta ccc ccg tgc agg agc tca caa aga aag ttc aca gtg aga tgg ttg gat gtg tgt-3'
Karlodinium armiger thiolated capture probe (CP)	5'- ttc att gag ttc gtc gta att ttt ttt ttt ttt tt-3'-C6-SH

Y represents the wobble C+T.

Polymerase Chain Reaction Conditions

DNA amplicons were produced by PCR in a T100 thermal cycler (Biorad) using the following protocol: 40 cycles at 95ºC for 30 seconds, 60ºC for 30 seconds, and 72ºC for 45 seconds, with a final elongation step at 72ºC for 5 minutes. The reaction mixture had 0.1 units of KOD XL, KOD XL buffer 1X, 199 nM of each primer (Karlo FwP-T and Karlo RvP), dGTP, dCTP, dTTP at 200 µM, dATP at 140 µM, dAEFcTP (60 µM) and KA target (1nM).

Electrode functionalisation with capture probe

Gold electrode arrays were fabricated on a soda-lime glass substrate, as previously described [20]. The array consisted of 3 circular working electrodes and 1 rectangular reference electrode with 1 mm^2 and 4 mm^2 surface area, respectively. To functionalize the working electrodes, the electrode array was cleaned using Milli-Q water and a commercial soap (Vajillas Super, from Sosmi S.A. Spain), rinsed with Milli-Q water and then dried with N_2. Thiolated capture probe (1 µL) solution was placed on each working electrode and incubated overnight at 22ºC in a humidity saturated chamber. The capture probe solution contained 1 µM capture probe (KA CP), 100 µM mercaptohexanol and 1 M KH_2PO_4. Following functionalization, the array was rinsed with Milli-Q and dried with N_2.

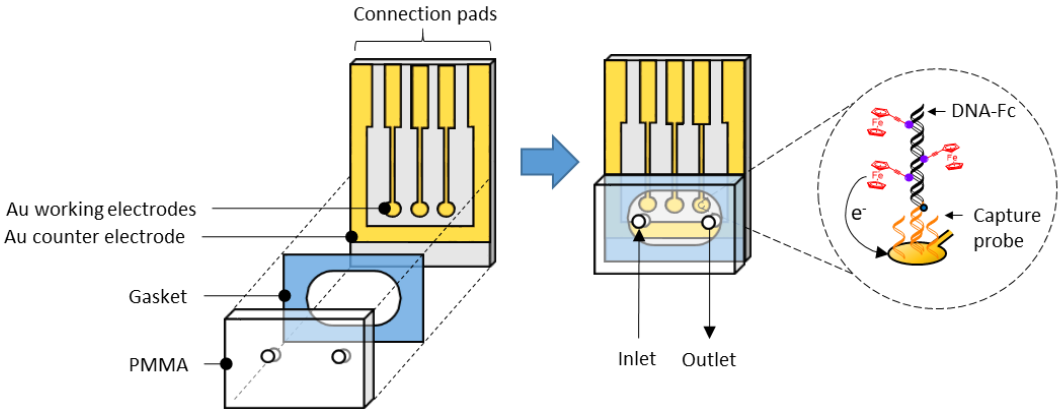

Figure 5.2. Schematic of electrode array showing the configuration and modification of the working electrode.

Microfluidic fabrication and mounting

As illustrated in Figure 5.2, a 7 µL microfluidic chamber was constructed using a PMMA cover sealed to the electrode array using a double adhesive gasket, and thus defining the area of the working and the counter electrodes. To complete the electrochemical cell, an external Ag/AgCl reference electrode was placed in the droplet formed on top of the PMMA when 100 µL of the electrolyte solution was added to the microfluidic chamber.

Amplicon hybridization on electrode arrays

Following PCR, 7 µL of the PCR product was injected into the microfluidic chamber and hybridization took place at 22ºC in a humidity saturated chamber for 30 minutes. The microfluidic chamber was then flushed 3 times with 200 µL of PBS Tween-20 and 200 µL of PBS. Prior to electrochemical measurements, the PBS solution was replaced with 200 µL of $Sr(NO_3)_2$ solution.

Electrochemical measurements

For cyclic voltammetry experiments, a PBSTAT 12 Autolab potentiostat/galvanostat and Nova 2.1.3 software were used. A pre-conditioning potential of 0 V was applied for 5 seconds and then cyclic staircase voltammetry was applied from 0V to 0.600 V using 10mV step at scan rates between 100 and 500-1000 mV s^{-1}. For short timescale experiments (< 250 µs), a custom built programmable function generator-potentiostat

was used. This instrument had a rise time of less than 10 ns and was used to apply potential steps of variable pulsewidth and amplitude directly to a two-electrode cell. A large area Pt foil and a reference electrode were combined to form a counter electrode. The foil lowered the resistance and provided a high frequency path. The current to voltage converter was based on a Comlinear CLC 203 AI operational amplifier with a 1500 Ω feedback resistance and a response time of less than 10 ns. The chronoamperograms were recorded using a HP54201A digital oscilloscope in 64X time-average mode. Cell time constants were extracted by fitting the i(t) vs. t responses to (multi-)exponential decays using software routines written in Microsoft Excel.

5.4 RESULTS AND DISCUSSION

Cyclic Voltammetry. Cyclic voltammetry can provide deep insights into the local microenvironment of the ferrocene moieties through the formal potentials and the dynamics of electron transfer across the electrode/monolayer as described by the standard heterogeneous electron transfer rate constant, $k^{o'}$. Here, a 153bp PCR amplicon containing ferrocene labelled deoxyadenosine and a single stranded DNA tail was hybridized to an electrode immobilized probe, which was complementary to the ssDNA tail. The ferrocene centers are located at discrete sites throughout the duplex, giving rise to different electron transfer distances that will affect their individual $k^{o'}$ values. Depending on the DNA surface coverage and the ferrocene loading, there may also be stabilizing or destabilizing lateral interactions. Using the formal potential, $E^{o'}$ and peak widths, cyclic voltammetry can provide insights into the thermodynamics and kinetics of electron transfer especially by varying the scan rate. These effects are likely to be influenced by the electrostatic charge on the DNA monolayer, the electrolyte concentration and the cation identity since the cations can associate with the negatively charged DNA. In particular, polyvalent ions can significantly change the secondary structure of the DNA, e.g., in solution they can convert linear strands into a tightly packed, circumferentially wound torus[21]. In monolayers, as well as these intra-molecular interactions, the close proximity of the adsorbates can lead to interactions between adjacent strands.

Figure 5.3 shows the voltammetric responses obtained for the DNA duplexes using 10 mM and 1000 mM $Sr(NO_3)_2$ as supporting electrolyte. The scan rates were 100 mV s^{-1}, 500 mV s^{-1} and 1000 mV s^{-1}. For both electrolyte concentrations, well defined peaks are observed corresponding to the oxidation and re-reduction of the bound ferrocenes. However, the peaks are significantly better defined in the more concentrated electrolyte and more ideally reflect the Gaussian response expected for surface confined electroactive species. The DNA surface coverage can be determined from the CV data. Assuming that in presence of $Sr(NO_3)_2$ 1000 M and with a low scan rate (100 mV/s), all ferrocene centers are electroactive, the charge passed under the CV wave gives a surface coverage of 3.5×10^{12} ferrocenes·cm^{-2} or 5.8×10^{-12} mol·cm^{-2}. Taking into account the flexibility of the C6 linker, the 15T vertical spacer and the C3 spacer and assuming a radius of gyration equal to the length of the fully extended hybridized DNA ($5{,}9 \cdot 10^{-8}$ m for a 153bp duplex), significant lateral interactions between

neighboring hybridized DNA molecules might be expected. The peak shape and full width at half of the peak maximum height (FWHM) can give insights into these lateral interactions within the monolayer. One electron reversible reactions with Nernstian behavior show a FWHM of 90.6 mV. For these systems, FWHM were 100-110 mV for the oxidation peak and 110-160 mV for the reduction peak for both electrolyte concentrations used. FWHM values higher than 90.6/n mV (where n=number of electrons transferred) may suggest weak (<6.7 kJ mol^{-1}) repulsive electrostatic lateral interactions between neighboring DNA strands. Another reason for the high FWHM values could be different formal potentials for the individual ferrocene centers distributed along the DNA strand due to different electrostatic environments

The formal potentials at 10 mM and 1000 mM are 321±1 mV and 288±7 mV, i.e., a shift of 33±7 mV for a 100 fold change in the electrolyte concentration. For a strongly ion paired system, or where Donnan potential effects are dominant[22], one would expect a 59 mV per decade change in the electrolyte concentration. Here, the formal potential is insensitive to the concentration of the supporting electrolyte suggesting that charge compensating ions are freely available within the monolayer and that the ferrocenium cation does not ion pair significantly with the charge compensating counterion, nitrate. Moreover, taking into account the surface coverage of the ferrocene centers, even at an electrolyte concentration of 10 mM, sufficient charge compensating ions could diffuse within less than 0.5 ms, i.e., approximately 2000 times faster than the highest scan rate employed here. Thus, it appears that neither the availability or the mass transport of charge compensating counterions controls the rate of redox switching in this system. Rather, electron transfer to/from the remote ferrocenium/ferrocene centers appears to control the rate.

The apparent standard heterogeneous electron transfer rate constant, $k^{o'}_{app}$, was determined by fitting the experimental CV data to a finite-diffusion model. The formal potential, $E^{o'}$, and surface coverage were measured using slow scan rate voltammetry to ensure equilibrium conditions. In fitting the model to the experimental CV response, the average $k^{o'}_{app}$ was the only freely adjustable variable. The rate constant was systematically varied to minimize the summed square of the residuals between the experimental and theoretical currents. As shown in Figure 5.3, satisfactory agreement is obtained between the theoretical and experimental responses and Table 5.2 details the apparent rate constants as a function of the electrolyte concentration and the scan rate.

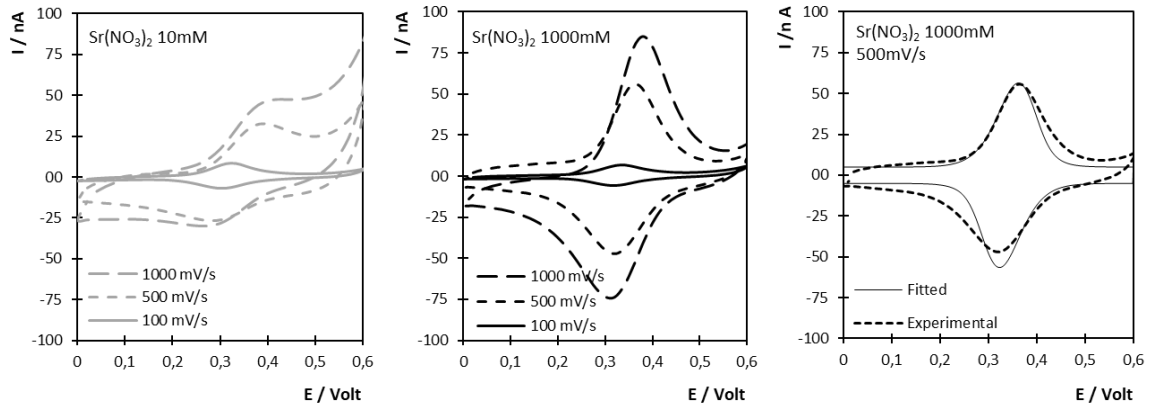

Figure 5.3. Cyclic voltammograms of target DNA hybridized on the electrode where the supporting electrolyte is 10 mM and 1000mM $Sr(NO_3)_2$. The scan rates are 100, 500

and 1000mV/s and an example of the best fit voltammogram obtained using a $k^{o'}_{app}$ value of 17.2 s^{-1} is shown.

Table 5.2. Dependence of the Apparent Standard Heterogeneous Electron Transfer Rate Constants, $k^{o'}_{app}$, and Peak-to peak Separation on Scan Rate and $Sr(NO_3)_2$ concentration.

	E_o-E_r /mV		$k^{o'}_{app}$ / s^{-1}	
Scan rate / mV s^{-1}	**10 mM $Sr(NO_3)_2$**	**1000 mM $Sr(NO_3)_2$**	**10 mM $Sr(NO_3)_2$**	**1000 mM $Sr(NO_3)_2$**
1000	93±12	60±10	10.9±1.1	19.7±2.1
500	84±10	40±10	6.4±0.7	17.2±2.0
100	50±10	10±10	2.5±0.3	12.5±1.3

For both electrolyte concentrations, the apparent rate constant is larger for higher scan rates. This behavior arises because ferrocenes located closer to the electrode surface, that have a higher rate of heterogeneous electron transfer, dominate the CV response at shorter timescales (faster scan rates). Significantly, for the more concentrated electrolyte solution, the $k^{o'}_{app}$ is approximately 2-3 fold higher for all scan rates investigated. Given that neither the availability or movement of electrolyte ions appears to control the redox switching rate, this result suggests that the average electron transfer distance is shorter for the higher electrolyte concentration. This behavior could arise due to more efficient screening of the negative charge on the DNA backbone by the higher electrolyte concentration allowing it to approach the electrode surface more closely. However, cyclic voltammetry is limited since the DNA conformation could change as the applied potential is scanned. Additionally, it is challenging to extract detailed kinetic information, especially with respect to the effect of the initial potential, and hence DNA conformation, on the apparent rate constant.

Interfacial Capacitance. One of the key issues to understanding the role of electrostatics is to determine the charge on the electrode surface. At the Potential of Zero Charge, PZC, there is no excess charge at the interface while it will be negatively or positively charged at applied potentials that are more negative or positive than the PZC, respectively. It is known that the adsorption of a monolayer at the electrode/solution interface alters the double layer structure and consequently changes the double layer capacitance, C_{dl}. The potential dependence of C_{dl} can be used to determine the potential of zero charge. Here, the capacitance was measured using small-amplitude potential step chronoamperometry. In these experiments, the potential was stepped from an initial value, E_i, with a pulse amplitude of 25mV, and the current response recorded from microsecond and longer time scales. Successive measurements were performed, increasing the E_i monotonically by 25 mV from 0.000 V to 0.700 V. The pulse amplitude is sufficiently small to allow the measured capacitance to be regarded as an approximate differential capacitance. For potentials far from the ferrocene $E^{o'}$, the step does not cause any change in the redox composition of the film, double layer charging dominates the response and the current decays according to a single-exponential decay. For potential steps close to the

ferrocene Eº', there are two time-resolved decays, that correspond to the double-layer charging and the faradaic reaction, respectively. The relatively slow rate of heterogeneous electron transfer, coupled with a short electrode response time, allow these processes to be resolved and fitting the early time data yields information about the resistance, R, and capacitance, C_{dl}.

The resistance and the double-layer capacitance at each potential was determined using Equation (1), where ΔE is the pulse amplitude, 25mV.

$$i_c = \frac{\Delta E}{R} e^{\frac{-t}{R \cdot C_{dl}}} \quad (1)$$

Figure 5.4 shows the potential dependence of C_{dl} for both the pristine gold electrode and following modification with the DNA-Ferrocene monolayer. The double layer capacitance is lower for the DNA modified electrode, which is consistent with the formation of a layer with a dielectric constant lower than water being formed at the interface, as well as ion displacement. Significantly, for both the modified and pristine electrodes, a local minimum in the C_{dl} is observed which is better defined for the DNA coated electrode. This minimum represents the PZC where there is no excess charge on the electrode. DNA layer formation induces a shift on PZC, from approximately 415 mV to 275 mV. This behavior is consistent with the adsorption of negatively charged molecules (i.e. DNA) at the electrode solution interface.

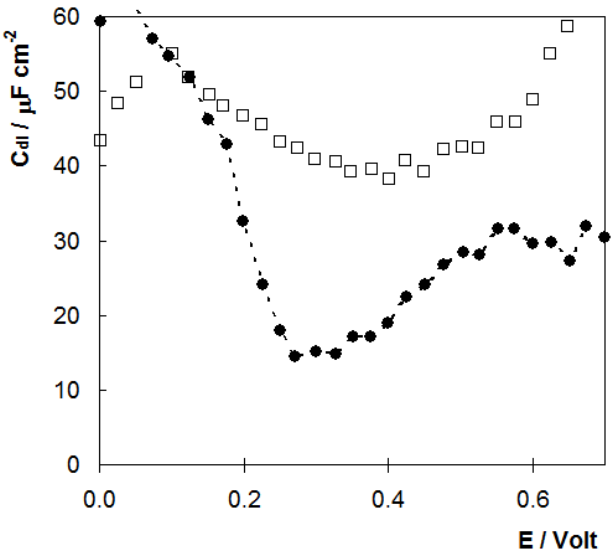

Figure 5.4. Dependence of the double layer capacitance, C_{dl}, on the applied potential. Data for a pristine gold electrode □ and following modification with a DNA-Fc duplex •. The electrolyte is 10 mM $Sr(NO_3)_2$ (pH 6.5).

Significantly, the formal potential of the ferrocene/ferrocenium couple, 321±1 mV and 288±7 mV for 10 or 1000mM $Sr(NO_3)_2$ respectively, is similar to the PZC which means that the electrode is negatively charged when the monolayer is in the reduced, ferrocene, state and positively charged when the film is oxidized to ferrocenium. Thus, one might expect electrostatic repulsion of the ferrocenium sites by the electrode.

However, the DNA backbone is negatively charged and its electrostatic interaction with the electrode will depend on the electrolyte concentration since a high electrolyte concentration will tend to screen the charge.

Potential Step Chronoamperometry. The effect of the electrode-film electrostatic interactions, as controlled by the initial potential and electrolyte concentration, on the electron transfer dynamics were probed using chronoamperometry. For an ideal electrochemical reaction involving a surface tethered species, the Faradaic current following a potential step that changes the redox composition exhibits a single exponential decay in time. For the ferrocene modified DNA monolayers considered here, a more complex response is anticipated because the redox centers are located at different distances from the electrode surface.

Figure 5.5 illustrates the effect of changing the initial potential on the chronoamperometry transients observed for the oxidation of the ferrocene centers (main figure) ($Fc - e^- \rightarrow Fc^+$) and the reduction (inset) of the ferrocenium centers ($Fc^+ + e^- \rightarrow Fc$), where the supporting electrolyte is 10 mM $Sr(NO_3)_2$ (pH 6.5). The uncompensated resistance is less than 500 Ω, which, in conjunction with the capacitance data shown in Figure 5.5, gives cell response times (product of resistance and capacitance) between 30 and 300 μs, i.e., at least 150 times shorter than the time constants for heterogeneous electron transfer. For ferrocenes linked to 20mer dsDNA film, the heterogeneous electron transfer rate constant is typically between 115 and 25 s^{-1} [23]. The dashed line, which represents the best fit to a single exponential decay, clearly fails to adequately model the experimental data, i.e., the experimental response deviates significantly from that expected for an ideal surface confined species. Ohmic drop can distort chronoamperometry responses since the flow of Faradaic and charging currents through a solution generates a potential that acts to weaken the applied potential by an amount iRu, where i is the total current. This ohmic drop can lead to severe distortions of experimental responses resulting in inaccurate measurements of the heterogeneous electron transfer rate. As illustrated in Figure 5.5, the Faradaic currents that flow in these chronoamperometry experiments are typically in the microampere range. Given that the uncompensated resistance is less than 500 Ω, an iRu drop of less than 5 mV is expected, which has a negligible impact on the current-time transients and does not explain the non-ideal behavior observed.

The response can be accurately modelled using a triple exponential decay:

$$i_F(t) = A\, k1\, Q \exp(-k1\, t) + B\, k2\, Q \exp(-k2\, t) + (1-A-B)\, k3\, Q \exp(-k3\, t) \quad (2)$$

where A and B are the fractions of the total charge passed, Q, for each of the electron transfer processes characterized by the three first order rate constants, k1, k2 and k3.

In fitting the experimental responses, the fraction of each species and its associated rate are freely adjustable parameters (open circles in Figure 5.5). The observation that more than one rate constant is required is not surprising given that there are ferrocene centers along the duplex that lead to different electron transfer distances and hence different heterogeneous electron transfer rate constants. The individual rate constants and population fractions are given in Table 5.3.

Table 5.3. Dependence of the rate constants extracted from chronoamperometry transients by fitting a triple exponential decay on the overpotential and $Sr(NO_3)_2$ concentration as supporting electrolyte. The fractional populations of each decay component are in brackets.

Electrolyte	Overpotential / V	k1 / s^{-1}	k2 /s^{-1}	k3 / s^{-1}
10 mM	-0.05	116±9.4 (0.55)	45±3.8 (0.30)	8±0.6 (0.15)
10 mM	0.046	8±0.6 (0.50)	2±0.2 (0.30)	0.7±0.6 (0.20)
1000 mM	-0.052	3±0.2 (0.60)	1±0.1 (0.24)	0.2±0.013 (0.16)
1000 mM	0.056	78±6.7 (0.65)	10±0.8 (0.20)	6±0.43 (0.15)

For DNA[24], the distance dependent electron tunneling parameter, α, is typically 0.2 $Å^{-1}$. Significantly, irrespective of the electrolyte concentration or the direction of the potential step, the difference between the fastest and slowest rate constants suggests that the electroactive ferrocene centers are distributed over 13.3±0.4Å, i.e., approximately four bases.

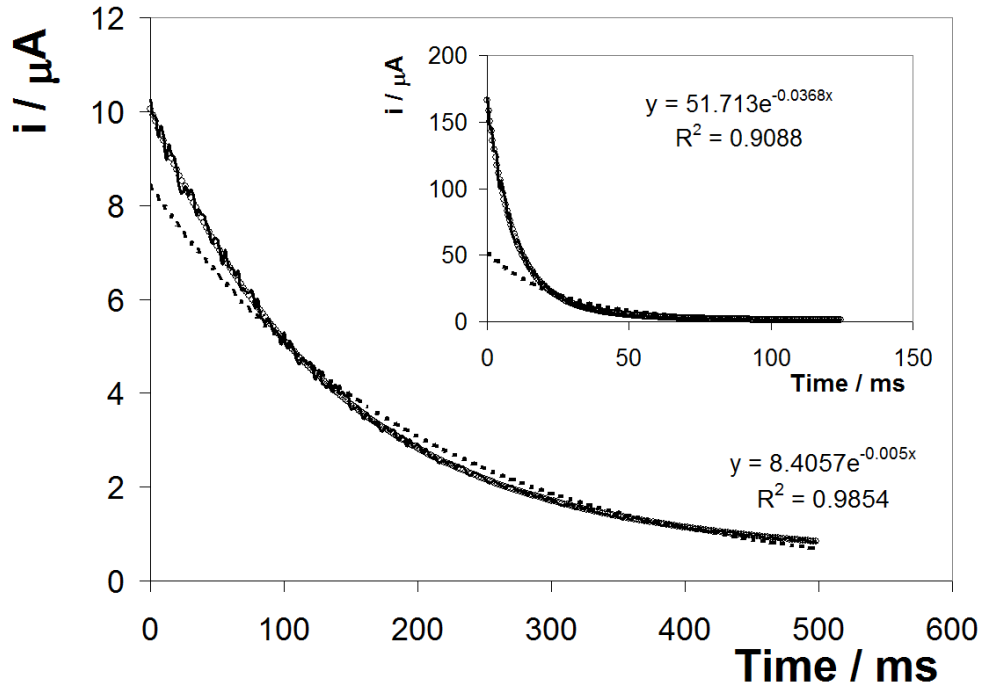

Figure 5.5. Current-time transients for the ferrocene containing DNA monolayer where the supporting electrolyte is 10 mM $Sr(NO_3)_2$ (pH 6.5). The main figure shows the response where the overpotential is +0.046 V (step triggers ferrocene oxidation), while the inset is where the overpotential is -0.05 V (step triggers ferrocenium reduction). The solid line represents the experimental response while the dashed line and open circles represent the best fit to a single a triple exponential decays, respectively.

The most striking feature of Figure 5.5 is that despite the absolute value of the overpotentials being indistinguishable in the two experiments, the rates of electron transfer depend on whether the monolayer is being reduced (highest k^o 117±7 s^{-1}) or oxidized (highest k^o 7.5±0.4 s^{-1}). Significantly, as shown in Figure 5.4, the PZC for the

monolayer, 275 mV, is very similar to the formal potential of the ferrocene couple, 321±1 mV and 288±7 mV for 10 or 1000mM $Sr(NO_3)_2$ respectively. Thus, prior to the potential step triggering oxidation of the ferrocene, Fc, to ferrocenium, Fc^+, the electrode is negatively charged. When the concentration of the supporting electrolyte is low (10 mM), significant charge repulsion between the negatively charged DNA backbone and the negatively electrode causes the DNA to adopt an extended configuration, increasing the average electron transfer distances and giving rise to a smaller rates of electron transfer. In contrast, for the reduction step, the electrode is initially poised positive of the PZC causing the negatively charged DNA to compress or concertina, bringing the ferrocenium centers closer to the electrode surface, leading to a higher rate of heterogeneous electron transfer.

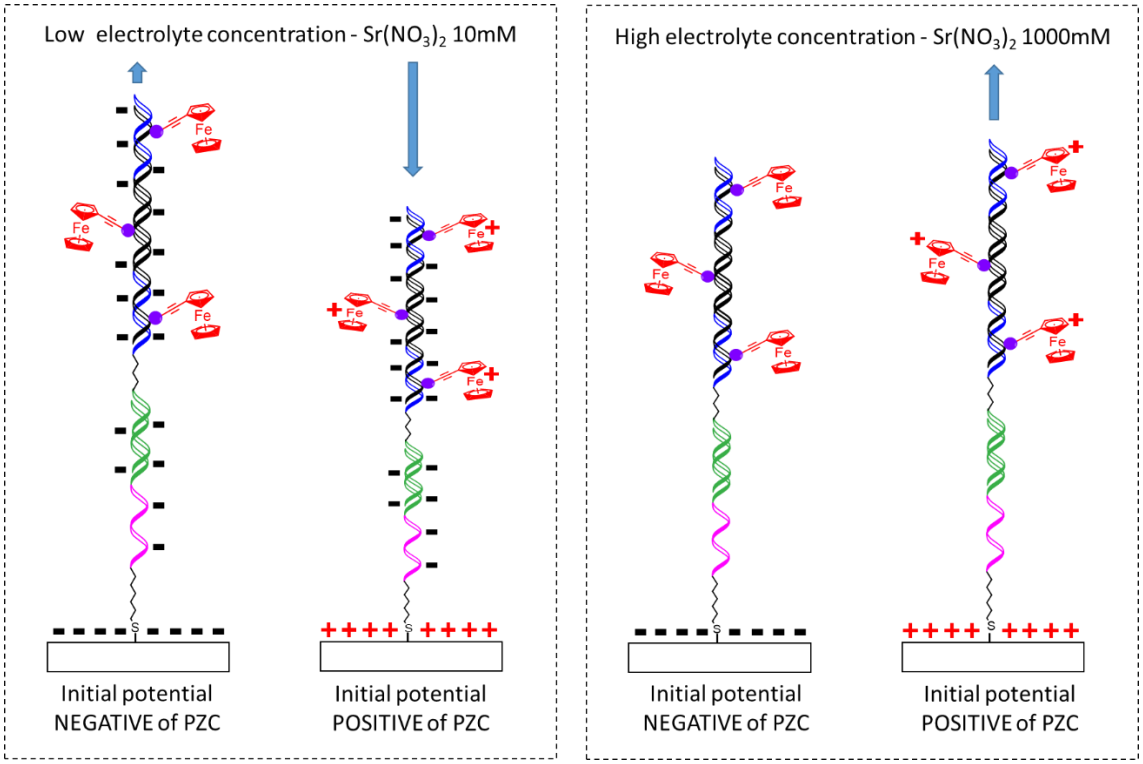

Figure 6. Schematic representation of the impact of the electrode potential on the extent of DNA compression where the concentration of supporting electrolyte is low and high.

The electrolyte concentration could influence the secondary structure of the DNA monolayer by shielding the charge present on the backbone. Figure 5.7 shows transients observed under similar conditions to Figure 5.5, except that the concentration of $Sr(NO_3)_2$ has been increased to 1000 mM. Increasing the electrolyte concentration does not significantly change the general features of the responses observed and the responses are well modelled by a triple exponential decay. However, the effect of the initial potential is significantly different. In the high concentration electrolyte, the state of charge of the ferrocene centers influences the response significantly. Specifically, in contrast to the 10 mM electrolyte data, the rate of heterogeneous electron transfer for the reduction is *lower* than that observed for oxidation. This behavior arises because the high Sr^{2+} concentration neutralizes or screens the charge present on the DNA backbone making the DNA secondary structure

more sensitive to the charge on the redox centers. At high electrolyte concentrations, when the initial potential is positive of $E^{o'}$, the positively charged ferrocenium centers are electrostatically repelled by the positively charged electrode and the rate of heterogeneous electron transfer for reduction is low. In contrast, for the oxidation reaction, the ferrocene centers are uncharged and can approach the electrode surface more closely giving a faster rate of heterogeneous electron transfer.

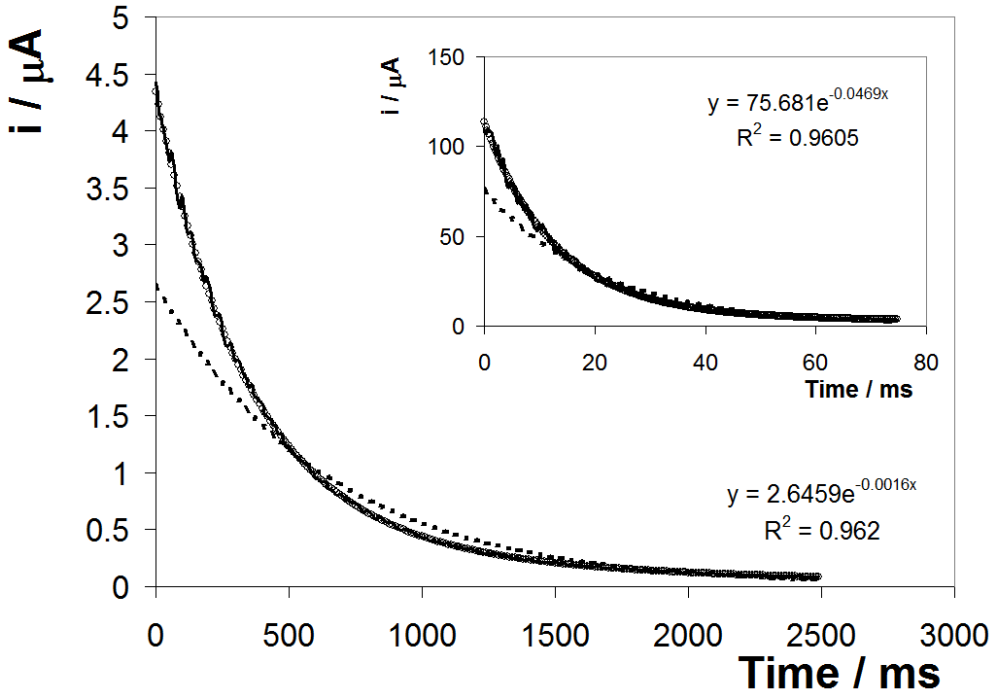

Figure 5.7. Current-time transients for the ferrocene containing DNA monolayer where the supporting electrolyte is 1000 mM $Sr(NO_3)_2$ (pH 6.5). The main figure shows the response where the overpotential is -0.052 V (step triggers ferrocenium reduction), while the inset is where the overpotential is +0.056 V (step triggers ferrocene oxidation). The solid line represents the experimental response while the dashed line and open circles represent the best fit to a single a triple exponential decays, respectively.

Potential Dependence of k. One of the great advantages of using chronoamperometry is that the redox composition of the ferrocene centers can be changed abruptly. This means that the response is not influenced by potential induced changes, e.g., changes in the electron transfer distance as a function of the applied potential, which can occur when the potential is scanned in CV. Moreover, the driving force for electron transfer can be systematically varied by changing the overpotential. Figure 5.8 illustrates Tafel plots of ln k vs. overpotential, η, where the supporting electrolyte is either 10 mM or 1000 mM $Sr(NO_3)_2$ at pH 6.5. As discussed above, the decay of the current over time following a step that changes the redox state of the ferrocene centers follows a multi-exponential model. For simplicity, only the fastest rate constant is considered here. Figure 5.8 shows that ln k depends approximately linearly on $|\eta|$ for values up to approximately 300 mV. This behavior is consistent with the Butler-Volmer formulation of electrode kinetics with the slopes being equal to $-\alpha_c nF/RT$ and $(1-\alpha_a)nF/RT$, for the

reduction and oxidation processes, where α_c and α_a are the cathodic and anodic transfer coefficients, respectively. In 10 mM electrolyte the Tafel slopes yield α_c and α_a values of 0.48±0.06 and 0.47±0.05, respectively. In 1000 mM electrolyte, while the transfer coefficients sum to unity, the α_c (0.61±0.06) and α_a (0.38±0.05) are statistically different from those expected for an ideal reversible reaction, 0.5, suggesting that the barrier to electron transfer is not symmetrical.

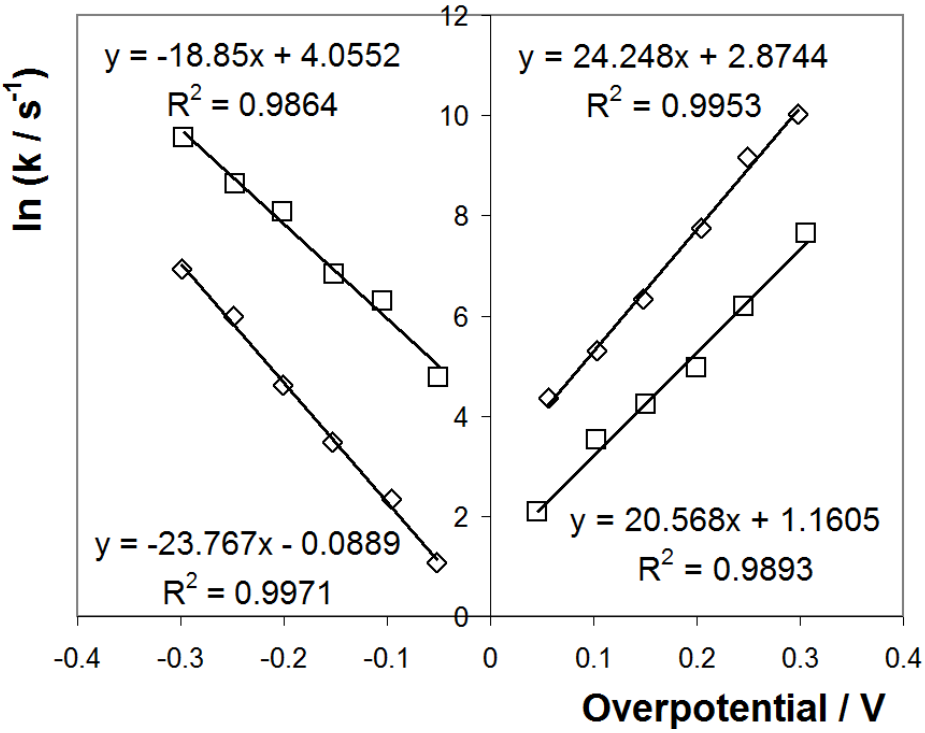

Figure 5.8. Dependence of the highest apparent rate constant on the overpotential. The supporting electrolyte is 10 mM $Sr(NO_3)_2$ □ or 1000 mM $Sr(NO_3)_2$ ◇. Error bars are smaller than, or comparable to, the size of the symbols.

As illustrated in Figure 5.8, specifying the overpotential with respect to the formal potential determined using cyclic voltammetry gives rate constants that are not equal for zero overpotential. Figure 5.8 shows that in 10 mM $Sr(NO_3)_2$ electrolyte, for $|\eta| = 0$, 'standard' heterogeneous electron transfer rate constants of 57.7±3.5 s^{-1} and 3.2±0.2 s^{-1} were obtained for reduction and oxidation of the redox centers within the monolayer, respectively. In 1 M electrolyte the corresponding values are 1.1±0.07 s^{-1} and 17.7±1.2 s^{-1}. The difference in apparent "standard" rate constants reflects the differences in the structure (electron transfer distance) that depends on the initial potential applied and the electrolyte concentration since these parameters control the electrostatic interactions of the DNA and the electrode.

Effect of DNA Coverage. It is important to probe the effect of the DNA surface coverage on the apparent electron transfer rates since inter-strand interactions could significantly influence the behavior observed. Here, the DNA coverage was reduced by diluting the deposition solution to 0.2 µM while keeping the deposition time the same. On the basis of square wave voltammetry, these conditions reduced the surface

coverage of the ferrocene-DNA by approximately 60%. Table 5.4 shows that irrespective of the electrolyte concentration, the rate constants obtained at high and low DNA coverage are indistinguishable. While the significant charge on the DNA is likely to keep them well separated as they are immobilized, it is important to acknowledge that the lower coverage may reflect the formation of DNA islands in which the local surface coverage is independent of the total number of molecules of DNA immobilized. However, the results obtained are consistent with lateral interactions between adjacent DNA strands not being important in controlling the rate of heterogeneous electron transfer.

Table 5.4. Effect of the DNA surface coverage on the rate constants determined using chronoamperometry. The fractional populations of each decay component are in brackets.

Electrolyte	Overpotential / V	k1 / s^{-1}	k2 s^{-1}	k3 s^{-1}
10 mM (high Γ)	-0.05	116±9(0.55)	45±3 (0.30)	8±0.7 (0.15)
10 mM (low Γ)	-0.05	105±8 (0.60)	55±4 (0.20)	10±0.6 (0.20)
10 mM (high Γ)	0.046	8±0.6 (0.50)	2±0.1 (0.30)	0.7±0.05 (0.20)
10 mM (low Γ)	0.048	11±0.9(0.60)	4±0.3 (0.20)	1.2±0.1 (0.20)
1000 mM (high Γ)	-0.052	3±0.2 (0.60)	1±0.1 (0.24)	0.2±0.015 (0.16)
1000 mM (low Γ)	-0.048	2.2±0.1 (0.50)	0.8±0.06 (0.3)	0.15±0.01 (0.20)
1000 mM (high Γ)	0.056	78±7 (0.65)	10±0.9 (0.20)	6±0.4 (0.15)
1000 mM (low Γ)	0.058	85±7 (0.65)	12±0.9 (0.15)	8±0.5 (0.20)

5.5 CONCLUSIONS

Direct labelling of DNA with ethynyl ferrocene moieties represents an attractive system for understanding the influence of electrostatic interactions between the underlying electrode and the DNA. Our data suggest a direct electron transfer mechanism from ferrocene centers to the electrode surface influenced by electrostatics in which the electrolyte concentration and the initial potential of the electrode affect the DNA layer apparent thickness and thus the apparent rate constant measured. It has been also observed that an increase in the $Sr(NO_3)_2$ concentration produce an increase in the apparent rate constant suggesting a closer distance from the ferrocene centers to the electrode surface due to compression and/or to a better screening of the electrostatic barrier on the electrode surface. Additionally, it has been also observed that for $Sr(NO_3)_2$ 10mM, electrostatic repulsion between the electrode and the dsDNA backbone predominates, while for $Sr(NO_3)_2$ 1M, DNA phosphate

backbone is better screened and the repulsion between the ferrocenium centers and the electrode surface predominates instead.
In summary, we demonstrated that electrolyte composition, concentration and initial potential are key parameters to control the DNA layer at the electrode surface to enable electron transfer.

ACKNOWLEDGEMENTS. This publication has emanated from research supported in part by a research grant from Science Foundation Ireland (SFI) under Grant Number 16/RC/3948 and co-funded under the European Regional Development Fund and by FutureNeuro industry partners. The work was also supported from Spanish Ministerio de Economía y Competitividad for CIGUASENSING BIO2017-87946-C2-1-R and SEASENSING BIO2014-56024-C2-1.

5.6 REFERENCES

(1) Hocek, M.; Fojta, M. Nucleobase Modification as Redox DNA Labelling for Electrochemical Detection. *Chem. Soc. Rev.* **2011**, *40* (12), 5802.
(2) Liu, T.; Barton, J. K. DNA Electrochemistry through the Base Pairs Not the Sugar - Phosphate Backbone. **2005**, 10160–10161.
(3) Kelley, S. O.; Jackson, N. M.; Hill, M. G.; Barton, J. K. Long-Range Electron Transfer through DNA Films. *Angew. Chem. Int.* **1999**, *38*, 941–945.
(4) Drummond, T. G.; Hill, M. G.; Barton, J. K. Electron Transfer Rates in DNA Films as a Function of Tether Length. **2004**, 15010–15011.
(5) Gorodetsky, A. A.; Buzzeo, M. C.; Barton, J. K. DNA-Mediated Electrochemistry. *Bioconjug Chem* **2008**, *19* (12), 2285–2296.
(6) Gorodetsky, A. A.; Green, O.; Yavin, E.; Barton, J. K. Coupling into the Base Pair Stack Is Necessary for DNA-Mediated Electrochemistry. *Bioconjug. Chem.* **2007**, *18* (5), 1434–1441.
(7) Abi, A.; Ferapontova, E. E. Unmediated by DNA Electron Transfer in Redox-Labeled DNA Duplexes End-Tethered to Gold Electrodes. *J. Am. Chem. Soc.* **2012**, *134*, 14499–14507.
(8) Mearns, F. J.; Wong, E. L. S.; Short, K.; Hibbert, D. B.; Gooding, J. J. DNA Biosensor Concepts Based on a Change in the DNA Persistence Length upon Hybridization. *Electroanalysis* **2006**, *18* (19–20), 1971–1981.
(9) Anne, A.; Demaille, C. Electron Transport by Molecular Motion of Redox-DNA Strands: Unexpectedly Slow Rotational Dynamics of 20-Mer Ds-DNA Chains End-Grafted onto Surfaces via C6 Linkers. *J. Am. Chem. Soc.* **2008**, *130* (30), 9812–9823.
(10) Kelley, S. O.; Barton, J. K.; Jackson, N. M.; McPherson, L. D.; Potter, A. B.; Spain, E. M.; Allen, M. J.; Hill, M. G. Orienting DNA Helices on Gold Using Applied Electric Fields. *Langmuir* **1998**, *14* (24), 6781–6784.
(11) Rouzina, I.; Bloomfield, V. A. DNA Bending by Small , Mobile Multivalent Cations. *Biophys. J.* **1998**, *74*, 3152–3164.
(12) Mcfail-isom, L.; Shui, X.; Williams, L. D. New Concepts in Biochemistry Divalent Cations Stabilize Unstacked Conformations of DNA and RNA by Interacting with

Base Π Systems. **1998**, *37* (49).

(13) Kelley, S. O.; Barton, J. K.; Jackson, N. M.; Hill, M. G. Electrochemistry of Methylene Blue Bound to a DNA-Modified Electrode. *Bioconjug. Chem.* **1997**, *8* (1), 31–37.

(14) Boon, E. M.; Salas, J. E.; Barton, J. K. An Electrical Probe of Protein-DNA Interactions on DNA-Modified Surfaces. *Nat. Biotechnol.* **2002**, *20* (3), 282–286.

(15) Springer, T.; Sípová, H.; Vaisocherová, H.; Stepánek, J.; Homola, J. Shielding Effect of Monovalent and Divalent Cations on Solid-Phase DNA Hybridization : Surface Plasmon Resonance Biosensor Study. *Nucleic Acids Res.* **2010**, *38* (20), 7343–7351.

(16) Tymoczko, J.; Schuhmann, W.; Gebala, M. Electrical Potential-Assisted DNA Hybridization. How to Mitigate Electrostatics for Surface DNA Hybridization. **2014**.

(17) Lipfert, J.; Doniach, S.; Das, R.; Herschlag, D. *Understanding Nucleic Acid – Ion Interactions*; 2015.

(18) Bai, Y.; Greenfeld, M.; Travers, K. J.; Chu, V. B.; Lipfert, J.; Doniach, S.; Herschlag, D. Quantitative and Comprehensive Decomposition of the Ion Atmosphere around Nucleic Acids. *J. Am. Chem. Soc.* **2007**, *129* (48), 14981–14988.

(19) Brázdilová, P.; Vrábel, M.; Pohl, R.; Pivoňková, H.; Havran, L.; Hocek, M.; Fojta, M. Ferrocenylethynyl Derivatives of Nucleoside Triphosphates: Synthesis, Incorporation, Electrochemistry, and Bioanalytical Applications. *Chem. - A Eur. J.* **2007**, *13*, 9527–9533.

(20) Magriñá, I.; Toldrà, A.; Campàs, M.; Ortiz, M.; Simonova, A.; Katakis, I.; Hocek, M.; O'Sullivan, C. K. Electrochemical Genosensor for the Direct Detection of Tailed PCR Amplicons Incorporating Ferrocene Labelled DATP. *Biosens. Bioelectron.* **2019**, *134* (January), 76–82.

(21) Gelbart, W. M.; Bruinsma, R. F.; Pincus, P. A.; Adrian Parsegian, V. DNA-Inspired Electrostatics. *Phys. Today* **2000**, *53* (9), 38–44.

(22) Ohki, S.; Ohshima, H. Donnan Potential and Surface Potential of a Charged Membrane. *Electrochem. Soc. Ext. Abstr.* **1985**, *85–1* (5), 645.

(23) Long, Y. T.; Li, C. Z.; Sutherland, T. C.; Chahma, M.; Lee, J. S.; Kraatz, H. B. A Comparison of Electron-Transfer Rates of Ferrocenoyl-Linked DNA. *J. Am. Chem. Soc.* **2003**, *125* (29), 8724–8725.

(24) Beratan, D. N. Why Are DNA and Protein Electron Transfer So Different? *Annu. Rev. Phys. Chem.* **2019**, *70* (1), 71–97.

CHAPTER 6

Tuning of Oxidation Potential of Ferrocene for Ratiometric Redox Labelling and Coding of Nucleotides and DNA

Tuning of Oxidation Potential of Ferrocene for Ratiometric Redox Labelling and Coding of Nucleotides and DNA

Anna Simonova,[1,2] Ivan Magriñá,[3] Veronika Sýkorová,[1] Radek Pohl,[1] Mayreli Ortiz,[3] Luděk Havran,[4] Miroslav Fojta,[4,5]* Ciara O'Sullivan,[3,6]* and Michal Hocek[1,2]*

[1] Institute of Organic Chemistry and Biochemistry, Academy of Sciences of the Czech Republic, Gilead & IOCB Research Centre, Flemingovo namesti 2, CZ-16610 Prague 6, Czech Republic
[2] Department of Organic Chemistry, Faculty of Science, Charles University in Prague, Hlavova 8, Prague-2 12843, Czech Republic.
[3] Departament d'Enginyeria Química, Universitat Rovira i Virgili, 26 Països Catalans, 43007, Tarragona, Spain
[4] Institute of Biophysics, Czech Academy of Sciences, Královopolská 135, 612 65 Brno, Czech Republic
[5] Central European Institute of Technology, Masaryk University, Kamenice 753/5, 625 00 Brno, Czech Republic
[6] Institució Catalana de Recerca i Estudis Avançats, Passeig Lluís Companys, 23, 08010, Barcelona, Spain

6.1 ABSTRACT

Three sets of 7-deazaadenine and cytosine nucleosides and nucleoside triphosphates bearing either unsubstituted ferrocene, octamethylferrocene and ferrocenecarboxamide linked through an alkyne tether to position 7 or 5, respectively, were designed and synthesized. The modified **dN^{FcX}TP**s were good substrates for KOD XL DNA polymerase in primer extension and were used for enzymatic synthesis of redox-labelled DNA probes. Square-wave voltammetry showed that the octamethylferrocene oxidation potential was shifted to lower values, whilst the ferrocenecarboxamide was shifted to higher potentials, as compared to ferrocene. Tailed PEX products containing different ratios of Fc-labelled A (**dA^{Fc}**) and FcPa-labelled C (**dC^{FcPa}**) were synthesized and hybridized with capture oligonucleotides immobilized on gold electrodes to study the electrochemistry of the redox-labelled DNA. Clearly distinguishable, fully orthogonal and ratiometric peaks were observed for the **dA^{Fc}** and **dC^{FcPa}** bases in DNA, demonstrating their potential for use in redox coding of nucleobases and for the direct electrochemical measurement of the relative ratio of nucleobases in an unknown sequence of DNA.

6.2 INTRODUCTION

Redox labelling of DNA bases by attachment of some oxidisable or reducible groups is used for diverse applications in bioanalysis and diagnostics[1,2]. The redox active group can be attached to 2'-deoxyribonucleoside triphosphate (dNTP) and used for polymerase mediated synthesis of redox-labelled DNA for subsequent electrochemical detection[2] with further possible applications for construction of electrochemical genosensors[3]. By using a combination of several orthogonal redox labels with differing redox potentials, an attractive option of redox coding of DNA bases[4] can be envisaged for applications in sequencing. Previously, we and others have reported the use of nitrophenyl[5], anthraquinone[4,6], benzofurazane[7] and azidophenyl[8] as reducible labels, some of which (combination of nitrophenyl with either benzofurazane or azidophenyl) were orthogonal and suitable for ratiometric redox coding of two bases, but none of the organic oxidizable labels, i.e. aminophenyl[5], methylene blue[4,9], methoxyphenol[10], or phenothiazines[4,11], was truly ideal and orthogonal for combination with another label(s). Ferrocene is a classical electrochemical standard[12] that has been used as an oxidizable electrochemical label for nucleotides and DNA[13,14] and has been exploited in sensors[3]. In order to develop a set of fully orthogonal oxidizable redox labels for the use in redox coding, herein we report the fine tuning of the oxidation potential of ferrocene by its substitution with electron-donating or electron-withdrawing substituents.

6.3 RESULTS AND DISCUSSION

Synthesis

In our design of modified ferrocene labels, we envisaged that multiple methylation of ferrocene, as in octamethylferrocene, can be used as electron-donating substituents to decrease the redox potential, whereas a substitution with an electron-withdrawing carboxamide should increase the oxidation potential. To easily synthesise the modified ferrocene-linked nucleosides and nucleotides through direct aqueous-phase Sonogashira cross-coupling reactions[15], we designed the corresponding terminal alkynes: 1-ethynyl-1',2,2',3,3',4,4',5-octamethylferrocene (**FcMe**)[16], and propargylaminocarbonylferrocene (**FcPa**)[17] as suitable building blocks and prepared them as previously reported.

The modified ferrocene-linked nucleosides were synthesized by Sonogashira cross-coupling reactions of unprotected halogenated nucleosides (dA^I or dC^I) in the presence of $Pd(PPh_3)_2Cl_2$ or $Pd(OAc)_2$ catalyst, PPh_3 or TPPTS (triphenylphosphine-3,3',3''-trisulfonate) ligand, CuI and Et_3N either in MeCN/water or in DMF to give labelled nucleosides dN^{FcMe} or dN^{FcPa} in high yields (Table 6.1, Scheme 6.1).

Table 6.1. Synthesis of nucleosides and dNTPs bearing acetylene-linked ferrocene labels.

Starting compound	Reagent	Catalyst	Solvent	Base	Product	Yield (%)
dA^{I}	**FcMe**	$Pd(OAc)_2$, CuI, TPPTS	MeCN/H_2O (1/1)	Et_3N	**dA^{FcMe}**	90
dC^{I}					**dC^{FcMe}**	86
dA^{I}	**FcPa**	$Pd(PPh_3)_2Cl_2$, CuI, PPh_3	DMF	Et_3N	**dA^{FcPa}**	98
dC^{I}					**dC^{FcPa}**	97
dA^{I}TP	**FcMe**	$Pd(PPh_3)_2Cl_2$, CuI, PPh_3	MeCN/H_2O (1/1)	Et_3N	**dA^{FcMe}TP**	38[a]
dC^{I}TP					**dC^{FcMe}TP**	30[a]
dA^{I}TP	**FcPA**	$Pd(PPh_3)_2Cl_2$, CuI, PPh_3	MeCN/H_2O (1/1)	Et_3N	**dA^{FcPa}TP**	13
dC^{I}TP					**dC^{FcPa}TP**	16
dC^{I}TP	ethynylferrocene	$Pd(OAc)_2$, CuI, TPPTS	MeCN/H_2O (1/1)	Et_3N	**dC^{Fc}TP**	27
dA^{FcPa}	1) $PO(OMe)_3$, $POCl_3$, 0°C; 2) $(NHBu_3)_2H_2P_2O_7$, Bu_3N, DMF, 0°C; 3) TEAB (2M)				**dA^{FcPa}TP**	22
dC^{FcPa}					**dC^{FcPa}TP**	18
dA^{FcMe}					**dA^{FcMe}TP**	15[a]
dC^{FcMe}					**dC^{FcMe}TP**	20[a]

[a] isolated **dN^{FcMe}TP**s were prone to oxidation on air

The corresponding modified dNTPs were prepared (Scheme 6.1, Table 6.1) either by phosphorylation of modified nucleosides (Approach A) or by direct aqueous-phase cross-coupling reactions of halogenated triphosphates **dN^{I}TP** with Fc-alkynes (Approach B). The cross-coupling reactions were performed analogously to the reaction of nucleosides using $Pd(PPh_3)_2Cl_2$ catalyst in acetonitrile/water for 1 h. The reactions reached completion but, due to partial hydrolysis of the triphosphates and difficulties in separation, the desired **dN^{FcMe}TP** or **dN^{FcPa}TP** were isolated in moderate yields (13-38 %) after isolation by HPLC. The alternative approach using triphosphorylation of nucleosides gave similarly moderate yields. In all cases, the modified **dN^{FcX}TPs** were prepared and isolated in sufficient quantities for the subsequent biochemical and electrochemical experiments. The dNTPs bearing

unsubstituted ethynylferrocene were also synthesised for comparison. **dA^{Fc}TP**s was prepared as previously reported[¡Error! Marcador no definido.] and the related **dC^{Fc}TP** was prepared analogously through Sonogashira reaction of **dC^{I}TP** with ethynylferrocene achieving a yield of 27 %.

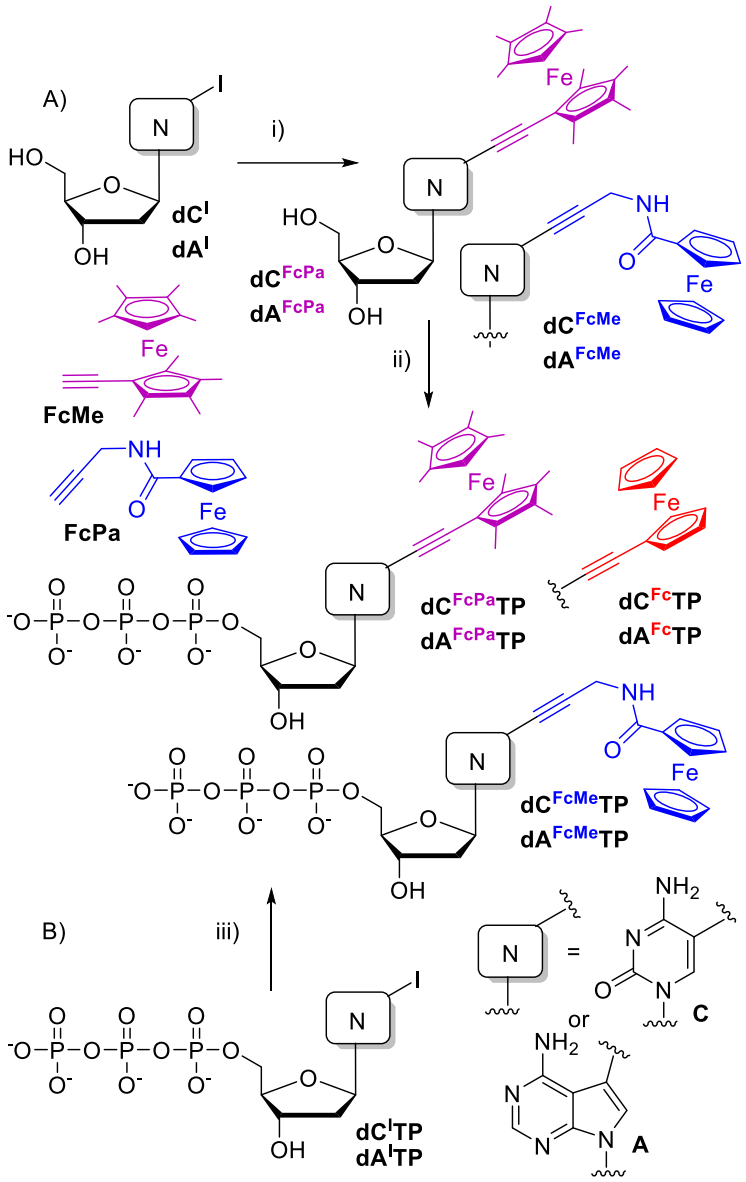

Scheme 6.1. Synthesis of modified nucleosides and dNTPs. Reagents and conditions: i) **FcPA** or **FcMe**, $Pd(PPh_3)_2Cl_2$ + PPh_3 or $Pd(OAc)_2$ + TPPTS, CuI, PPh_3, DMF (75 °C, 1 h) or $MeCN/H_2O$ (1:1) (50 °C, 40 min.); ii) 1. $POCl_3$, $PO(OMe)_3$, 0 °C, 3 h; 2. $(NHBu_3)_2H_2P_2O_7$, Bu_3N, DMF, 0 °C, 1.5 h; 3. TEAB; iii) **FcPA** or **FcMe**, $Pd(PPh_3)_2Cl_2$, CuI, PPh_3, $MeCN/H_2O$ (1:1), 60 °C, 1 h.

Biochemistry

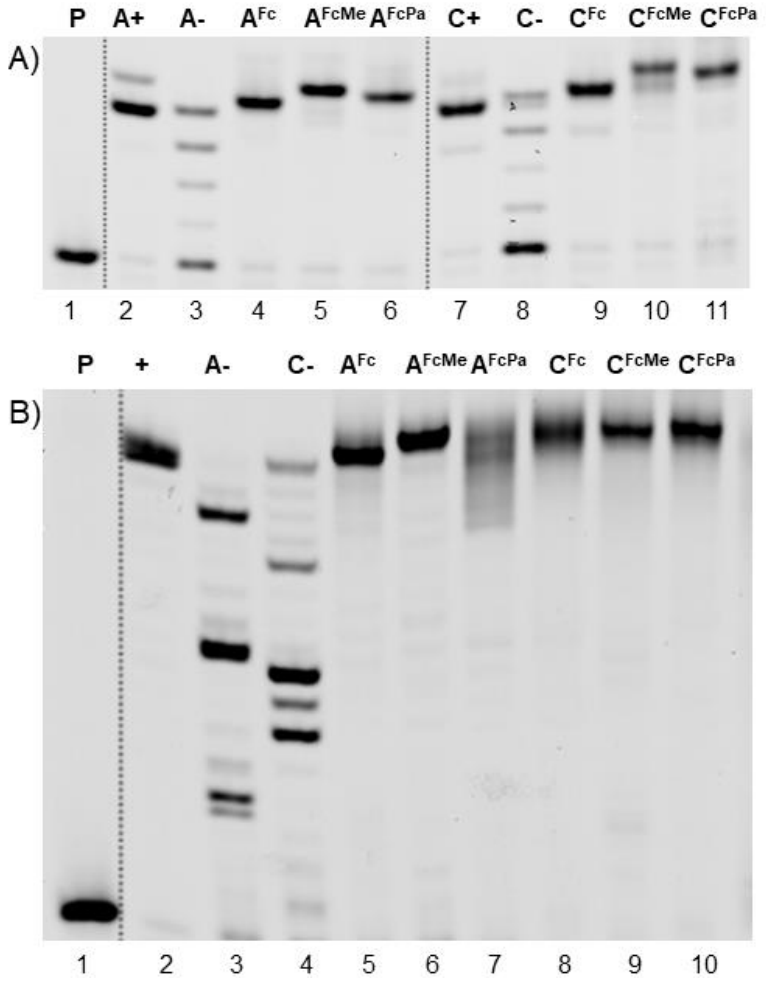

Figure 6.1. Primer extension with a KOD XL polymerase using either (A) 19-mer template temp^{A} or temp^{C} and prim^{rnd}; or (B) 31-mer temp^{rnd16} and prim^{rnd}: (P) primer (5'-6-FAM-labelled); (A+, C+ or +) natural dNTPs; (A-) dCTP, dTTP, dGTP; (C-) dATP, dTTP, dGTP; (A^{Fc}) **dA^{Fc}TP**, dCTP, dTTP, dGTP; (C^{Fc}) **dC^{Fc}TP**, dATP, dTTP, dGTP; (A^{FcMe}) **dA^{FcMe}TP**, dCTP, dTTP, dGTP; (C^{FcMe}) **dC^{FcMe}TP**, dATP, dTTP, dGTP; (A^{FcPa}) **dA^{FcPa}TP**, dCTP, dTTP, dGTP; (C^{FcPa}) **dC^{FcPa}TP**, dATP, dTTP, dGTP.

The Fc-modified **dN^{FcX}TP**s were then tested as substrates for DNA polymerases in primer extension (PEX) reactions using KOD XL DNA polymerase and either a 19-mer (temp^{A} or temp^{C}) or 31-mer (temp^{rnd16}) template and 15-mer primer prim^{rnd} (for sequences of all oligonucleotides, see Table S1 in Annex 1). Figure 6.1 shows the PAGE analysis confirming that in all cases, full-length PEX products containing either 1 or 4 modified nucleotides were formed. The identity of most of the PEX products was also confirmed by MALDI analysis (Table 6.2) of single-stranded oligonucleotides (ssONs) after PEX with biotinylated template and magnetoseparation. Only in the case of 31-mers containing 4 **dN^{FcMe}** bases the mass of the full-length products, was not observed, probably due to the limited stability of the octamethylferrocene label, which is prone to oxidation in air.

Table 6.2. List of MALDI data of PEX products bearing modified or non-modified Fc labels.

oligonucleotide	M calcd. (Da)	M found (Da)
31ON_4A^{Fc}	10445.5	10447.0
31ON_4A^{FcPa}	10673.7	10674.1
31ON_4C^{Fc}	10449.5	10451,9
31ON_4C^{FcPa}	10677.7	10679.6
19ON_1A^{Fc}	6182.0	6183.2
19ON_1A^{FcPa}	6239.0	6238.6
19ON_1A^{FcMe}	6294.0	6295.4
19ON_1C^{Fc}	6159.0	6160.2
19ON_1C^{FcPa}	6216.0	3389.4
19ON_1C^{FcMe}	6271.0	6272.3

Electrochemistry of nucleosides and nucleotides

The electrochemical behavior of Fc-modified nucleosides and dNTPs was studied using Square-wave voltammetry (SWV) on a pyrolytic graphite electrode (PGE) in acetate buffer (pH 5.0). Samples of nucleosides **dN^{FcX}** and triphosphates **dN^{FcX}TP** show voltammetric peaks corresponding to reversible oxidation of the ferrocene moiety (see Fig. S14-15 in SI for the evidence of signal reversibility/irreversibility given by components of the SWV current). In the case of 7-deazaadenine derivatives, an additional peak of irreversible oxidation of the pyrrolopyrimidine moiety was observed at 1.03-1.10 V (vs Ag|AgCl). As expected and designed, the substitution of ferrocene strongly influences the oxidation potential. The electron rich octamethylferrocene is shifted to lower oxidation potentials by ca. 300 mV (Table 6.3). This easier oxidation, however, leads to limited stability of these labels in air. On the other hand, the electron-poor amide-linked ferrocene derivatives are shifted to higher potentials by ca. 100 mV. Compounds containing octamethylferrocene give an additional irreversible peak (denoted as X in Figure 6.2) at 1.20 V.

Table 6.3. Redox potentials of FcX-labelled nucleosides and dNTPs[a]

Compound	FcX/V	A*^{ox}/V	X/V
dA^{Fc}	0.470	1.100	
dA^{FcMe}	0.160	1.040	1.280
dA^{FcPa}	0.550	1.030	
dA^{Fc}TP	0.380	1.030	
dA^{FcMe}TP	0.060	1.050	-----
dA^{FcPa}TP	0.470	1.080	
dC^{Fc}	0.325		
dC^{FcMe}	0.115		1.200
dC^{FcPa}	0.550		
dC^{Fc}TP	0.325		
dC^{FcMe}TP	0.070		1.125
dC^{FcPa}TP	0.440		

[a] Peak potentials of net SWV signals measured at the PGE against Ag|AgCl|3M KCl. For more details, see Figure 6.2.

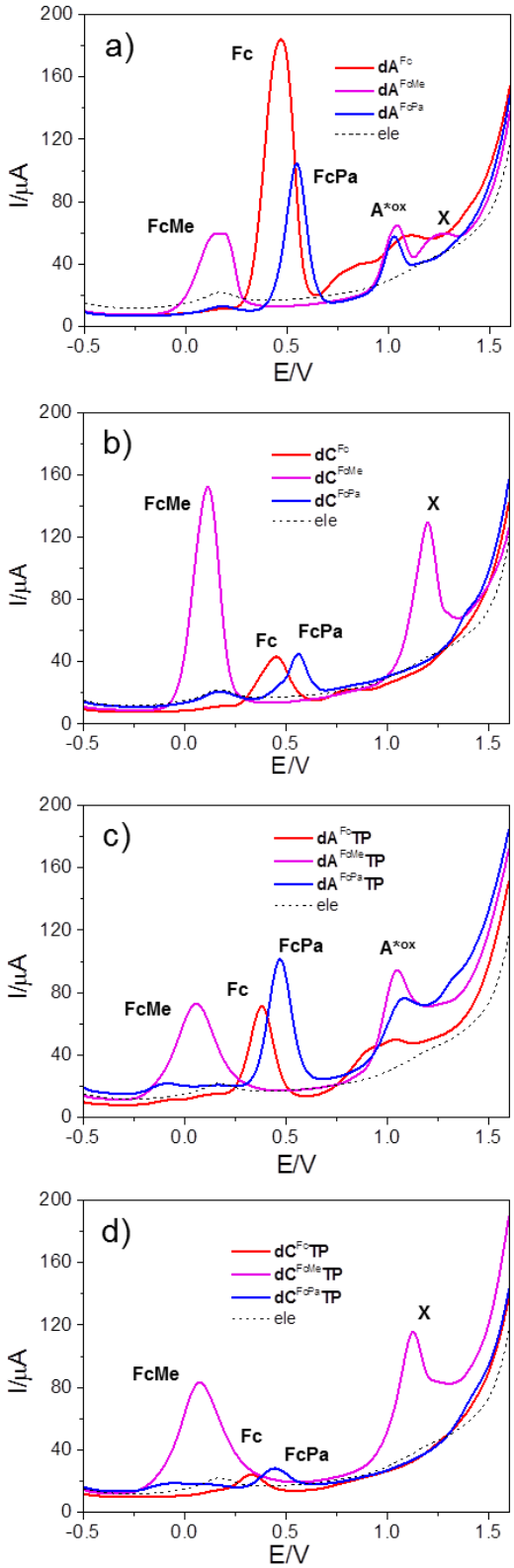

Figure 6.2. Square-wave voltammograms of modified nucleosides (a, b) or 40 μM dNTPs (c, d) measured at a pyrolytic graphite electrode in 0.2 M acetate buffer (pH 5.0).

Design, synthesis and electrochemistry of modified DNA probes

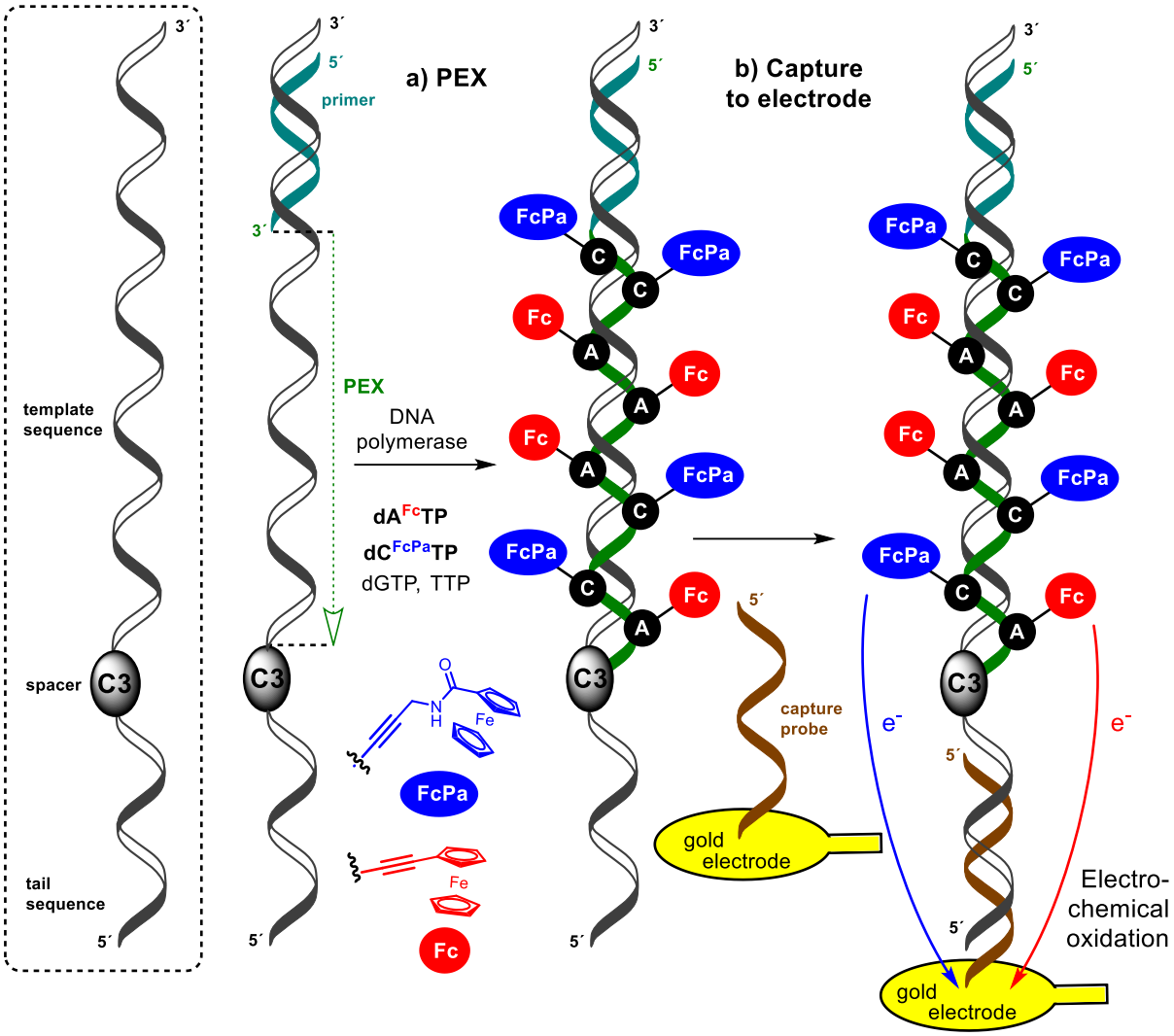

Scheme 6.2. PEX synthesis of the modified DNA probes and their capture on electrode.

In order to study the electrochemistry of redox-labelled DNA, we initially tried to synthesize FcX-modified ssONs by PEX with magnetoseparation and studied their SWV on carbon paste electrodes (analogously to our previous works[¡Error! Marcador no definido.]). Unfortunately, we did not observe any significant signals, probably because of low amounts of the modified ssONs and problems with their adsorption on electrodes. Therefore, we applied our recently reported approach[¡Error! Marcador no definido.] based on the synthesis of tailed-PEX products and their capture on gold electrodes (Scheme 6.2). Since the octamethylferrocene-labelled nucleotides and ONs were prone to oxidation with air, we focused only on the stable unsubstituted ferrocene (**Fc**) and carboxamidoferrocene (**FcPa**) labels.

To test whether the **Fc** and **FcPa** labels can be distinguished and electrochemically quantified, we designed two 55-mer and one 37-mer template bearing a 20-mer ON sequence at the 3'-end separated through a $-(CH_3)_3-$ (C3) spacer (Table S1, annex 1).

The two 55-mer tailed templates were designed for the synthesis of PEX products containing either a combination of 8 **dA^{Fc}** and 2 **dC^{FcPa}** (**DNA_8A^{Fc}_2C^{FcPa}**) or a combination of 2 **dA^{Fc}** and 8 **dC^{FcPa}** (**DNA_2A^{Fc}_8C^{FcPa}**). The shorter 37-mer template was designed for PEX synthesis of DNA containing equimolar numbers of 4 **dA^{Fc}** and 4 **dC^{FcPa}** (**DNA_4A^{Fc}_4C^{FcPa}**). The role of the 3'-tail was to facilitate hybridization of the PEX product to a complementary capture probe immobilised on the gold electrode and the role of the C3 spacer was to prevent further extension during the PEX, maintaining the tail as ssON.

Agarose gel electrophoresis (Figure 6.3) shows the PEX product formation using either set of natural dNTPs (+) or combination of **dA^{Fc}TP**, **dC^{FcPa}TP** with TTP and GTP (*Fc). In all cases, the formation of the full-length PEX product was observed confirming that even the combination of two Fc-modified dNTPs can be used for polymerase construction of double-redox-labelled DNA. The labelled PEX products were then hybridized to the complementary capture probe immobilised on gold electrode, washed and used for electrochemical interrogation by SWV. $Ca(NO_3)_2$ 0,1M was selected as the electrolyte solution due to the ability of divalent cations to shrink, compact and bend DNA, whilst also shielding electrostatic repulsions between neighbour DNA strands.

The square-wave voltammograms (Figure 6.4) of the three individual labelled PEX products show two clearly distinguishable peak maxima corresponding to the oxidation of **Fc** (0.3 V vs Ag/AgCl) and **FcPa** (0.4 V vs Ag/AgCl), respectively. After peak deconvolution, the ratios of the intensities of the two oxidation peaks correlated very well with the expected A/C nucleobase ratio present in each PEX product: 3.6 ± 0.5 (**DNA_8A^{Fc}_2C^{FcPa}**), 0.27 ± 0.02 (**DNA_2A^{Fc}_8C^{FcPa}**) and 1.04 ± 0.15 (**DNA_4A^{Fc}_4C^{FcPa}**).

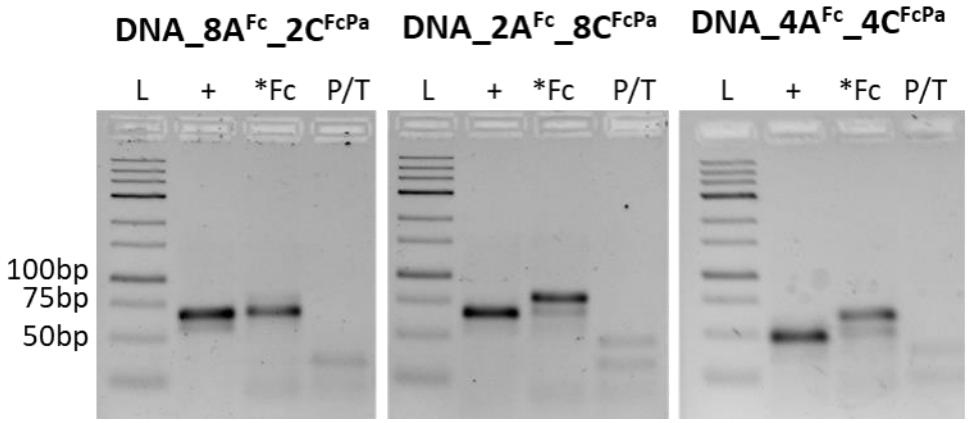

Figure 6.3. Agarose gel electrophoresis of PEX products using temp^{8A,2C}, temp^{8C,2A} or temp^{4C,4A} templates and Primer$^{8/2_4/4}$ obtained in presence of (a) all four natural dNTPs (+), or combination of **dA^{Fc}TP**, **dC^{FcPa}TP** with TTP and GTP (*Fc). P/T corresponds to primer hybridized to template in the absence of polymerase**.**

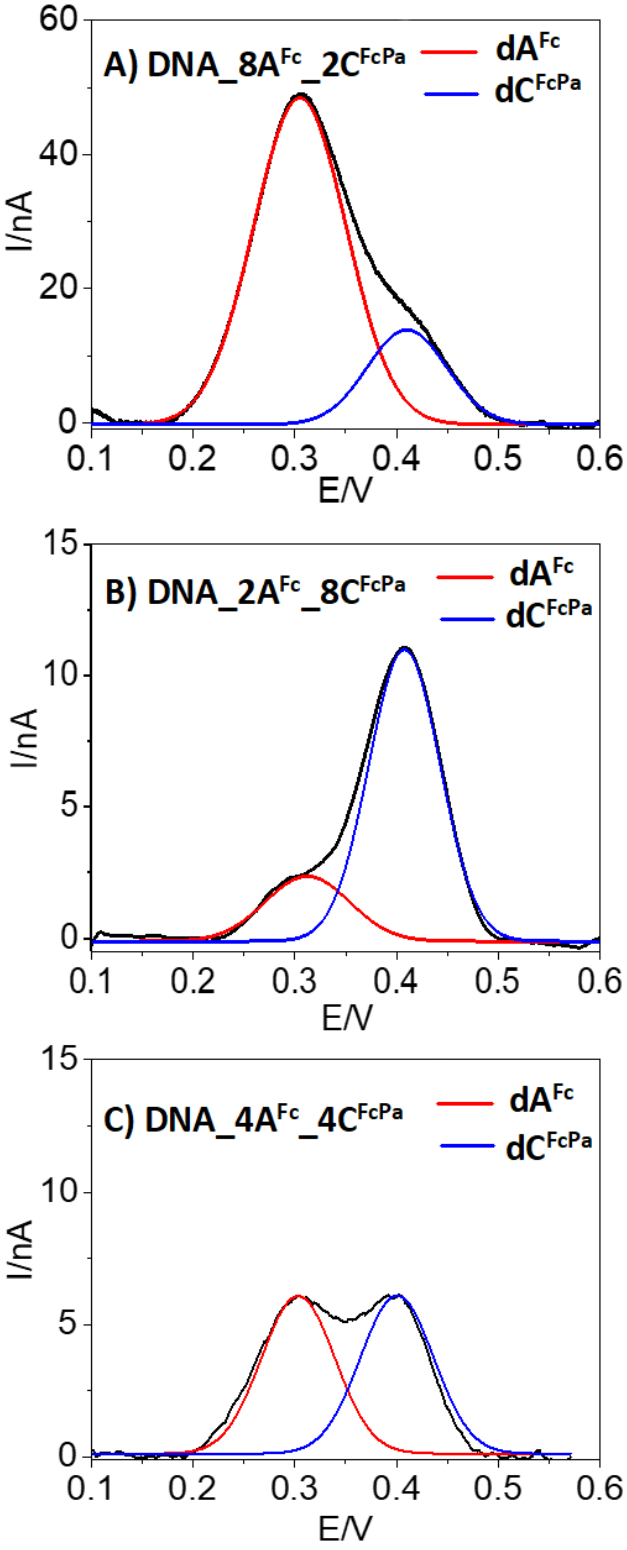

Figure 6.4. Square-wave voltammograms of the oxidation peaks of **dA^{Fc}** and **dC^{FcPa}** on PEX products and then hybridized to a complementary surface tethered thiol-end sequence for detection. The black traces correspond to the experimental SWV signals for **dA^{Fc}/dC^{FcPa}** ratios equal to: 8:2 (A), 2:8 (B) and 4:4 (C). Red and blue traces correspond to the deconvoluted signals of **dA^{Fc}** and **dC^{FcPa}** respectively. SWVs were recorded in 0.1 M $Ca(NO_3)_2$ vs Ag/AgCl reference electrode.

6.4 CONCLUSIONS

We have designed and synthesized nucleosides and dNTPs bearing three differently substituted ferrocene labels. Substitution with eight electron-donating methyl groups led to a significant decrease of the oxidation potential of ferrocene (by 300 mV), whilst the attachment of the electron-withdrawing carboxamide shifted the redox potential to 100 mV higher values. The octamethyferrocene-linked nucleosides and nucleotides were insufficiently stable due to their spontaneous oxidation in air. However, the unsubstituted ferrocene (Fc) and ferrocenecarboxamide (FcPa) labels were stable and useful for electrochemical labelling. The corresponding redox-labelled **dN^{FcX}TP**s were good substrates for KOD XL DNA polymerase and were efficiently used for the enzymatic synthesis of DNA probes containing either one or even two redox-labelled nucleotides using PEX. The oxidation peaks associated with **dA^{Fc}** and **dC^{FcPa}** were clearly distinguishable and ratiometric. Thus, for the first time, we describe a set of two fully orthogonal and ratiometric oxidisable labels for DNA suitable for the redox-coding of nucleobases. The PEX using tailed templates and hybridization with capture probes on gold electrodes is a very efficient and straightforward strategy to study the incorporation of the two redox labels to DNA and thus directly measure the relative abundance of A and C in an unknown target sequence of DNA.

6.5 EXPERIMENTAL

Complete experimental procedures and methods, characterization of all compounds, additional figures and copies of spectra are given in the Annex 1.

ACKNOWLEDGEMENTS

This work was supported by the the Academy of Sciences of the Czech Republic (Praemium Academiae award for M. H.), by the European Regional Development Fund; OP RDE (No. CZ.02.1.01/0.0/0.0/16_019/0000729 to M.H.) and institutional support from the IBP CAS (No. 68081707). The work was also supported from Spanish Ministerio de Economía y Competitividad for CIGUASENSING BIO2017-87946-C2-1-R and SEASENSING BIO2014-56024-C2-1.

6.6 REFERENCES

(1) E. Paleček, M. Bartošík, *Chem. Rev.* **2012**, *112*, 3427–3481.
M. Hocek, M. Fojta, *Chem. Soc. Rev.* **2011**, *40*, 5802–5814.

(2) I. Magriñá, A. Toldrà, M. Campàs, M. Ortiz, A. Simonova, I. Katakis, M. Hocek, C. K. O'Sullivan, *Biosens. Bioelectron.* **2019**, *134*, 76-82.

(3) A. M. Debela, S. Thorimbert, B. Hasenknopf, C. K. O'Sullivan, M. Ortiz, *Chem. Commun.* **2016**, *52*, 757–759.

(4) H. Cahová, L. Havran, P. Brázdilová, H. Pivonková, R. Pohl, M. Fojta, M. Hocek, *Angew. Chem. Int. Ed.* **2008**, *47*, 2059–2062.
(a) A. A. Gorodetsky, O. Green, E. Yavin, J. K. Barton, *Bioconjug. Chem.,* **2007**, *18*, 1434–1441. (b) J. Balintová, M. Plucnara, P. Vidláková, R. Pohl, L. Havran, M. Fojta, M. Hocek, *Chem. Eur. J* **2013**, *19*, 12720–12731.

(5) J. Balintová, M. Plucnara, P. Vidláková, R. Pohl, L. Havran, M. Fojta, M. Hocek, *Chem. Eur. J* **2013**, *19*, 12720–12731.

(6) J. Balintová, J. Špaček, R. Pohl, M. Brázdová, L. Havran, M. Fojta, M. Hocek, *Chem. Sci.* **2015**, *6*, 575–587.

(7) C. G. Feeney, J. K. Barton, *Langmuir* **2012**, *28*, 7063-7070.

(8) A. Simonova, J. Balintová, R. Pohl, L. Havran, M. Fojta, M. Hocek, *ChemPlusChem* **2014**, *79*, 1703 – 1712.

(9) A. Simonova, L. Havran, R. Pohl, M. Fojta, M. Hocek, *Org. Biomol. Chem.* **2017**, *15*, 6984–6996.

(10) D. R. Van Staveren, N. Metzler-Nolte, *Chem. Rev.* **2004**, *104*, 5931-5985. (a) D. A. Di Giusto, W. A. Wlassoff, S. Geisebrecht, J. J., Gooding, G. C. King, *J. Am. Chem. Soc.* **2004**, *126*, 4120-4121. (b) D. A. Di Giusto, W. A. Wlassoff, S. Geisebrecht, J. J., Gooding, G. C. King, *Angew. Chem., Int. Ed.* **2004**, *43*, 2809-2812. (c) W. A. Wlassoff, G. C. King, *Nucleic Acids Res.* **2002**, *30*, e58. (d) S. S. W. Yeung, T. M. H. Lee, I-M. Hsing, *J. Am. Chem. Soc.* **2006**, *128*, 13374-13275. (e) F. Patolsky, Y. Weizmann, I. Willner, *J. Am. Chem. Soc.* **2002**, *124*, 770-772. (f) C. J. Yu, H. Yowanto, Y. J. Wan, T. J. Meade, Y. Chong, M. Strong, L. H. Donilon, J. F. Kayyem, M. Gozin, and G. F. Blackburn, *J. Am. Chem. Soc.* **2000**, *122*, 6767-6768.

(13) P. Brázdilová, M. Vrábel, R. Pohl, H. Pivonková, L. Havran, M. Hocek, M. Fojta, *Chem. Eur. J* **2007**, *13*, 9527–9533.

(14) (a) K. H. Shaughnessy, *Molecules* **2015**, *20*, 9419–9454. (b) J. H. Cho, C. D. Prickett, K. H. Shaughnessy, *Eur. J. Org. Chem.* **2010**, 3678–3683

(15) P. Jutzi, B. Kleinebekel, *J. Organometal. Chem.* **1997**, *545–546*, 573–576.

(16) A. E. Beilstein, M. W. Grinstaff, *Chem. Commun.*, **2000**, 509–510.

(17) T. Špringer, H. Šípová, H. Vaisocherová, J. Štěpánek, J. Homola, *Nucleic Acids Res.* **2010**, *38*, 7343–7351.

UNIVERSITAT ROVIRA I VIRGILI
DEVELOPMENT OF ELECTROCHEMICAL DNA SENSORS BASED ON THE INCORPORATION OF FERROCENE LABELLED DATP
Ivan Magriñá Lobato

CHAPTER 7

CONCLUSIONS AND FUTURE PERSPECTIVES

CONCLUSIONS

We contributed to the field of biosensors by developing a generic 3 steps electrochemical DNA sensor approach that consist in the genomic DNA extraction, target amplification in presence of $dA^{EFc}TP$ and tailed primers and a further tailed amplicon hybridization and electrochemical detection.

First of all, we presented a novel simple and generic approach to perform primer extension (PEX), hybridisation and electrochemical detection using redox labelled dNTPs. Specifically, we proved that KOD XL polymerase is able to incorporate $dA^{EFc}TP$ in a long and complex template that contains, A, AA and AAA repetitions within the sequence without an early termination of the PEX even when 100% $dA^{EFc}TP$ is used in the PEX mixture.

Then we moved to a more challenging approach in which target DNA is not only extended but also amplified in presence of $dA^{EFc}TP$ and tailed primers, process than involves not only incorporation of $dA^{EFc}TP$ but also the use of an hipermodified template with ferrocene as a tempalte for the polymerase. The concept has been successfully applied to the singleplex detection of the *K. armiger* (toxic microalgae) and the duplex detection of *B. anthracis* (causative agent of anthrax) from genomic DNA extracted from real samples.

During the optimization process we concluded that $dA^{EFc}TP$ can be incorporated by KODXL polymerase at different $dA^{EFc}TP$:dATP ratios in both primer extension and amplification experiments and we also determined that the increase in $dA^{EFc}TP$:dATP ratio increases the ferrocene peak intensity obtained and the limit of detection achieved, but it decreases the DNA amplification yield. This facts, combined with the numbers of cycles in the PCR amplification allows to tune and adapt the limit of detection of the assay to the specific needs of the target. Typically, a limit of detection of 1fM with a dynamic range of 1,5 decades can be achieved in aproximately 2h.

We also discovered that the ferrocene electron transfer and ferrocene oxidation peak obtained from hybridized target on the electrode surface are strongly dependent on the electrolyte composition and concentration, requiring the presence of divalent or trivalent cations to be effective. Indeed, we proved that the electrolyte composition, concentration and electrode initial potential are key parameters to control the DNA layer at the electrode surface to enable the electron transfer.

Finally, we proved that $dA^{EFc}TP$ can be used in combination with $dC^{FcPa}TP$ to obtain distinguishable redox peaks to directly measure the relative abundace of A and C in an unknown target sequence of DNA.

FUTURE PERSPECTIVES

As mentioned in the summary, the use of electrochemical DNA sensors as point-of–need devices is still limited because they require several steps including, #1: the amplification of the target sequence, #2: the generation of single stranded DNA following amplification, #3: target hybridization with a complementary capture probe and finally #4: the need of reporting steps to detect the hybridized target DNA sequence.

With the use of tailed primers and $dA^{EFc}TP$, we overcame the need for single stranded DNA generation (#2) and the need for further labelling steps (#4), respectively, while retaining the analytical performance required to detect target sequences in genomic DNA samples.

However, there are still problems to be adressed to fully implement the method in a point-of-need device. As in other PCR based methods, the need for a thermocycler for the amplification step (#1) decreases the portability and increases the cost and power consumption of the assay. In order to replace the thermocycler with a more portable and cost-effective incubator we propose the use of tailed primers and $dA^{EFc}TP$ in combination with isothermal amplification methods such as recombinase polymerase amplification, that is simple and operates at a low and constant 37-41ºC.

Additionally, the use of tailed primers to perform liquid phase amplification could be replaced by a solid-phase amplification format in which one or both primers are immobilized on the elctrode surface. This approach is more challenging than liquid-phase amplification due to a limited amount of primers, an inherent reduced mobility of the surface-confined primers as well as a limited availability of enzymes. Despite these drawbacks, solid-phase amplification facilitates reduced/null primer-dimers, multiplexing capabilities and direct production of the amplicon on the electrode surface, which eliminates the need for post amplification hybridization (#3).

In the near future we envisage the development of a new generation of multiplexed electrochemical DNA sensors based on isothermal solid-phase amplification in combination with ferrocene labelled dNTPs. This new two-step point-of-need device, would only require a genomic DNA extraction module, an electrode array, a portable incubator and portable potentiostat to proceed with the genomic DNA extraction and the single-pot multiple target amplification and detection fullfilling the ASSURED (affordable, sensitive, specific, user-friendly, rapid and robust, equipment-free and deliverable to end-users) criteria outlined by the World Health Organisation (WHO) for developing point-of-care devices for resource-limited settings.

UNIVERSITAT ROVIRA I VIRGILI
DEVELOPMENT OF ELECTROCHEMICAL DNA SENSORS BASED ON THE INCORPORATION OF FERROCENE LABELLED DATP
Ivan Magriñá Lobato

ANNEXES

Annex 1. Supplementary information Chapter 6

Tuning of Oxidation Potential of Ferrocene for Ratiometric Redox Labelling and Coding of Nucleotides and DNA

Anna Simonova, Ivan Magriñá, Veronika Sýkorová, Radek Pohl, Mayreli Ortiz, Luděk Havran, Miroslav Fojta,* Ciara O'Sullivan,* and Michal Hocek*

Supplementary information

Contents

1. Additional results and schemes

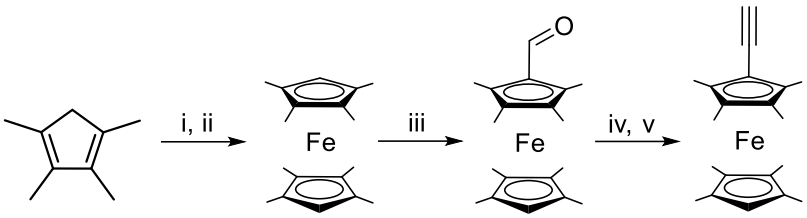

Scheme S1. Synthesis of 1-ethynyl-1',2,2',3,3',4,4',5-octamethylferrocene. Reagents and conditions: i) tetramethylcyclopentadiene in benzene, CH_3Li in E_2O, 25 °C, reflux for 4 h, ii) $FeCl_2$ (0.7 equiv.), THF, 0 °C to 25 °C, 12 h (48 %); iii) $POCl_3$ (7.8 equiv.), DMF, 60 °C, 6 h (79 %); iv) $[Ph_3PCH_2Cl]Cl$ (1.0 equiv.), THF, n-BuLi (2.5 equiv.), 25 °C, 3 h, v) t-BuOK (2.0 equiv.), reflux for 1 day (56 %).

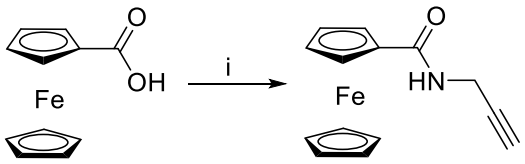

Scheme S2. Synthesis of ferrocenoyl propargylamide. Reagents and conditions: i) DCC (1.5 equiv.), DMAP (0.1 equiv.), propargylamine (1.0 equiv.), CH_2Cl_2, 25 °C, 24 h (25 %).

2. Experimental section – organic chemistry

General remarks

NMR spectra were recorded on 400 (400.0 MHz for ^{1}H, 162 MHz for ^{31}P, 100 MHz for ^{13}C), 500 (500 MHz for ^{1}H, 125.7 MHz for ^{13}C, 470.4 MHz for ^{19}F and 202.3 for ^{31}P) or 600 (600.1 MHz for ^{1}H, 150.9 MHz for ^{13}C) spectrometers from sample solutions in D_2O, DMSO-d_6, CD_3CN or CD_3OD. Chemical shifts (in ppm, δ scale) were referenced as follows: D_2O (referenced to dioxane as internal standard in 1 mm coaxial capillary; 3.75 ppm for ^{1}H NMR and 69.3 ppm for ^{13}C NMR); CD_3OD (referenced to solvent signal: 3.31 ppm for ^{1}H NMR and 49.00 ppm for ^{13}C NMR); DMSO-*d6* (referenced to solvent signal: 2.50 ppm for ^{1}H NMR and 39.7 ppm for ^{13}C NMR); CD_3CN (referenced to solvent signal: 1.94 ppm for ^{1}H NMR and 1.32 ppm for ^{13}C NMR). ^{31}P chemical shifts were referenced to H_3PO_4 as external reference. Chemical shifts are given in ppm (δ scale), coupling constants (*J*) in Hz. Complete assignment of all NMR signals was achieved by using a combination of H,H-COSY, H,C-HSQC, and H,C-HMBC experiments. Mass spectra were measured on LCQ classic (Thermo-Finnigan) spectrometer using ESI or Q-Tof Micro (Waters, ESI source, internal calibration with lockspray). Preparative HPLC separations were performed on a column packed with 10 µm C18 reversed phase (Phenomenex, Luna C18(2)). High resolution mass spectra were measured on a LTQ Orbitrap XL (Hermo Fischer Scientific) spectrometer using ESI ionization technique. Mass spectra of functionalised DNA were measured by Maldi-TOF, Reflex IV (Bruker) with nitrogen laser.

Synthesis of ferrocene labels

1,1',2,2',3,3',4,4'-octamethylferrocene

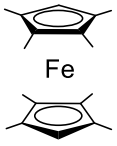

Yield: 48 %. Spectral data were in accordance with literature.[1a]

1-formyl-1',2,2',3,3',4,4',5-octamethylferrocene

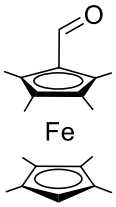

Yield: 79 %. Spectral data were in accordance with literature.[1b]

1-ethynyl-1',2,2',3,3',4,4',5-octamethylferrocene (FcMe)

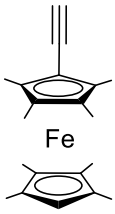

Yield: 56 %. Spectral data were in accordance with literature.[1c]

Ferrocenoyl propargylamide (FcPa)

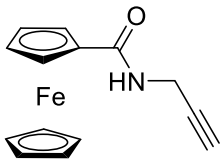

Yield: 25 %. Spectral data were in accordance with literature.[2]

Synthesis of ferrocene-labeled nucleosides

Synthesis of modified nucleosides - Sonogashira cross-coupling:

Method A: A 1:1 mixture of H_2O-CH_3CN (2 mL) was added through a septum to an argon-purged flask containing a halogenated nucleoside **dN^I** (1 equiv.), **FcX** (1.5 equiv.), CuI (10 mol %), TPPTS (2 mol %) and $Pd(OAc)_2$ (5 mol %) followed by Et_3N (10 equiv.). The reaction mixture was stirred at 50 ºC for 40 min until complete consumption of the starting material and then evaporated under vacuum. The products were purified by silica gel column chromatography using chloroform/methanol (0 to 10 %) as eluent.

Method B: Dry DMF (3 mL) was added to an argon-purged flask containing **FcX** (1.5 equiv.), a nucleoside analogue **dN^I** (1 equiv.), CuI (10 mol %), PPh_3 (2 mol %) and $[Pd(PPh_3)_2Cl_2]$ (5 mol %) followed by Et_3N (10 equiv.). The reaction mixture was stirred at 75 °C for 1 h until complete consumption of the starting material and then evaporated in vacuo. The products were purified by silica gel column chromatography using chloroform/methanol (0 to 10 %) as eluent.

7-(1',2,2',3,3',4,4',5-Octamethylferrocene-1-yl-ethynyl)-7-deaza-2'-deoxyadenosine (dA^{FcMe})

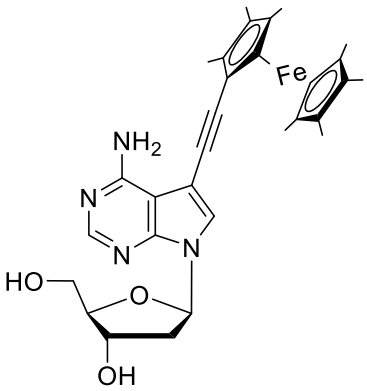

Compound **dA^{FcMe}** was prepared from **dA^I** according to Method A. The product was isolated as a yellow solid (45 mg, 90 %); ^{1}H NMR (500.0 MHz, CD_3OD): 1.38, 1.41, 1.53, 1.56 (4 × bs, 24H, CH_3-ferrocene); 2.32 (ddd, 1H, J_{gem} = 13.6, $J_{2'b,1'}$ = 6.0, $J_{2'b,3'}$ = 2.6 H-2'b); 2.66 (ddd, 1H, J_{gem} = 13.6, $J_{2'a,1'}$ = 8.3, $J_{2'a,3'}$ = 5.9, H-2'a); 3.58 (bs, 1H, H-ferrocene); 3.73 (dd, 1H, J_{gem} = 12.1, $J_{5'b,4'}$ = 3.5, H-5'b); 3.81 (dd, 1H, J_{gem} = 12.1, $J_{5'a,4'}$ = 3.2, H-5'a); 4.00 (ddd, 1H, $J_{4',5'}$ = 3.5, 3.2, $J_{4',3'}$ = 2.6, H-4'); 4.52 (dt, H, $J_{3',2'}$ = 5.9, 2.6, $J_{3',4'}$ = 2.6, H-3'); 6.49 (dd, 1H, $J_{1',2'}$ = 8.3, 6.0, H-1'); 7.56 (s, 1H, H-6); 8.10 (s, 1H, H-2).

^{13}C NMR (125.7 MHz, CD_3OD): 9.15, 9.97, 10.89, 11.02 (CH_3-ferrocene); 41.56 (CH_2-2'); 63.61 (CH_2-5'); 73.00 (CH-3'); 74.28 (CH-ferrocene); 82.03 (C5-**C**≡C-ferrocene); 83.85, 84.13 (C-ferrocene); 86.69 (CH-1'); 89.19 (CH-4'); 92.58 (C5-C≡**C**-ferrocene); 97.87 (C-5); 104.43 (C-4a); 126.38 (CH-6); 149.81 (C-7a); 153.22 (CH-2); 159.39 (C-4).

MS (ESI-): *m/z* (%): 571.2 (100) [M]; HRMS (ESI-): calcd. 571.2366 for $C_{31}H_{39}O_3N_4Fe$, found 571.2362.

5-(1',2,2',3,3',4,4',5-Octamethylferrocene-1-yl-ethynyl)-2'-deoxycytidine (**dC^{FcMe}**)

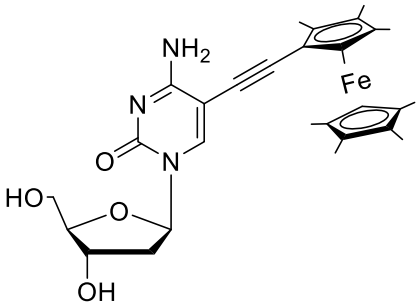

Compound **dC^{FcMe}** was prepared from **dC^{I}** according to Method A. The product was isolated as a yellow solid (40 mg, 86 %); ^{1}H NMR (500.0 MHz, CD_3OD): 0.35 – 1.24 (bm, 24H, CH_3-ferrocene); 2.10 (dt, 1H, J_{gem} = 13.6, $J_{2'b,1'}$ = $J_{2'b,3'}$ = 6.2, H-2'b); 2.37 (ddd, 1H, J_{gem} = 13.6, $J_{2'a,1'}$ = 6.2, $J_{2'a,3'}$ = 4.0, H-2'a); 3.68 (dd, 1H, J_{gem} = 12.1, $J_{5'b,4'}$ = 3.5, H-5'b); 3.74 (dd, 1H, J_{gem} = 12.1, $J_{5'a,4'}$ = 3.2, H-5'a); 3.92 (ddd, 1H, $J_{4',3'}$ = 4.0, $J_{4',5'}$ = 3.5, 3.2, H-4'); 4.31 (dt, 1H, $J_{3',2'}$ = 6.2, 4.0, $J_{3',4'}$ = 4.0, H-3'); 6.19 (t, 1H, $J_{1',2'}$ = 6.2, H-1'); 8.31 (bs, 1H, H-6); (CH-ferrocene not detected).

^{13}C NMR (125.7 MHz, CD_3OD): 8.77, 9.41, 10.28, 10.59 (CH_3-ferrocene); 42.39 (CH_2-2'); 62.39 (CH_2-5'); 71.77 (CH-3'); 76.70 (C5-**C**≡C-ferrocene); 87.96 (CH-1'); 89.12 (CH-4'); 94.68 (C-5); 97.24 (C5-C≡**C**-ferrocene); 143.46 (CH-6); 156.57 (C-2); 165.49 (C-4); (C,CH-ferrocene not detected)

MS (ESI-): *m/z* (%): 547.2 (100) [M]; HRMS (ESI-): calcd. 547.2328 for $C_{29}H_{37}O_4N_3Fe$, found 547.2131.

7-[3-(Ferrocene-1-carboxamido)prop-1-yn-1-yl]-7-deaza-2'-deoxyadenosine (**dA^{FcPa}**)

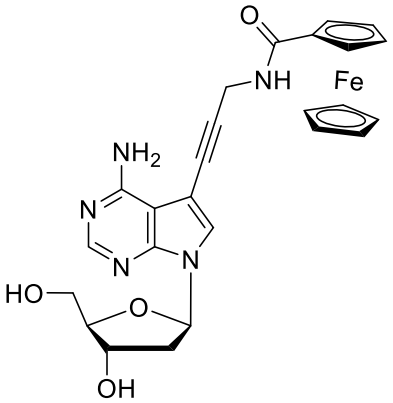

Compound **dA^{FcPa}** was prepared from **dA^{I}** according to Method B. The product was isolated as a yellow solid (52 mg, 98 %); ^{1}H NMR (500.0 MHz, CD_3OD): 2.31 (ddd, 1H, J_{gem} = 13.7, $J_{2'b,1'}$ = 6.0, $J_{2'b,3'}$ = 2.7 H-2'b); 2.61 (ddd, 1H, J_{gem} = 13.7, $J_{2'a,1'}$ = 8.0, $J_{2'a,3'}$ = 6.0, H-2'a); 3.70 (dd, 1H, J_{gem} = 12.1, $J_{5'b,4'}$ = 3.7,H-5'b); 3.77 (dd, 1H, J_{gem} = 12.1, $J_{5'a,4'}$ = 3.3,H-5'a); 3.99 (ddd, 1H, $J_{4',5'}$ = 3.7, 3.3, $J_{4',3'}$ = 2.7, H-4'); 4.21 (bs, 5H, H-cp); 4.25 (bs, 2H, CH_2N); 4.37 – 4.45 (m, 2H, H-2",5"); 4.49 (dt, H, $J_{3',2'}$ = 6.0, 2.7, $J_{3',4'}$ = 2.7, H-3'); 4.83 – 4.85 (m, 2H, H-3",4"); 6.46 (dd, 1H, $J_{1',2'}$ = 8.0, 6.0, H-1'); 7.58 (s, 1H, H-6); 8.15 (bs, 1H, H-2).

^{13}C NMR (125.7 MHz, CD_3OD): 30.90 (CH_2N); 41.55 (CH_2-2'); 63.61 (CH_2-5'); 69.52, 69.54 (CH-3",4"); 70.82 (CH-cp); 72.04 (CH-2",5"); 72.96 (CH-3'); 75.74, 75.86 (C-1", C5-**C**≡C-CH_2); 86.63 (CH-1'); 89.18 (CH-4'); 90.43 (C5-C≡**C**-CH_2); 97.16 (C-5); 104.77 (C-4a); 127.78 (CH-6); 149.83 (C-7a); 153.49 (CH-2); 159.00 (C-4); 174.14 (CONH).

MS (ESI-): *m/z* (%): 516.1 (90) [M]; 538.1 (100) [M+Na]; HRMS (ESI-): calcd. 516.1329 for $C_{25}H_{26}O_4N_5Fe$, found 516.1327; calcd. 538.1148 for $C_{25}H_{25}O_4N_5FeNa$, found 538.1148.

5-[3-(Ferrocene-1-carboxamido)prop-1-yn-1-yl]-2'-deoxycytidine (**dC^{FcPa}**)

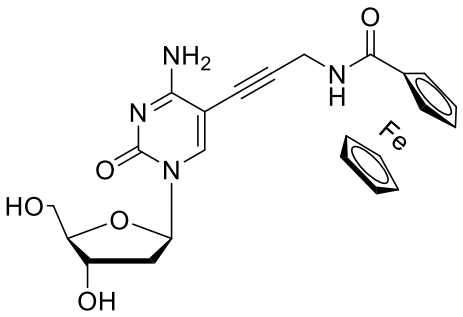

Compound **dC^{FcPa}** was prepared from **dC^{I}** according to Method B. The product was isolated as a yellow solid (48 mg, 97 %); ^{1}H NMR (600.1 MHz, DMSO-d_6): 1.95 (ddd, 1H, J_{gem} = 13.2, $J_{2'b,1'}$ = 7.2, $J_{2'b,3'}$ = 6.0, H-2'b); 2.12 (ddd, 1H, J_{gem} = 13.2, $J_{2'a,1'}$ = 5.9, $J_{2'a,3'}$ = 3.3, H-2'a); 3.52, 3.57 (2 × ddd, 2 × 1H, J_{gem} = 11.9, $J_{5',OH}$ = 5.2, $J_{5',4'}$ = 3.5, H-5'); 3.77 (q, 1H, $J_{4',3'}$ = $J_{4',5'}$ = 3.5, H-4'); 4.18 (m, 8H, H-3', CH_2N, H-cp); 4.38 (m, 2H, H-2",5"); 4.81 (m, 2H, H-3",4"); 5.07 (bt, 1H, $J_{OH,5'}$ = 5.2, OH-5'); 5.21 (bd, 1H, $J_{OH,3'}$ = 4.2, OH-3'); 6.09 (dd, 1H, $J_{1',2'}$ = 7.2, 5.9, H-1'); 6.84, 7.88 (2 × bs, 2 × 1H, NH_2); 8.12 (s, 1H, H-6); 8.29 (t, 1H, J = 5.4, NH).

^{13}C NMR (150.9 MHz, DMSO-d_6): 29.68 (CH_2N); 40.98 (CH_2-2'); 61.29 (CH_2-5'); 68.47 (CH-3",4"); 69.57 (CH-cp); 70.45 (CH-3', CH-2",5"); 74.23 (C5-**C**≡C-CH_2); 75.83 (C-1"); 85.56 (CH-1'); 87.68 (CH-4'); 89.71 (C-5); 93.58 (C5-C≡**C**-CH_2); 143.72 (CH-6); 153.67 (C-2); 164.69 (C-4); 169.67 (CONH).

MS (ESI-): *m/z* (%): 493.1 (10) [M]; 515.1 (100) [M+Na]; HRMS (ESI-): calcd. 493.1169 for $C_{23}H_{25}O_5N_4Fe$, found 493.1164; calcd. 515.0988 for $C_{23}H_{24}O_5N_4FeNa$, found 515.0983.

Synthesis of ferrocene-labeled dNTPs

Synthesis of modified nucleoside triphosphates - Sonogashira cross-coupling

Method A: A 1:1 mixture of H_2O-CH_3CN (2 mL) was added through a septum to an argon-purged flask containing a halogenated nucleotide **dN^{I}TP** (1 equiv.), **FcX** (1.5 equiv.), CuI (10 mol %), Et_3N (10 equiv.), PPh_3 (2 mol %) and $[Pd(PPh_3)_2Cl_2]$ (5 mol %). The flask was evacuated and purged with argon, and then the reaction mixture was stirred at 60 ºC for 1 h until complete consumption of the starting material and then evaporated under vacuum. Product was isolated from the crude reaction mixture by HPLC on a C18 column with the use of a linear gradient of 0.1 M TEAB (triethylammonium bicarbonate) in H_2O to 0.1 M TEAB in H_2O–MeOH (1:1) as eluent. Several co-distillations with water followed by freeze-drying from water gave a solid product.

Synthesis of modified nucleoside triphosphates - triphosphorylation

Method B: $POCl_3$ (2.5 equiv) in $PO(OMe)_3$ (1 ml) was added through a septum to an argon-purged flask containing modified nucleosides **dN^{EPT}** (1 equiv.), Reaction mixture was then stirred at 0 ºC for 12 h until complete consumption of the starting material. Then an ice-cooled solution of $(NHBu_3)_2H_2P_2O_7$ (5 equiv) and Bu_3N (4.2 equiv) in dry DMF (2 ml) was added and the mixture was stirred at 0 °C for another 1.5 h. The reaction was quenched by addition of 2 M aqueous TEAB (triethylammonium bicarbonate) (2 ml) and the solvents were evaporated under vacuum and the residue was co-distilled with water three times. The product was isolated by HPLC on a C18 column with the use of a linear gradient of 0.1 M TEAB in H_2O to 0.1 M TEAB in H_2O–MeOH (1:1) as eluent. Several co-distillations with water followed by freeze-drying from water gave solid product.

7-(1',2,2',3,3',4,4',5-Octamethylferrocene-1-yl-ethynyl)-7-deaza-2'-deoxyadenosine 5'-*O*-triphosphate (dA^{FcMe}TP)

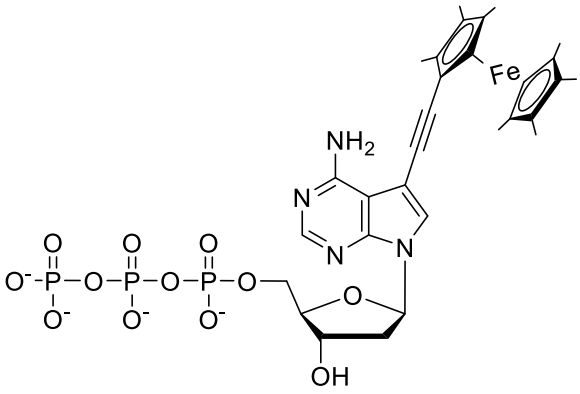

Compound **dA^{FcMe}TP** was prepared from **dA^{I}TP** by aqueous Sonogashira cross-coupling (Method A, 20 mg, 38 %) and from **dA^{FcMe}** according to the general triphosphorylation procedure (Method B, 8 mg, 15 %). The product was isolated as a yellow solid. ^{1}H and ^{13}C NMR spectra were not possible to analyze because of partial oxidation of ferrocene moiety.

^{31}P{^{1}H} NMR (162 MHz, D_2O): -20.41 (t, *J* = 19,6 P_{β}); -10.29 (d, *J* = 19.6, P_{α}); -4.10 (d, *J* = 20.2, P_{γ}).

MS (ESI-): *m/z* (%): 729.2 (100) [M-H_2PO_3]; 649.2 (60) [M-$H_3P_2O_6$]; HRMS (ESI-): calcd 808.1132 for $C_{31}H_{39}O_{12}N_4FeP_3$, found 808.1119.

5-(1',2,2',3,3',4,4',5-Octamethylferrocene-1-yl-ethynyl)-2'-deoxycytidine 5'-*O*-triphosphate (dC^{FcMe}TP)

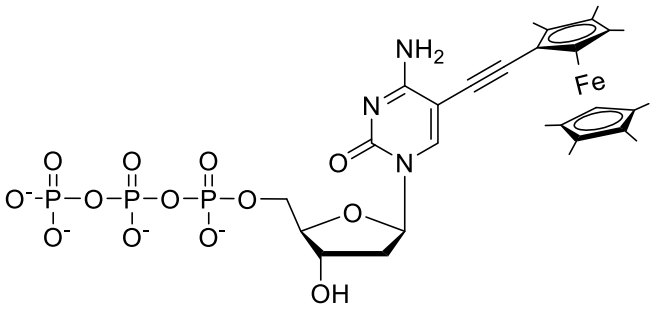

Compound **dC^{FcMe}TP** was prepared from **dC^{I}TP** by aqueous Sonogashira cross-coupling (Method A, 18 mg, 30 %) and from **dC^{FcMe}** according to the general triphosphorylation procedure (Method B, 7 mg, 20 %). The product was isolated as a yellow solid. ^{1}H and ^{13}C NMR spectra were not possible to analyse because of the partial oxidation of the ferrocene moiety.

^{31}P{^{1}H} NMR (162 MHz, D_2O): -19.62 (t, *J* = 20.5, P_{β}); -9.40 (d, *J* = 20.1, P_{α}); -3.48 (d, *J* = 20.5, P_{γ}).

MS (ESI-): *m/z* (%): 706.1 (100) [M-H_2PO_3]; 626.2 (50) [M-$H_3P_2O_6$]; HRMS (ESI-): calcd. 785.0972 for $C_{29}H_{38}O_{13}N_3FeP_3$, found 785.0964.

7-[3-(Ferrocene-1-carboxamido)prop-1-yn-1-yl]-7-deaza-2'-deoxyadenosine 5'-*O*-triphosphate (dA^{FcPa}TP)

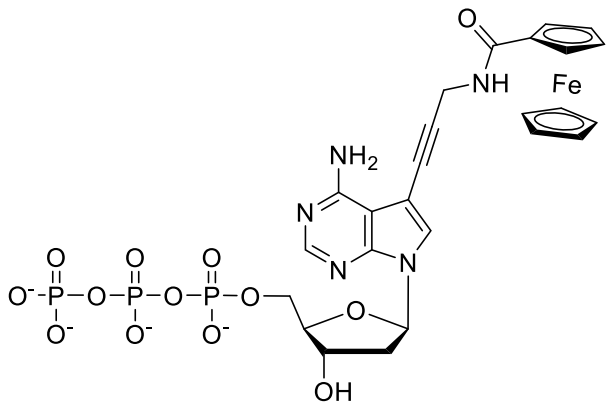

Compound **dA^{FcPa}TP** was prepared from **dA^{I}TP** by aqueous Sonogashira cross-coupling (Method A, 8 mg, 13 %) and from **dA^{FcPa}** according to the general triphosphorylation procedure (Method B, 25 mg, 22 %). The product was isolated as a yellow solid. ^{1}H NMR (500.0 MHz, D_2O): 1.20 (bm, 36H, C**H$_3$**CH$_2$N); 2.43 (ddd, 1H, J_{gem} = 13.7, $J_{2'b,1'}$ = 6.0, $J_{2'b,3'}$ = 3.4 H-2'b); 2.61 (ddd, 1H, J_{gem} = 13.7, $J_{2'a,1'}$ = 7.8, $J_{2'a,3'}$ = 6.0, H-2'a); 3.11 (bm, 24H, CH$_3$C**H$_2$**N); 4.04 – 4.13 (m, 2H, H-5'); 4.17 (q, 1H, $J_{4',3'}$ = $J_{4',5'}$ = 3.4, H-4'); 4.22 (bs, 5H, H-cp); 4.26 (bs, 2H, CH$_2$N); 4.46 (m, 2H, H-2",5"); 4.68 (dt, H, $J_{3',2'}$ = 6.0, 3.4, $J_{3',4'}$ = 3.4, H-3'); 4.79 (bs, 2H, H-3",4"); 6.46 (dd, 1H, $J_{1',2'}$ = 7.8, 6.0, H-1'); 7.60 (s, 1H, H-6); 8.03 (bs, 1H, H-2).

^{13}C NMR (125.7 MHz, D_2O): 10.94 (**CH$_3$**CH$_2$N); 32.68 (CH$_2$N); 41.15 (CH$_2$-2'); 42.97 (CH$_3$**C**H$_2$N); 68.28 (d, $J_{C,P}$ = 4.9, CH$_2$-5'); 71.19, 71.21 (CH-3",4"); 72.74 (CH-cp); 73.69 (CH-3'); 74.50 (CH-2",5"); 75.88 (C-1"); 7.47 (C5-**C**≡C-CH$_2$); 85.50 (CH-1'); 87.96 (d, $J_{C,P}$ = 8.7, CH-4'); 92.15 (C5-C≡**C**-CH$_2$); 99.01 (C-5); 105.56 (C-4a); 128.80 (CH-6); 151.18 (C-7a); 154.90 (CH-2); 159.84 (C-4); 176.97 (CONH).

^{31}P NMR (202.3 MHz, D_2O): -22.36 (bt, J = 19.4, P_β); -10.75 (d, J = 19.4, P_α); - 7.87 (bd, J = 19.4, P_γ).

MS (ESI-): 754.0 [M-H]; 674.0 [M-H$_2$PO$_3$]; HRMS (ESI-): calcd. 754.0173 for $C_{25}H_{27}O_{13}N_5FeP_3$, found 754.0169.

5-[3-(Ferrocene-1-carboxamido)prop-1-yn-1-yl]-2'-deoxycytidine 5'-*O*-triphosphate (dC^{FcPa}TP)

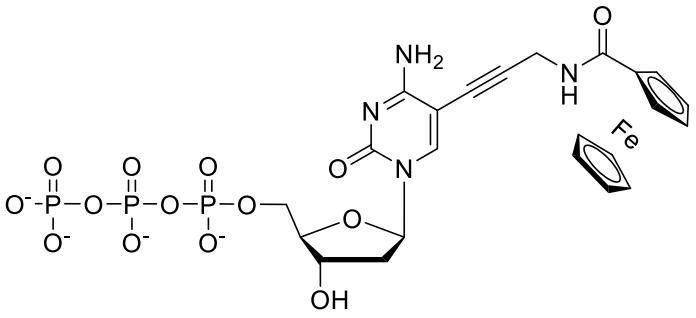

Compound **dC^{FcPa}TP** was prepared from **dC^{I}TP** by aqueous Sonogashira cross-coupling (Method A, 10 mg, 16 %) and from **dC^{FcPa}** according to the general triphosphorylation procedure (Method B, 20 mg, 18 %). The product was isolated as a yellow solid. ^{1}H NMR (500.0 MHz, D_2O): 1.26 (bm, 36H, C**H$_3$**CH$_2$N); 2.26 (dt, 1H, J_{gem} = 13.7, $J_{2'b,1'}$ = 6.8, $J_{2'b,3'}$ = 6.4, H-2'b); 2.40 (ddd, 1H, J_{gem} = 13.7, $J_{2'a,1'}$ = 6.1, $J_{2'a,3'}$ = 4.7, H-2'a); 3.17 (bm, 24H, CH$_3$C**H$_2$**N); 4.17 (m, 1H, H-4'); 4.18 – 4.26 (m, 2H, H-5'); 4.26 – 4.33 (m, 7H, CH$_2$N, H-cp); 4.54 (m, 2H, H-2",5"); 4.58 (dt, H, $J_{3',2'}$ = 6.4, 4.7, $J_{3',4'}$ = 4.7, H-3'); 4.85 (m, 2H, H-3",4"); 6.22 (dd, 1H, $J_{1',2'}$ = 6.8, 6.1, H-1'); 8.18 (s, 1H, H-6).

^{13}C NMR (125.7 MHz, D_2O): 10.98 (**C**H$_3$CH$_2$N); 32.52 (CH$_2$N); 42.02 (CH$_2$-2'); 49.33 (CH$_3$**C**H$_2$N); 67.75 (d, $J_{C,P}$ = 4.6, CH$_2$-5'); 71.30, 71.34 (CH-3",4"); 72.69 (CH-3'); 72.84 (CH-cp); 74.64, 74.65 (CH-2",5"); 75.73 (C1", C5-**C**≡C-CH$_2$); 88.21 (d, $J_{C,P}$ = 8.6, CH-4'); 88.82 (CH-1'); 95.05 (C-5); 95.60 (C5-C≡**C**-CH$_2$); 147.67 (CH-6); 158.68 (C-2); 167.83 (C-4); 177.10 (CONH).

^{31}P NMR (202.3 MHz, D_2O): -22.42 (t, J = 20.0, P_β); -10.83 (d, J = 20.0, P_α); -8.33 (bd, J = 20.0, P_γ).

MS (ESI-): 731.0 [M-H]; 651.0 [M-H$_2$PO$_3$]; HRMS (ESI-): calcd. 731.0013 for $C_{23}H_{26}O_{14}N_4FeP_3$, found 731.0006.

5-(Ferrocene-1-yl-ethynyl)-2'-deoxycytidine 5'-*O*-triphosphate (**dC^{Fc}TP**)

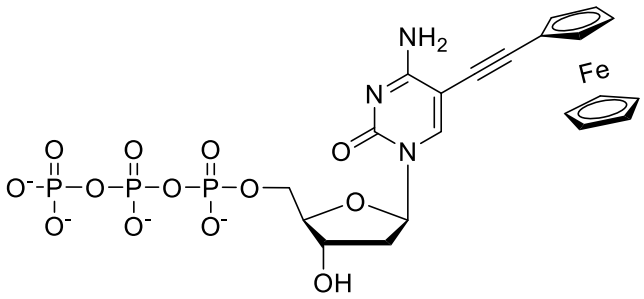

Compound **dC^{Fc}TP** was prepared in analogy to the literature [7] by the Sonogashira coupling of **dC^{I}TP** (0.05 mmol) with ethynylferrocene (16 mg, 0.078 mmol) in presence of $Pd(OAc)_2$ (0.6 mg, 5 mol %), CuI (1 mg, 10 mol %) and TPPTS (tris(3-sulfonatophenyl)phosphine) (7.5 mg, 25 mol %) in H_2O/acetonitrile (2:1, 1 ml) containing Et_3N (58 µL, 8 equiv.). The mixture was stirred under argon at 70 °C for 1 h, evaporated and the product isolated by reverse phase HPLC on C18 column with a linear gradient of 0.1 M TEAB (triethylammonium bicarbonate) in H_2O to 0.1 M TEAB in H_2O/MeOH (1:1), followed by repeated coevaporation with water and conversion to sodium salt using Dowex 50WX8 in Na^+ cycle. The product was obtained as a trisodium salt by freeze-drying from water in 27 % yield. ^{1}H NMR (600.1 MHz, D_2O): 2.34, 2.45 (2 × m, 2 × 1H, H-2'); 4.17-4.28 (m, 3H, H-4',5'); 4.34 (bs, 5H, cp); 4.40 (bs, 2H, H-3",4"); 4.60-4.68 (bm, 3H, H-3' and H-2",5") 6.48 (bt, 1H, $J_{1',2'}$ = 5.9, H-1'); 7.72 (s, 1H, H-8); 8.23 (bs, 1H, H-2).

^{13}C NMR (150.9 MHz, D_2O): 41.70 (CH2-2'); 65.92 (C-1"); 67.97 (d, $J_{C,P}$ = 5.3, CH_2-5'); 72.31 (CH-3",4"); 72.89 (CH-cp); 73.02 (CH-3'); 74.28 (CH-2",5"); 78.26 (C≡C-fer); 88.20 (d, $J_{C,P}$ = 8.5, CH-4'); 89.02 (CH-1'); 96.19 (C≡C-fer); 98.22 (C-5); 146.16 (CH-6); 158.76 (C-2); 167.58 (C-4).

^{31}P{^{1}H} NMR (202.3 MHz, D_2O): -21.70 (t, J = 19.2, P_β); -11.08 (d, J = 19.2, P_α); -5.91 (d, J = 19.2, P_γ).

MS (ESI-): *m/z* (%): 739.9 (15) [M]; 717.9 (100) [M-Na]; 696.0 (85) [M-Na_2]; 616.0 [M-Na_2PO_3]; 594.0 [M-Na_3PO_3]; 514.0 [M-$Na_3P_2O_6$]; HRMS (ESI-): calcd. 739.92570 for $C_{21}H_{20}O_{13}N_3FeNa_3P_3$; found: 739.92571.

3. Experimental section - biochemistry

General remarks

All gels were analysed by fluorescence imaging using Typhoon FLA 9500 (GE Healthcare). Mass spectra of oligonucleotides were measured on UltrafleXtreme MALDI-TOF/TOF (Bruker) mass spectrometer with 1 kHz smartbeam II laser. UV-Vis spectra were measured at room temperature in a NanoDrop1000 (ThermoScientific). Synthetic oligonucleotides (primers labelled at 5´-end with a 6-carboxyfluorescein (6-FAM), templates and biotinylated templates; for sequences see Table S1) were purchased from Generi Biotech (Czech Republic). Natural nucleoside triphosphates (dATP, dGTP, dTTP, dCTP) were purchased from ThermoScientific. KOD XL DNA polymerase and corresponding polymerase reaction buffer from Merck (Sigma Aldrich), Pwo DNA polymerase and Terminal transferase (TdT) were purchased from New England Biolabs. Streptavidin magnetic particles (Roche) were obtained from Sigma Aldrich. Milli-Q water was used for all experiments. PAGE stop solution used after PEX reactions contains: 95 % [v/v] formamide, 0.5 mM EDTA, 0.025 % [w/v] bromophenol blue and 0.025 % [w/v] xylene cyanol, 0.025 % [w/v] SDS and Milli-Q water. Samples after PEX reactions were separated with a 12.5 % PAGE (acrylamide/bisacrylamide 19:1, 25 % urea) under denaturing conditions (TBE 1X). Other chemicals were of analytical grade.

Table S1. List of sequences of primers and templates.

Name	Sequence
primer^{rnd}	5'-CATGGGCGGCATGGG-3'
temp^{rnd16}	5'-CTAGCATGAGCTCAGTCCCATGCCGCCCATG-3'
temp^{A}	5'-CCCTCCCATGCCGCCCATG-3'
temp^{C}	5'-CCCGCCCATGCCGCCCATG-3'
temp^{termA}	5'-TCCCATGCCGCCCATG-3'
temp^{termC}	5'-GCCCATGCCGCCCATG-3'
temp$^{1A,1C\text{-}bio}$	5´-CCACCATCCGCC CAT GCC GCC CAT G-3´
temp$^{rnd16\text{-}bio}$	5'-CTAGCATGAGCTCAGTCCCATGCCGCCCATG-3'
temp$^{1\text{-}C3\text{-}1A,1C}$	5´-ATTACGACGAACTCAATGAA-**C3**-CCACCATCCGCCCATGCCGCCC ATG - 3´
temp$^{2\text{-}C3\text{-}rnd16}$	5´- ATTACGACGAACTCAATGAA-**C3**-CTAGCATGAGCTCAGTCCCATG CCGCCCATG - 3´
temp$^{3\text{-}C3\text{-}Repet4*A,C}$	5´-ATTACGACGAACTCAATGAA-**C3**-ACTGACTGACTGACTGCCCATG CCGCCCATG - 3´
primer$^{8/2_4/4}$	5’-CATGGGCGGCCATTG G-3’
temp^{8A,2C}	5’-ATTACGACGAACTCAATGAA – **C3** – TCGATAGCCTACCTACAC CACACCTCAATACACTACCTACCAATGGCCGCCCATG-3´
temp^{8C,2A}	5’-ATTACGACGAACTCAATGAA – **C3** – GCTAGATCCGACCGACAC CACACCGCAAGACACGACCGACCAATGGCCGCCCATG-3’
temp^{4C,4A}	5’-ATTACGACGAACTCAATGAA – **C3** – GCTATAGCCTACGCAAGA CCTCCAATGGCCGCCCATG-3’
Capture probe	5’- TTCATTGAGTTCGTCGTAATTTTTTTTTTTTTTT-3’-**C6-SH**

In the template ONs the segments forming duplex with the primer are underlined.

Primer extension experiment – analysis and isolation of PEX products

Single incorporation (templates temp^A and temp^C)

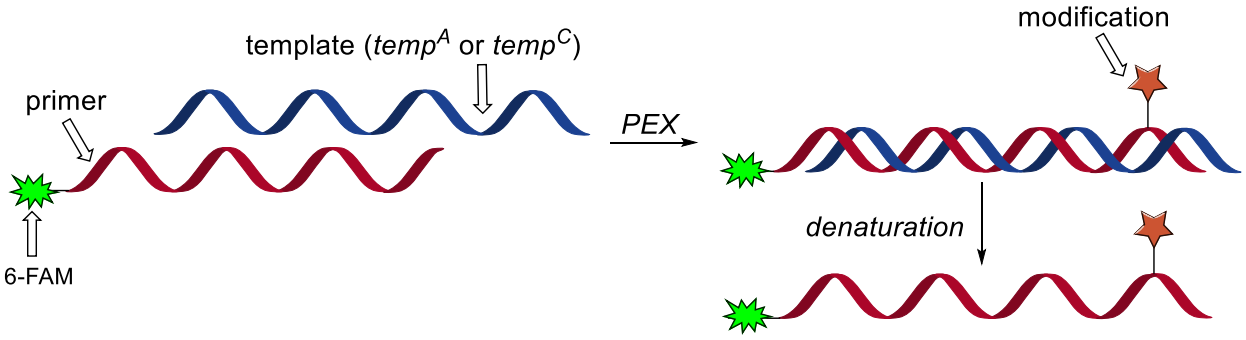

Scheme S3. Single nucleotide incorporation by PEX.

Method A: Reaction mixture (20 µL) contained temp^A (3 µM, 1 µl), 5'-6-(FAM)-labelled primer^{rnd} (3 µM, 1.5 µl), dGTP (4 mM, 0.1 µl), either dATP or **dA^{FcX}TP** (4 mM, 1 µl) KOD XL DNA polymerase (0.125 U) and reaction buffer (10X, 2 µL) as supplied by the manufacturer. The reaction mixture was incubated for 40 minutes at 60 °C. The PEX reaction was stopped by addition of PAGE stop solution (20 µL) and heated for 2 minutes at 95 °C. Samples were analysed with a 12.5 % denaturing polyacrylamide gel electrophoresis (1 h, 50 °C) and visualised using fluorescence imaging (Figure S1).

Method B: PEX reactions with temp^C were performed in the same way as described for temp^A except either dCTP or **dC^{FcX}TP** (4 mM, 1µl) were used (Figure S1).

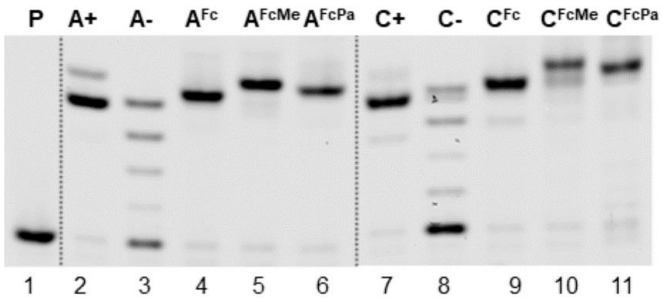

Figure S1. Primer extension with a KOD XL DNA polymerase using prim^{rnd}, temp^A, and temp^C: (P) primer (5'-6-FAM-labelled); (A+) dATP, dGTP; (A-) dGTP; (A^{Fc}) **dA^{Fc}TP**, dGTP; (A^{FcMe}) **dA^{FcMe}TP**, dGTP; (A^{FcPa}) **dA^{FcPa}TP**, dGTP; (C+) dCTP, dGTP; (C-) dGTP; (C^{Fc}) **dC^{Fc}TP**, dGTP; (C^{FcMe}) **dC^{FcMe}TP**, dGTP; (C^{FcPa}) **dC^{FcPa}TP**, dGTP.

Multiple incorporation (template $temp^{rnd16}$)

The reaction mixture (20 µL) contained template $temp^{rnd16}$ (3 µM, 1 µl), 5'-(FAM)-labelled $primer^{rnd}$ (3 µM, 1.5 µl), dNTP (either natural or modified, 4 mM, 1 µl), KOD XL DNA polymerase (0.25 U) and reaction buffer (10X, 2 µL) as supplied by the manufacturer. The reaction mixture was incubated for 40 minutes at 60 °C. The PEX reaction was stopped by addition of PAGE stop solution (20 µL) and heated for 2 minutes at 95 °C. Samples were analysed with a 12.5 % denaturing polyacrylamide gel electrophoresis (1 h, 50 °C) and visualised using fluorescence imaging (Figure S2).

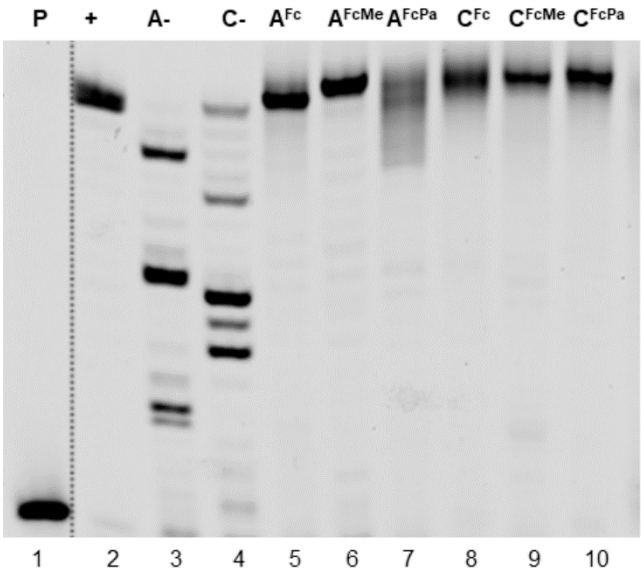

Figure S2. Primer extension with KOD XL DNA polymerase using $prim^{rnd}$, $temp^{rnd16}$: (P) primer (5'-6-FAM-labelled); (+) natural dNTPs; (A-) dCTP, dTTP, dGTP; (C-) dATP, dTTP, dGTP; (A^{Fc}) **$dA^{Fc}TP$**, dCTP, dTTP, dGTP; (C^{Fc}) **$dC^{Fc}TP$**, dATP, dTTP, dGTP; (A^{FcMe}) **$dA^{FcMe}TP$**, dCTP, dTTP, dGTP; (C^{FcMe}) **$dC^{FcMe}TP$**, dATP, dTTP, dGTP; (A^{FcPa}) **$dA^{FcPa}TP$**, dCTP, dTTP, dGTP; (C^{FcPa}) **$dC^{FcPa}TP$**, dATP, dTTP, dGTP.

Kinetics of incorporation of modified dNTPs (templates $temp^{termA}$ and $temp^{termC}$)

The simplified kinetics studies in the presence of KOD XL DNA polymerase were performed to examine the incorporation efficiency of modified **$dN^{FcX}TP$**s by PEX experiments in comparison with natural dNTPs (Figures S3-S6). The rates of the PEX with natural dNTPs or modified nucleotides were revealed using templates $temp^{termA}$ or $temp^{termC}$ and $primer^{rnd}$. The incorporation of natural dATP or dCTP were complete

in 2 minutes and ferrocenene-labelled nucleotides were fully incorporated within a maximum of 1-2 minutes. The slowest extension was observed in the experiment with **dA^{FcMe}TP**.

The rate of incorporation was compared by preparation of samples with natural and modified dNTPs with various time periods. PEX reaction mixture (20 µl) was performed with 5'-6-(FAM)-labelled prim^{rnd} (3 µM, 1 µl), temp^{termA} (3 µM, 1.5 µl) or temp^{termC} (3 µM, 1.5 µl), dNTPs (4 mM, 1 µl) with KOD XL DNA polymerase (0.125 U) in the enzyme reaction buffer (10X, 2 µL) as supplied by the manufacturer, followed by stopping of the reaction using the PAGE stop solution (20 µL) and immidiately heating for 2 minutes at 95 °C. Samples were analysed with a 12.5 % denaturing polyacrylamide gel electrophoresis (1 h, 50 °C) and visualised using fluorescence imaging.

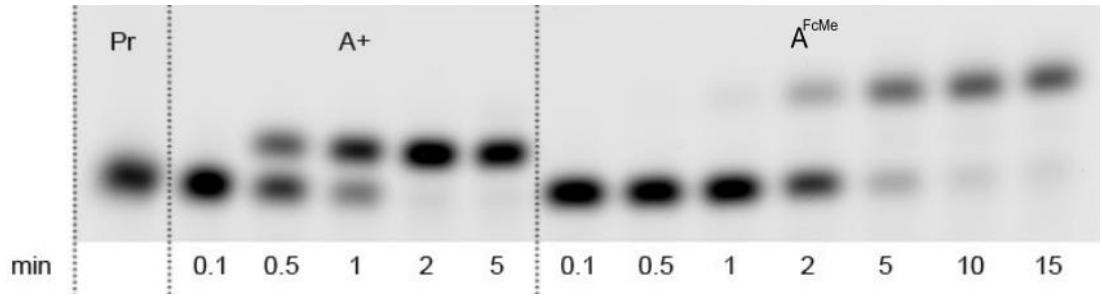

Figure S3. Comparison of incorporation of natural and modified dATPs to DNA with temp^{termA}: (Pr) primer (5'-6-FAM-labelled); (A+) dATP; (A^{FcMe}) **dA^{FcMe}TP**.

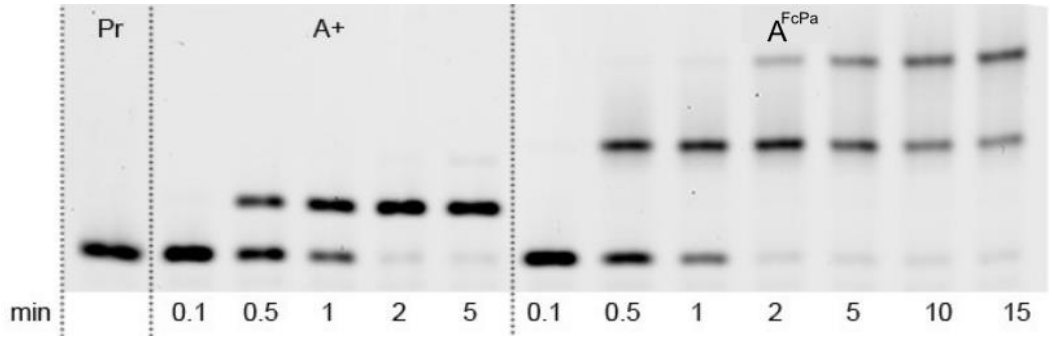

Figure S4. Comparison of incorporation of natural and modified dATPs to DNA with temp^{termA}: (Pr) primer (5'-6-FAM-labelled); (A+) dATP; (**A**^{FcPa}) **dA^{FcPa}TP**.

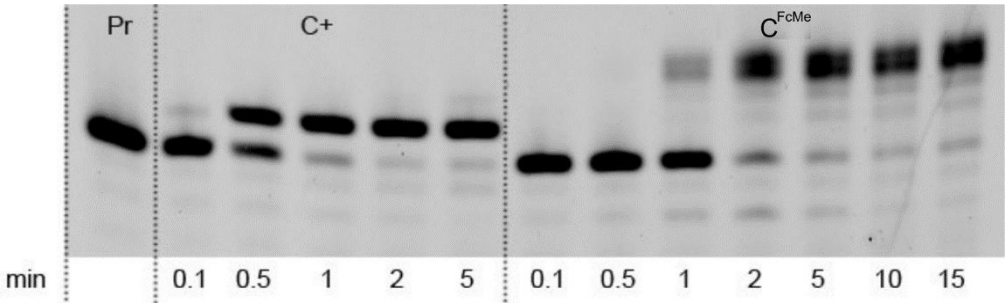

Figure S5. Comparison of incorporation of natural and modified dCTPs to DNA with temp^{termC}: (Pr) primer (5'-6-FAM-labelled); (C+) dCTP; (C^{FcMe}) **dC^{FcMe}TP**.

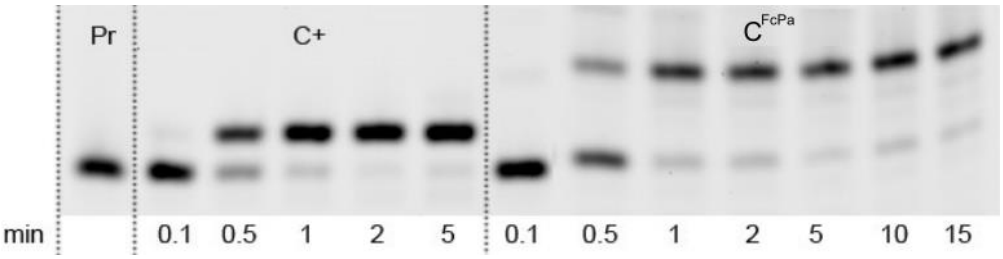

Figure S6. Comparison of incorporation of natural and modified dCTPs to DNA with temp^{termC}: (Pr) primer (5'-6-FAM-labelled); (C+) dCTP; (C^{FcPa}) **dC^{FcPa}TP**.

Isolation of single-strand oligonucleotides by the DBStv magnetoseparation procedure (templates temp^{rnd16}, temp^{A} and temp^{C})

The reaction mixture (50 µL) contained biotinylated temp^{rnd16} (temp^{A} or temp^{C}) (100 µM, 1.6 µL), primer^{rnd} (100 µM, 1.6 µL), dNTPs (4 mM, 2.6 µL), and KOD XL DNA polymerase (0.75 U) in the enzyme reaction buffer (5 µL) as supplied by the manufacturer. The reaction mixture was incubated for 1 h at 60 °C in a thermal cycler. The reaction was stopped by cooling to 4 °C. Streptavidin magnetic particles (Roche, 100 µL) were washed with Binding buffer TEN 100 (10 mM Tris, 1 mM EDTA, 100 mM NaCl, pH 7.5; 3 × 200 µL). The reaction mixture after PEX was diluted with the Binding buffer TEN 100 (50 µL), and the solution was added to the prewashed magnetic beads and incubated for 30 min at 15 °C and 1400 rpm. After the incubation, the magnetic beads were collected on a magnet (DynaMag-2, Invitrogen) and the solution was discarded. The beads were washed successively with Wash buffer TEN 500 (10 mM Tris, 1 mM EDTA, 500 mM NaCl, pH 7.5; 3 × 200 µL), and water (3 × 200 µL). Water (50 µL) was then added and the sample was denatured for 2 min at 70 °C and 1000 rpm. The beads were collected on a magnet and the solution was transferred to a clean vial. The product was analysed using MALDI-TOF mass spectrometry (Table S2).

MALDI-TOF measurements

The MALDI-TOF spectra were measured with 1 kHz smartbeam II laser technology. The measurements were carried out in reflectron and linear mode using the droplet technique, with the mass range up to 30 kDa. The matrix consisted of 3-hydroxypicolinic acid (HPA)/picolinic acid (PA)/ ammonium tartrate in ratio 9/1/1. The matrix (1 µL) was applied to the target (ground steel) and dried down at room temperature. The sample (1 µL) and matrix (1 µL) were mixed and added on the top of the dried matrix preparation spot and dried at room temperature.

Table S2. List of MALDI data of PEX products bearing modified or non-modified Fc labels.

oligonucleotide	M calcd. (Da)	M found (Da)
31ON_4A^{Fc}	10445.54	10447.0
31ON_4A^{FcPa}	10673.70	10674.1
31ON_4C^{Fc}	10449.54	10451,9
31ON_4C^{FcPa}	10677.70	10679.6
19ON_1A^{Fc}	6182.0	6183.2
19ON_1A^{FcPa}	6239.0	6238.6
19ON_1A^{FcMe}	6294.0	6295.4
19ON_1C^{Fc}	6159.0	6160.2
19ON_1C^{FcPa}	6216.0	3389.4
19ON_1C^{FcMe}	6271.0	6272.3

Single incorporation (template temp$^{1A,1C\text{-}bio}$)

The PEX reaction mixture (200 µL) contained 5'-(6-FAM)-labelled 15nt primer prim^{rnd} (3 µM, 10 µL), 25nt biotinylated template temp$^{1A,1C\text{-}bio}$ (3 µM, 15 µL), KOD XL DNA polymerase (2.5 U/µL, 0.5 µL), natural dNTPs (1 mM, 2 µL), modified dATP or dCTP (4 mM, 2.5 µL) in enzyme reaction buffer (10X, 20 µL) as supplied by the manufacturer. The reaction mixture was incubated for 10 min at 60 °C in a thermal cycler.

Small aliquots (5 µL) of the finished PEX mixture was mixed with 5 µL of PAGE stop solution and heated for 5 min at 95 °C prior to loading. Samples were separated with a 12.5 % PAGE under denaturing conditions (42 mA, 30 min). Visualisation was performed using fluorescence imaging (Figure S7).

The rest of the PEX reaction mixture was then used for the isolation of single-stranded oligonucleotides bearing one modification by magnetoseparation procedure (see below).

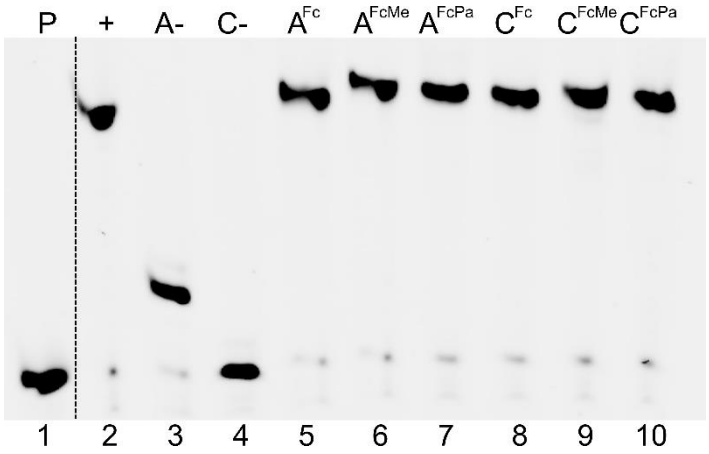

Figure S7. Primer extension with KOD XL DNA polymerase using prim*rnd* and temp$^{1A,1C\text{-}bio}$: (P) primer (5'-6-FAM-labelled); (+) natural dNTPs; (A-) dCTP, dTTP, dGTP; (C-) dATP, dTTP, dGTP; (A^{Fc}) **dA^{Fc}TP**, dCTP, dTTP, dGTP; (A^{FcMe}) **dA^{FcMe}TP**, dCTP, dTTP, dGTP; (A^{FcPa}) **dA^{FcPa}TP**, dCTP, dTTP, dGTP; (C^{Fc}) **dC^{Fc}TP**, dATP, dTTP, dGTP; (C^{FcMe}) **dC^{FcMe}TP**, dATP, dTTP, dGTP; (C^{FcPa}) **dC^{FcPa}TP**, dATP, dTTP, dGTP.

Multiple incorporation (template temp$^{rnd16\text{-}bio}$)

The PEX reaction mixture (200 µL) contained 5'-(6-FAM)-labelled 15nt primer prim*rnd* (3 µM, 10 µL), 31nt biotinylated template temp$^{rnd16\text{-}bio}$ (3 µM, 15 µL), KOD XL DNA polymerase (2.5 U/µL, 3 µL), natural dNTPs (4 mM, 10 µL), modified dATP or dCTP (4 mM, 25 µL) in enzyme reaction buffer (10X, 20 µL) as supplied by the manufacturer. The reaction mixture was incubated for 30 min at 60 °C in a thermal cycler.

Small aliquots (5 µL) of the finished PEX mixture was mixed with 5 µL of PAGE stop solution and heated for 5 min at 95 °C prior to loading. Samples were separated with a 12.5 % PAGE under denaturing conditions (42 mA, 30 min). Visualisation was performed using fluorescence imaging (Figure S8).

The rest of the PEX reaction mixture was then used for the isolation of single-stranded oligonucleotides bearing four modifications by magnetoseparation procedure (see below).

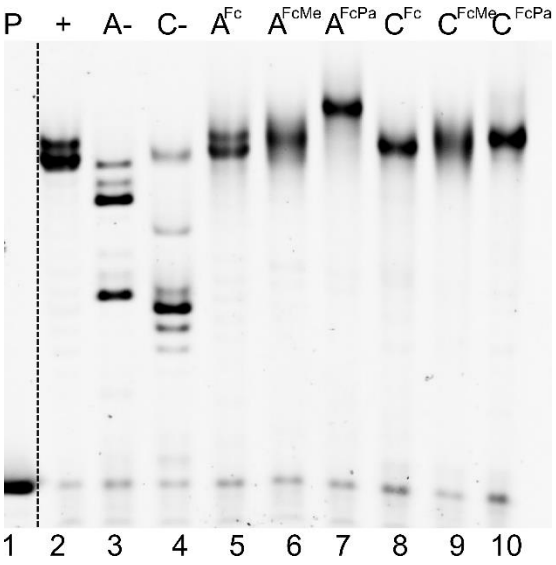

Figure S8. Primer extension with KOD XL DNA polymerase using prim^{rnd} and temp$^{rnd16\text{-}bio}$: (P) primer (5'-6-FAM-labelled); (+) natural dNTPs; (A-) dCTP, dTTP, dGTP; (C-) dATP, dTTP, dGTP; (A^{Fc}) **dA^{Fc}TP**, dCTP, dTTP, dGTP; (A^{FcMe}) **dA^{FcMe}TP**, dCTP, dTTP, dGTP; (A^{FcPa}) **dA^{FcPa}TP**, dCTP, dTTP, dGTP; (C^{Fc}) **dC^{Fc}TP**, dATP, dTTP, dGTP; (C^{FcMe}) **dC^{FcMe}TP**, dATP, dTTP, dGTP; (C^{FcPa}) **dC^{FcPa}TP**, dATP, dTTP, dGTP.

Magnetoseparation procedure (template $temp^{1A,1C\text{-}bio}$ and $temp^{rnd16\text{-}bio}$)

Streptavidin magnetic particles (Roche, 450 µL) were washed with Binding buffer TEN 100 (10 mM Tris, 1 mM EDTA, 100 mM NaCl, pH 7.5; 3 × 200 µL). The reaction mixture after PEX (195 µL) was mixed with the Binding buffer TEN 100 (1000 µL), and the solution was then added to the prewashed magnetic beads and incubated for 30 min at 15 °C and 1400 rpm. After the incubation, the magnetic beads were collected on a magnet (DynaMag-2, Invitrogen) and the solution was discarded. The beads were washed successively with Wash buffer TEN 500 (10 mM Tris, 1 mM EDTA, 500 mM NaCl, pH 7.5; 3 × 500 µL), and Milli-Q water (4 × 300 µL). Water (100 µL) was then added and the sample was denatured for 2 min at 72 °C and 900 rpm. The beads were collected on a magnet and the solution was transferred to a clean vial.

After magnetoseparation, small aliquots (2 µL) of all samples were mixed with 3 µL of PAGE stop solution and 10 µL of Milli-Q water and heated for 5 min at 95 °C prior to loading. Samples were separated with a 12.5 % PAGE under denaturing conditions (42 mA, 30 min). Visualisation was performed using fluorescence imaging (Figure S9).

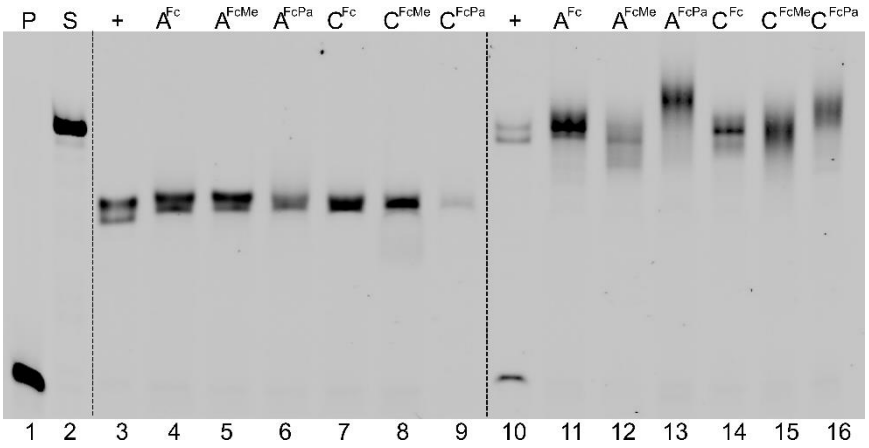

Figure S9. 12.5 % PAGE after magnetoseparation procedure. Single-stranded oligonucleotide products (Lines 3-9) with one Fc modification, 25-mer product; (Lines 10-16) with four Fc modifications, 31-mer product. (P) 15nt primer (5'-6-FAM-labelled); (S) 31nt oligonucleotide with complementar sequence to $temp^{rnd16}$ (5'-6-FAM-labelled).

All single-stranded oligonucleotide products were lyophilized, and before use were dissolved in 10 µL of Milli-Q water.

Enzymatic synthesis of ON using tailed-templates with C3-spacer

Single incorporation (template $temp^{1\text{-}C3\text{-}1A,1C}$)

The PEX reaction mixture (20 µL) contained 5'-(6-FAM)-labelled 15nt primer $prim^{rnd}$ (3 µM, 1 µL), template $temp^{1\text{-}C3\text{-}1A,1C}$ (3 µM, 1.5 µL), KOD XL DNA polymerase (0.125 U/µL, 1 µL), natural dNTPs (0.2 mM, 1 µL), modified dATP or dCTP (0.8 mM, 1.5 µL) in enzyme reaction buffer (10X, 2 µL) as supplied by the manufacturer. The reaction mixture was incubated for 10 min at 60 °C in a thermal cycler.

The finished PEX mixture was mixed with 20 µL of PAGE stop solution and heated for 5 min at 95 °C prior to loading. Samples were separated with a 12.5 % PAGE under denaturing conditions (42 mA, 30 min). Visualisation was performed using fluorescence imaging (Figure S10-A).

Moreover, the enzymatic synthesis was then five times scaled-up (100 µL total volume of PEX reaction mixture) in order to obtain sufficient amount of modified DNA for electrochemical experiments.

After the PEX synthesis at a higher scale, small aliquots (5 µL) of all samples were mixed with 5 µL of PAGE stop solution and heated for 5 min at 95 °C prior to loading. Samples were separated with a 12.5 % PAGE under denaturing conditions (42 mA, 30 min). Visualisation was performed using fluorescence imaging (Figure S10-B).

The remaining volume (~ 95 µL) of all samples was mixed with 20 µL of hybridization solution (H7140, Sigma Aldrich) and freezed to - 80 °C.

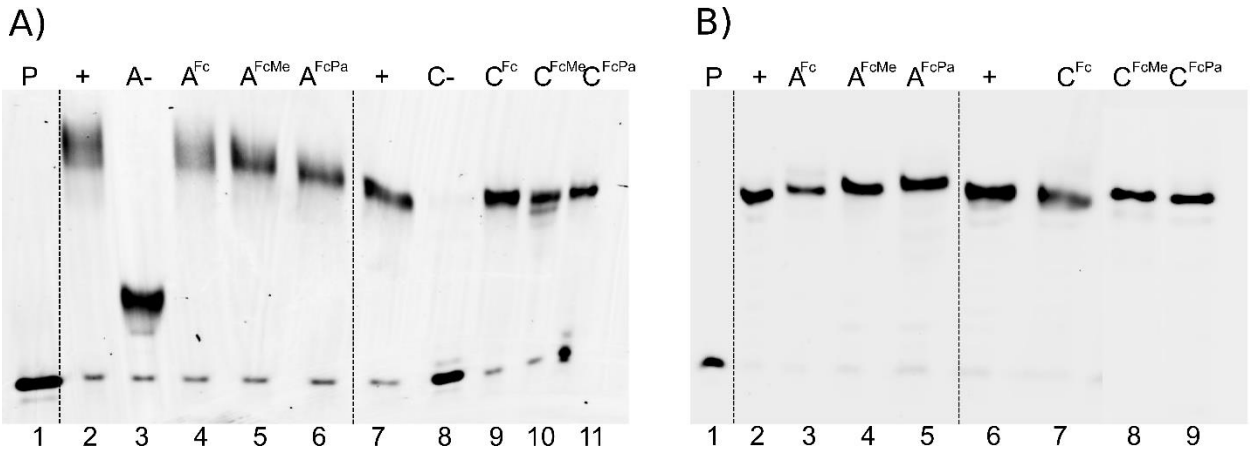

Figure S10. Primer extension with KOD XL DNA polymerase using $prim^{rnd}$ and **$temp^{1\text{-}C3\text{-}1A,1C}$**: A) PEX in small scale (20 µL); B) PEX in larger scale (100 µL); (P) primer (5'-6-FAM-

labelled); (+) natural dNTPs; (A-) dCTP, dTTP, dGTP; (C-) dATP, dTTP, dGTP; (A^{Fc}) **$dA^{Fc}TP$**, dCTP, dTTP, dGTP; (A^{FcMe}) **$dA^{FcMe}TP$**, dCTP, dTTP, dGTP; (A^{FcPa}) **$dA^{FcPA}TP$**, dCTP, dTTP, dGTP; (C^{Fc}) **$dC^{Fc}TP$**, dATP, dTTP, dGTP; (C^{FcMe}) **$dC^{FcMe}TP$**, dATP, dTTP, dGTP; (C^{FcPa}) **$dC^{FcPa}TP$**, dATP, dTTP, dGTP.

Multiple incorporation (templates $temp^{1\text{-}C3\text{-}1A,1C}$ or $temp^{3\text{-}C3\text{-}Repet4*A,C}$)

The PEX reaction mixture (20 µL) contained 5'-(6-FAM)-labelled 15nt primer $prim^{rnd}$ (3 µM, 1 µL), templates $temp^{1\text{-}C3\text{-}1A,1C}$ or $temp^{3\text{-}C3\text{-}Repet4*A,C}$ (3 µM, 1.5 µL), KOD XL DNA polymerase (0.75 U/µL, 1 µL),

A) in the case of **$dA^{FcX}TP$**: natural dNTPs (4 mM, 1 µL), modified dATP (4 mM, 2.5 µL)
B) in the case of **$dC^{FcX}TP$**: natural dNTPs (4 mM, 0.5 µL), modified dCTP (4 mM, 2.5 µL)

in enzyme reaction buffer (10X, 2 µL) as supplied by the manufacturer. The reaction mixture was incubated for 20 min at 60 °C in a thermal cycler.

The finished PEX mixture was mixed with 20 µL of PAGE stop solution and heated for 5 min at 95 °C prior to loading. Samples were separated with a 12.5 % PAGE under denaturing conditions (42 mA, 30 min). Visualisation was performed using fluorescence imaging (Figure S11-A, Figure S12|-A).

Moreover, the enzymatic synthesis was then five times scaled-up (100 µL total volume of PEX reaction mixture) in order to obtain a sufficient amount of modified DNA for electrochemical experiments.

After the PEX synthesis at a higher scale, small aliquots (5 µL) of all samples were mixed with 5 µL of PAGE stop solution and heated for 5 min at 95 °C prior to loading. Samples were separated with a 12.5 % PAGE under denaturing conditions (42 mA, 30 min). Visualisation was performed using fluorescence imaging (Figure S11-B, Figure S12-B).

The remaining volume (~ 95 µL) of all samples was mixed with 20 µL of hybridization solution (H7140, Sigma Aldrich) and freezed to - 80 °C.

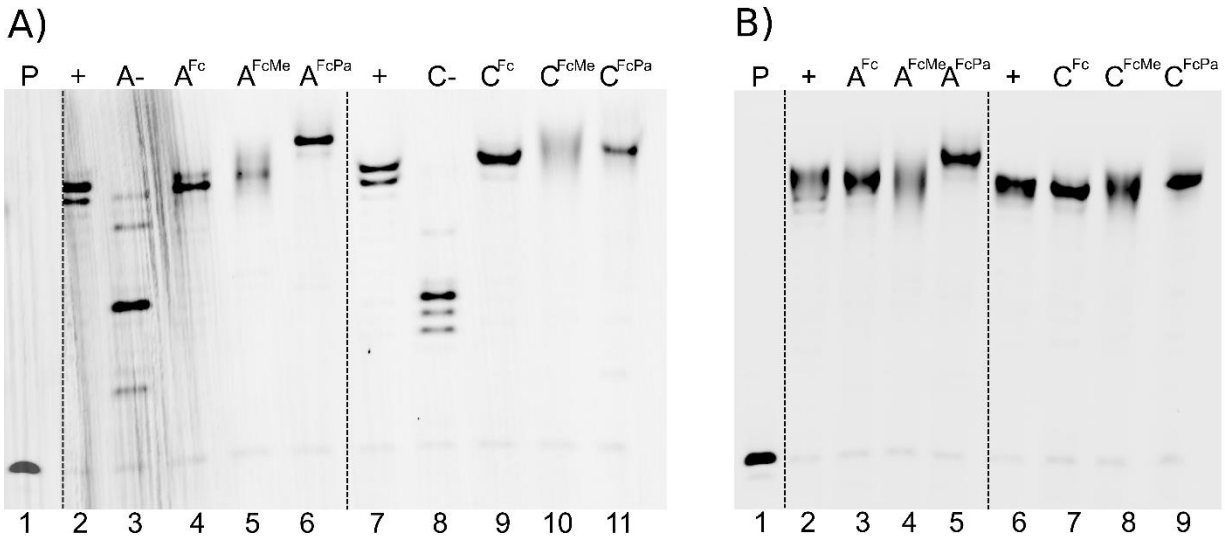

Figure S11. Primer extension with KOD XL DNA polymerase using prim^{rnd} and **temp$^{2\text{-}C3\text{-}rnd16}$**: A) PEX in small scale (20 µL); B) PEX in larger scale (100 µL); (P) primer (5'-6-FAM-labelled); (+) natural dNTPs; (A-) dCTP, dTTP, dGTP; (C-) dATP, dTTP, dGTP; (A^{Fc}) **dA^{Fc}TP**, dCTP, dTTP, dGTP; (A^{FcMe}) **dA^{FcMe}TP**, dCTP, dTTP, dGTP; (A^{FcPa}) **dA^{FcPa}TP**, dCTP, dTTP, dGTP; (C^{Fc}) **dC^{Fc}TP**, dATP, dTTP, dGTP; (C^{FcMe}) **dC^{FcMe}TP**, dATP, dTTP, dGTP; (C^{FcPa}) **dC^{FcPa}TP**, dATP, dTTP, dGTP.

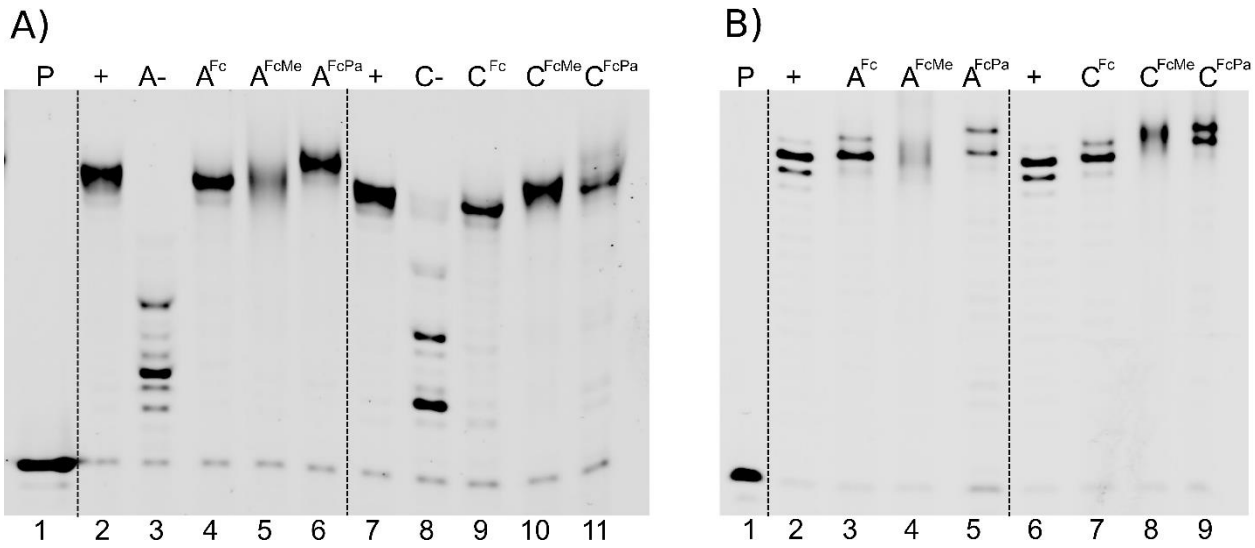

Figure S12. Primer extension with KOD XL DNA polymerase using prim^{rnd} and **temp$^{3\text{-}C3\text{-}Repet4*A,C}$**: A) PEX in small scale (20 µL); B) PEX in larger scale (100 µL); (P) primer (5'-6-FAM-labelled); (+) natural dNTPs; (A-) dCTP, dTTP, dGTP; (C-) dATP, dTTP, dGTP; (A^{Fc}) **dA^{Fc}TP**, dCTP, dTTP, dGTP; (A^{FcMe}) **dA^{FcMe}TP**, dCTP, dTTP, dGTP; (A^{FcPa}) **dA^{FcPa}TP**, dCTP, dTTP, dGTP; (C^{Fc}) **dC^{Fc}TP**, dATP, dTTP, dGTP; (C^{FcMe}) **dC^{FcMe}TP**, dATP, dTTP, dGTP; (C^{FcPa}) **dC^{FcPa}TP**, dATP, dTTP, dGTP.

4. Experimental section – electrochemistry

Electrochemical analysis of nucleosides

Modified nucleosides and dNTPs were studied by *in situ* square-wave voltammetry (SWV) at a basal plane-oriented pyrolytic graphite electrode (PGE). SWV settings: initial potential -0.5 V, end potential 1.6 V, frequency 200 Hz, amplitude 50 mV; background electrolyte: 0.2 M sodium acetate pH 5.0. Concentration of the compounds was 40 µM. All measurements were performed at room temperature using an Autolab analyzer (Eco Chemie, The Netherlands) in connection with VA-stand 663 (Metrohm, Herisau, Switzerland). The three-electrode system was used with Ag/AgCl/3M KCl electrode as a reference and platinum wire as an auxiliary electrode (Figure S14-S15).

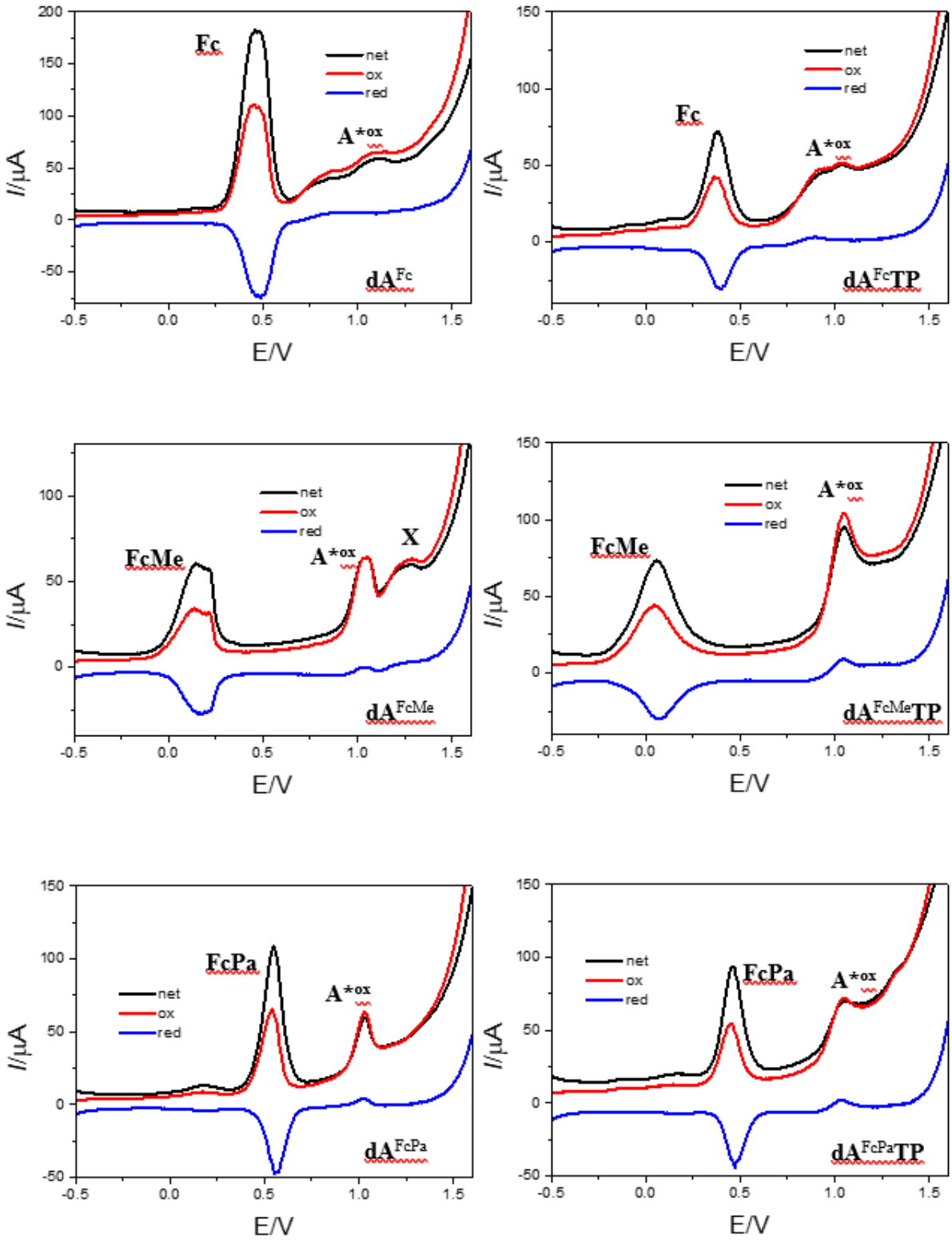

Figure S14. Components of square-wave voltammograms of $\mathbf{A^{FcMe}}$ and $\mathbf{A^{FcPa}}$-modified nucleosides and dNTPs (for experimental conditions see Figure 2 in the article). Red curves – forward component, blue – backward component, black – net current. Negative (reduction) counterpeaks on the backward curve at potentials close to those of forward positive (oxidation) peaks indicate reversibility of the system (ferrocene/ferrocenium). Absence of the negative peaks (or presence of small positive peaks at the backward curve) indicate an irreversible oxidation process.

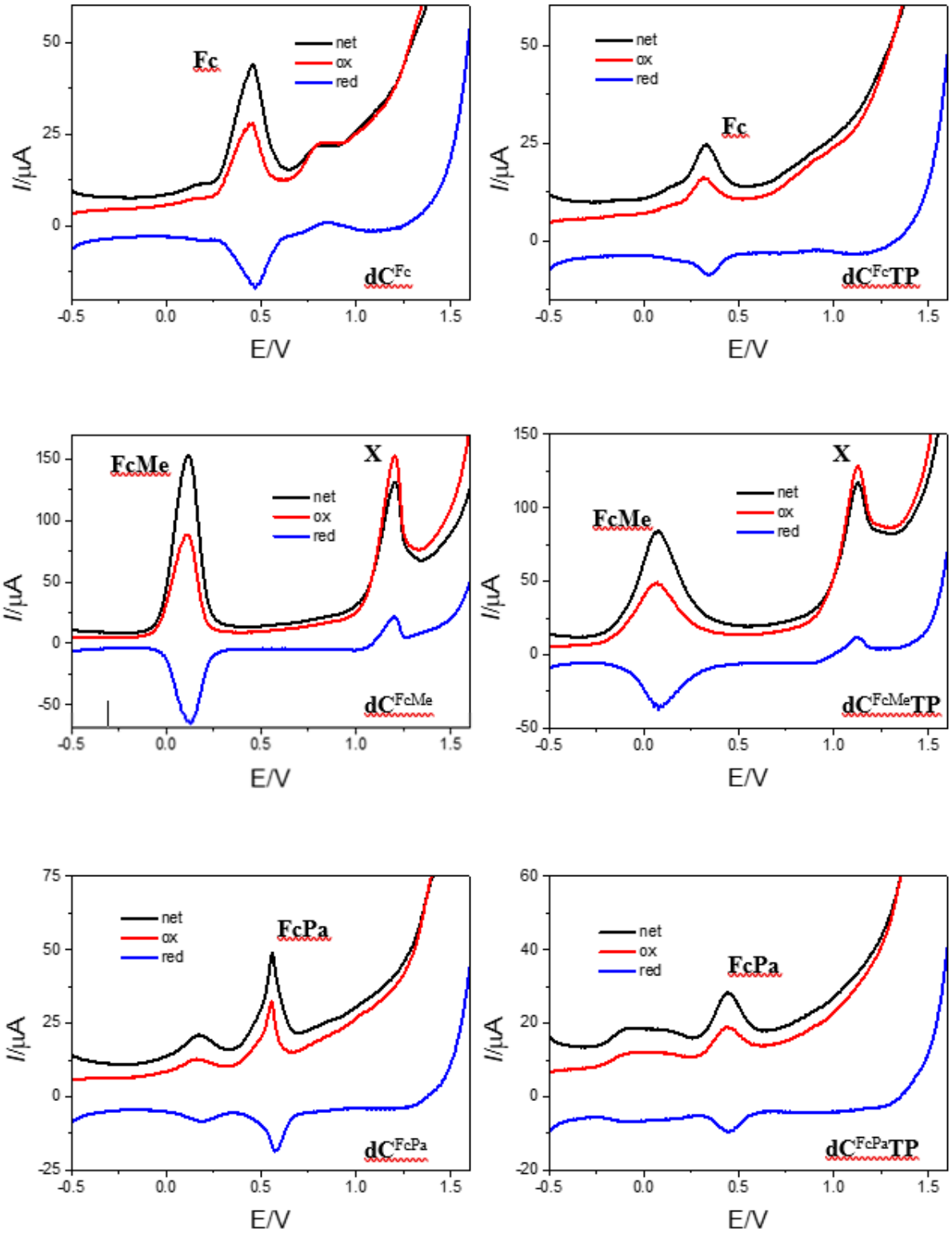

Figure S15. Components of square-wave voltammograms of C^{FcMe} and C^{FcPa}-modified nucleosides and dNTPs (for experimental conditions see Figure 2 in the article). Red curves – forward component, blue – backward component, black – net current. Negative (reduction) counterpeaks on the backward curve at potentials close to those of forward positive (oxidation) peaks indicate reversibility of the system (ferrocene/ferrocenium). Absence of the negative peaks (or presence of small positive peaks at the backward curve) indicate an irreversible oxidation process.

Electrochemical analysis of oligonucleotides

Electrode fabrication and functionalisation

Gold sputtered electrode arrays consisting of 3 groups of 3 circular working electrodes (1 mm^2), were fabricated on a glass substrate as described previously.[3] Prior to functionalisation, the electrodes were cleaned by sonicating for 5 minutes in acetone, followed by 5 minutes in isopropanol and were then rinsed with Milli-Q water and dried with N_2. Subsequently, the electrodes were electrochemically cleaned in KOH (0.1 M) using cyclic voltammetry with a scan rate of 100 mV/s, from 0 to -1.2 V vs Ag/AgCl, for 10 scans. The electrodes were then rinsed with Milli-Q water, dried with N_2, and again electrochemically cleaned, this time in H_2SO_4 (0.1 M), with a scan rate of 100 mV/s from 0 to 1.6 V vs Ag/AgCl, again for 10 cycles, before a final rinse with Milli-Q water and drying with N_2.

A capture probe cocktail solution was prepared to contain 1 µM capture probe, 100 µM of mercaptohexanol and 1 M KH_2PO_4. One microlitre of the capture probe cocktail was dropcast on to each working electrode and the array was then incubated for 3 h at 22 ºC in a humidity saturated chamber. Following functionalisation, the electrodes were rinsed with Milli-Q and then dried with N_2. A 7 µL volume chamber was created to host the PEX purified products for hybridisation and electrochemical detection, by placing a PMMA cover over a patterned double adhesive gasket. Once assembled, the microfluidic chambers were washed with 20 µL of PBS Tween-20, then 200 µL of milli-Q and finally dried them with N_2 prior to use.

Primer extension and hybridisation

Primer extension (PEX) was performed in a T100 thermal cycler (Biorad) by heating the sample to 60 ºC for 30 minutes. The PEX reaction mixture (20 µL) contained 1.2 units of KOD XL DNA polymerase, KOD XL buffer (1X), 200 nM primer, 300 nM template and 200 µM of dGTP, dTTP, **$dA^{Fc}TP$** and **$dC^{FcPa}TP$**. The PEX product was mixed with 4 µL of hybridisation solution (2X) and 7 µL of the mixture were added to a functionalised electrode array and incubated for 30 minutes at 22 ºC in a humidity chamber. The

microfluidic chambers were then washed with 3 x 200 µL of PBS Tween-20 and 200 µL of 0.1 M $Ca(NO_3)_2$.

Agarose gel electrophoresis

PEX products were visualised using agarose gel electrophoresis, which was prepared with ultra low pure agarose (4 % w/v) in 1× Tris-Borate-EDTA buffer (TBE) and stained with GelRed™nucleic acid stain. PEX product (3 µL) was added to 3 µL of loading buffer 2X (stock buffer 6X contained glycerol 30 %, bromphenol blue 0,25 %) per well, and electrophoresis was carried out with an applied voltage of 100 V for 40 min. The DNA was imaged using a UV transilluminator (λ = 254 nm) (Figure S16).

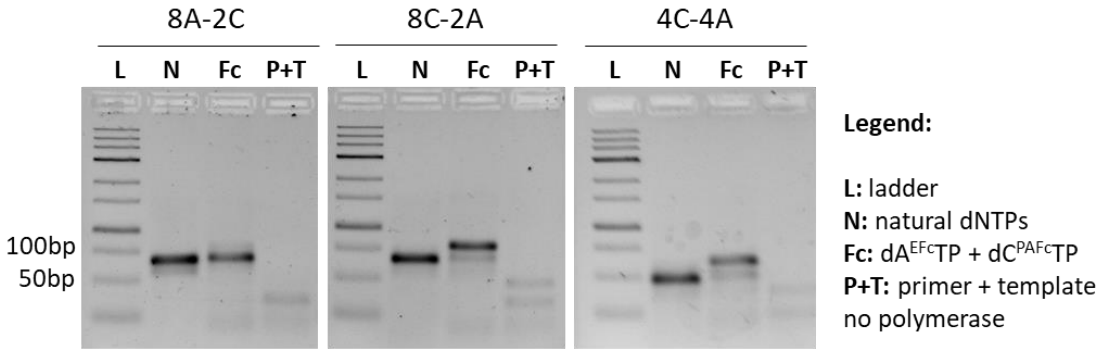

Figure S16. Agarose gel electrophoresis of PEX products using $temp^{8A,2C}$, $temp^{8C,2A}$ or $temp^{4C,4A}$ templates and $primer^{8/2\_4/4}$ obtained in the presence of (a) all four natural dNTPs (+), or combination of **$dA^{Fc}TP$**, **$dC^{FcPa}TP$** with TTP and GTP (*Fc). P/T corresponds to primer hybridised to template in the absence of polymerase.

Electrochemical measurements of PEX products

Square wave voltammetry was performed using a potentiostat/galvanostat PBSTAT 12 Autolab controlled with Nova 2.1.3 software. Following hybridisation, measurements were carried out in 0.1 M $Ca(NO_3)_2$ electrolyte solution using an external Ag/AgCl reference electrode and the internal counter and working gold electrodes on the electrode array, with a step potential from 0 V to 0.6 V using a 1 mV step, 20 mV modulation amplitude and 50 Hz of frequency.

Hybridisation for liquid phase PEX products

PEX product (7 µL) was added to each electrode array chamber (3 working electrodes/chamber, for triplicate measurements) for 30 minutes at 22 ºC in a humidity saturated chamber. Following hybridisation the electrode array chambers were flushed with 3 x 200 µL of PBS-Tween and then with 200 µL of 0.1 M $Ca(NO_3)_2$.

Electrochemical detection - Square wave voltammetry

Square wave voltammetry was carried out using a potentiostat/galvanostat PGSTAT 12 Autolab controlled with Nova 2.1.3 software. Following hybridisation, measurements were taken in 0.1 M $Ca(NO_3)_2$ electrolyte solution using an external Ag/AgCl reference electrode and the internal counter and working gold electrodes on the electrode array. For square wave voltammetry experiments, a step potential from 0.2 V to 0.6 V was used, with a 5 mV step, 25 mV modulation amplitude and 50 Hz frequency. For cyclic voltammetry experiments the potential was cycled between 0 and 0.6 V vs Ag/AgCl at a scan rate of 100 mV/s.

5. Copies of MALDI-TOF mass spectra

a) prim^{rnd} 3'-GGGTACGGCGGGTAC-5'

temp^{rnd16} 5'-CTAGCATGAGCTCAGTCCCATGCCGCCCATG-3'

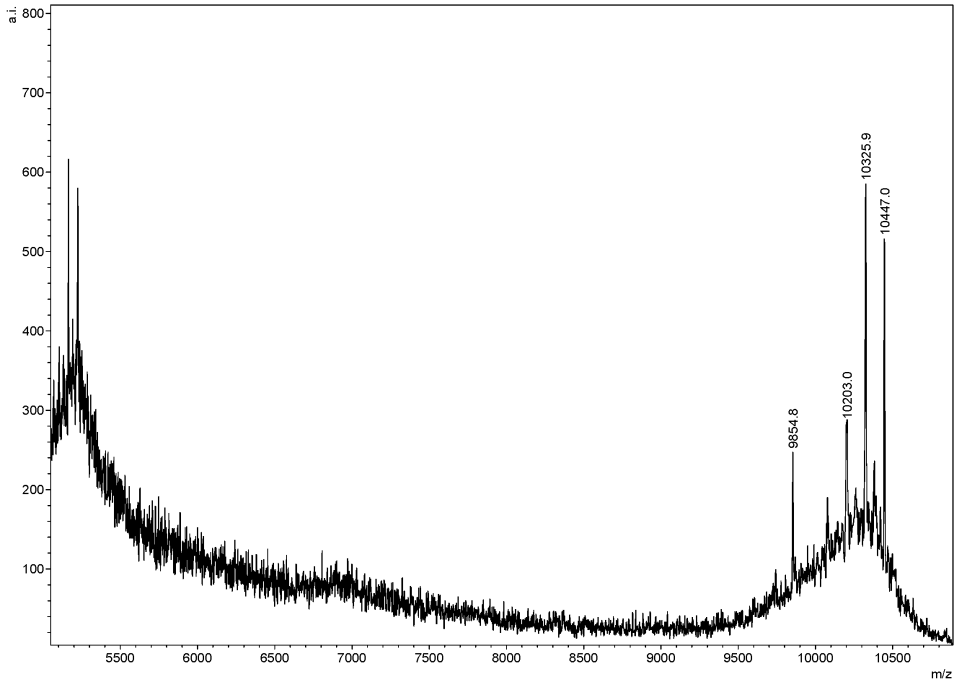

Figure S17. Mass (ssDNA: **dA^{Fc}TP,** dCTP, dTTP**,** dGTP): calculated: 10445,54 Da; found: 10447.0 Da; Δ = 1.46 (M = 10325.9 Da is full product minus one Cp ring with Fc; M = 10203.0 Da is full product minus two Cp rings with two Fc)

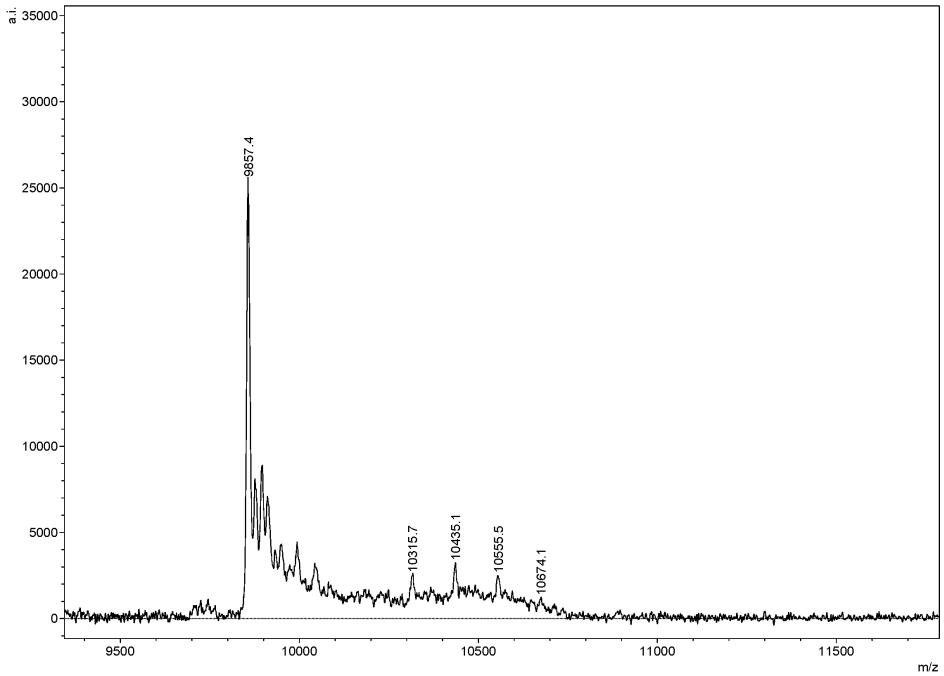

Figure S18. Mass (ssDNA: **dA^{FcPa}TP,** dCTP, dTTP**,** dGTP): calculated: 10673,7 Da; found: 10674.1 Da; Δ = 1.46 (M = 9857.4 Da is a peak of template; M = 10555.5 Da is full product minus one Cp ring with Fc; M = 10435.0 Da is full product minus two Cp rings with two Fc; M = 10315.7 Da is full product minus three Cp ring with three Fc) (Sample was measured in linear mode).

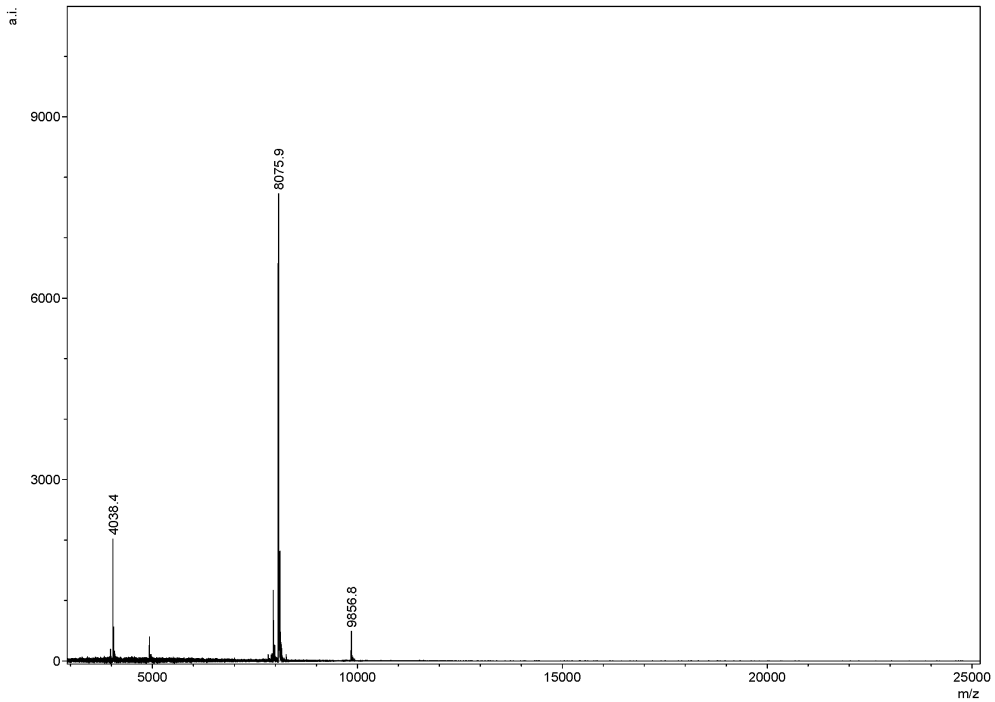

Figure S19. Mass (ssDNA: **dA^{FcMe}TP,** dCTP, dTTP**,** dGTP): calculated: 10894,38 Da; found: 8075.9 Da; (M = 9856.8 Da is a peak of template; M = 8075.9 Da is product of not fully incorporated product 5'-CATGGGCGGCATGGG**A^{FcMe}**CTG**A^{FcMe}**GCTC-3')

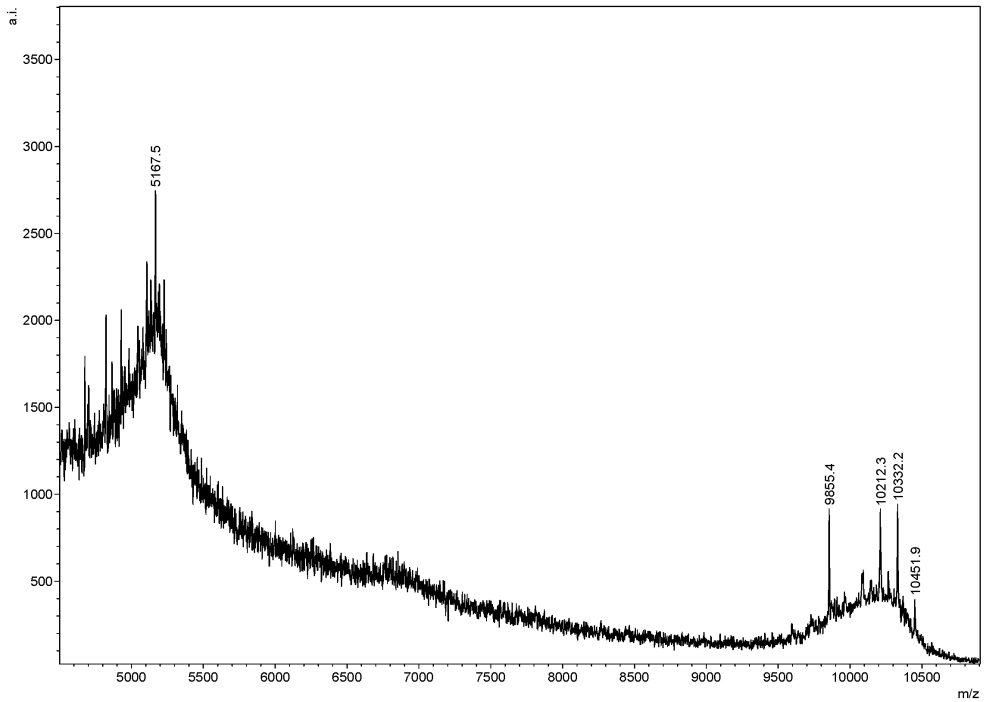

Figure S20. Mass (ssDNA: **dC^{Fc}TP,** dATP, dTTP**,** dGTP): calculated: 10449,54 Da; found: 10451.9 Da; Δ = 2.36 (M = 10332.2 Da is full product minus one Cp ring with Fc; M = 10212.3 Da is full product minus two Cp rings with two Fc).

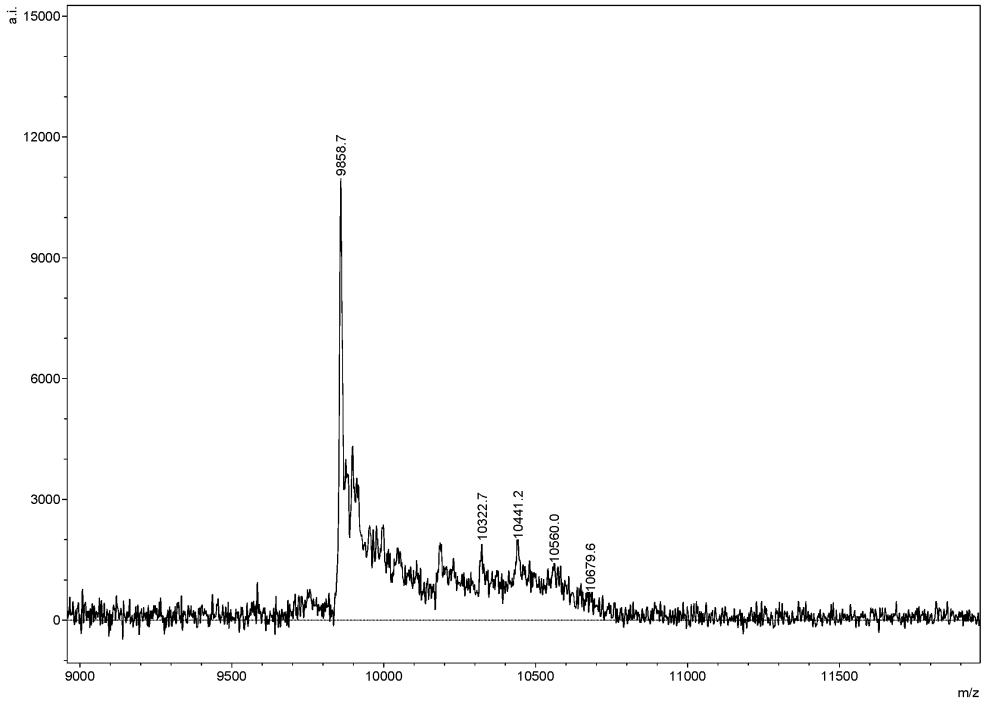

Figure S21. Mass (ssDNA: **dC^{FcPa}TP,** dATP, dTTP**,** dGTP): calculated: 10677,7 Da; found: 10679.6 Da; Δ = 1.9 (M = 9858.7 Da is a peak of template; M = 10560.0 Da is full product minus one Cp ring with Fc; M = 10441.2 Da is full product minus two Cp rings with two Fc; M = 10322.7 Da is full product minus three Cp ring with three Fc) (Sample was measured in linear mode)

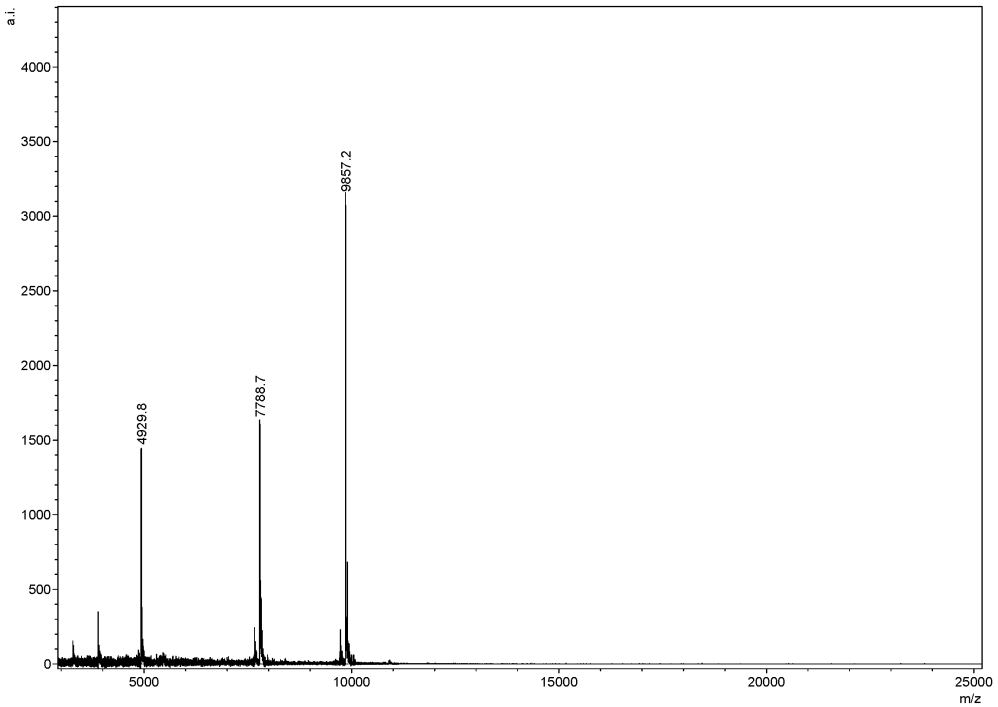

Figure S22. Mass (ssDNA: dC^{FcMe}TP, dATP, dTTP**,** dGTP): calculated: 10898,38 Da; found: 7788.7 Da; (M = 9857.2 Da is a peak of template; M = 7788.7 Da is product of not fully incorporated product 5'-CATGGGCGGCATGGGA**C^{FcMe}**TGAG**C^{FcMe}**T-3')

b) prim^{rnd} 3’-GGGTACGGCGGGTAC-5’

temp^{A} 5‘-CCCTCCCATGCCGCCCATG-3‘

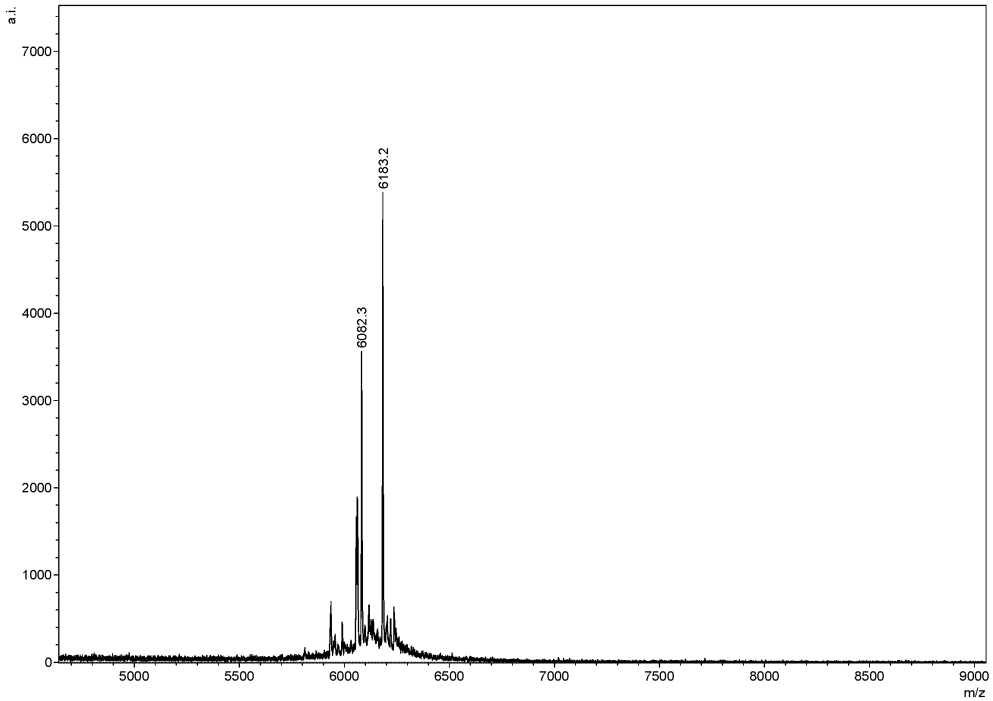

Figure S23. Mass (ssDNA: **dA^{Fc}TP,** dGTP): calculated: 6182,03 Da; found: 6183.2 Da; Δ = 1.17 (M = 6082.3 Da is a peak of template)

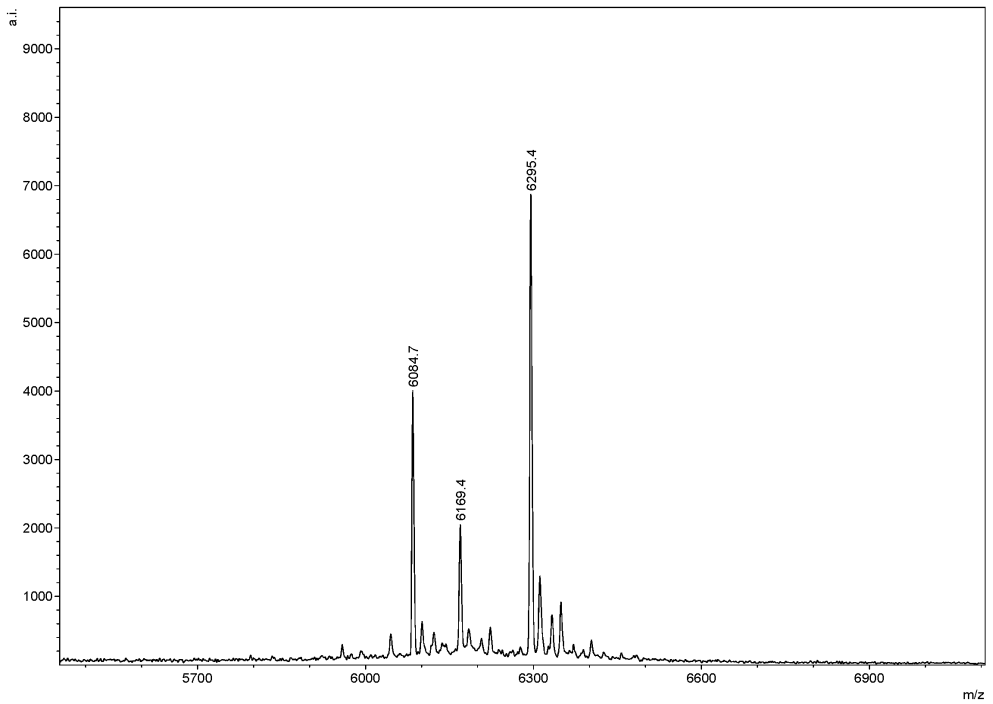

Figure S24. Mass (ssDNA: **dA^{FcMe}TP,** dGTP): calculated: 6293,96 Da; found: 6295.4 Da; Δ = 1.44

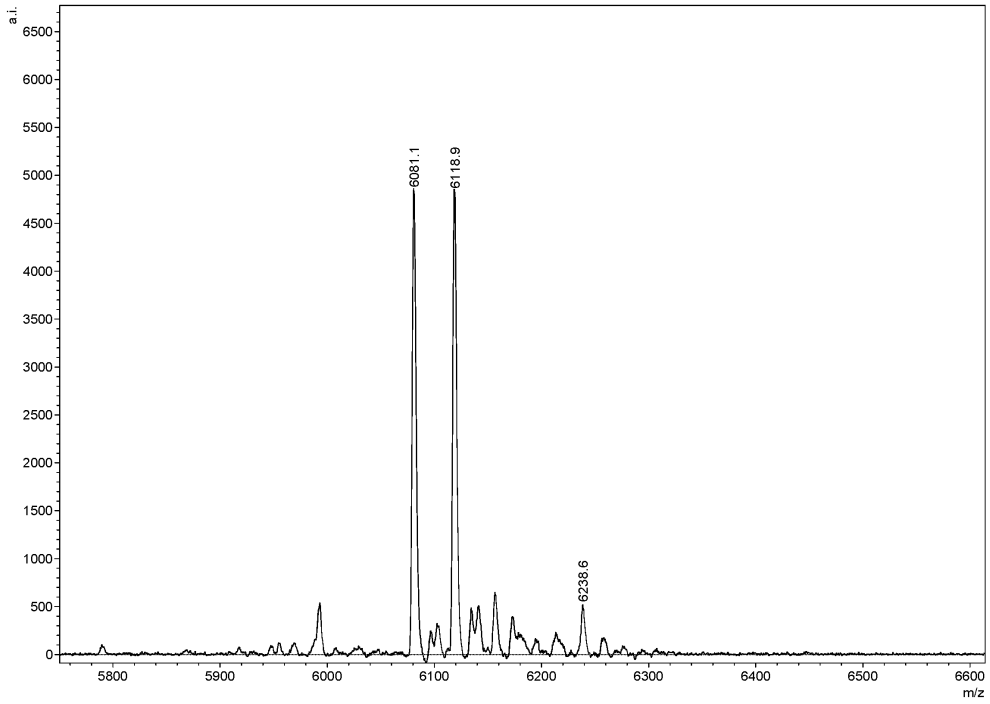

Figure S25. Mass (ssDNA**: dA^{FcPa}TP,** dGTP): calculated: 6239,01 Da; found: 6238.6 Da; Δ = 0.41 (M = 6081.1 Da is a peak of template; M = 6118.9 Da is full product minus Cp ring with Fc)

c) prim^{rnd} 3’-GGGTACGGCGGGTAC-5’

temp^{C} 5‘-CCCGCCCATGCCGCCCATG-3‘

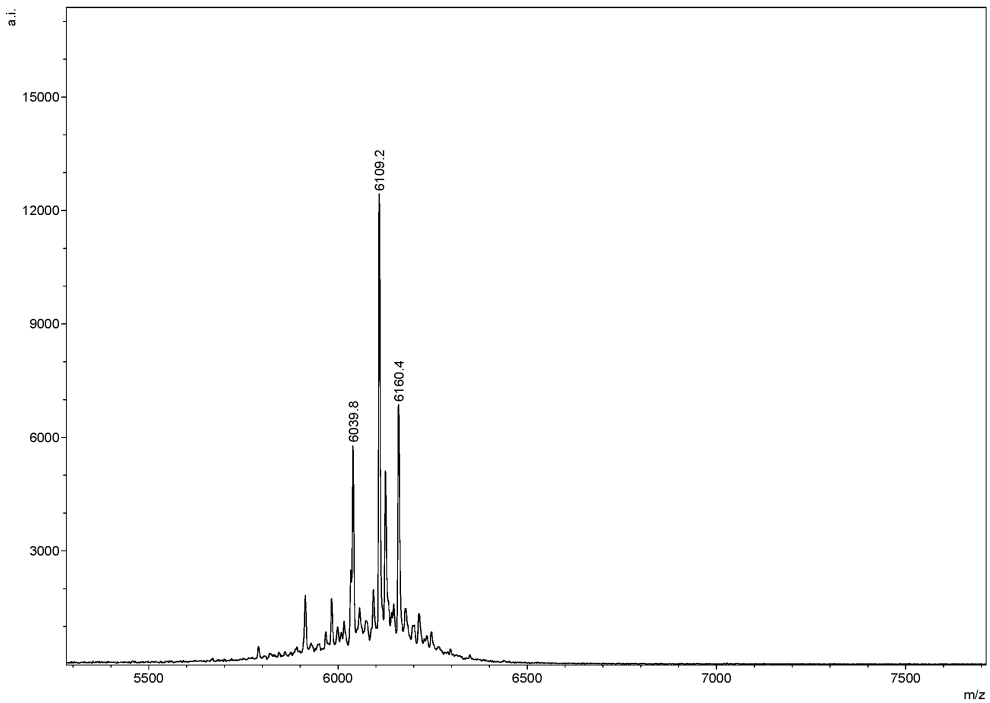

Figure S26. Mass (ssDNA: **dC^{Fc}TP,** dGTP): calculated: 6158,96 Da; found: 6160.2 Da; Δ = 1.24 (M = 6109.2 Da is a peak of template; M = 6039.8 Da is full product minus Cp ring with Fc).

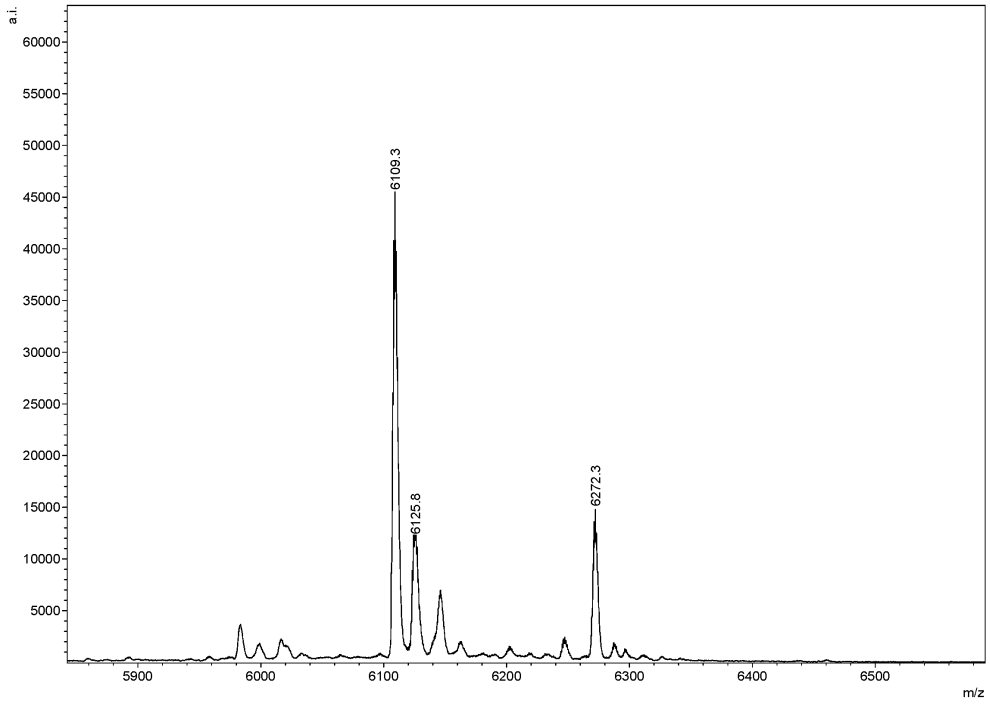

Figure S27. Mass (ssDNA: **dC^{FcMe}TP,** dGTP): calculated: 6270,96 Da; found: 6272.3 Da; Δ = 1.34.

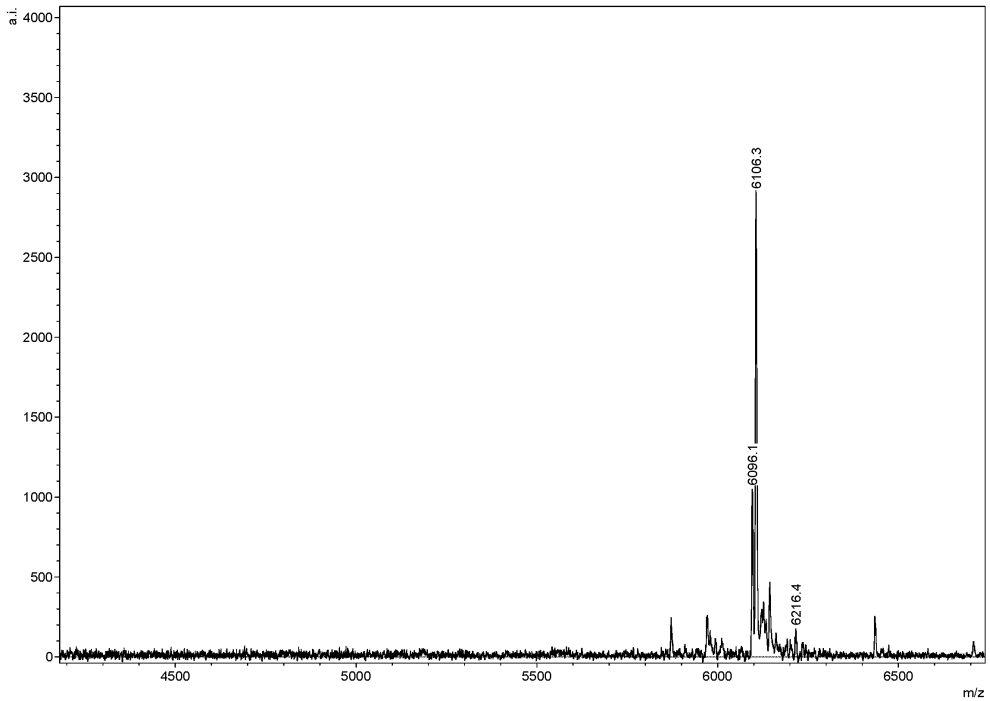

Figure S28. Mass (ssDNA: **dC^{FcPa}TP,** dGTP): calculated: 6216,01 Da; found: 6216.4 Da; Δ = 0.39 (M = 6106.3 Da is a peak of template; M = 6096.1 Da is full product minus Cp ring with Fc).

6. Copies of NMR spectra

dA^{FcMe}

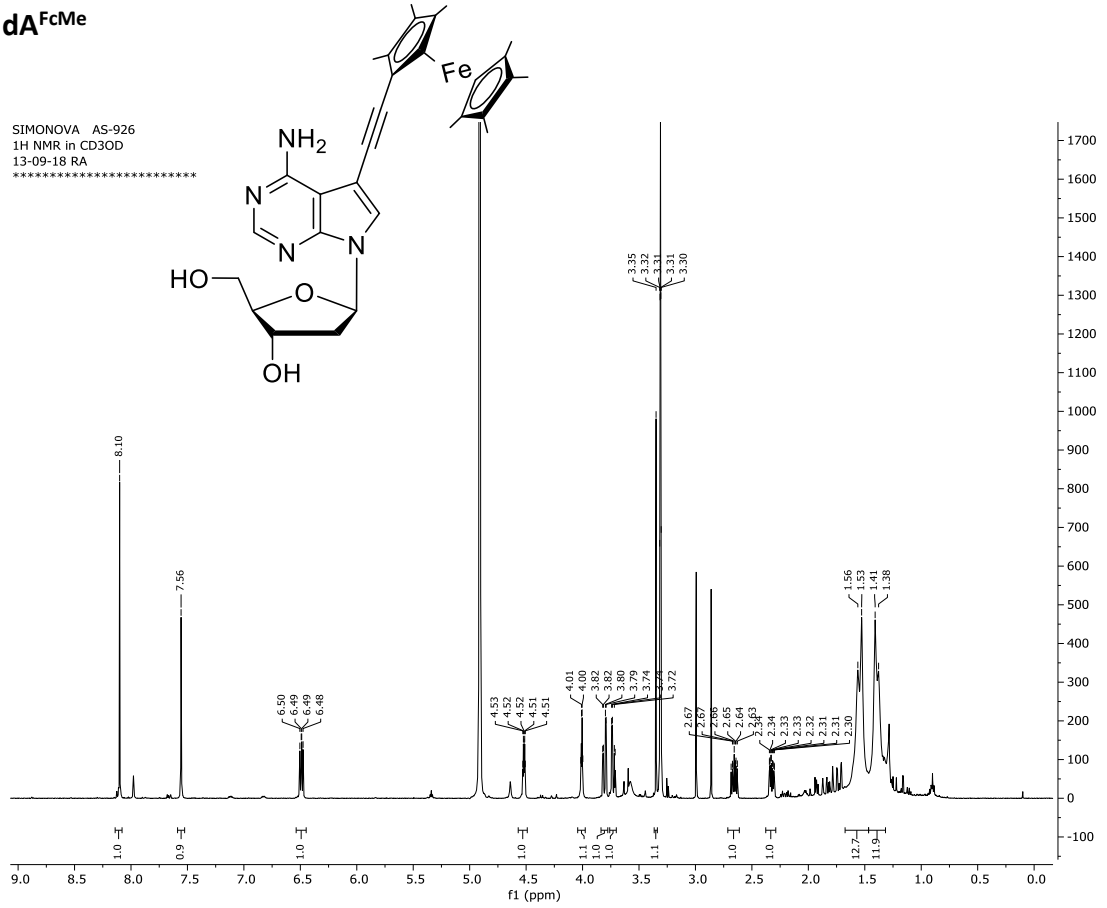

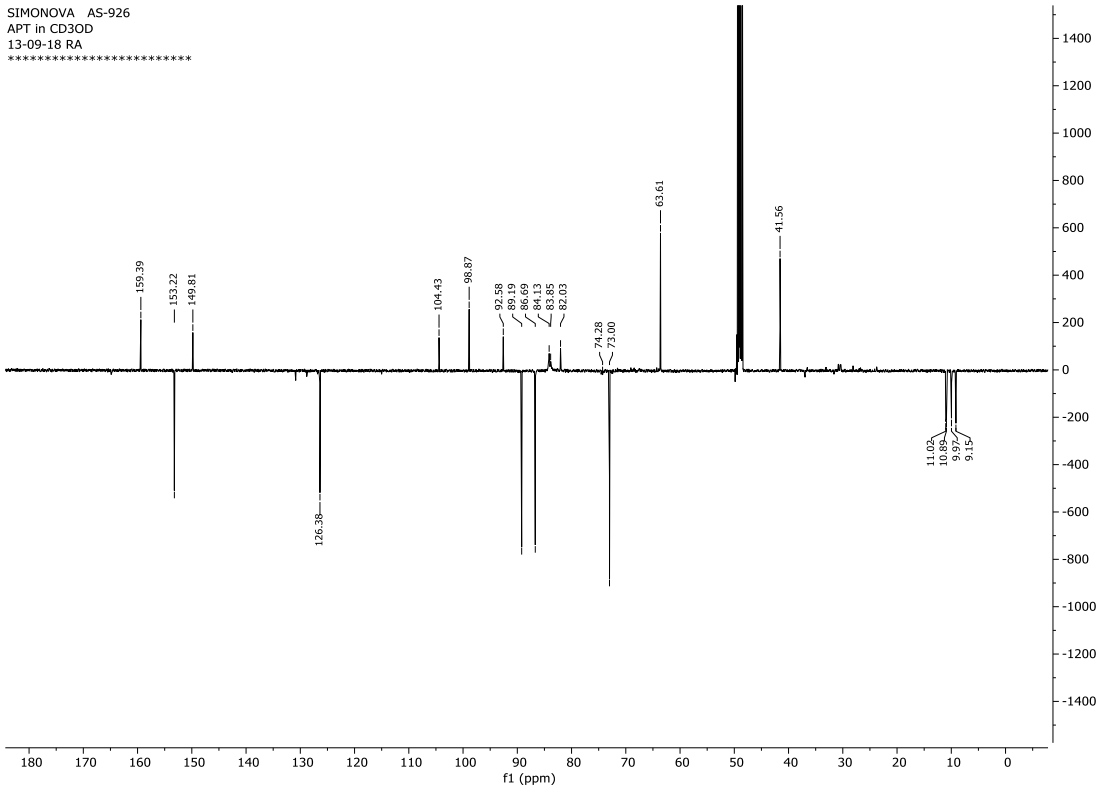

dC^{FcMe}

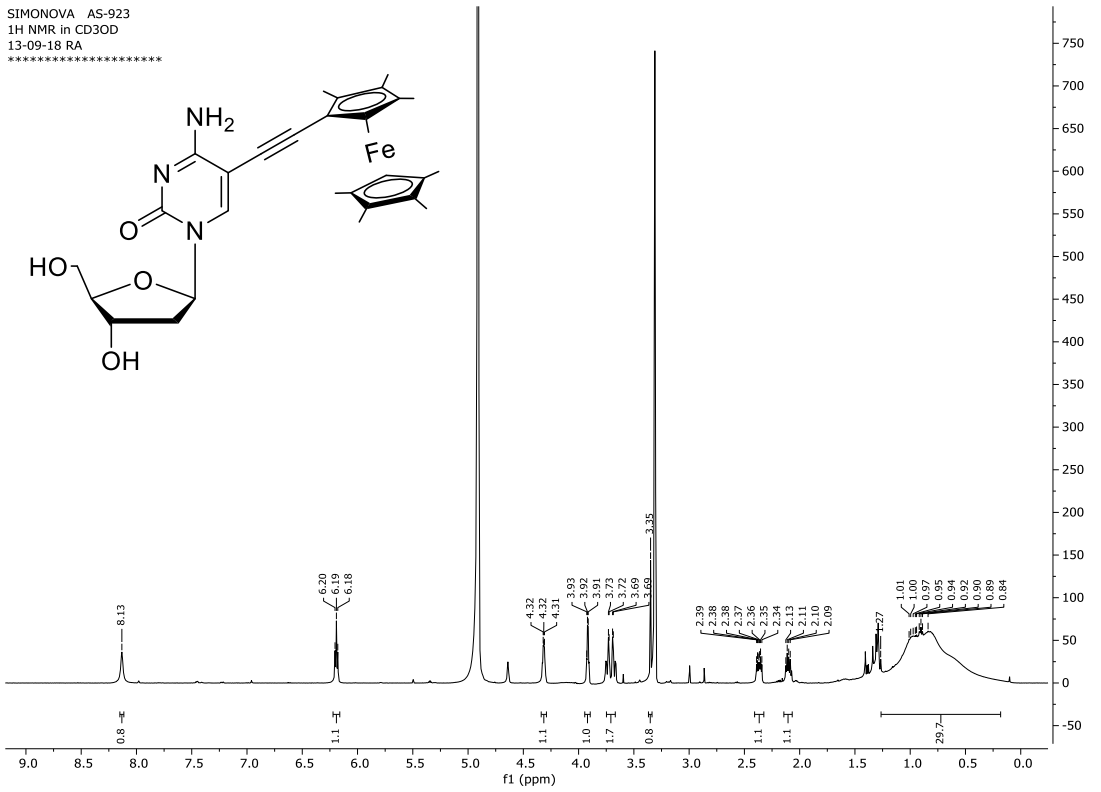
SIMONOVA AS-923
1H NMR in CD3OD
13-09-18 RA
****
NH2
N
O
N
HO
O
OH
Fe
f1 (ppm)

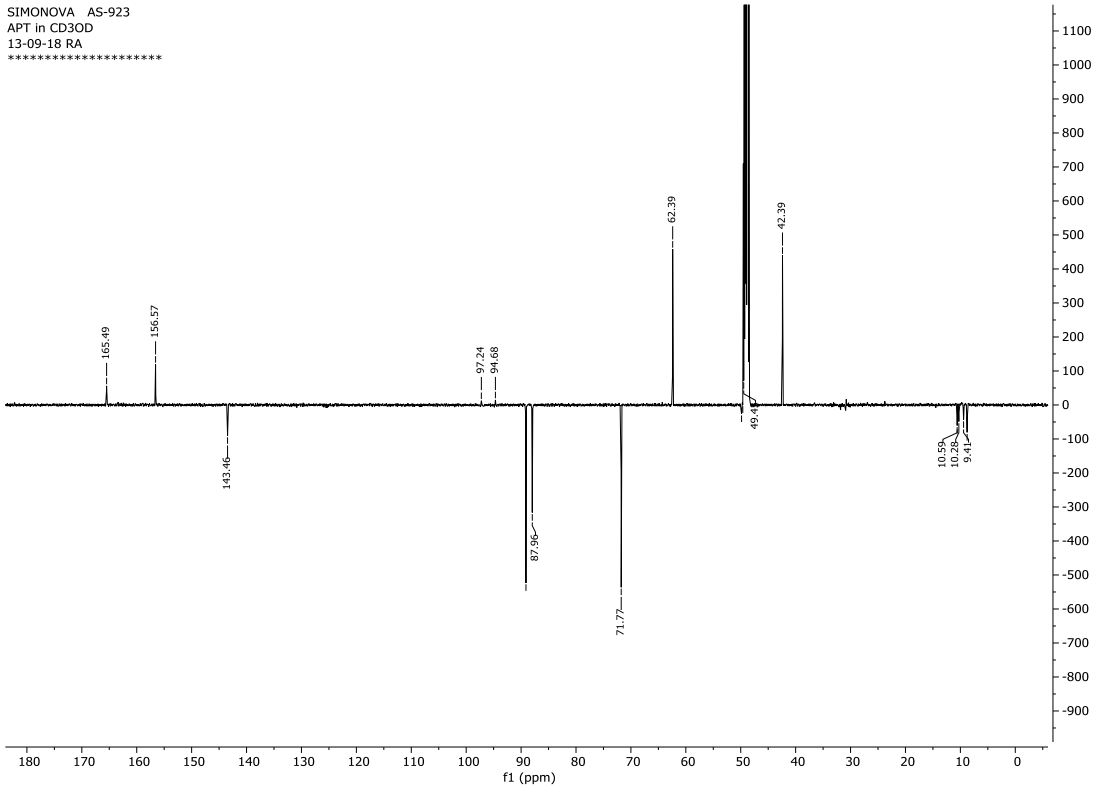
SIMONOVA AS-923
APT in CD3OD
13-09-18 RA
****
f1 (ppm)

dA^{FcPa}

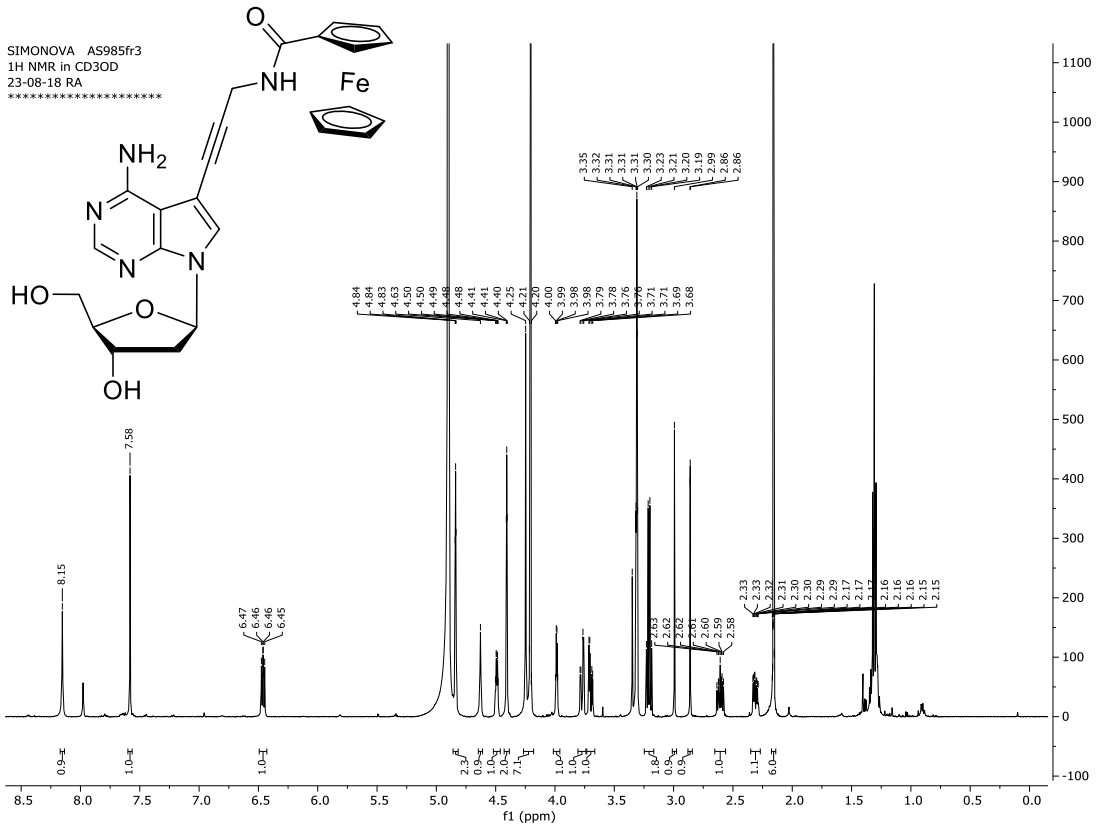
SIMONOVA AS985fr3
1H NMR in CD3OD
23-08-18 RA
****
O
NH
Fe
NH2
N
N
N
HO
O
OH
f1 (ppm)

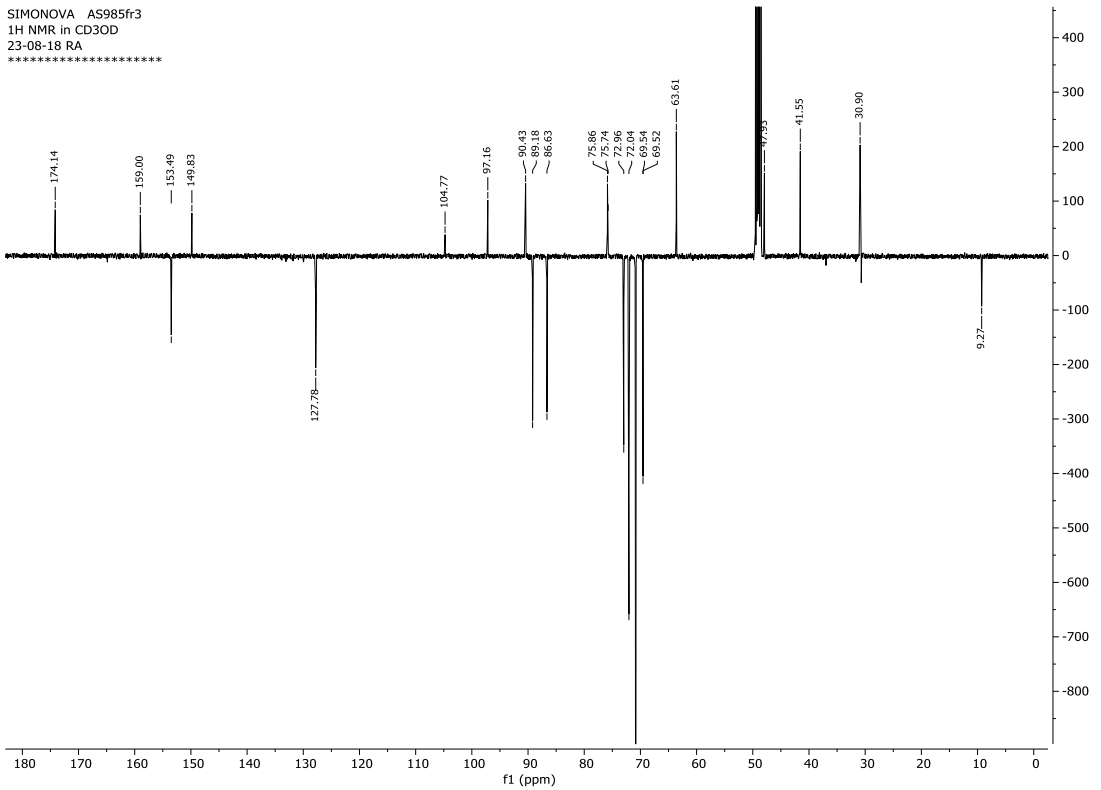
SIMONOVA AS985fr3
1H NMR in CD3OD
23-08-18 RA
****
f1 (ppm)

dC^{FcPa}

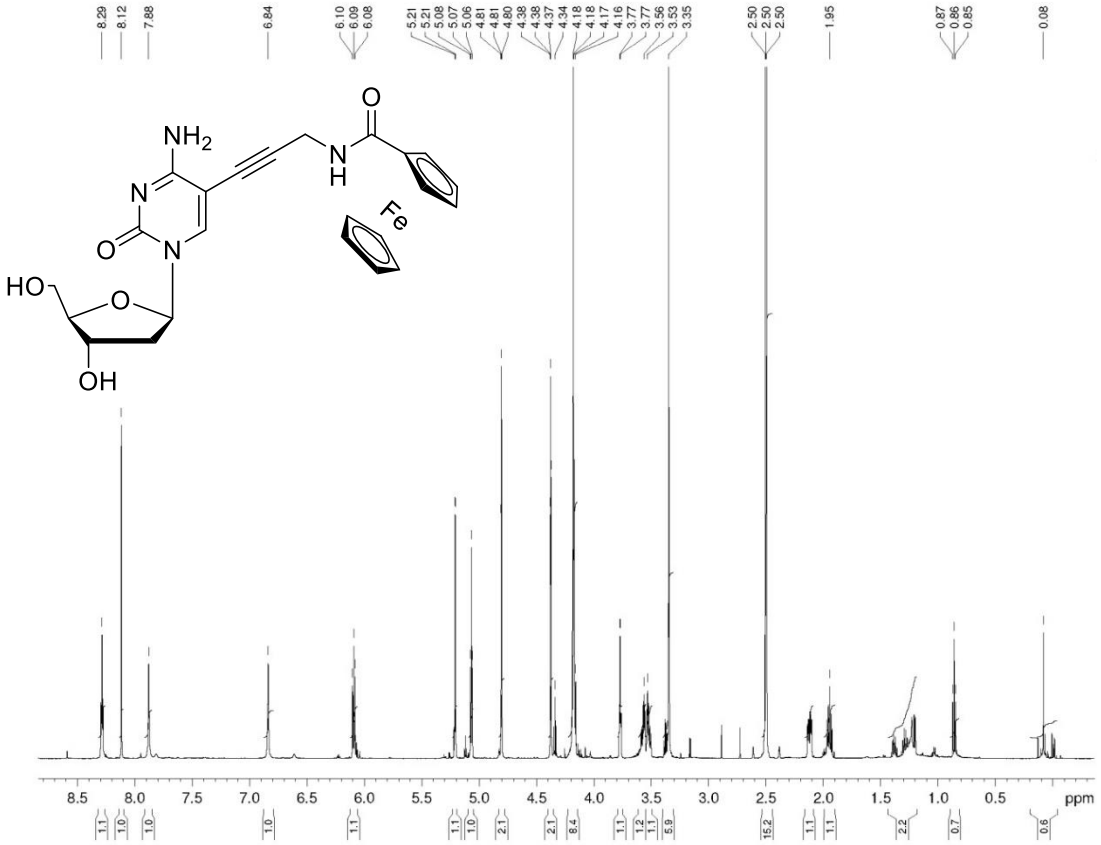
8.29
8.12
7.88
6.84
6.10
6.09
6.08
5.21
5.21
5.08
5.07
5.06
4.81
4.81
4.80
4.38
4.38
4.37
4.34
4.18
4.18
4.17
4.16
3.77
3.77
3.56
3.53
3.35
2.50
2.50
2.50
1.95
0.87
0.86
0.85
0.08
NH2
N
O
N
H
O
Fe
HO
O
OH
8.5
8.0
7.5
7.0
6.5
6.0
5.5
5.0
4.5
4.0
3.5
3.0
2.5
2.0
1.5
1.0
0.5
ppm
1.1
1.0
1.0
1.0
1.1
1.1
1.0
2.1
2.1
8.4
1.1
1.2
1.1
5.9
15.2
1.1
1.1
2.2
0.7
0.6

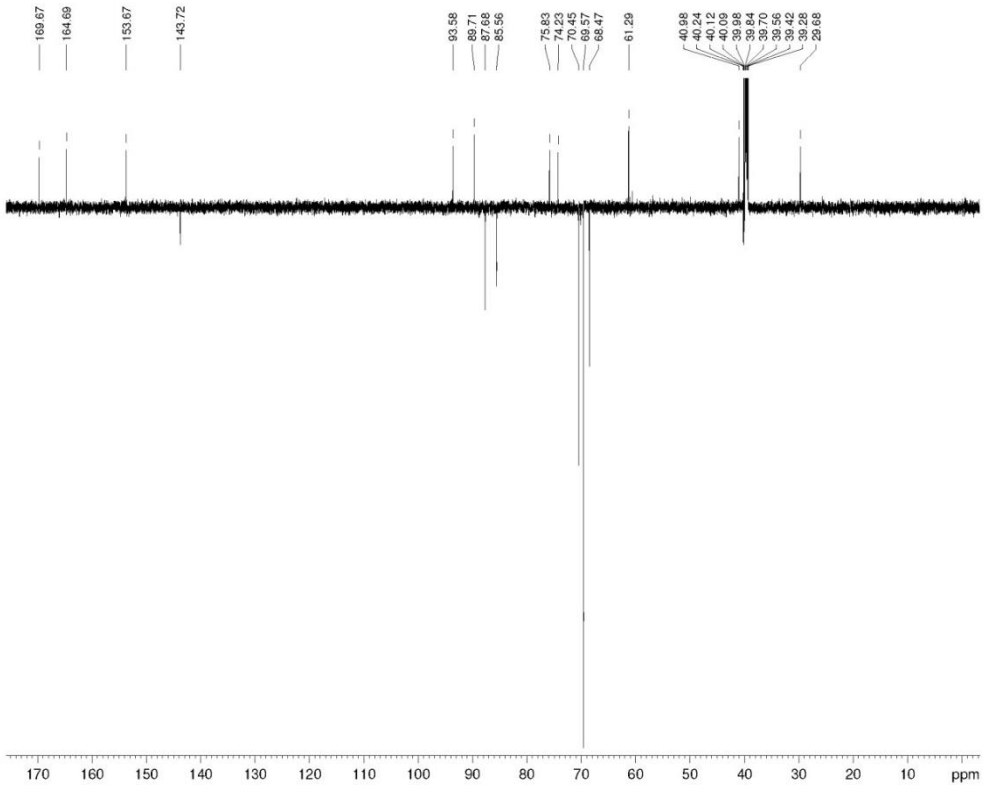
169.67
164.69
153.67
143.72
93.58
89.71
87.68
85.56
75.83
74.23
70.45
69.57
68.47
61.29
40.98
40.24
40.12
40.00
39.98
39.84
39.70
39.56
39.42
39.28
29.68
170
160
150
140
130
120
110
100
90
80
70
60
50
40
30
20
10
ppm

dA^{FcMe}TP

^{1}H and ^{13}C NMR spectra were not possible to analyse because of partial oxidation of ferrocene moiety.

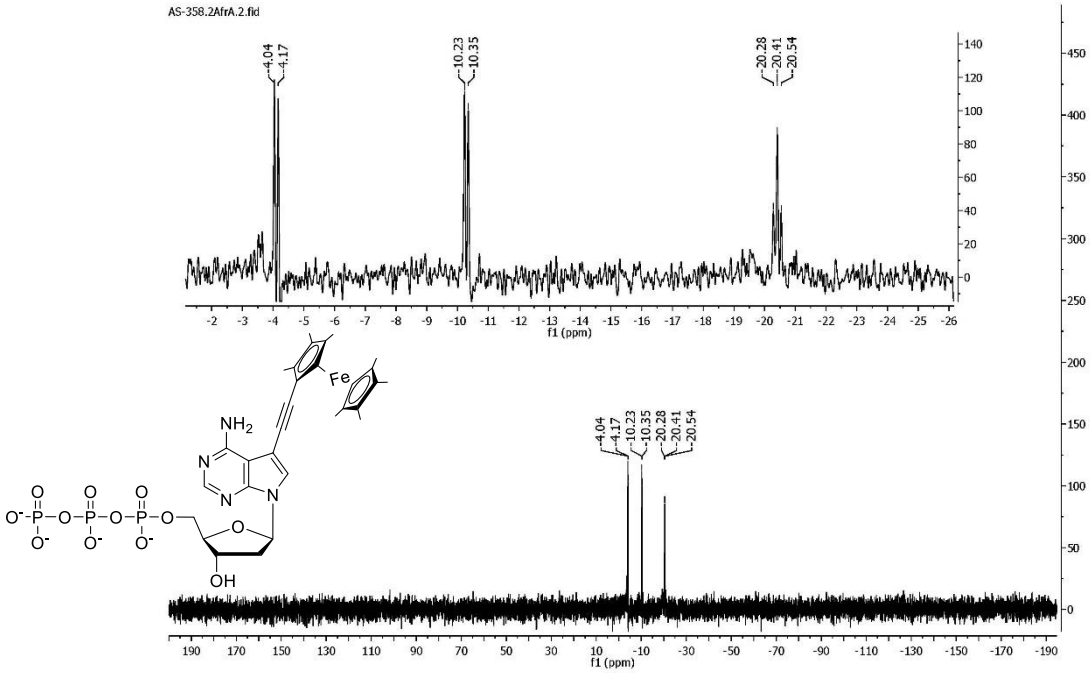

dC^{FcMe}TP

^{1}H and ^{13}C NMR spectra were not possible to analyse because of partial oxidation of ferrocene moiety.

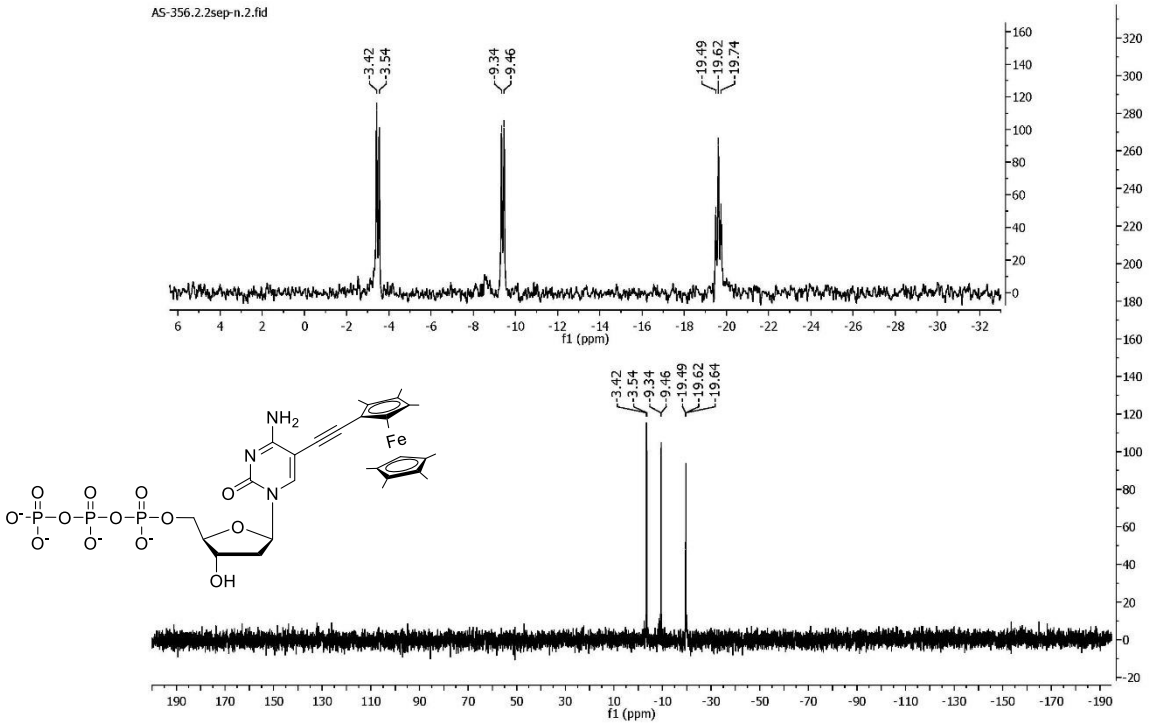

dA^{FcPa}TP

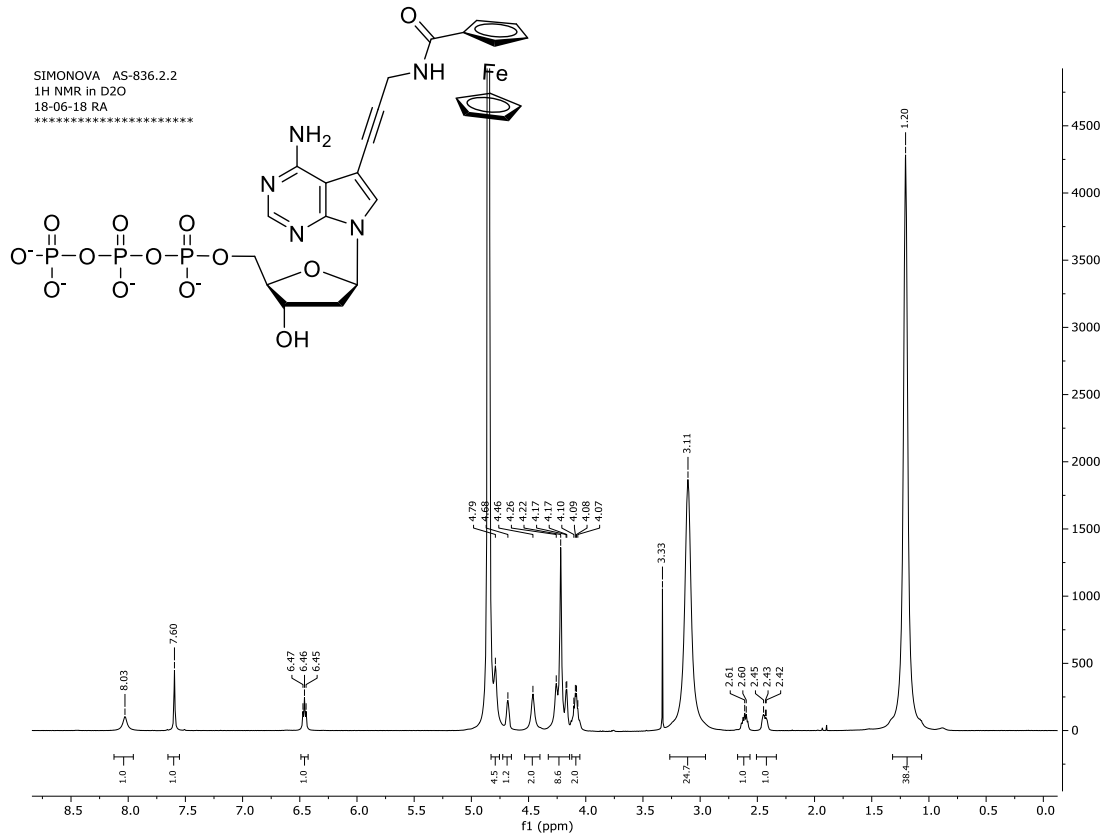
SIMONOVA AS-836.2.2
1H NMR in D2O
18-06-18 RA
f1 (ppm)

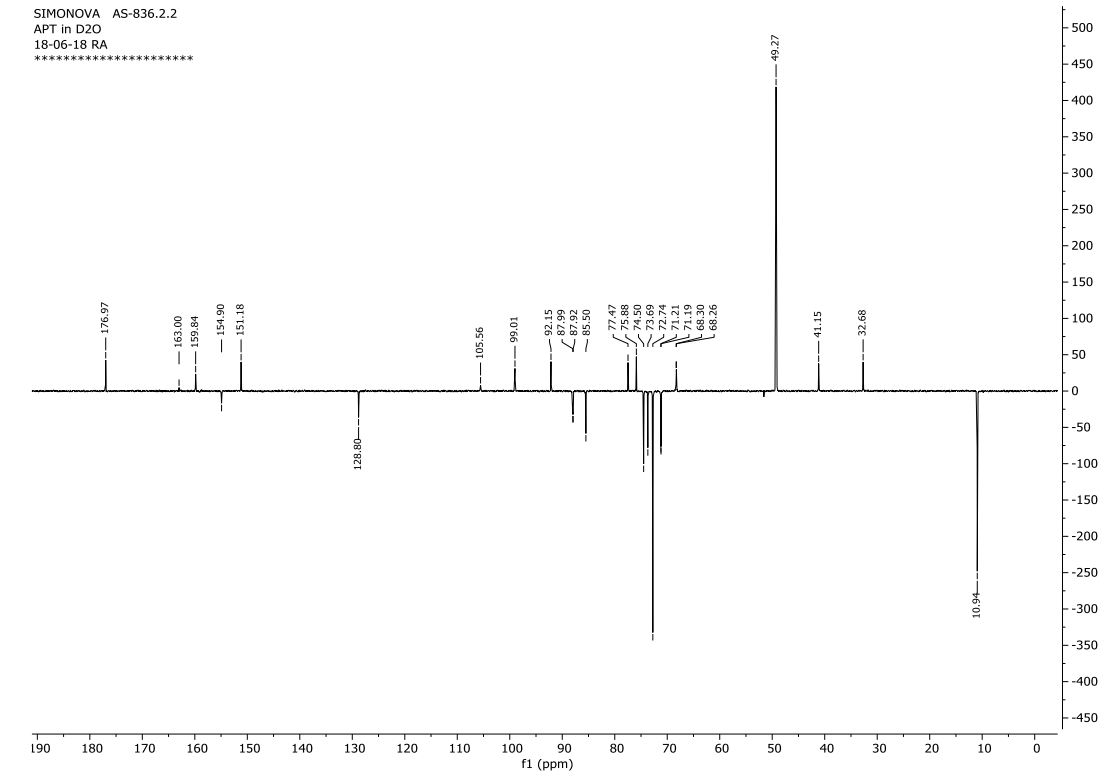
SIMONOVA AS-836.2.2
APT in D2O
18-06-18 RA
f1 (ppm)

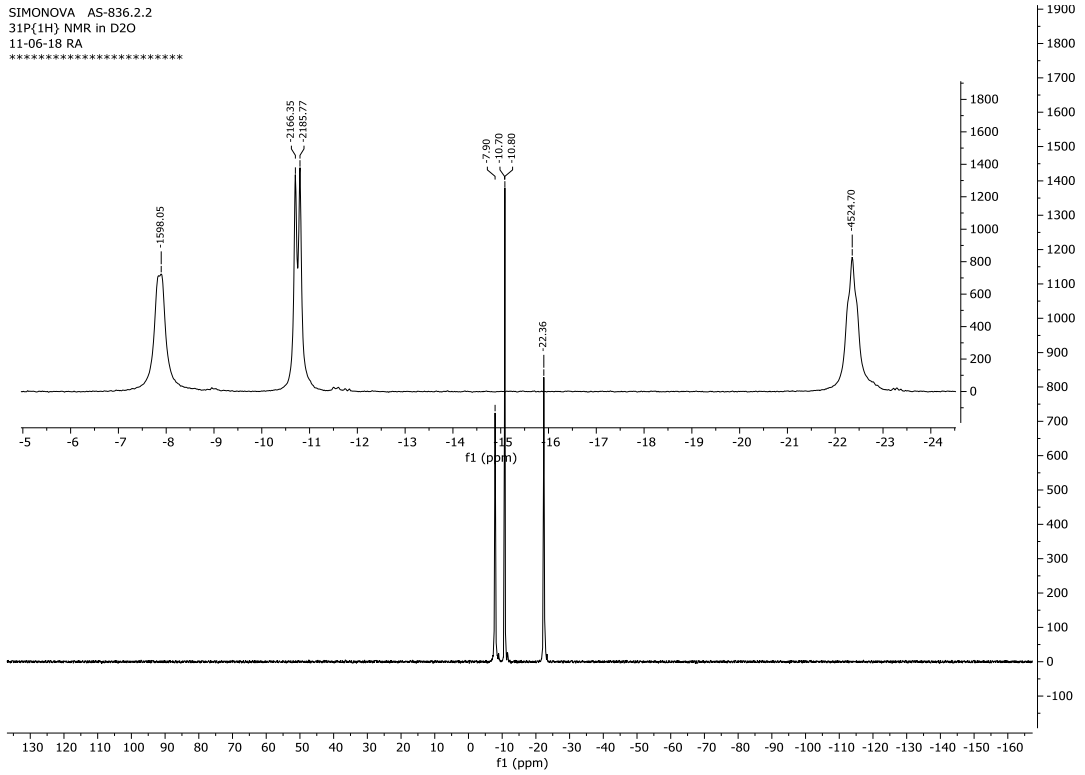
SIMONOVA AS-836.2.2
31P{1H} NMR in D2O
11-06-18 RA
****
-1598.05
-2166.35
-2185.77
-7.90
-10.70
-10.80
-22.36
-4524.70
f1 (ppm)

dC^{FcPa}TP

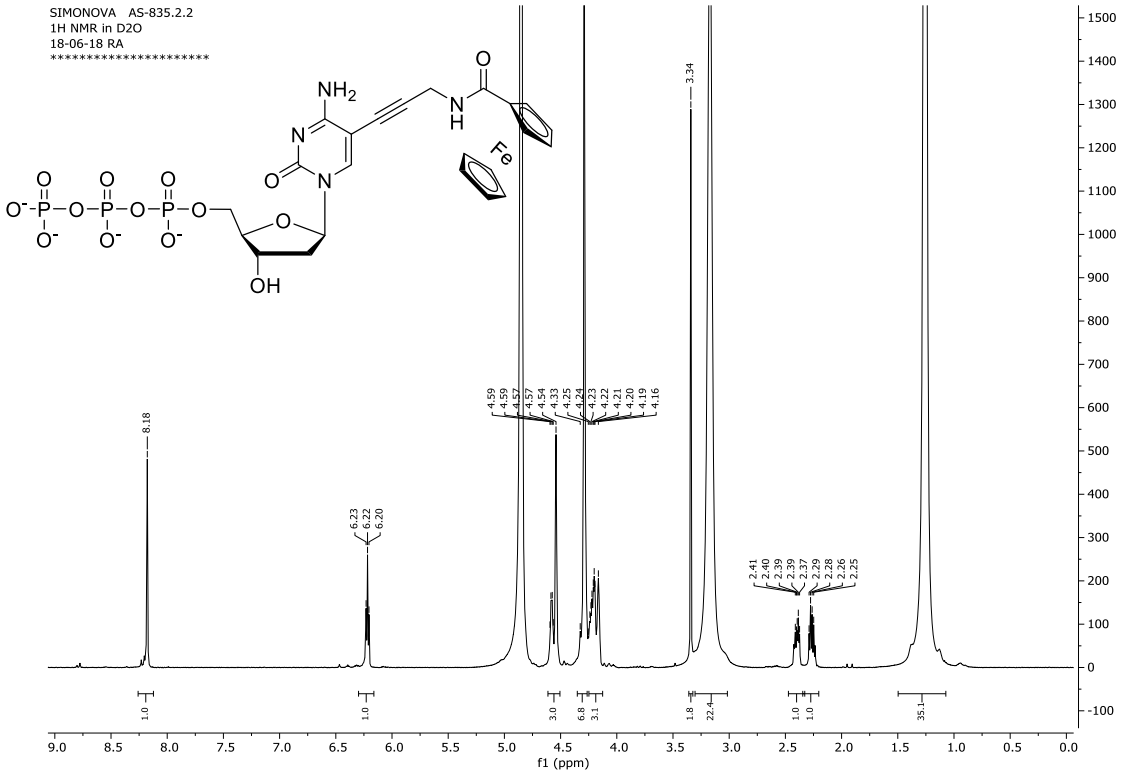
SIMONOVA AS-835.2.2
1H NMR in D2O
18-06-18 RA
****
NH2
N
O
N
H
Fe
O
O-P-O-P-O-P-O
O- O- O-
OH
8.18
6.23
6.22
6.20
4.59
4.59
4.57
4.57
4.54
4.33
4.25
4.24
4.23
4.22
4.21
4.20
4.19
4.16
3.34
2.41
2.40
2.39
2.39
2.37
2.29
2.28
2.26
2.25
1.0
1.0
3.0
6.8
3.1
1.8
22.4
1.0
1.0
35.1
f1 (ppm)

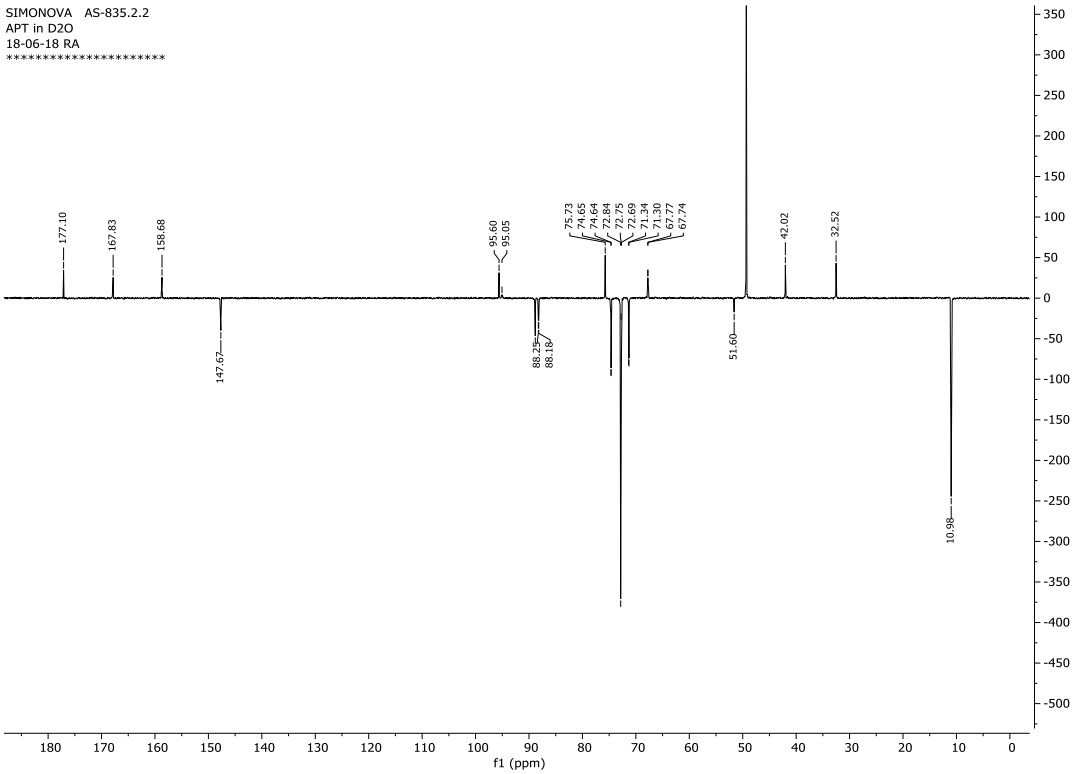
SIMONOVA AS-835.2.2
APT in D2O
18-06-18 RA
****
177.10
167.83
158.68
147.67
95.60
95.05
88.25
88.18
75.73
74.65
74.64
72.84
72.75
72.69
71.34
71.30
67.77
67.74
51.60
42.02
32.52
10.98
f1 (ppm)

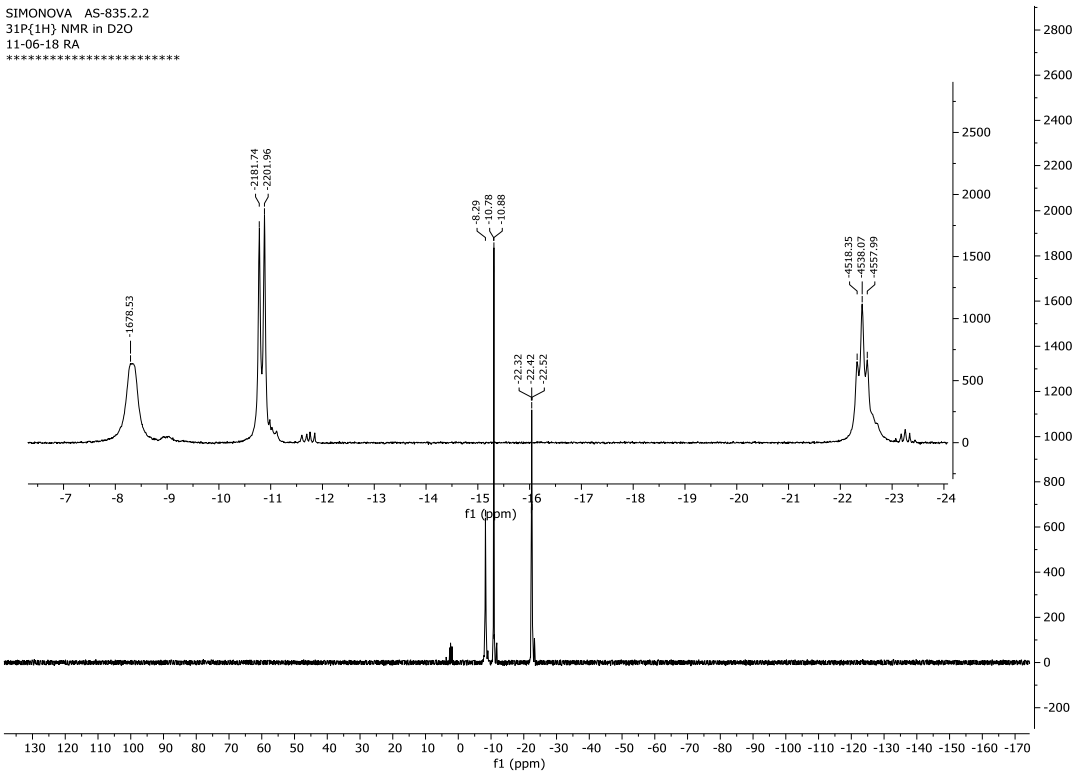
SIMONOVA AS-835.2.2
31P{1H} NMR in D2O
11-06-18 RA
****
-1678.53
-2181.74
-2201.96
-8.29
-10.78
-10.88
-22.32
-22.42
-22.52
4518.35
4538.07
4557.99
f1 (ppm)

dC^{Fc}TP

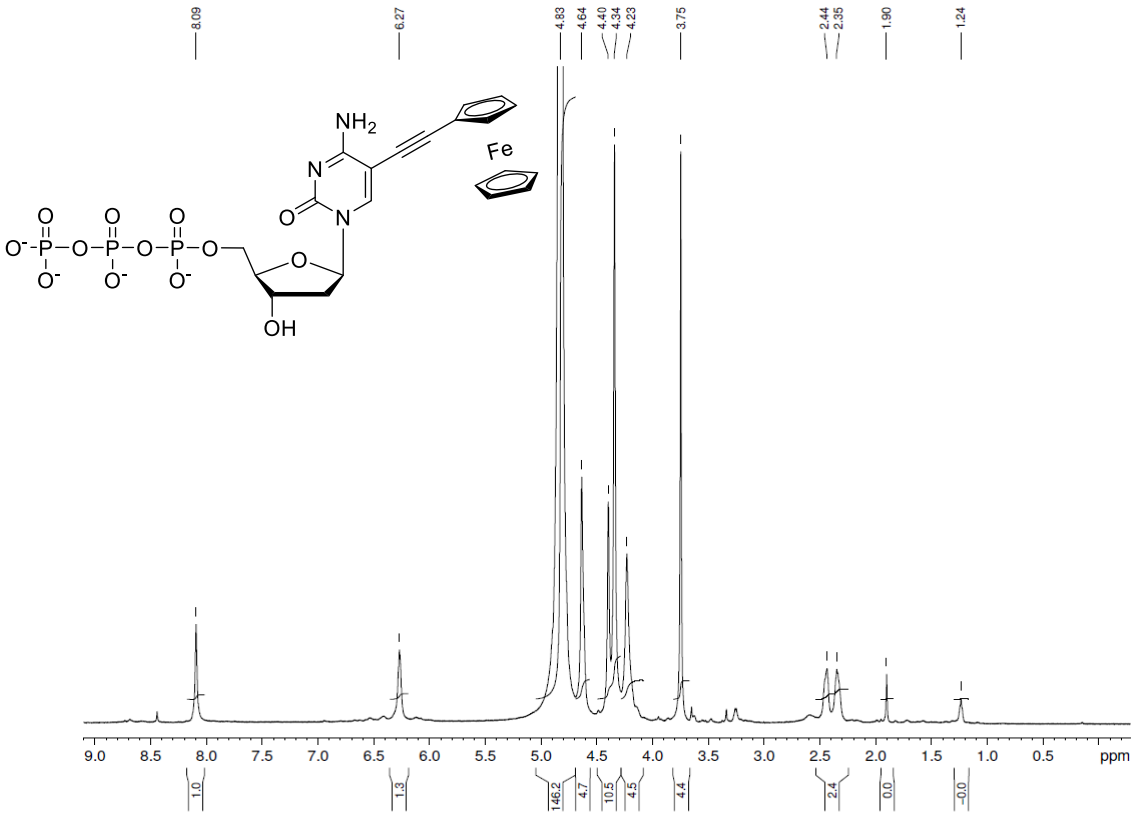
8.09
6.27
4.83
4.64
4.40
4.34
4.23
3.75
2.44
2.35
1.90
1.24
NH2
N
O
N
Fe
O
O
O
O
O
O
O
O
O
O
O
O
OH
9.0
8.5
8.0
7.5
7.0
6.5
6.0
5.5
5.0
4.5
4.0
3.5
3.0
2.5
2.0
1.5
1.0
0.5
ppm
1.0
1.3
146.2
4.7
10.5
4.5
4.4
2.4
0.0
0.0

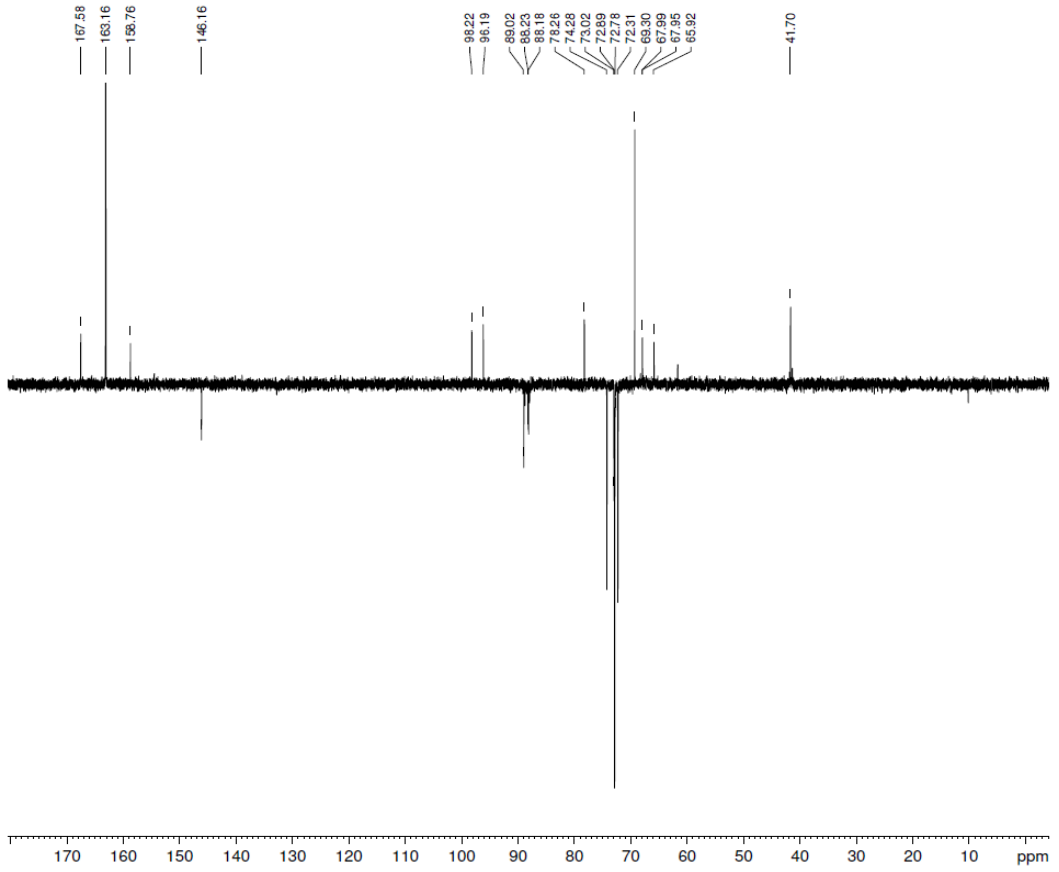
167.58
163.16
158.76
146.16
98.22
96.19
89.02
88.23
88.18
78.26
74.28
73.02
72.89
72.78
72.31
69.30
67.99
67.95
65.92
41.70
170
160
150
140
130
120
110
100
90
80
70
60
50
40
30
20
10
ppm

7. References

1. a) S. K. Ghag, M. L. Tarlton, E. A. Henle, E. M. Ochoa, A. W. Watson, L. N. Zakharov, E. J. Watson, *Organometallics*, **2013**, *32*, 1851–1857; b) C. Zou and M. S. Wrighton*, J. Am. Chem. Soc.,* **1990**, *112,* 7578-7584; c) P. Jutzi, B. Kleinebekel, *J. Organometal. Chem.*, **1997**, *545–546*, 573–576.
2. A. E. Beilstein, M. W. Grinstaff, *Chem. Commun.*, **2000**, 509–510.
3. I. Magriñá, A. Toldrà, M. Campàs, M. Ortiz, A. Simonova, I. Katakis, M. Hocek, C.K. O'Sullivan, *Biosens. Bioelectron.*, **2019**, *134*, 76–82.

Annex 2. List of figures

Annex 3. List of tables

Annex 4. Abbreviations

Abbreviation	Definition
α	Transfer coefficient
A	Adenine
ALP	Alkaline phosphatase
B. anthracis	*Bacillus anthracis*
bp	Base pair
C	Cytosine
Cdl	Double layer capacitance
CE	Counter electrode
CV	Cyclic voltammetry
dATP	deoxyadenosine triphosphate
$dA^{EFc}TP$	Ethynylferrocene labelled dATP
dCTP	deoxycytidine triphosphate
dGTP	deoxyguanosine triphosphate
DNA	Desoxyribonucleic acid
dNTP	Deoxynucleotide triphosphate
dsDNA	Double stranded DNA
dTTP	deoxythymidine triphosphate
DVD	Digital versatile disc
E^0	Formal potential
EDTA	Ethylenediaminetatraacetic acid
EFc	Ethynylferrocene
ET	Electron transfer
Fc	Ferrocene
FCA	Fast chronoamperometry
FcPA	Propargylaminocarbonylferrocene
FWHM	Full width at half of the peak màximum height
G	Guanine
HDA	Helicase-dependent amplification
HPV 16	Human papilloma virus 16
HPLC	High pressure liquid cromatography
k^o	Standard heterogeneous electron transfer rate constant
K. armiger	*Karlodinium armiger*
LAMP	Loop mediated isothermal amplification
LNA	Locked nucleid acid
mRNA	Messenger RNA
η	Overpotential
NA	Nucleic acid
NASBA	Nucleic acid sequence-based amplification
NTC	Non-template control
PEX	Primer extension
PBS	Phosphate buffered saline
PCR	Polymerase chain reaction
PMMA	polymethylmethacrylate
PNA	Peptide nucleic acid
POC	Point-of-care
POM	Polyoxometalate
PZC	Potential of Zero Charge
qPCR	Quantitative PCR

RCA	Rolling circle amplification
RE	Reference electrode
RNA	Ribonucleic acid
RPA	Recombinase polymerase amplification
SDA	Strand displacement amplification
SELEX	Systematic evolution of ligands by exponential enrichment
ssbp	Single stranded binding proteins
ssDNA	Single stranded DNA
SNP	Single nucleotide polymorphism
SWV	Square wave voltammetry
T	Thymine
TMB	3,3',5,5'-tetramethylbenzidine
TRIS	Tris(hydroxymethyl)aminomethane
UV	ultraviolet
WE	Working electrode

Annex 5. Short CV

SCIENTIFIC PUBLICATIONS AND OWN CONTRIBUTION

The development of this thesis has led to the publication of seven scientific publications, six of them as a first author, and four of them currently under review. To achieve this, different institutions and researchers have been involved. The aim of this section is to provide a list of these publications and a statement of my personal contribution to each of them.

This thesis includes one publication found in chapter 3 and three manuscripts under revision found in chapters 4, 5 and 6.

1. Magriñá, I.; Toldrà, A.; Campàs, M.; Ortiz, M.; Simonova, A.; Katakis, I.; Hocek, M.; O'Sullivan, C. K. Electrochemical Genosensor for the Direct Detection of Tailed PCR Amplicons Incorporating Ferrocene Labelled dATP. *Biosens. Bioelectron.* **2019**, *134*, 76–82. (Chapter 3)

Personal contribution:

- The design and fabrication of the electrode array and microfluidic adhesive and gasket.
- The development and optimization of the electrochemical DNA sensor methodology.
- Calibration curve and the analysis of the genomic seawater samples.
- The extraction of the genomic DNA from spiked seawater samples.
- The validation of the method with qPCR.
- The study of the effect of $dA^{EFc}TP$:dATP ratio on PCR amplification yield and electrochemical sensitivity.
- Determination of the electrode stability

2. Magriñá, I.; Jauset-Rubio, M.; Ortiz, M.; Tomaso, H.; Simonova, A.; Hocek, M.; O'Sullivan, C.K. Duplex electrochemical DNA sensor to detect B. anthracis CAP and PAG DNA targets based on the incorporation of tailed primers and ferrocene labelled dATP. (Submitted to ACS:Omega) (Chapter 4)

Personal contribution:

- The design and fabrication of the electrode array and microfluidic adhesive and gasket.
- The development and optimization of the electrochemical DNA sensor methodology.
- Cross-reactivity study.
- Study of the effect of electrolyte composition and concentration on ferrocene oxidation peak.
- Duplex calibration curve and the analysis of real samples.
- Validation of the method with qPCR.

3. Magriñá, I.; Ortiz, M.; Simonova, A.; Katakis, I.; Hocek, M.; O'Sullivan , C.K.; Forster, R. Controlling DNA monolayer structure through electrostatics. *(Manuscript to be submitted to JACS)* (Chapter 5)

Personal contribution:

- The design and fabrication the electrode array and microfluidic adhesive and gasket.
- Generation of the ferrocene labelled DNA.
- Performing the cyclic voltammetry experiments and simulations.

4. Simonova, A.; Magriñá, I.; Sýkorová, V.; Pohl, R.; Ortiz, M.; Havran L.; Fojta, M.; O'Sullivan C.; Hocek, M. Tuning of oxidation potential of ferrocene for radiometric redox labelling and coding of nucleotides and DNA. *(Submitted to Chemistry – A European Journal)*. (Chapter 6)

Personal contribution:

- The design and fabrication of the electrode array and microfluidic adhesive and gasket.
- The design of sequences to study the incorporation of the ferrocene labelled dNTPs via hybridization and electrochemical detection.
- Primer Extension, hybridization and electrochemical detection of the aforementioned sequences bearing the ferrocene labelled dNTPs.

Moreover, three publications, including a review, a forum article and a full article have been achieved.

5. Magriñá, I.; O'Sullivan C.K. Recombinase polymerase amplification: basics, application and recent advances. *Trend. Anal. Chem.* **2018,** *98*, 19-35. (Annex 1)

Personal contribution:

- Writing the manuscript.

6. Magriñá, I.; O'Sullivan C.K. Solid-phase amplification. *(Submitted to Trends in Biotechnology)* (Annex 2)

Personal contribution:

- Writing the manuscript.

7. del Río, J. S.; Lobato, I. M.; Mayboroda, O.; Katakis, I.; O'Sullivan, C. K. Enhanced Solid-Phase Recombinase Polymerase Amplification and Electrochemical Detection. *Anal. Bioanal. Chem.* **2017**, *409* (12), 3261–3269.

Personal contribution:

- Comparison the effect of dsDNA vs ssDNA vertical spacers.
- Analysis of genomic DNA.

CONFERENCES

During the development of this thesis I had the chance to attend and participate in numerous national and international conferences.

ORAL PRESENTATIONS

2019. 25-29 August**. ACS Fall 2019 National Meeting and exposition.** San Diego, USA. Duplex electrochemical DNA sensor to detect *B.anthracis CAP and PAG* DNA targets based on the incorporation of tailed primers and ferrocene labelled dATP

2018. 20-21 September. ***XXII Transfrontier meeting on sensors and biosensors***. Barcelona, Spain. Duplex electrochemical DNA mothed to detect B. anthracis based on tailed primers, the incorporation of ferrocene labelled dATP and signal amplification mediated by ruthenium hexaamine.

2018. 3-6 June. ***17th International conference on Electroanalysis***. Electrochemical DNA method to detect *K. armiger* based on tailed primers, the incorporation of ferrocene labelled dATP and signal amplification mediated by $Ru(NH_6)^{+3}$

2018. 23 May. ***12th Doctoral day***. Tarragona, Spain. Electrochemical DNA sensor for *K. armiger*based on incorporation of ferrocene labelled dATP and tailed primers

2017. 21-22 September. ***XXII Transfrontier meeting on sensors and biosensors***. Montpellier, France. *A novel PCR method combining tailed primers and ferrocene labelled dNTPs for the electrochemical detection of Karlodinium Armiger*

POSTER PRESENTATIONS

2017. 24 May. **11th Doctoral day**. Tarragona, Spain. *Isothermal bridge amplification and electrochemical detection for reliable and cost effective molecular diagnostics.*

2016. 29-30 September. **XXI Transfrontier meeting on sensors and biosensors**. Barcelona, Spain. *Isothermal bridge amplification and electrochemical detection for reliable and cost effective molecular diagnostics.*

2016. 7-8 July. **X International workshop on sensors and molecular recognition.** Valencia, Spain. *Isothermal bridge amplification and electrochemical detection for reliable and cost effective molecular diagnostics.*

ATTENDANCES

2016. 23-34 June. 6th Early Stage Researchers Workshop in Nanoscience. Madrid, Spain.

UNIVERSITAT ROVIRA I VIRGILI
DEVELOPMENT OF ELECTROCHEMICAL DNA SENSORS BASED ON THE INCORPORATION OF FERROCENE LABELLED DATP
Ivan Magriñá Lobato

UNIVERSITAT ROVIRA I VIRGILI
DEVELOPMENT OF ELECTROCHEMICAL DNA SENSORS BASED ON THE INCORPORATION OF FERROCENE LABELLED DATP
Ivan Magriñá Lobato

UNIVERSITAT
ROVIRA i VIRGILI